Selection and Characterization of DNA Aptamers for the Detection of Antibiotics

By

Yichen Zhao

A thesis

presented to the University of Waterloo

in fulfilment of the

thesis requirement for the degree of

Doctor of Philosophy

in

Chemistry (Nanotechnology)

Waterloo, Ontario, Canada, 2024

©Yichen Zhao 2024

Examining Committee Membership

The following served on the Examining Committee for this thesis. The decision of the Examining Committee is by majority vote.

External Examiner	**Dr. Maxim V. Berezovski** Professor, Department of Chemistry and Biomolecular Sciences University of Ottawa, Ottawa, Canada
Supervisor	**Dr. Juewen Liu** Professor, Department of Chemistry, University of Waterloo, Waterloo, Canada
Internal Member	**Dr. Thorsten Dieckmann** Associate Professor, Department of Chemistry, University of Waterloo, Waterloo, Canada
Internal Member	**Dr. Richard Manderville** Professor, Department of Chemistry, University of Guelph, Guelph, Canada
Internal-external Member	**Dr. Veronika Magdanz** Assistant Professor, Department of Systems Design Engineering

University of Waterloo, Waterloo, Canada

Author's Declaration

This thesis consists of material all of which I authored or co-authored: see Statement of Contributions included in the thesis. This is a true copy of the thesis, including any required final revisions, as accepted by my examiners.

I understand that my thesis may be made electronically available to the public.

Statement of Contributions

The work presented in this thesis is the result of work performed by the authors and other scientific collaborators. Contributions from each scientist and the resulting publications are listed below.

The work in Chapter 2 has been published as follows:

Yichen Zhao, Steven Ong, Yijing Chen, Po-Jung Jimmy Huang, and Juewen Liu. Label-free and dye-free fluorescent sensing of tetracyclines using a Capture-Selected DNA aptamer. *Analytical Chemistry,* **2022**, 94 (28), 10175–10182. Fluorescence polarization experiments were done by Yijing Chen and fluorescence titration of TC and DOX were done by Steven Ong. All other experiments were done by Yichen Zhao. The manuscript was written by Yichen Zhao and Juewen Liu.

Yichen Zhao., Biwen Gao, Peihuan Sun and Juewen Liu. Metal and pH-Dependent Aptamer Binding of Tetracyclines Enabling Highly Sensitive Fluorescence Sensing. Biosensors 2022, 12, 717. Some of the metal ion binding curves were done by Biwen Gao and Peihuan Sun. All other experiments were done by Yichen Zhao. The manuscript was written by Yichen Zhao and Juewen Liu.

Yichen Zhao., Nikesh Patel, Peihuan Sun, Karen Faulds, Duncan Graham, and Juewen Liu. (2023). Light-up split aptamers: binding thermodynamics and kinetics for sensing. The Analyst, 148(22), 5612–5618. Temperature dependent fluorescence was measured by Peihuan Sun, The AuNP excitation was measured by Nikesh Patel. All other experiments were done by Yichen Zhao. The manuscript was written by Yichen Zhao and Juewen Liu.

The work in Chapter 3 has been published as: Yichen Zhao, Biwen Gao., Yijing Chen and Juewen Liu. (2023). An aptamer array for discriminating tetracycline antibiotics based on binding-

enhanced intrinsic fluorescence. The Analyst, 148(7), 1507–1513 and Yichen Zhao., Biwen Gao., and Juewen Liu (2024). Characterization of the Binding Properties of Ten Aptamers Using the Intrinsic Fluorescence of Oxytetracycline. *ChemistryOpen*. Biwen Gao and Yichen Zhao contributed equally to the experiments this work. The data analysis was done by Yichen Zhao and Juewen Liu. The manuscript was written by Yichen Zhao and Juewen Liu.

The work in Chapter 4 has been published as: Yichen Zhao, Albert Zehan Li and Juewen Liu. (2023). Capture-SELEX for Chloramphenicol Binding Aptamers for Labeled and Label-Free Fluorescence Sensing. Environment & Health, 1(2), 102–109. Albert Zehan Li performed the Thioflavin-T titration curve. All other experiments were done by Yichen Zhao. The manuscript was written by Yichen Zhao and Juewen Liu.

For Chapter 5, all experiments were performed by Yichen Zhao.

Abstract

DNA is a naturally occurring biomacromolecule that plays many roles in living organisms. While the majority of natural DNA is double stranded, chemical synthesis allows the production of single-stranded DNA oligonucleotides that can carry chemical functions for molecular recognition, and these are known as DNA aptamers. There is wide range of targets that DNA can bind, from metabolites, drugs, toxins, and other small molecules to proteins and even cells and tissues. Aptamers are generally selected through an iterative process called Systematic Evolution of Ligands by Exponential Enrichment (SELEX). After this process is completed, the newly selected aptamers can then be subject to binding assays for characterization before finally becoming useful for sensing. Compared to the traditional methods of sensing such as HPLC, mass spectroscopy, or antibodies, aptamers are cheaper, easier to transport and use, have longer shelf lives, and can have a wider range of targets. This focus of this thesis is to use a method called capture-SELEX to isolate new aptamers for a few important antibiotics. While aptamers have been reported for them, they were mostly obtained by the immobilization of target molecules. In capture-SELEX, the DNA library is immobilization allowing the use of free target molecules.

In Chapter 1, background information is given about nucleic acid structure, DNA, and the current state of aptamers. The SELEX process is also discussed in detail as well as some characterization methods and sensor applications.

In Chapter 2, a new DNA aptamer for the family of tetracycline antibiotics was selected using capture-SELEX and oxytetracycline (OTC) as the target. This new aptamer was called OTC5 and had a dissociation constant (K_d) of 150 nM OTC measured using ITC. This aptamer could also enhance the intrinsic fluorescence of the tetracycline antibiotics and this property could be exploited for label free and dye free sensing. Follow-up studies were done on the OTC5 aptamer.

It was found that metal ions (specifically Mg^{2+}) had an effect on the binding of OTC5 to the tetracyclines. pH also affected binding with pH 6 promoting binding more than higher pH values. Studies were also done on splitting the OTC5 aptamer. The split aptamer retained its binding with doxycycline.

In Chapter 3, from the remaining SELEX pool of the selection in Chapter 2, 10 other aptamers were identified to have binding with the tetracyclines. Some of these could distinguish between tetracycline, doxycycline, and oxytetracycline which led to the development of an aptamer sensor array that could differentiate these antibiotics with statistical significance.

In Chapter 4, a new aptamer called CAP1 was selected for chloramphenicol (CAP) using capture-SELEX. Previous aptamers for CAP were selected by target immobilization which omitted a portion of the CAP molecule. When subjected to ITC, this previous aptamer did not show any indications of binding to the full CAP molecule. The newly selected CAP1 showed a fitted K_d of 9.8 μM using ITC. A sensor was also developed using Thioflavin-T fluorescence and had a limit of detection of 1.8 μM in lake water and 3.8 μM in wastewater.

In Chapter 5, the effect of pH on aptamer selection was studied by a parallel selection at pH 6 and pH 8 for the aminoglycoside antibiotic kanamycin A. The selection at pH 6 showed better convergence than pH 8 and yielded an aptamer (KAN6-1). This aptamer had a K_d of around 300 nM from ITC. pH and salt studies were done using Thioflavin-T fluorescence assays and the optimal condition for binding was at pH 6 with no added salts. When KAN6-1 was tried with thioflavin-T under pH 8 selection conditions, there was no evidence of any binding. A sensor was then designed using KAN6-1 and had a limit of detection of 0.1 μM in lake water.

Acknowledgements

I would like to extend a very special thank you to Dr. Juewen Liu, my supervisor of many years for his invaluable advice, constant encouragement and great mentorship.

I would also like to thank Dr. Thorsten Dieckmann, Dr. Richard Manderville and Dr. Vivek Masheshwari for being on my advisory and examining committee as well as their evaluation of my research. Also, thank you to Dr. Maxim Berezovski and Dr. Veronika Magdanz for agreeing to be my examiners for this dissertation.

Thank you to all the past and present members of the Liu lab for fostering a welcoming and productive work environment: Dr. Po-Jung Jimmy Huang, Dr. Yibo Liu, Dr. Mohamed (MoMo) Zandieh, Dr. Kaya Wong, Yuzhe Ding and Jennifer Moon.

Finally, I would like to thank my friends and family, especially my parents Li and Yingming for their unending love and support.

Table of Contents

Author's Declaration ..... **iv**
Statement of Contributions ..... **v**
Abstract ..... **vii**
Acknowledgements ..... **ix**
Chapter 1 Introduction **1**
1.1 Nucleic Acids **1**
1.1.1 Nucleic Acids Structure 1
1.2 Aptamers **3**
1.2.1 Brief Overview of Nucleic Acid Aptamers 3
1.2.2 History of Aptamers 3
1.2.3 DNA vs RNA vs Antibodies 4
1.2.4 Protein Targets and Examples 5
1.2.5 Small Molecule Targets and Examples 6
1.2.6 Aptamers for Antibiotics 7
1.2.7 Previously reported aptamers for antibiotics 8
1.3 Aptamers That Cannot Bind Their Targets **20**
1.4 The SELEX Process **24**
1.4.1 General Overview and Types of SELEX 25
1.4.2 Library Design 26
1.4.3 Methods to Monitor Enrichment 28
1.4.4 Sequencing Analysis and Binding Assays 29
1.4.5 Post-SELEX Modifications 31
1.4.6 Sensor Development 34

1.5 Thesis goals 35

Chapter 2 An Aptamer for Tetracycline Antibiotics 36

2.1 Introduction 36

2.2 Materials and Methods 37

2.2.1 Chemicals 38

2.2.2 Preparation of OTC solutions 38

2.2.3 SELEX for OTC Aptamers 39

2.2.4 ITC 40

2.2.5 Fluorescence polarization 40

2.2.6 Fluorescence Measurements 40

2.2.7 Detection in milk 41

2.2.8 Fluorescence biosensor based on strand displacement 41

2.2.9 Split Aptamer Studies 41

2.3 Results and Discussion 42

2.3.1 Aptamer selection 42

2.3.2 Aptamer binding assay using ITC 45

2.3.3 Intrinsic Fluorescence Enhancement by The OTC5 aptamer 46

2.3.4 pH and Metal Ion Dependency 49

2.3.5 pH and Mg^{2+}- dependent fluorescence of the tetracyclines 52

2.3.6 pH and Mg^{2+} dependent aptamer binding 53

2.3.7 pH and Mg^{2+} Binding Assay using ITC 56

2.3.8 Effect of other metal ions 57

2.3.9 Sensing of the Tetracyclines using OTC5. 58

2.3.10 Sensing of OTC in milk 61

2.3.11 Labeled fluorescent sensing of OTC 62

2.4 A Split aptamer biosensor 63

2.4.1 Splitting the OTC5 aptamer 64

2.4.2 Fluorescence change and binding affinity at different stem lengths 66

2.4.3 Temperature-dependent binding 67

2.4.4 Thermodynamics of binding using ITC 68

2.4.5 Binding Kinetics of the Split Aptamers 70

2.5 Conclusions 72

Chapter 3 Characterization of an Aptamer Array for the Tetracyclines 74

3.1 Materials and Methods 75

3.1.1 Chemicals 75

3.1.2 Fluorescence Spectroscopy 75

3.1.3 Fluorescence Lifetime 75

3.1.4 Isothermal Titration Calorimetry (ITC) 76

3.1.5 Selectivity of the sensors 76

3.1.6 Sensor array 76

3.2 Results and Discussion 76

3.2.1 The ten oxytetracycline binding aptamers 76

3.2.2 Effect of Mg^{2+} 77

3.2.3 High affinity binding aptamers. 79

3.2.4 Fluorescence lifetime. 80

3.2.5 Isothermal Titration Calorimetry 81

3.2.6 Aptamer binding induced fluorescence changes. 82
3.2.7 Highly sensitive detection. 86
3.2.8 A sensor array for discriminating the three antibiotics. 87
3.3 Conclusions 89
Chapter 4 An Aptamer for Chloramphenicol 90
4.1 Introduction 90
4.2 Materials and Methods 91
4.2.1 Chemicals. 91
4.2.2 Capture-SELEX for CAP. 92
4.2.3 ITC. 93
4.2.4 Biosensor based on the strand displacement reaction 93
4.2.5 Thioflavin-T (ThT) based fluorescence sensing. 93
4.3 Results and Discussion 94
4.3.1 Capture selection of CAP binding aptamers. 94
4.3.2 Three families of CAP binding aptamers. 95
4.3.3 Binding Assay using ITC. 97
4.3.4 Comparison with previously reported aptamers 100
4.3.5 Strand displacement reaction for sensing of CAP 102
4.3.6 Fluorescence Sensing Using ThT 103
4.3.7 Real Water Samples with the ThT-based Sensor. 106
4.4 Conclusions 107
Chapter 5 pH-Directed Capture-SELEX Aptamers for Kanamycin Detection 109
5.1 Introduction 109

5.2 Materials and Methods **110**

5.2.1 Chemicals. 110

5.2.2 Buffer and Kanamycin Solution Preparation 111

5.2.3 Kanamycin Selection. 111

5.2.4 Isothermal Titration Calorimetry. 112

5.2.5 Thioflavin-T Fluorescence Assay. 112

5.3 Results and Discussion **112**

5.3.1 Capture-SELEX of Kanamycin Binding Aptamers at Two pH Values 112

5.3.2 A Strong Effect of pH for Binding in High Salt Buffers 115

5.3.3 pH-insensitive Binding in Low Salt Buffers 117

5.3.4 Mutation Studies 120

5.3.5 Comparison with previously published aptamers 121

5.3.6 Selectivity of the KAN6-1 aptamer 123

5.3.7 Detection of kanamycin A in Lake Water 124

5.4 Conclusions **125**

Chapter 6 Conclusions and Future Work **127**

6.1 Conclusions **127**

6.2 Original Contributions **129**

6.3 Future Work **130**

Letters of Copyright Permission **131**

References **146**

List of Figures

Figure 1.1 Chemical Structure of (A) double stranded DNA showing the components of a nucleotide, the phosphate backbone and Watson-Crick base pairing. (B) A single strand of RNA. 2

Figure 1.2. 3D representation of the thrombin aptamer bound to thrombin. 6

Figure 1.3 (A) Predicted secondary structure of the theophylline aptamer TCT8-4. (B) K_d values of the TCT8-4 aptamer with theophylline and caffeine measured using a competitive equilibrium filtration binding assay. 7

Figure 1.4. The chemical structures of common antibiotics. (A) Tetracycline (B) Kanamycin (C) Ampicillin (D) Chloramphenicol. 8

Figure 1.5 (A) Sequence alignment of the selection done by Berens et al. (B) Secondary structures of cb28 (left) and cb32 (right). 10

Figure 1.6. (A) Gel electrophoresis showing the lead induced cleavage of the cb28 aptamer. (B) Fluorescence titrations of the cb32 aptamer to determine K_d of TC and DOX. 10

Figure 1.7. (A) SPR peaks of P2MC aptamer for K_d determination.(B) Fluorescence titration showing specificity of P2MC for DOX compared to the previously selected Tet aptamer from Berens *et al*. (C) SPR peaks of the P1MC aptamer (D) Fluorescence titration of showing no reactivity with TC from the P1MC aptamer. 11

Figure 1.8. The secondary structure of the No.4 aptamer selected by Niazi *et al*. for oxytetracycline. 12

Figure 1.9. (A) Sequence alignment from the selection by Niazi *et al*. (B) Equilibrium filtration binding assays to determine K_d. 13

Figure 1.10 (A). Active sequences and their measured K_d from the selection of Burke *et al*. (B) Inferred secondary structures of 3 isolates..... 14

Figure 1.11 (A) Sequence alignment of the random regions from the selection done by Mehta *et al*. (B) Secondary structure of the truncated CAP aptamer.(C) Secondary structures of full length aptamers from A.(D) Specificity of aptamers 7 and 16. 15

Figure 1.12. (A) Sequence alignment of the random region from the selection by Duan et al. (B) Predicted secondary structure of No.4 and No.5 from (A) for chloramphenicol. (C) Measured K_d of aptamer candidates. (D) Specificity of No.4 and No.5 by equilibrium filtration. 16

Figure 1.13. (A) The chemical structure of free CAP (B) CAP base, the form available after conjugation to beads. (C) Immobilization of CAP base using a carboxylic acid as done by Duan *et al.* (D) Immobilization of CAP base using p-toluenesulfonyl (tosyl) groups done by Mehta *et al*. 17

Figure 1.14 (A) Predicted structure of the 3_19 aptamer. (B) Sequence and predicted structure of the K16-1 aptamer..... 18

Figure 1.15 (A) Selectivity of the 3-19 aptamer compared to the other compounds used in its selection target solution. (B) Elution assay for to determine K_d for different aptamer candidates from the selection by Mehta et. al. (C) Restriction enzyme SELEX protocol from the Heemstra group. (D) Comparison of microscale thermophoresis studies between the 3-19 and K16-1 kanamycin aptamers..... 19

Figure 1.16. The principle of a colorimetric gold nanoparticle assay..... 21

Figure 1.17. (A) Colorimetric nanoparticle assay comparing Ars-3 and a random 30-mer DNA. (B) ITC traces comparing As (III) into a buffer control and Ars-3 (left) and As(V) into Ars-3 and a buffer control(right). 22

Figure 1.18 (A) Thermograms of ampicillin in the AMP17, AMP4, and AMP18 aptamers. (B) Thermograms of AMP18 in different buffers. 23

Figure 1.19. (A) ITC trace of chloramphenicol into the truncated 7 aptamer. (B) ITC trace of the 7 aptamer into its complementary strand. Gold nanoparticle assay of kanamycin into the ky2 aptamer, 2 mutants and a random sequence (C) without and (D) with NaCl. 24

Figure 1.20. The general overview of the capture-SELEX process using ssDNA.[65] 26

Figure 1.21. Different possible library designs. (A) Stem-loop (B) Three-way junctions (C) Other structures.[70] 28

Figure 1.22. The dissociation constant..... 30

Figure 1.23. (A) Schematic of an Isothermal Titration Calorimeter . (B) Thermogram generated by ITC. 31

Figure 1.24. (A) Structure and mutants of the Caff203 aptamer. (B) ITC traces of caffeine into Mutant-1 and Mutant-2. (C) Structure and mutants of the CSS.1 aptamer. (D)ITC traces of cortisol into CSS.1 (left), CSS.1-mt1(middle), CSS.1-mt2 (right). 32

Figure 1.25. (A) Structure and truncation of Uri1 aptamer (B) ITC traces of uridine into the Uri1 aptamer (left) and Uri-m (right). (C) Structure and truncations of SRhB1 aptamer. (D) Fluorescence titration and fitted K_d of the SRhB1 mutants. 33

Figure 1.26. (A) Schematic of a paper-based sensor for kanamycin detection. (B) Potentiometric response of sensor with increasing amounts of kanamycin and (D) calibration curve generated. 34

Figure 1.27. (A) Schematic of a lateral flow sensor using an aptamer for dopamine. (B) visual observation of the effect of dopamine concentration on color intensity of the test line; (C) peak area value of intensity to quantify dopamine presence at 15 min. 35

Figure 2.1. (A) The structures of the three tetracycline antibiotics used in this study. (B) Alignment of the most abundant 15 sequences. Within each family, the nucleotides in green can base pair, while those in blue are identical. Mfold predicted secondary structures of (C) the OTC1 aptamer, (D) the OTC5 aptamer and (E) a truncated OTC5 aptamer with the small hairpin removed. 44

Figure 2.2. Alignment of previously reported No. 4 aptamer with the top 10 sequences from our selection. 44

Figure 2.3. ITC traces and integrated heat of (A) titrating OTC into the OTC1 aptamer; and titrating (B) OTC, (C) TC and (D) DOX into the OTC5 aptamer. For each titration, 150 μM of target was titrated into 9 μM of DNA aptamer in the SELEX buffer at 25°C..... 46

Figure 2.5. (A) Fluorescence spectra of 100 nM OTC in the presence of various concentration of the OTC5 aptamer with 370 nm excitation. The fluorescence increases of 100 nM (B) OTC, (C) TC, and (D) DOX with increasing concentration of the OTC5 aptamer. The data were fitted to a one-site binding curve. In (B), the non-binding mutant was also tested..... 47

Figure 2.6. Fluorescence of OTC witht and without the OTC aptamer. 48

Figure 2.7. (A) The general structure of the tetracyclines with their respective pK_a values.[129] pK_a values adapted from ref.129(B) The structure of tetracyclines at pH 6 and pH 8.3. (C) The

secondary structure of the OTC5 aptamer. (D) A cartoon showing the fluorescence enhancement of the tetracyclines upon aptamer binding. 51

Figure 2.8 The fluorescence of the tetracycline antibiotics at pH 6.0 and 8.3 in the presence of increasing concentration of Mg^{2+}: (A) DOX, (B) OTC and (C) TC. The fluorescence intensity of 100 nM (D) DOX, (E) OTC, and (F) TC alone and with 2 μM of the OTC5 aptamer with increasing concentration of Mg^{2+} in 10 mM MES, pH 6.0 with 50 mM NaCl. 53

Figure 2.9. (A) Fluorescence spectra of 100 nM OTC in the absence and presence of 2 μM OTC5 aptamer at pH 6.0. (B) pH-dependent fluorescence of 1 μM OTC in the absence and presence of 2 μM OTC5 aptamer. pH 4 and 5: acetate buffer; pH 6, 7: phosphate buffer; pH 8: Tris buffer. All with 10 mM Mg^{2+}. (C) The fold of fluorescence enhancement at different pH due to the addition of OTC5. 54

Figure 2.10. Aptamer binding curves for (A, B) DOX, (C, D) OTC, and (E, F) TC in (A, C, E) pH 6.0 buffer and (B, D, F) pH 8.3 buffer in the absence or presence of 2 mM Mg^{2+}. 55

Figure 2.12. The fluorescence of 100 nM OTC alone and with 2 μM OTC5 aptamer as a function of (A) Ca^{2+}, (B) Mn^{2+} and (C) Zn^{2+} concentration. All in pH 6.0 MES buffer. (D) The fluorescence of 100 nM OTC as a function of OTC5 aptamer concentration in 0.5 mM Mn^{2+} alone and with 0.5 mM Mn^{2+} and 2 mM Mg^{2+} mixture. The buffer was 10 mM MES, pH 6.0 with 100 mM NaCl. 58

Figure 2.13. (A) Fluorescence difference of various molecules in the absence and presence of 2 μM OTC5 aptamer. (B) Fluorescence intensity at 520 nm of 100 nM of each of the molecules excited at 370 nm. The buffer was 10 mM Tris HCl, pH 7.8, 60 mM NaCl, 2 mM $MgCl_2$, 1 mM KCl. 59

Figure 2.14. Fluorescence intensity of (A) DOX, (B) OTC, and (C) TC in the absence (black dots) and presence (red dots) of 2 μM OTC5 aptamer. Fluorescence difference of (D) DOX, (E) OTC, and (F) TC in the absence and presence of 2 μM OTC5 aptamer. The measurements were performed in pH 6 buffer with 2 mM Mg^{2+}. 60

Figure 2.15. Selectivity of the OTC5 aptamer in (A) pH 6.0 MES buffer and (B) pH 8.3 Tris buffer each with 2 mM Mg^{2+}. 2 μM of OTC5 was added to 100 nM of antibiotic. Samples were scanned at an excitation wavelength of 370 nm and emission of 530 nm. (C) The fluorescence difference at pH 6.0 and 8.3 with and without OTC5. 61

Figure 2.16. Fluorescence intensity as a function of OTC concentration in spiked milk samples after extraction without and with 2 μM OTC5 aptamer at (A) pH 6.0 with 2 mM Mg^{2+}. (B) Fluorescence difference as a function of OTC concentration at pH 6.0. 62

Figure 2.17. (A) Schematic of the strand-displacement biosensing system with a covalently linked fluorophore and quencher. (B) Kinetics traces of the sensor in the presence of various concentrations of OTC in the selection buffer. OTC was added at 5 min. (C) Fluorescence intensity as a function of OTC concentration. Inset: linear response at lower concentrations. (D) Sensor selectivity against various antibiotics at 8 μM. 63

Figure 2.18. (A) The full-length OTC5 aptamer and the strategy of splitting. In this study, the OTC5a strand was fixed and the length of OTC5b strand varied to tune the number of base pairs. In the current figure, the two stems have 7 and 5 base pairs, respectively. (B) Fluorescence spectra of 1 μM doxycycline in the absence and presence of 2 μM of the full length OTC5 aptamer. Buffer for OTC5: 2 mM Mg2+, 10 mM MES, pH 6.0. (C) Photograph showing fluorescence enhancement

of 2 μM doxycycline in the presence and absence of 5 μM C5 in the previously mentioned buffer. 66

Figure 2.19. Fluorescence titration of each split aptamer into1 μM doxycycline. Fitted K_d values in μM are in brackets. Split aptamers were pre-annealed at 90°C for 5 min and allowed to cool to room temperature before measurements. 67

Figure 2.20. Temperature-dependent 1 μM doxycycline fluorescence in the presence of 2 μM of the full-length or the split (5/6 bp) OTC5 aptamer. The measurement was performed in 10 mM MES buffer pH 6.0, 1 mM $MgCl_2$ and 50 mM NaCl. 68

Figure 2.21. ITC traces of (A) the full length OTC5, (B) OTC5a+ OTC5b7/5 aptamer, and (C) OTC5a+OTC5b5/4. All aptamers were pre-annealed for 5 min at 90°C and allowed to cool to room temperature before loading. Experiments were carried out at 20°C. 70

Figure 2.22. Kinetics of the split OTC5a and OTC5b5/4. Black: OTC5a and OTC5b5/4 were pre-annealed at 90°C and 1 μM of the annealed solutions was added at 180 s. Red: 1 μM OTC5a was added at 180 s followed by 1 μM OTC5b5/4 at 360 s. Green: 1 μM OTC5b5/4 was added at 180 s followed by 1 μM OTC5a at 360 s. Excitation was at 370 nm and emission at 535 nm. 200 nM doxycycline in MES pH 6.0 buffer with 1 mM $MgCl_2$ was read for 180 s to ensure a stable background before the addition of the split aptamer. 71

Figure 3.1. The Mfold predicted secondary structures of the ten OTC aptamers studied in this work: (A) OTC1, (B) OTC8, (C) OTC11, (D) OTC26, (E) OTC34, (F) OTC2, (G) OTC22, (H) OTC23, (I) OTC43 and (J) OTC5. The structures of (K) tetracycline, (L) oxytetracycline and (M) doxycycline. 77

Figure 3.2. (A) The fluorescence intensity ratios of 100 nM OTC in the presence and absence of 2 μM of various aptamers. (B) The fluorescence of 100 nM OTC in the presence various concentrations of OTC2 aptamer at different Mg^{2+} concentrations..... 78

Figure 3.3. Titration curves of various aptamers: (A) OTC1, (B) OTC2, (C) OTC3, (D) OTC5, (E) OTC8, (F) OTC11, (G) OTC22, (H) OTC23, (I) OTC26 and (J) OTC43. 79

Figure 3.4. (A) Fluorescence lifetime decay traces of 1 μM OTC alone and in the presence of 2 μM aptamers. (B) Average lifetime of the samples. (C) Average fluorescence lifetime vs folds of fluorescence enhancement. The measurements were performed in 10 mM pH 6.0 MES buffer with 50 mM NaCl and 2 mM $MgCl_2$. 80

Figure 3.5. ITC traces of (A) OTC2, (B) OTC22, and (C) OTC43. All experiments were done in 10 mM pH 6.0 MES buffer with 50 mM NaCl and 2 mM Mg^{2+}, 9 μM aptamer and 150 μM OTC at 25°C. 81

Figure 3.6. (A) Fluorescence spectra of 100 nM OTC before and after adding 2 μM OTC2 aptamer. (B) A fluorescent photograph of 500 nM OTC with (right) and without (left) 2 μM OTC2 aptamer. (C) The fold of fluorescence enhancement of the ten aptamers to the three tetracyclines. (D) The K_d values of the three aptamers. Note the *y*-axis is in log scale. (E) Structures showing aptamers binding to OTC in three different ways, which can explain their selectivity for the three tetracycline antibiotics. 84

Figure 3.7. The aptamer-dependent fluorescence enhancement of 100 nM of the three tetracyclines in pH 6.0 buffer with 2 mM Mg^{2+} with (A) OTC1, (B) OTC8, (C) OTC11, (D) OTC26, (E) OTC34, (F) OTC2, (G) OTC22, (H) OTC23, (I) OTC43 and (J) OTC5 aptamers. 84

Figure 3.8. (A) The secondary structure of the OTC7, which is an orphan sequence that cannot be assigned to a family. (B) The change of fluorescence of the three antibiotics in the presence of increasing concentration of OTC7. The lack of fluorescence change indicates no binding. 85

Figure 3.9. The fluorescence of (A) free OTC and after adding 2 μM OTC43 aptamer, (B) free TC and after adding 2 μM OTC2 aptamer, and (C) free DOX and after adding 2 μM OTC22 aptamer. The fluorescence intensity difference before and after adding the aptamers for the detection of (D) OTC, (E) TC, and (F) DOX using their respective aptamers. 87

Figure 3.10. Discrimination of different antibiotics using the sensor array. (A) Fluorescence intensity increase among different antibiotics. (B) Canonical score plots of fluorescence responses obtained for different antibiotics at 50 nM antibiotic. (C) Score plots for fluorescence response obtained using varying concentrations of OTC. (D) Plots of PC1 vs concentration of OTC. 88

Figure 4.1. (A) Structures of CAP and CAP base. (B) Top 10 most abundant sequences after sequencing from the first (Seq1) and the second (Seq2) sequencing. The bases in red are conserved within each family, whereas the remaining sequences have little to no homology. The number of copies of each sequence is in brackets for the selected sequences. The sequences without a copy number contained less than 10 copies. Secondary structures of the (C) CAP1, (D) CAP3, and (E) CAP4 aptamers predicted using Mfold. 96

Figure 4.2. Alignment of selection results with CAM80 with the help of ClustalOmega. From the results, CAM80 and other sequences from a selection done by Duan *et al* (No, 1,4,5,6 and 10), do not align with the sequences obtained in this work. 97

Figure 4.3. ITC traces of (A) 0.4 mM CAP into 20 μM CAP1 aptamer, (B) 0.4 mM CAP into 20 μM of CAP3, and (C) 2 mM CAP into 50 μM CAP4 at 25°C. Aptamers were pre-annealed at 90°C for 5 min in 1× SB. 99

Figure 4.4. ITC traces of (A) a truncated CAP1 (CAP1short) aptamer, and (B) a mutant of CAP1 (CAP1mut2) titrated with 0.4 mM CAP and 20 μM aptamer at 25°C in 1× SB. (C) ITC trace of 20 μM CAM80 and 1 mM CAP using the original selection buffer conditions (20 mM Tris-HCl pH 7.6, 100 mM NaCl, 5 mM KCl, 2 mM $MgCl_2$, 1 mM $CaCl_2$). (D) ITC trace of CAP1 without pre-annealing. 100

Figure 4.5. Secondary structures of (A) the full length 80-mer CAP aptamer, (C) the truncated 40-mer of the CAP aptamer (from the yellow region in panel (B)) predicted by Mfold (top) and from the literature (bottom). (C) The RNA aptamer for CAP. (D) ITC of 3 mM CAP into 34.5 μM previously reported 80-nt CAM80 aptamer. 102

Figure 4.6. (A) Schematic of the strand displacement fluorescent sensor. (B) Kinetics of 100 nM sensor with the addition of 0.5 mM CAP in 1× SB. (C) Fluorescence intensity as a function of CAP concentration. Inset: linear response at low concentrations. (D) Selectivity of sensor against 0.15 mM antibiotic: penicillin (PEN), kanamycin (KAN), streptomycin (STR), oxytetracycline (OTC), tetracycline (TC), and doxycycline (DOX). 103

Figure 4.8.(A) The effect of different concentrations of NaCl and $MgCl_2$ on the fluorescence change of the CAP1-ThT system. (B) Titration curve of CAP1 aptamer into 2.5 μM Thioflavin-T in 20 mM Tris-HCl pH 7.8, 10 mM $MgCl_2$. A K_d of 2.3 μM was fitted.(C) CAP3 (K_d = 46 μM), and (C) CAP4 (unable to fit K_d) and 0.5 μM ThT. 106

Figure 4.9. Fluorescence intensity of ThT/CAP1 after the addition of varying amounts of CAP in wastewater. The wastewater was buffered the same way as the lake water. A LOD of 3.6 μM was achieved. 107

Figure 5.1. (A) The structure of kanamycin A and the pK_a values of its four amino groups.[32] The secondary structures of the (B) KAN6-1 and (C) KAN6-5 aptamers. (D) The top 20 most abundant sequences from SELEX done at pH 6, and the top 4 sequences from SELEX done at pH 8 as well as the previously selected aptamers. The number of copies of each sequence is in brackets. The colored regions are the conserved sequences..... 115

Figure 5.2. (A) A scheme showing the ThT-based fluorescence assay of kanamycin A (KAN) binding and it can also be used as a label-free detection method. Fluorescence titration curve of adding kanamycin A into 1 μM KAN6-1 aptamer in the presence of 1 μM ThT in either (B) high salt buffers (50 mM MES, pH 6 or HEPES, pH 7 and 8 with 300 mM NaCl, 10 mM MgCl2, and 5 mM KCl), or (C) no salt buffers 50 mM MES (pH 6) or HEPES (pH 7 and 8) buffer but with 2 mM EDTA. 119

Figure 5.3. The fluorescence of Thioflavin-T with and without a non-binding aptamer sequence for control. (A) No salt in 50 mM pH 6 MES buffer, pH 7 HEPES, and pH 8 HEPES all with 2mM EDTA.(B) Same buffers but all with 300 mM NaCl, 10 mM $MgCl_2$, and 5 mM KCl..... 119

Figure 5.4. ITC trace of titrating 100 μM kanamycin A into 10 μM KAN6-1 aptamer in (A) 50 mM pH 6.0 MES with 300 mM NaCl, 10 mM MgCl2, 5 mM KCl; (B) 50 mM pH 8.0 HEPES with 300 mM NaCl, 10 mM MgCl2, 5 mM KCl. (C) ITC trace of titrating 200 μM kanamycin A into 20 μM KAN6-5 aptamer in pH 6.0 SB1 buffer. 120

Figure 5.5. (A) Two aptamer mutants based on KAN6-1. (B) Fluorescence binding assays of mutant 1 and 2 using ThT. 121

Figure 5.6. Alignment of the top 7 sequences from our pH 6 kanamycin selection and previously reported aptamers (Ky2, K16-1, 3_17) using Clustal Omega. There is little sequence homology between our newly selected aptamers and the previously reported ones..... 122

Figure 5.7 (A) The secondary structure of Ky2 predicted my Mfold. (B) Thioflavin-T assay of the Ky2 aptamer in its selection buffer (20 mM Tris-HCl pH 8.0 100 mM NaCl, 5 mM MgCl2, 5 mM KCl). (C) ITC trace of 100 μM kanamycin A into 10 μM Ky2 aptamer in its selection buffer.123

Figure 5.8 (A) Structures of the antibiotics used in the selectivity study. The highlighted regions in TOB are the differences between tobramycin and kanamycin A. The red line represents a possible binding region for the aptamers. (B) Selectivity of the KAN6-1 aptamer with 1 μM different antibiotics in SB1 buffer. (C) A ThT fluorescence titration curve of tobramycin. 124

Figure 5.9. ThT-based assay using (A) pH 6 MES buffer with 2 mM EDTA. (B) Filtered Lake Ontario water. Inset: Linear region at low concentrations of kanamycin. 125

List of Tables

Table 1.1 Advantages and Disadvantages of RNA vs DNA Aptamers vs Antibodies 4

Table 2.1 DNA Sequences used in this study. 38

Table 2.2 Thermodynamic values of the aptamers based on ITC. Binding ratio (N), dissociation constant (Kd), enthalpy change (ΔH) and entropy change (ΔS) of the binding reactions are supplied. 46

Table 2.3 Thermodynamic Values of the Aptamers Based on ITC. Binding ratio (N), dissociation constant (Kd), enthalpy change (ΔH), and entropy change (ΔS) of the binding reactions are supplied. 56

Table 2.3 Fitted thermodynamic values of ITC experiments. 70

Table 3.1. Fitted thermodynamic values of ITC traces. 81

Table 4.1 List of sequences used in this study 91

Table 4.2. Thermodynamic values of titrating CAP into various aptamers based on ITC. 99

Table 5.1. DNA sequences used in this work 111

Table 5.1. SELEX parameters and dissociation constants of previous selections for kanamycin A. 113

Table 5.2. Fitted thermodynamic values from ITC traces. 120

Chapter 1 Introduction

1.1 Nucleic Acids

1.1.1 Nucleic Acids Structure

Nucleic acids are biomolecules found in nature and help regulate many of the processes in the body. There are two main types of nucleic acids found in nature. Ribonucleic acid (RNA) is found in all living cells and carries instructions from DNA for the synthesis of proteins or other information. Deoxyribonucleic acid (DNA) is a functional biomacromolecule that carries our genetic information and is packaged in the nucleus of cells. Both RNA and DNA are composed of smaller units called nucleotides. Each nucleotide is composed of a phosphate group, a pentose sugar (deoxyribose in DNA and ribose in RNA), and a nucleobase (Figure 1.1). Two nucleotides are linked together through phosphodiester bonds between the sugar and phosphates leading to a phosphate rich backbone. Each nucleotide also contains one nucleobase. These include adenine (A), thymine (T) in DNA or uracil (U) in RNA, guanine (G), and cytosine (C). These bases can form hydrogen bonds, giving DNA a double helix conformation whereas RNA is generally single-stranded. Canonical Watson-Crick base pairing in DNA is A-T and G-C, though non-canonical pairing is also possible.

Compared to RNA, DNA is more chemically stable. The role of RNA in cells is a transient messenger and is chemically unstable due to the 2′-OH group on the ribose sugar (Figure 1.1B) backbone. This makes RNA very susceptible to hydrolysis[1] and has a half-life of only a few seconds in serum.[2] DNA does not have the 2′-hydroxyl group and can have a half-life up to several hours.[3,4]

In cells, DNA is replicated during cellular division through the use of specialized enzymes such as DNA helicase and DNA polymerases. DNA helicase unwinds the double stranded DNA and DNA polymerases synthesize the new DNA from the parent strand. DNA polymerases are also what is used to synthesize new DNA strands in *in vitro* conditions such as polymerase chain reaction. RNA is transcribed from DNA also through the use of enzymes called RNA polymerases. Both of these nucleic acids can be synthesized *in vitro* as well.

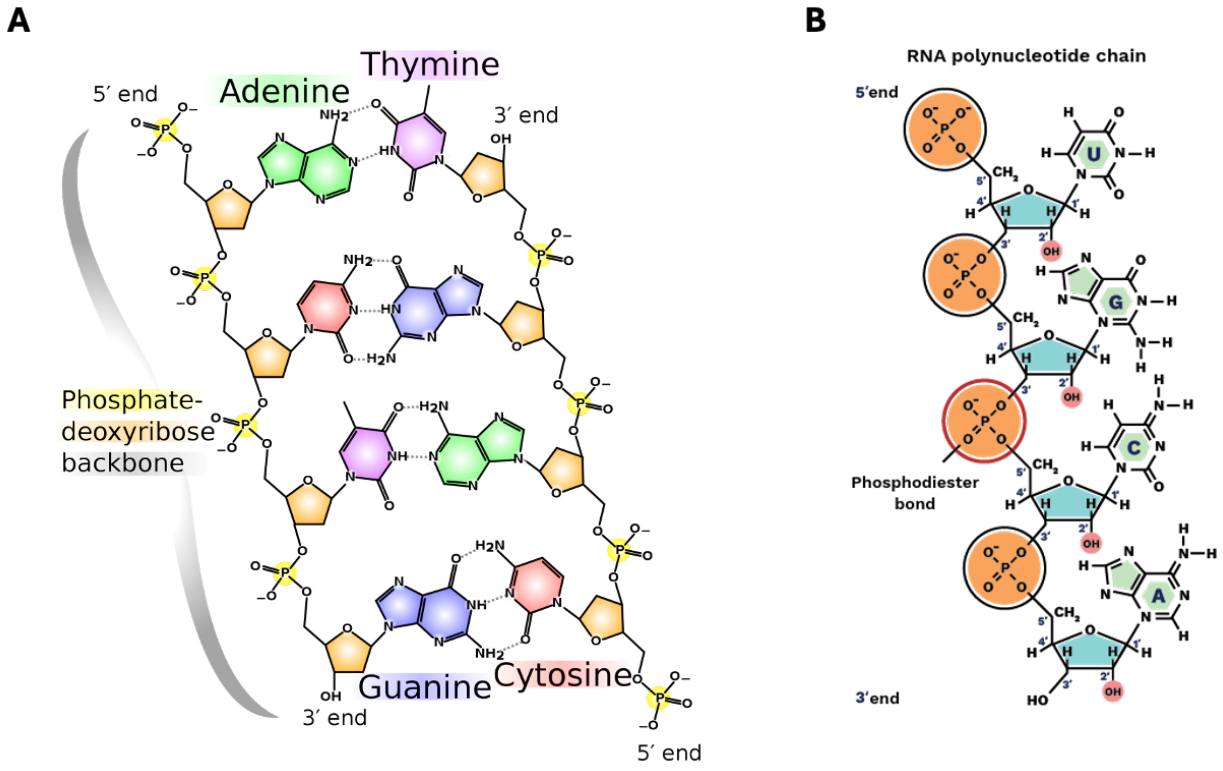


Figure 1.1 Chemical Structure of (A) double stranded DNA showing the components of a nucleotide, the phosphate backbone and Watson-Crick base pairing. (B) A single strand of RNA.

1.2 Aptamers

1.2.1 Brief Overview of Nucleic Acid Aptamers

Aptamers are single-stranded oligonucleotides can specifically bind different ligands with good affinity and can be made from either RNA or DNA. They are generally 20-80 nucleotides long and can fold into various three-dimensional structures in order to bind to their respective targets. Aptamers are generally found through a selection process called the Systematic Evolution of Ligands by Exponential Enrichment (SELEX) where a library of nucleic acids with a region of random nucleobases is screened to find sequences that bind to a specific target. These targets can vary from proteins, amino acids, metal ions, and other small molecules to viruses, bacteria, and whole cells.[5] These selected aptamers can then be modified and used for many applications such as biosensing either *in vitro* or *in vivo*.

1.2.2 History of Aptamers

Aptamers were first described in 1990 by Tuerk and Gold who found RNA sequences that bind to bacteriophage T4 polymerase using the SELEX procedure[6]. Around the same time Ellington and Szotak also selected an RNA sequence that bind to a variety of organic dyes and were the first to coin the term aptamer[7] which comes from the Latin terms *aptus* meaning to fit and *meros* meaning part. In 1992, Ellington and Szotak also selected the first DNA aptamers using the same SELEX procedure that also bind to organic dyes.[8] In 1999, Homann and Goringer were the first to use live cells to select RNA aptamers that bind to African trypanosomes and was later coined cell-SELEX.[9] The first FDA approved aptamer drug pegaptanib (brand name Macugen), was approved for use in 2004 and is an anti-VEGF (vascular endothelial growth factor) RNA aptamer developed by NeXstar Pharmaceuticals (later Eyetech Pharmaceuticals) in the mid 1990s for the treatment of age related macular degeneration (AMD).[10] The second FDA approved

aptamer drug was called avacincaptad pegol (Izervay),[11] a PEGylated RNA aptamer that binds to the complementary protein C5, inhibiting it cleavage into its biologically active fragments. This is also a treatment for AMD. More recent advances in aptamer technology include different approaches in the aptamer screening process by modifying the original SELEX protocol to accommodate different targets and achieve better affinity. There are many other methods such as magnetic bead (MB-SELEX),[12] capture-SELEX,[13] and graphene-oxide (GO-SELEX).[14]

1.2.3 DNA vs RNA vs Antibodies

Although many of the first aptamers were RNA-based, more and more recent selections are shifting to using DNA. While both have been successfully selected to bind specific ligands, there are some different advantages to using DNA instead of RNA, which are briefly summarized in Table 1. During the SELEX process, an essential step that is required for RNA aptamers is the reverse transcription of the library for each round of selection[15]. Native DNA libraries can be directly used. Another reason to use DNA is the stability.[123,4]

The major competitor against nucleic acid aptamers are antibodies. Antibodies have been used for sensing the same targets as aptamers for many years using assays such as the enzyme-linked immunosorbent assay (ELISA).[16] However, there are many advantages to using aptamers compared to antibodies. First, antibodies are expensive to produce, have great batch-to-batch variations, and are not as shelf stable whereas aptamers can be chemically synthesized for much cheaper and are stable at ambient temperatures. Second, aptamers can be recycled and regenerated after use which antibodies cannot.[17] Finally, it is difficult to generate antibodies to non-immunogenic molecules such as small molecule antibiotics or metal ions.

Table 1.1 Advantages and Disadvantages of RNA vs DNA Aptamers vs Antibodies

	DNA	RNA	Antibodies
Advantages	- Direct use of library - More chemically stable and more resistant to degradation	- Can form more diverse and intricate 3-D structures - Forms smaller structures - Riboswitches	- Lower limits of detection - "gold standard" assay
Disadvantages	- May not bind as tightly to target as RNA (higher K_d)	- Library must be first reverse transcribed for each round of selection - Not as stable as native DNA aptamers	- More expensive - Can not be regenerated - Large batch variations

1.2.4 Protein Targets and Examples

Aptamers can be selected for different targets from small molecules to larger proteins. Protein targets can be of great interest as they act as biomarkers and control many of the physiological and pathological events in living organisms. The EpCAM aptamer was selected for the membrane protein, epithelial cell adhesion molecule[18] which is a structural protein that is overexpressed in cancerous cells[19,20] and is used as a biomarker. Other targets that have aptamers include IGA1, IGA2, and IGA3 for insulin[21] a protein which regulates blood glucose and is important in monitoring diseases such as diabetes[22] and the DSA1N5[23] and the C7 aptamer[24] for

the SARS-CoV-2 spike protein. The thrombin aptamer is another well-known aptamer for the blood clotting factor, thrombin[25] (Figure 1.2).

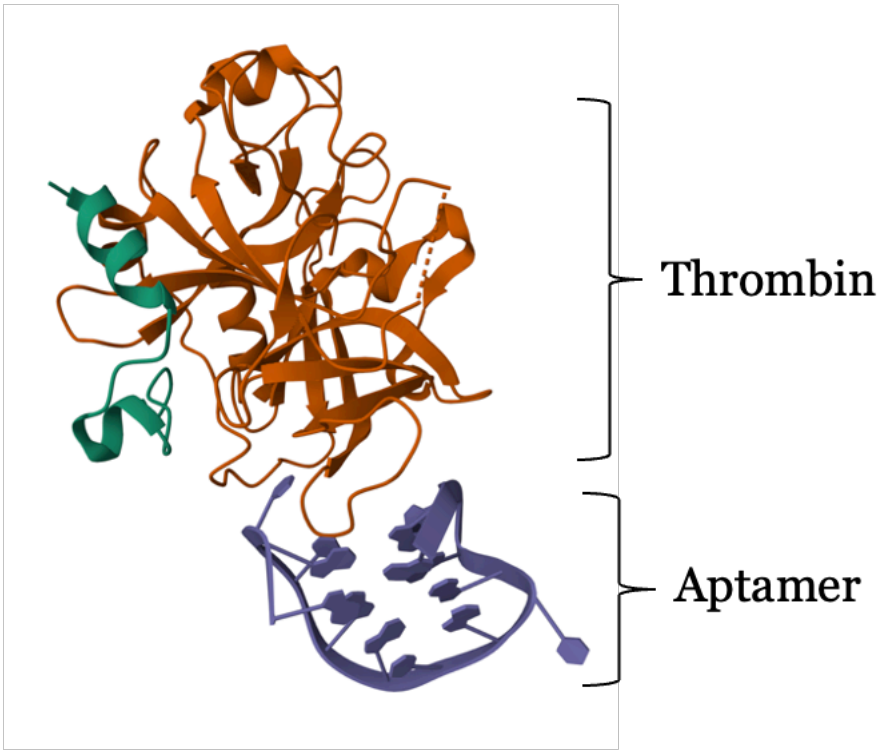


Figure 1.2. 3D representation of the thrombin aptamer bound to thrombin. PDB ID: 4DII.

1.2.5 Small Molecule Targets and Examples

A more applicable target for aptamers is small molecules. These molecules can come from a variety of sources and are used or need to be monitored. These can include aptamers for industrial wastes such as melamine and polychlorinated biphenyls[26,27], environmental toxins such as bisphenol A[28], dyes [29], therapeutic drugs such as quinolone and streptomycin[30,31] and more. The traditional methods of monitoring and detecting these molecules require the use of big and expensive machinery as well as professionally trained personnel to operate them. These include methods such as high-performance liquid chromatography (HPLC) and mass spectrometry. Another classic example of small molecule RNA aptamers is the RNA aptamer for the

bronchodilator theophylline.[32] This aptamer has very good selectivity for theophylline over caffeine, a molecule that only differs from theophylline by one methyl group. The K_d for theophylline is 10,000 times lower than for caffeine (Figure 1.3).

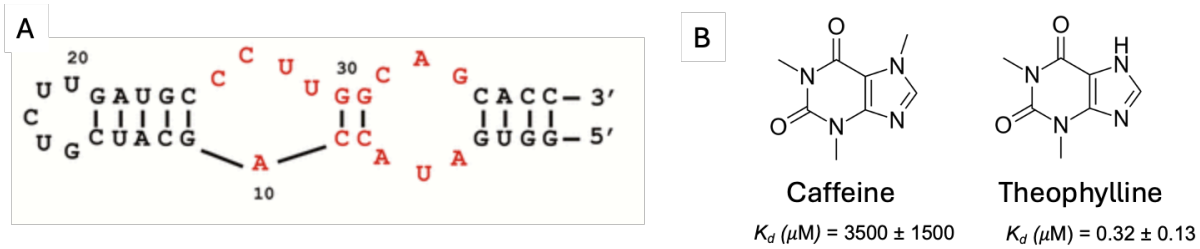


Figure 1.3 (A) Predicted secondary structure of the theophylline aptamer TCT8-4. Adapted with permission from Ref [32] Copyright 2020 American Chemical Society (B) K_d values of the TCT8-4 aptamer with theophylline and caffeine measured using a competitive equilibrium filtration binding assay. K_d values from Ref [53].

1.2.6 Aptamers for Antibiotics

Antibiotics are a subset of these small molecules and are therapeutical drugs used in both humans and veterinary medicine as well as agriculture. More and more recently antibiotics are being overused and is leading to many problems such as antibiotic resistance[33], pollution and toxicity from animal by-products[34]. Aptamers present a novel, cost effective, and easy to use method of monitoring and sensing these molecules compared to the traditional methods mentioned above. Many aptamers have previously been selected for different classes of antibiotics (Figure 1.4) such as tetracyclines[35–37], aminoglycosides[38–41], beta-lactams[42–44], chloramphenicol[45,46], and more and has shown much promise as the future of antibiotic sensing.

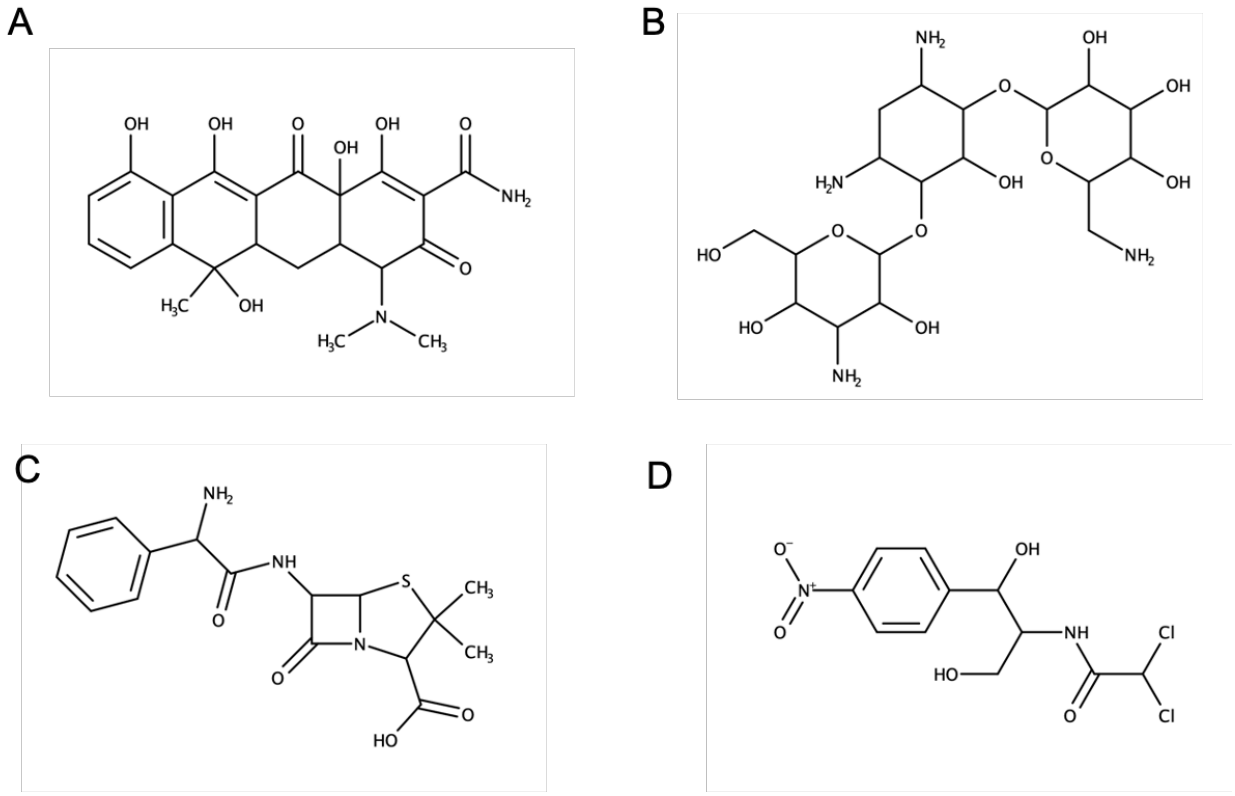


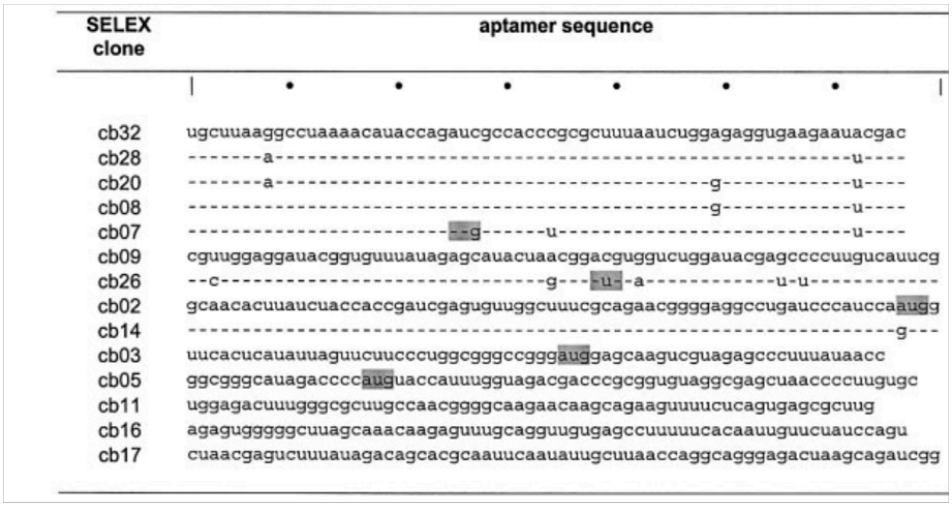
Figure 1.4. The chemical structures of common antibiotics. (A) Tetracycline (B) Kanamycin (C) Ampicillin (D) Chloramphenicol.

1.2.7 Previously reported aptamers for antibiotics

Selecting aptamers for antibiotics has been reported in the past. The tetracyclines have had multiple RNA and DNA aptamers selected for them. An early RNA aptamer was selected by Berens *et. al* in 2001.[47] This aptamer called cb28 (Figure 1.5B) was isolated by immobilizing tetracycline on to epoxy-activated Sepharose beads. The K_d of cb28 was determined to be 1 μM tetracycline by probing the Pb^{2+} dependent cleavage of the RNA backbone. This is generally a good method to probe RNA structure and conformational changes[48] upon ligand binding since base paired regions are not cleaved whereas unstructured flexible regions are cleaved.[49] Upon the

addition of tetracycline (TC), regions of the cb28 that were cleaved before became protected and unable to be cleaved, showing a conformation change which meant ligand binding interactions (Figure 1.6A). This binding also proved to be magnesium dependent as lead was able to cleave cb28 in those areas without the addition of magnesium (Figure 1.6A, lanes 4 and 5). Another RNA aptamer from the same selection (cb32) was also later characterized to have binding to tetracycline (K_d = 0.77 nM), oxytetracycline (OTC) (K_d = 1.18 nM) and doxycycline (DOX) (K_d = 118 nM) characterized by fluorescence titration spectroscopy (Figure 1.6 B).[50,51] These aptamers are quite long and limited work was done using them as biosensors.

A



B

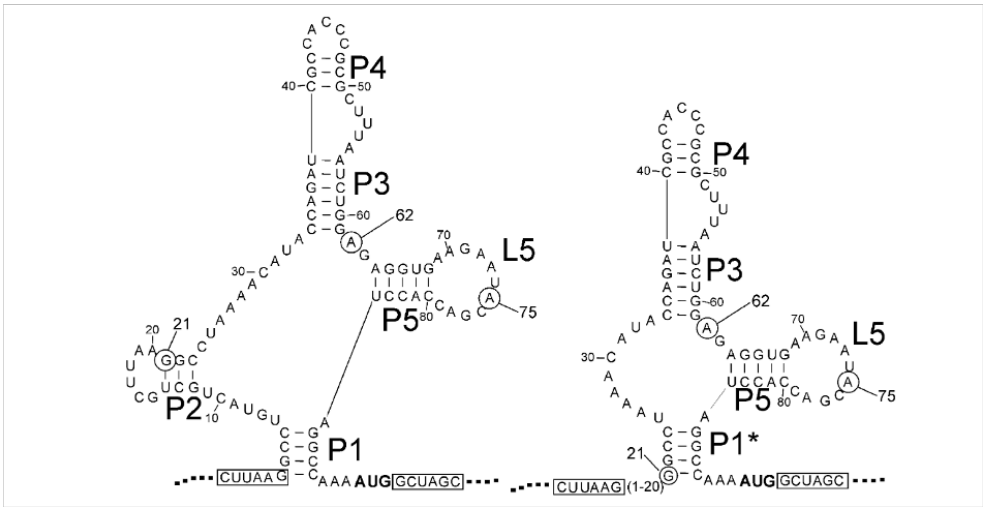


Figure 1.5 (A) Sequence alignment of the selection done by Berens et al. (B) Secondary structures of cb28 (left) and cb32 (right). Figures adapted from ref [50] by permission of Oxford University Press.

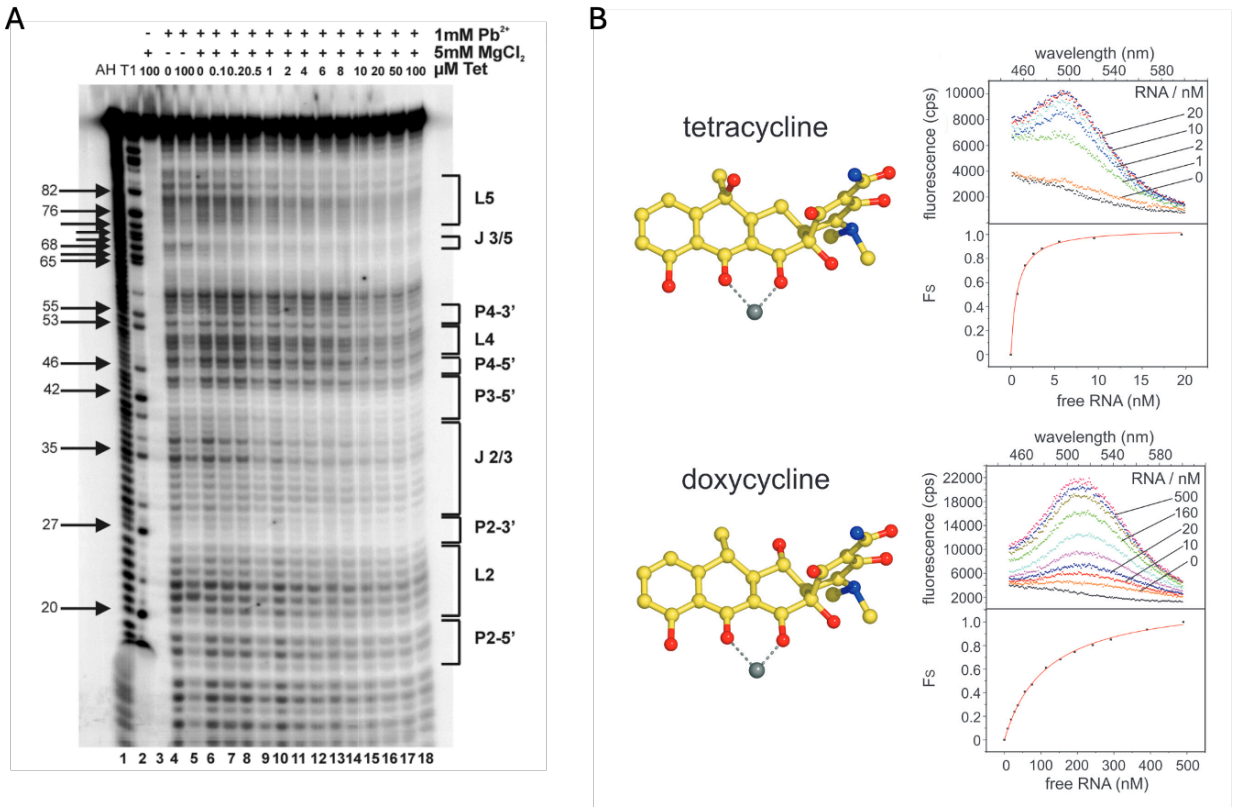


Figure 1.6. (A) Gel electrophoresis showing the lead induced cleavage of the cb28 aptamer. Adapted from Ref [47], Copyright (2001) with permission from Elsevier. (B) Fluorescence titrations of the cb32 aptamer to determine K_d of TC and DOX adapted from Ref [51] by permission of Oxford University Press.

Tickner et al. then selected an aptamer specific to doxycycline by using libraries that were selectively randomized versions of the previously mentioned cb32 aptamer and different DNA polymerases. After four rounds of selection using a DOX, two consensus sequences P2MC and P1MC were tested using surface plasmon resonance and both had a K_d of around 7 nM (Figure

1.7A and B).[52] P2MC was able to distinguish between DOX and TC using fluorescence titration (Figure 1.7C and D).

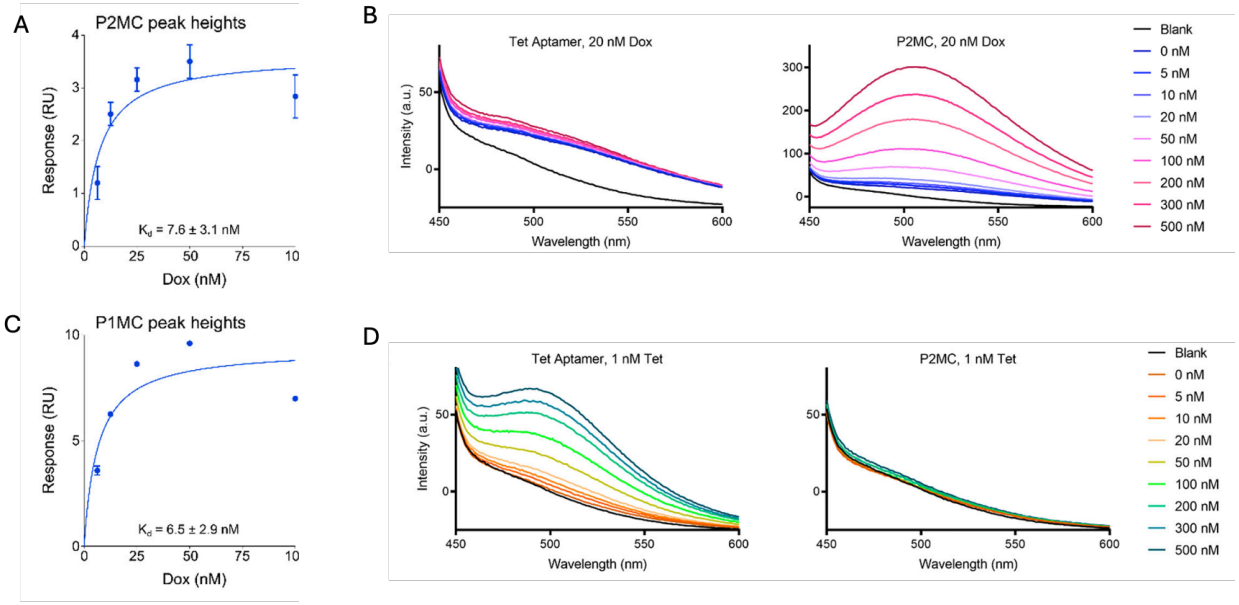


Figure 1.7. (A) SPR peaks of P2MC aptamer for K_d determination.(B) Fluorescence titration showing specificity of P2MC for DOX compared to the previously selected Tet aptamer from Berens *et al*. (C) SPR peaks of the P1MC aptamer (D) Fluorescence titration of showing no reactivity with TC from the P1MC aptamer. Adapted with permission from Ref [52] Copyright 2020 American Chemical Society.

In addition to RNA aptamers for the tetracyclines, there have also been previously selected DNA aptamers. Niazi *et al*. selected DNA aptamers for OTC. By immobilizing OTC onto tosylated magnetic beads, they selected an aptamer that they named No.4 with a K_d of around 10 nM (Figure 1.8).[35] Later, they would also select aptamers that could bind TC, DOX and OTC by being specific for the tetracycline back bone with K_d ranging from 63-483 nM (Figure 1.9B).[53] These K_d were determined using equilibrium filtration[54] in which the target and aptamer were allowed to bind in solution before passing through a dialysis membrane. The solution that remained above the cut-

off molecular weight contained free target, free aptamer, and bound complexes, and the filtrate contained only free target equivalent to the initial concentration of target. This amount of free target in the filtrate and the retentate would then be compared to the initial concentration of the target to determine the fraction bound. However, Niazi et al. only mentioned that the filtrate was measured and not the retentate which assumes that all of the free target passed through the membrane and could possibly misrepresent the measured K_d. In addition, the aptamers reported by Niazi *et al* were also very long, typically longer than 76 nucleotides and they do not have a well-defined secondary structure making truncation difficult.

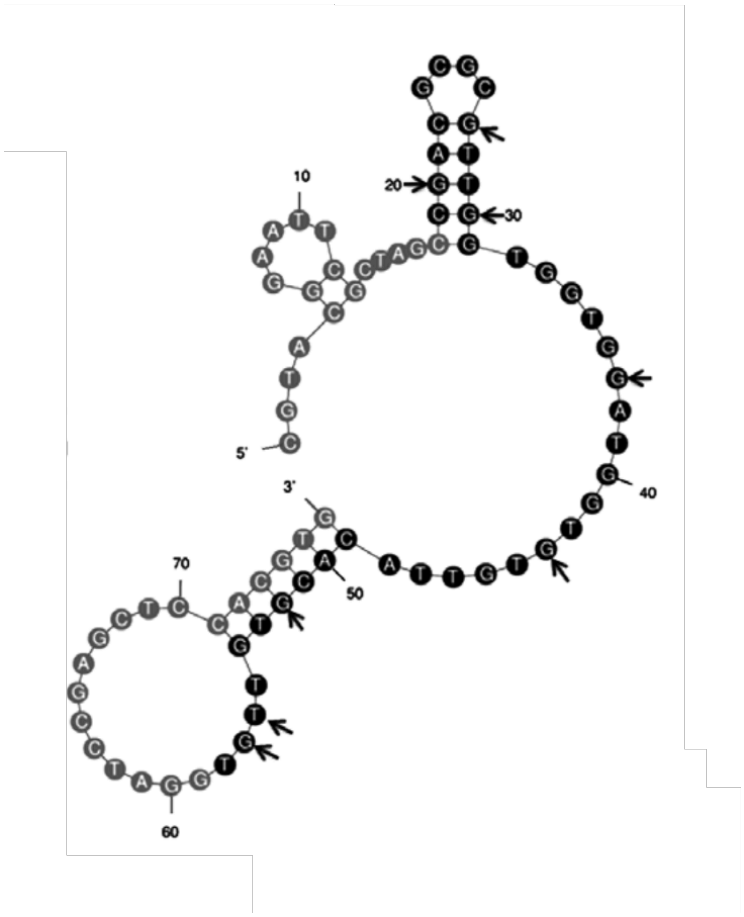
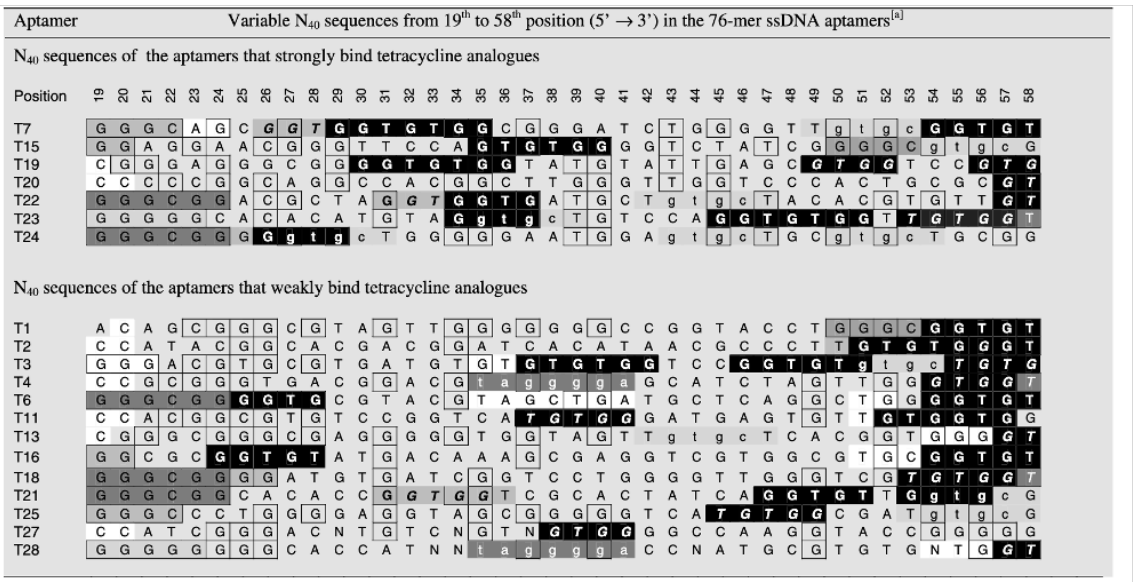


Figure 1.8. The secondary structure of the No.4 aptamer selected by Niazi *et al*. for oxytetracycline. Reprinted from Ref [35] Copyright (2008), with permission from Elsevier

A



B

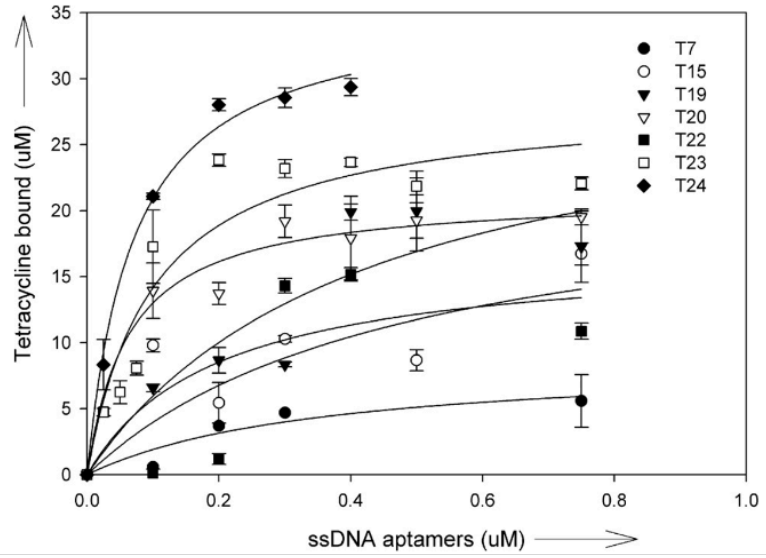


Figure 1.9. (A) Sequence alignment from the selection by Niazi *et al*. (B) Equilibrium filtration binding assays to determine K_d. Reprinted from Ref [53] Copyright (2008), with permission from Elsevier

Chloramphenicol (CAP) acts by inhibiting peptidyl transferase, preventing peptide bond formation and has had some aptamers selected for it. Early RNA aptamers for CAP were selected in 1997 by Burke *et. al* by target immobilization.[55] The authors obtained a series of sequences after

12 rounds of selection that could bind CAP with K_d ranging from 2 μM to 275 μM, based on a microconcentrator spin assay (Figure 1.10A). This is a size exclusion assay which partitions the RNA based on the folded bound structure of the RNA-CAP complex. This work was mainly about probing the interactions between RNA and CAP and not used for sensing.

A

Cm-binding behavior of 40 RNAs.

	Retained*	% Eluted	K_d (μM)
Active isolates			
70Cm3 (2)	1.0	7.1	
70Cm4†	18.3	6.2	
70Cm4‡	0.2‡	20.1‡	
70Cm6 (4)	9.8	18.9	2.1 ± 0.3
70Cm9 (3)†	12.0	25.4	8 ± 4
70Cm12 (3)	0.9	23.4	50 ± 10
70Cm12§	5.2§	75.5§	
70Cm14	0.8	5.8	
70Cm15 (2)	2.7	20.3	140 ± 50
70Cm19 (4)‡	5.2	4.1	66 ± 10
70Cm19§	13.7§	20.1§	
70Cm24	1.9	8.1	
70Cm29 (2)	2.3	34.0	130 ± 30
70Cm42	1.8	17.4	275 ± 150
70Cm45 (2)	1.2	21.6	17 ± 10
70Cm53 (2)	1.0	20.2	7 ± 2
70Cm55†	12.1	18.8	
80Cm1 (2)	1.8	20.3	110 ± 60
80Cm7	4.3	12.5	
80Cm10	0.9	17.2	
80Cm15	0.9	9.8	
80Cm19	1.7	28.2	110 ± 60
80Cm30	2.0	20.2	30 ± 5
80Cm31 (2)†	10.9	7.2	
80Cm33	0.7	19.0	165 ± 50
80Cm45	1.8	10.6	
80Cm46	4.0	16.7	216 ± 75
80Cm47†	6.7	2.5	
80Cm50†	22.4	10.0	
80Cm50‡	1.3‡	29.1‡	25 ± 3
80Cm55	1.1	21.0	195 ± 75
80Cm59	3.6	20.9	96 ± 20

B

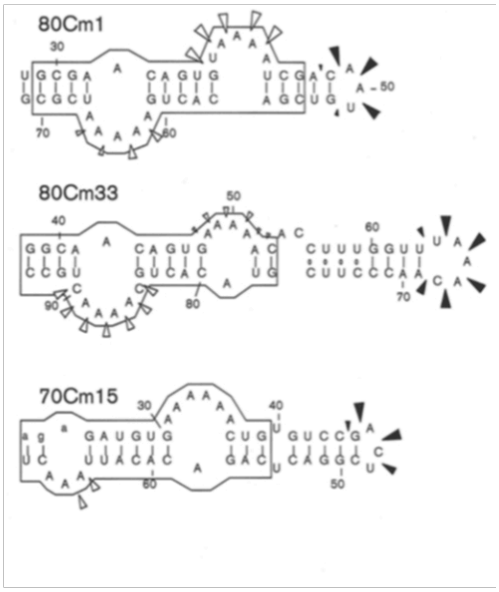


Figure 1.10 (A). Active sequences and their measured K_d from the selection of Burke *et al*. (B) Inferred secondary structures of 3 isolates. Reprinted from Ref [55] Copyright (1997), with permission from Elsevier.

Later, Mehta *et al*. selected DNA aptamers using target-immobilized magnetic bead SELEX. They did 7 rounds of selection and 1 round of counter selection with uncoated beads for a total of 8

rounds. The resulting aptamers were 80 nucleotides long and had a various K_d's with the best one being 0.77 µM (called sequence number 7).[46] This was determined using fluorescence binding assay (Figure 1.11A). Fluorescein labelled aptamer was incubated with a CAP coated bead column and then eluted. The eluted aptamer concentration was then compared to the initial concentration of aptamer to obtain a K_d. Sequence number 7 also showed to be specific to CAP in a competitive assay against other similarly structured molecules (Figure 1.11D) A truncated 40 nucleotide version of this aptamer was used for biosensor design (Figure 1.11B).[45,56]

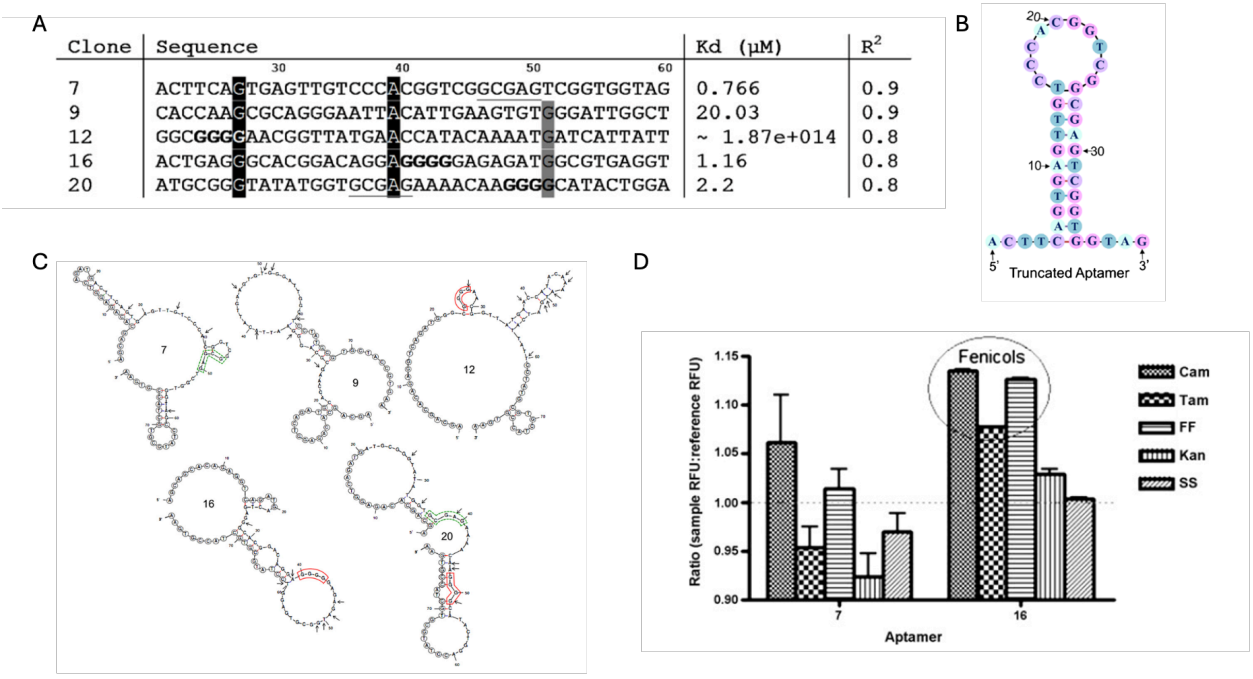


Figure 1.11 (A) Sequence alignment of the random regions from the selection done by Mehta *et al*. (B) Secondary structure of the truncated CAP aptamer.(C) Secondary structures of full length aptamers from A.(D) Specificity of aptamers 7 and 16. (A), (C), and (D) Reprinted from Ref [46] Copyright (2011), with permission from Elsevier. (B) adapted from Ref [69], 2020, Springer Nature.

Duan et al. also used target immobilization to select DNA aptamers for CAP (Figure 1.12B).[57] After 10 rounds of selection they obtained aptamers with K_d in the range of 0.03 μM to 0.32 μM using a fluorescein assay similar to the one used by Mehta *et al*. and also showed good specificity for CAP by equilibrium filtration (Figure 1.12D).

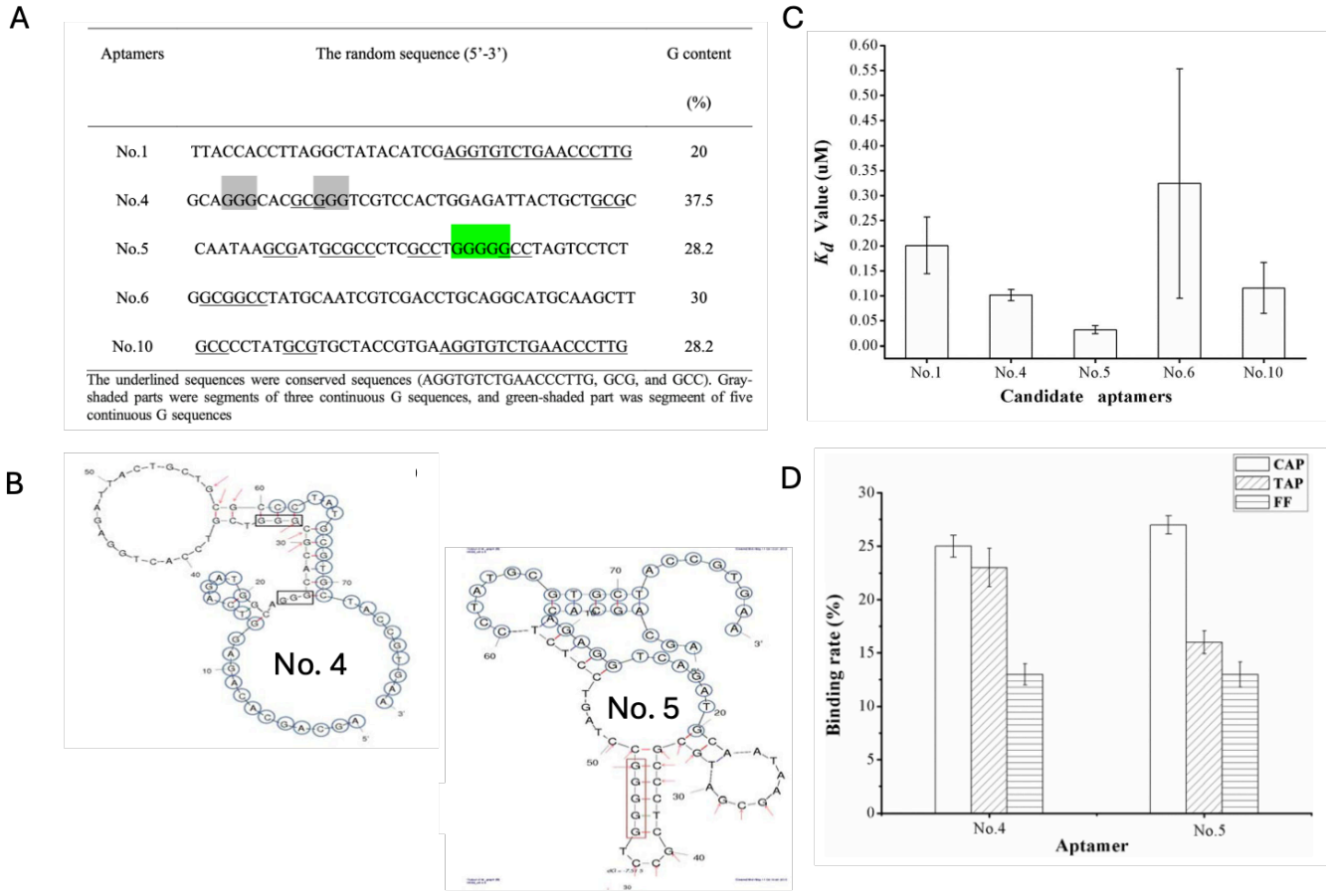


Figure 1.12. (A) Sequence alignment of the random region from the selection by Duan et al. (B) Predicted secondary structure of No.4 and No.5 from (A) for chloramphenicol. (C) Measured K_d of aptamer candidates. (D) Specificity of No.4 and No.5 by equilibrium filtration. Figures adapted from Ref [57] reproduced with permission from SNCSC.

The previous selections for the CAP molecule have all used the target immobilization method. However, in order to immobilize CAP onto the beads, an important portion of the molecule

containing the chlorine atoms is omitted due to the coupling reaction that occurs (Figure 1.13). Many of the aptamers selected this way may not bind to the free molecule in solution.

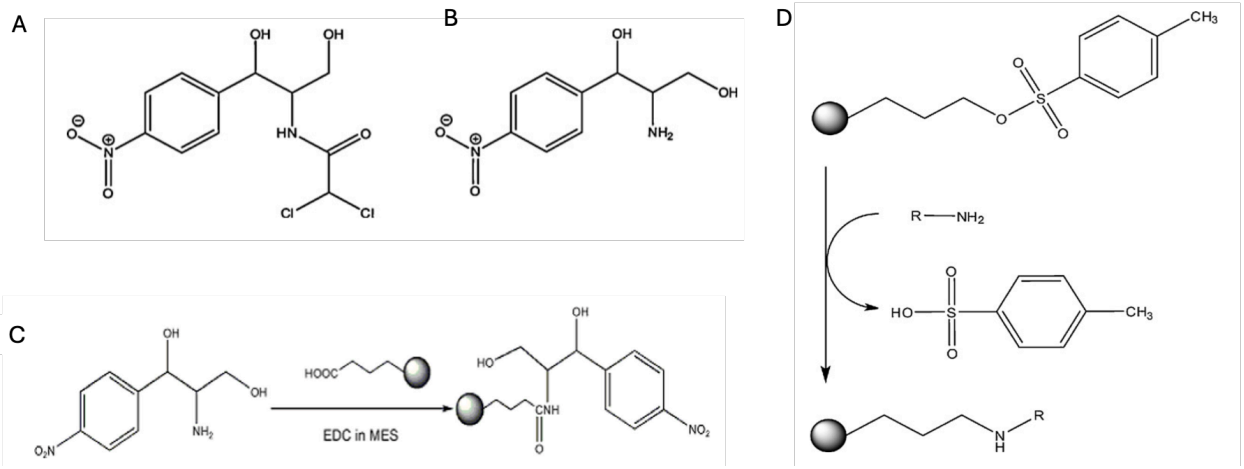


Figure 1.13. (A) The chemical structure of free CAP (B) CAP base, the form available after conjugation to beads. (C) Immobilization of CAP base using a carboxylic acid as done by Duan *et al.* Figures adapted from Ref [57] reproduced with permission from SNCSC. (D) Immobilization of CAP base using p-toluenesulfonyl (tosyl) groups done by Mehta *et al*. Reprinted from Ref [46] Copyright (2011), with permission from Elsevier.

Kanamycin is an antibiotic that is part of the aminoglycoside family along and commonly exists as a mixture of Kanamycin A, B, and C. Kanamycin A and C are isomers whereas Kanamycin B has different functional groups and is a byproduct from biosynthesis. The majority of the mixture is kanamycin A with B and C in trace amounts. An RNA aptamer targeting kanamycin B was selected in 2001 by Kwon et al. using target immobilization.[58] This aptamer called K8 showed a K_d of 181 nM for kanamycin B and 4400 nM for kanamycin A determined using fluorescence anisotropy. However, this aptamer showed an even higher affinity for tobramycin with a K_d of 11.6 nM. DNA aptamers have been isolated for kanamycin A by Song *et. al*.[59] The Ky2 aptamer was selected with target immobilization on Sepharose beads and showed a K_d of 78.8 nM for a

kanamycin A 83.5 nM for kanamycin B and 103 nM for tobramycin. This was measured by elution and quantification of fluorescein labelled aptamer with each target. This aptamer was a minimized version of the Kana2 sequence from the selection results. Stoltenburg *et al*. used library immobilized capture-SELEX to isolate a kanamycin A binding aptamer using a target solution that was a mixture of 4 pharmaceutical compounds (kanamycin A, sulfocarbamide, sulfomethoxazole, and sotalol hydrochloride)[60]. After sequencing, 10 representatives from the resulting aptamer families were tested against each of the four compounds and 3_19 was found to have the best affinity for kanamycin A at a K_d of 3.9 μM (Figure 1.14A, Figure 1.15A and B), measured using the fluorescence method similar to Song et al.

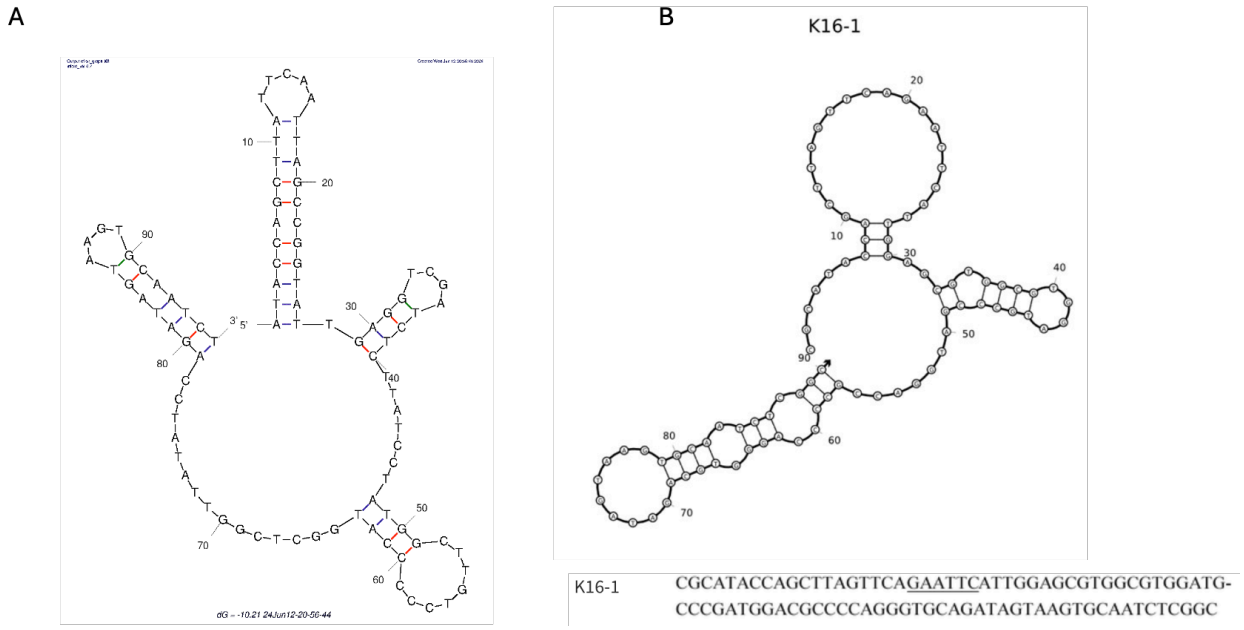


Figure 1.14 (A) Predicted structure of the 3_19 aptamer. Figure adapted from Ref [60] (B) Sequence and predicted structure of the K16-1 aptamer. Figure adapted from Ref [61].

However, the Heemstra group tested the 3_19 sequence using microscale thermophoresis and found the K_d to be almost 100-fold higher than reported. They then did their own selection for

kanamycin A.[61] Their selection protocol used library immobilized capture-SELEX and the restriction enzyme EcoRI-HF (Figure 1.15C) to cleave portions of the library that did not bind to the target. An initial step where the library was incubated with EcoRI-HF and the cleaved fragments were ligated back together to ensure that the resistance to cleavage was target dependent. After 11 rounds of selection and sequencing they obtained an aptamer called K16-1(Figure 1.14B) which had a K_d of 340 μM measured using microscale thermophoresis. They also truncated this aptamer (K16-1c) and it retained its binding with a K_d of 400 μM of kanamycin A (Figure 1.15D).

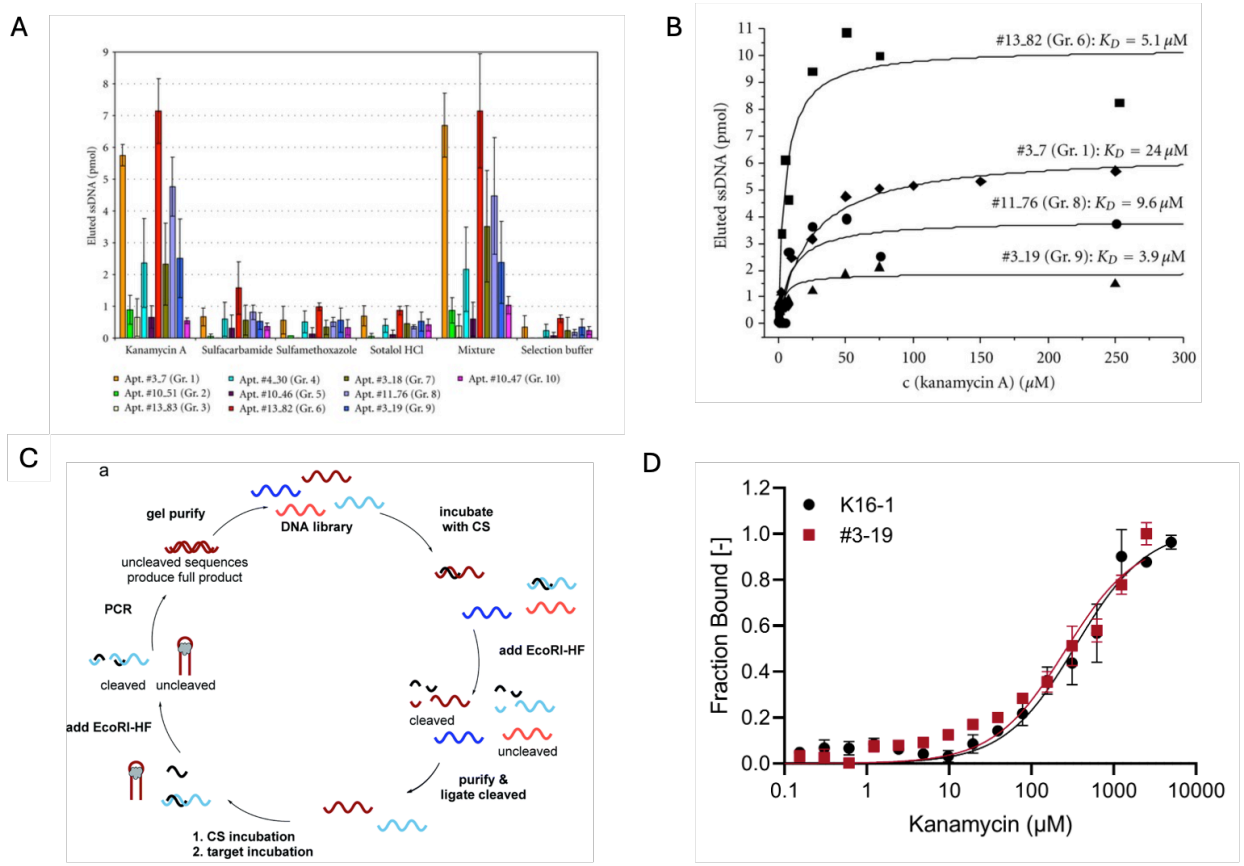


Figure 1.15 (A) Selectivity of the 3-19 aptamer compared to the other compounds used in its selection target solution. (B) Elution assay for to determine K_d for different aptamer candidates from the selection by Mehta et. al. (C) Restriction enzyme SELEX protocol from the Heemstra

group. (D) Comparison of microscale thermophoresis studies between the 3-19 and K16-1 kanamycin aptamers. (A) and (B) adapted from ref [60]. (C) and (D) adapted from Ref [61].

1.3 Aptamers That Cannot Bind Their Targets

Characterization of aptamer binding is a crucial step to ensure the discovery of true aptamers that bind to their target. However, the steps required to ensure accurate characterization are not always consistent amongst all selected aptamers and skipping these steps can result in reporting non-aptamer sequences as aptamers. Some examples are given below.

Arsenic is an environmental toxin that appears most commonly in the +3 (As(III)) and +5 (As(V)) oxidation states.[62] The Ars-3 aptamer was selected in 2009 for the removal of arsenic from groundwater.[63] 10 rounds of selection were done by using immobilized As(II) (as 4-aminophenylarsine oxide) on an Affinity gel 10 resin and Ars-3 was the most abundant sequence. Next, binding was characterized using surface plasmon resonance (SPR) by covalently linking As(III) and As(V) onto a gold surface.[63] Using this method a K_d of 5 nM for As(III) and 7 nM for As(V) was measured. However, DNA itself has been known to have an affinity for gold surfaces and could also explain the shift in SPR signal. Follow-up studies have used this aptamer for biosensor design, mostly for As(III).[64,65]

These sensors have been designed using gold nanoparticles (Au-NPs) and inducing a color change. The general idea behind these assays is that when the target is added to the aptamer, it would cause the aptamer to fold into a compact structure and unable to absorb on to the surface of the AuNPs. The addition of salt would then cause the unprotected AuNPs to aggregate causing a

red-blue color shift (Figure 1.16)[66]. However, many of these studies neglect to account for the interaction between the target and AuNPs themselves.

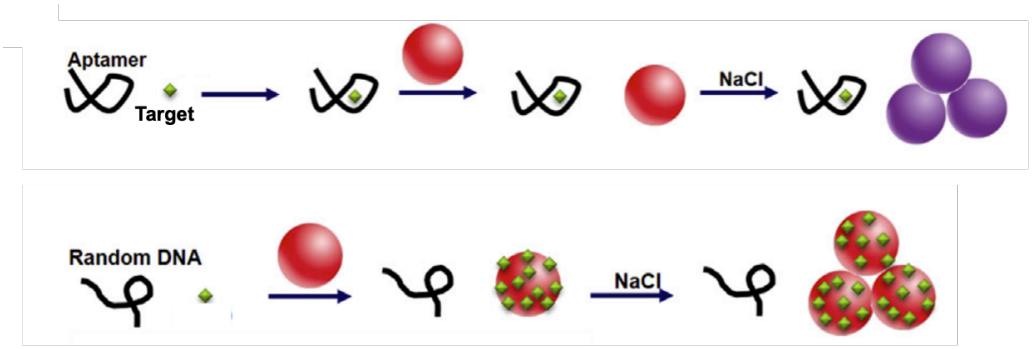


Figure 1.16. The principle of a colorimetric gold nanoparticle assay. Figure adapted from Ref [66].

This was what likely occurred in the case of the Ars-3 aptamer. A study was done to analyze the interactions of arsenic and AuNPs and showed that the color change was most likely due to the adsorption of As(III) onto the surface of AuNPs as opposed to the binding of As-3 confirmed by using a non-binding control sequence (Figure 1.17A). ITC studies further confirmed that there was no interaction between As(III) and As(V) with Ars-3 (Figure 1.17B) since the traces line up closely with the buffer control.[67]

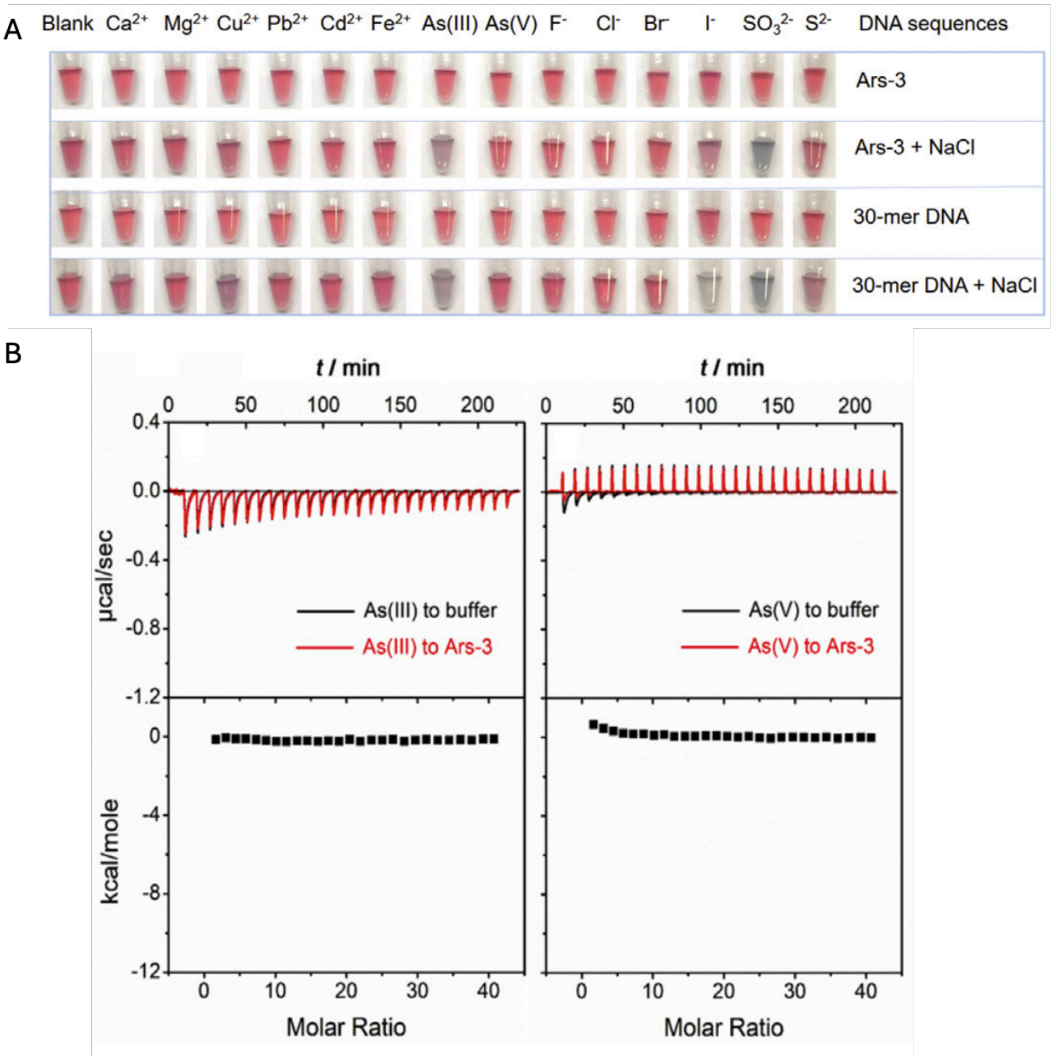


Figure 1.17. (A) Colorimetric nanoparticle assay comparing Ars-3 and a random 30-mer DNA. (B) ITC traces comparing As (III) into a buffer control and Ars-3 (left) and As(V) into Ars-3 and a buffer control(right). Adapted with permission from Ref [67] Copyright (2019) American Chemical Society.

Some of the previously mention aptamers for antibiotics also appear to not their respective targets. The ampicillin aptamers (AMP4, AMP17, and AMP18) showed no signs of binding when subjected to ITC (Figure 1.18). [68]

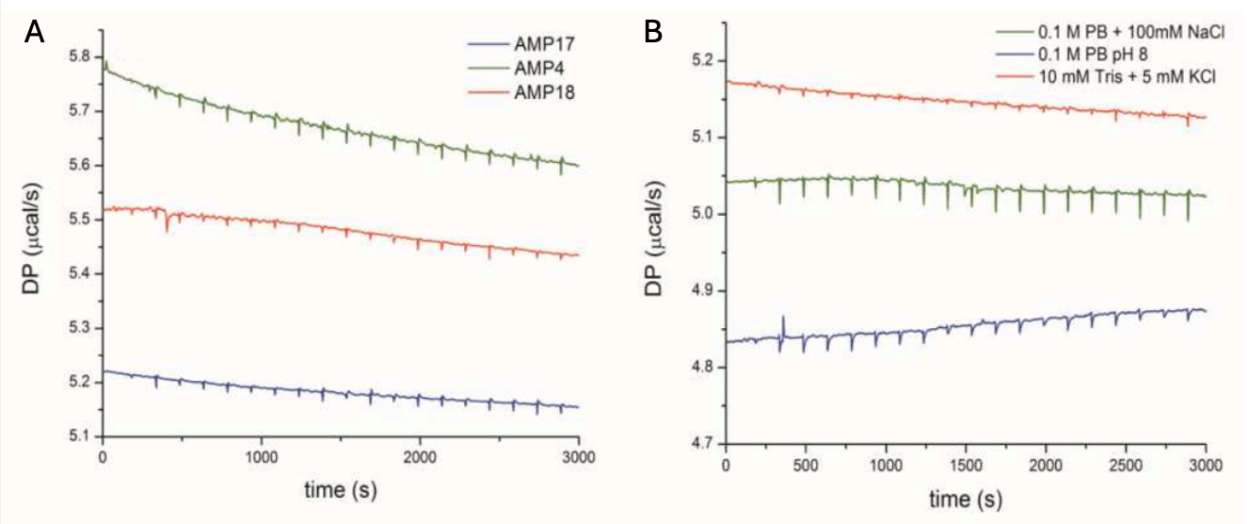


Figure 1.18 (A) Thermograms of ampicillin in the AMP17, AMP4, and AMP18 aptamers. (B) Thermograms of AMP18 in different buffers. Adapted with permission from Ref [68] Copyright (2020) American Chemical Society.

Also, both the chloramphenicol aptamer (7 from section 1.2.7) and the kanamycin aptamer (Ky2) do not show signs of binding to their respective targets when subjected to ITC (Figure 1.19A and B)[69] or due to target-gold interactions (Figure 1.19C and D).[70]

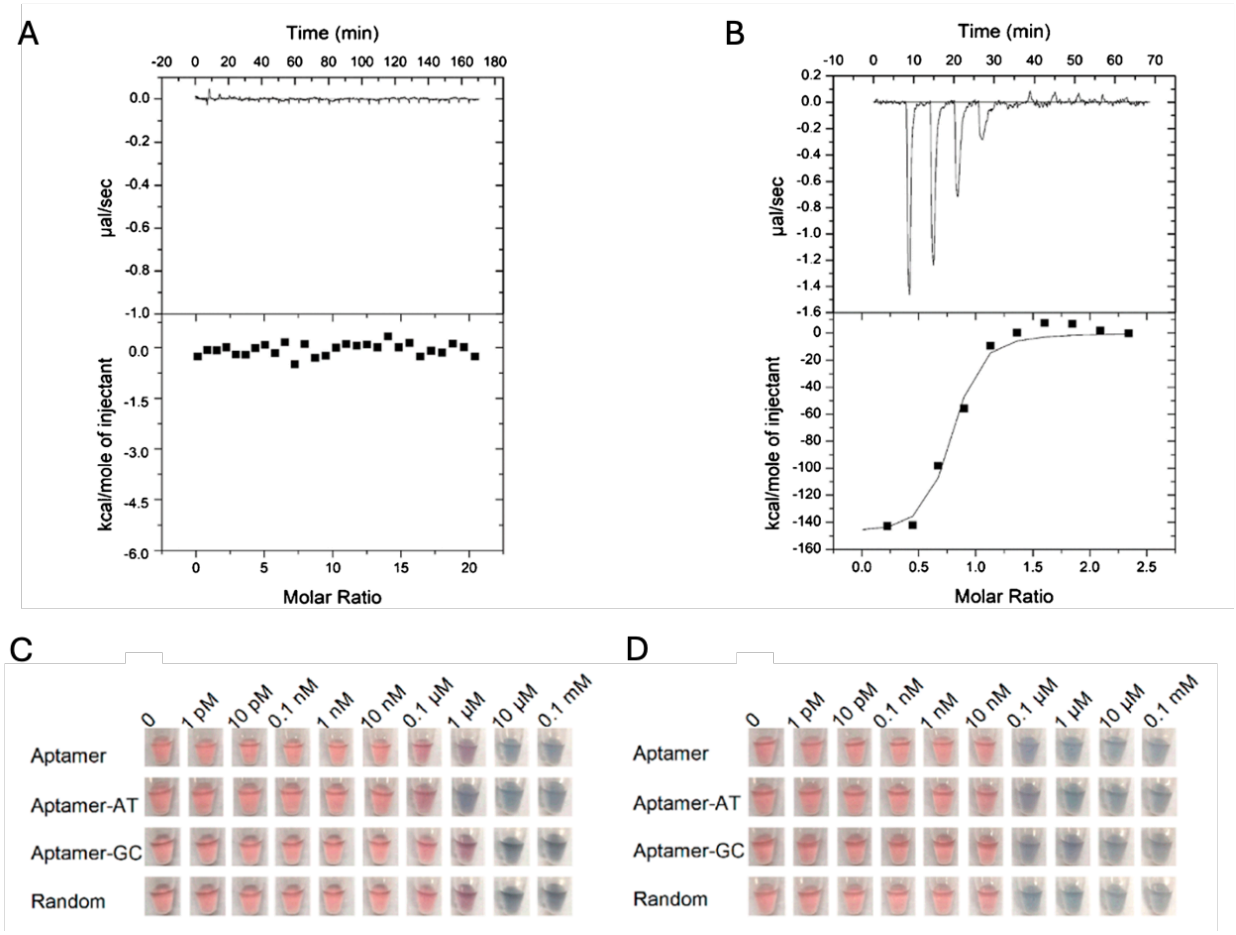


Figure 1.19. (A) ITC trace of chloramphenicol into the truncated 7 aptamer. (B) ITC trace of the 7 aptamer into its complementary strand. Gold nanoparticle assay of kanamycin into the ky2 aptamer, 2 mutants and a random sequence (C) without and (D) with NaCl. (A) and (B) adapted from Ref [69], 2020, Springer Nature. (C) and (D) dapted with permission from Ref [70] Copyright (2020) American Chemical Society.

1.4 The SELEX Process

The process of selecting new nucleic acid aptamers for a specific target is generally done through an *in vitro* screening process called the **S**ystematic **E**volution of **L**igands by **EX**ponential Enrichment (**SELEX**) and was coined by Tuerk and Gold in 1990[6]. Depending on the type of

nucleic acid being used (RNA or single-stranded DNA), the steps in the selection process may vary slightly.

1.4.1 General Overview and Types of SELEX

In general, SELEX is a process that screens a vast initial library of oligonucleotides down to only the sequences that bind the desired target. The discussion in this thesis is focused on SELEX for small molecule targets, especially antibiotics. The process starts with an initial oligonucleotide library that is incubated with the target molecule to allow binding to occur. Next, the bound and unbound sequences are separated, and the bound sequences eluted. The number of bound sequences is then monitored for progress. The target is then removed from the sequences and the sequences are amplified through polymerase chain reaction (PCR). The remaining pool of sequences is then separated into single strands and acts as the next library in the next round of SELEX and this repeats over and over until sufficient affinity is achieved through monitoring. The SELEX process generally takes around 15-20 rounds[71]. If RNA is used as the ligand, the PCR products would need to undergo reverse transcription to retrieve the RNA sequence.

There are different types of SELEX protocols. Traditional SELEX (or target immobilized SELEX) is when the target is chemically modified to bind with a solid substrate (i.e magnetic beads[57,72]) and the library is flowed through to allow binding. Some drawbacks to this method include the need to chemically modify the target thus not allowing access to the entire target molecule or omitting possible binding sites on the targets due to the modification.

However, one type of SELEX called capture-SELEX[73] is as easily implemented as traditional SELEX and can have many possible targets. As opposed to traditional SELEX, capture-SELEX immobilizes the nucleic acid library instead of the target molecule (Figure 1.20). This is usually done by adding a biotin tag at the end of the library sequences and binding to streptavidin

coated beads due to the biotin-streptavidin affinity[73,74]. The target is then flowed through and the sequences that bind will elute off the beads and can be collected for amplification. The advantages of this method are that the entire target molecule can be accessed for binding and the partitioning of bound and unbound sequences is easily done. The following discussion will all be based on capture-SELEX using single-stranded DNA (ssDNA) libraries.

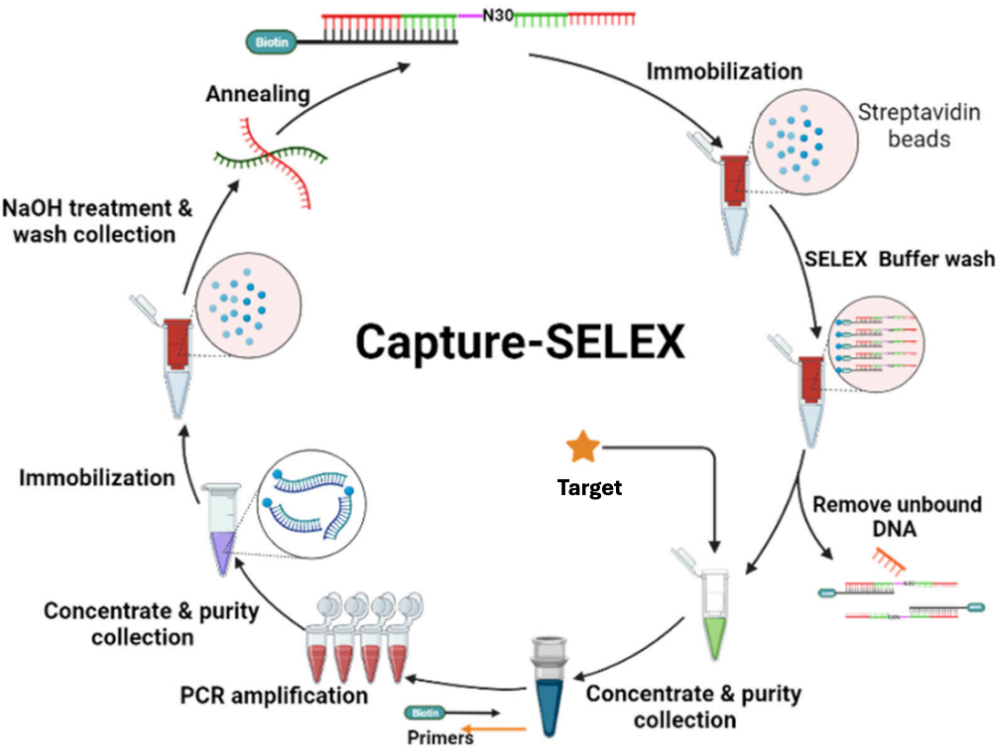


Figure 1.20. The general overview of the capture-SELEX process using ssDNA. Figure adapted from Ref [73].

1.4.2 Library Design

Designing the initial library is the first step in capture-SELEX. The sequences in the initial library generally require to be designed having three main components. A docking sequence, which hybridizes with a shorter strand of complementary DNA which typically has a biotin tag to

anchor it streptavidin beads (the solid substrate used in most capture-SELEX processes). Two primer binding regions for PCR amplification are also required so that eluted sequenced can be replicated. Finally, there needs to be a region of random bases which can vary in length. This random region is where the target will bind to during the SELEX process.

The docking sequence can be designed in different ways (Figure 1.21)[75] and can either use one of the primer binding regions or a separate docking sequence elsewhere on the strand[76]. The primer binding regions are required for PCR. These regions flank the two ends of the strand. In order to have high PCR efficiency, these regions must be designed so that they don't self-dimerize or hetero-dimerize and have a similar melting temperature (T_m)[77]. The melting temperature is when half of the duplex DNA are single stranded and can be used as a measure of duplex stability. The random region of the library sequences is where the target is meant to bind and is generally in the length of N_8 – N_{60} where N is the number of randomly generated A, C, T, and G bases. While larger N includes all the subsets of the smaller N, it may be advantageous to use smaller libraries to scan the entire receptor space the sequences encompass[78]. Generally, random regions of N_{30} – N_{40} seem to yield good results for most selections[77,79].

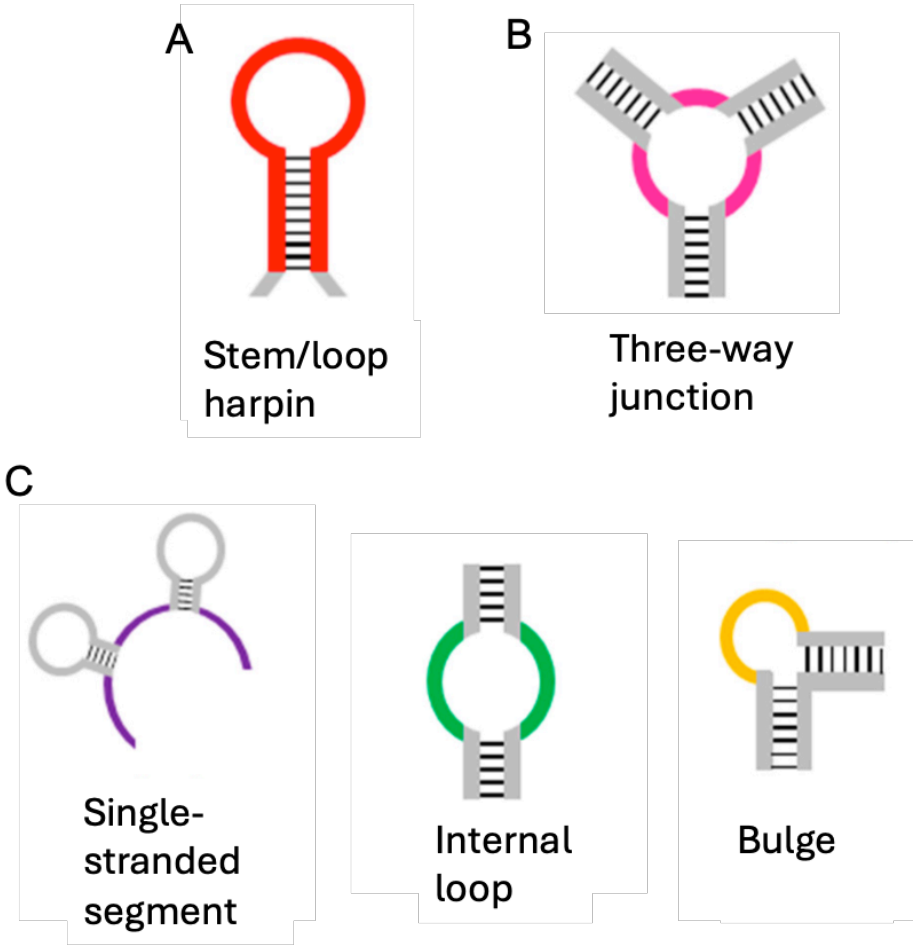


Figure 1.21. Different possible library designs. (A) Stem-loop (B) Three-way junctions (C) Other structures. Figure adapted from Ref [75] under an Open Access License.

1.4.3 Methods to Monitor Enrichment

There are different methods to monitor the progress of selection. This is necessary to ensure that the selection is advancing and can indicate an ending point. Some widely used methods include labelling the library using fluorescent dyes[80] or non-labelled methods such as real-time PCR[81] (or qPCR).

1.4.4 Sequencing Analysis and Binding Assays

After a stopping point has been declared, the resulting library will be sequenced and analyzed for the best aptamer candidates. Traditionally, Sanger sequencing was done but this method is slower and cannot handle very big libraries. Newer technologies such as high-throughput sequencing (HTS)[82] and other next-generation sequencing (NGS) methods[83] have now replaced the Sanger sequencing and can handle large libraries with fast turnaround times. Post sequencing analysis includes the identification of aptamer candidates by searching for conserved base sequences or secondary structures in resulting library. After these have been identified, binding assays can be done to confirm that the candidates are true aptamers.

Many different binding assays can be done to determine parameters such as the dissociation constant (K_d). The K_d is an equilibrium constant that describes the concentration of free target at which half of the target is bound to the aptamer (Figure 1.22) and can be used as a gauge of how well the aptamer binds its target with lower K_d indicating stronger binding.

$$A + T \underset{k_{off}}{\overset{k_{on}}{\rightleftharpoons}} AT$$

$$K_d = \frac{[A][T]}{[AT]} = \frac{k_{off}}{k_{on}} = \frac{1}{K_a}$$

[A] - Concentration of Aptamer
[T] - Concentration of Target
k_{on} - rate constant of association
k_{off} - rate constant of dissociation
K_a - Association Constant
K_d - Dissociation Constant

Figure 1.22. The dissociation constant.

Isothermal titration calorimetry (ITC) can be considered the "gold standard" when it comes to evaluating aptamer binding. ITC is a method that uses instrumentation to measure the amount of power (in μcal/sec) needed to maintain a constant temperature between a sample cell and a reference cell[84] (Figure 1.23). When an aptamer binds to its target, the formation of the bound complex is often accompanied by a small change in temperature that is either exothermic or endothermic in nature and changes the temperature in the sample cell. One ITC experiment can give the K_d, as well as other thermodynamic constants such as enthalpy and entropy and the binding stoichiometry.

Another type of binding assay is fluorescence-based assays. Fluorescence based assays make the use of a fluorophore containing compound that will emit light at a specific emission wavelength under excitation. This change in the fluorescence can be measured using a fluorimeter or spectrophotometer and be used to characterize binding interactions. These can either be attached to the aptamer (labelled) or free floating in solution (label-free). In some cases, the fluorescent compound could be the target itself. Other methods to measure aptamer binding include colorimetric gold nanoparticle (AuNP) assays and enzyme digestion. However, some of these methods are not as reliable due to factors such as target nanoparticle interactions when using AuNP assays leading to some false aptamers as described in section 1.3. Multiple binding assays are also recommended as different assays have shown to give vastly different K_d values for the same aptamer.[85]

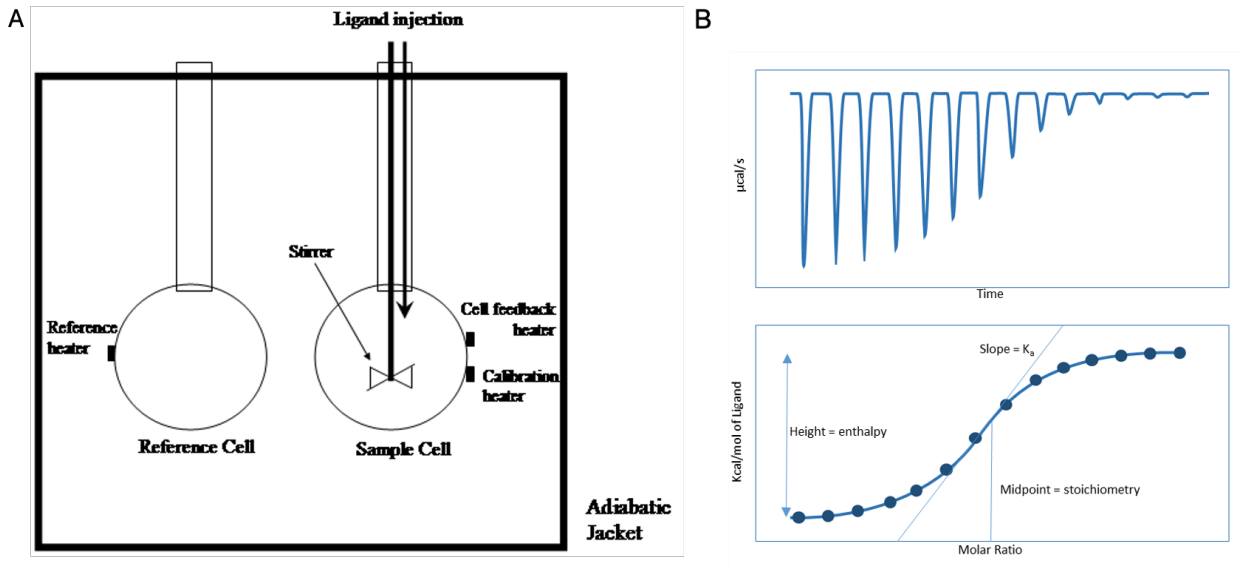


Figure 1.23. (A) Schematic of an Isothermal Titration Calorimeter . (B) Thermogram generated by ITC.

1.4.5 Post-SELEX Modifications

After confirmation of the aptamer binding the target, modifications can be made to the aptamer. These modifications can be used to probe more binding characteristics. Mutations of certain nucleobases within the aptamer sequence can help probe which sections of the aptamer are involved in the binding.[86] An aptamer for caffeine (Caff203) was isolated using capture-SELEX with a K_d of 2.2 µM, measured by ITC. A mutation study was done on this aptamer by shuffling around bases on its two loops (Figure 1.24A) resulting in two mutants (Mutant-1 and Mutant-2).[87] These mutations resulted in a loss of binding and showing that the binding observed was specific for caffeine (Figure 1.24B). Another aptamer selected for cortisol (CSS1)[82] had two base mutations on its main loop which also resulted in a loss of binding to its target[88] (Figure 1.24C and D).

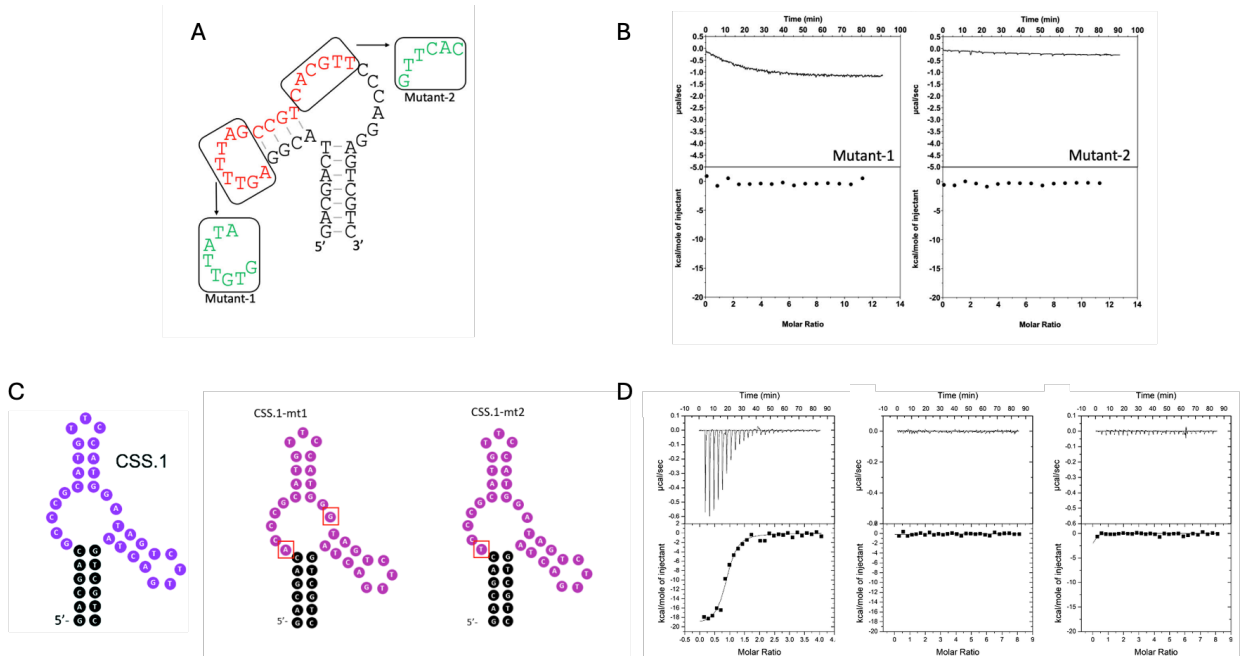


Figure 1.24. (A) Structure and mutants of the Caff203 aptamer. (B) ITC traces of caffeine into Mutant-1 and Mutant-2. (C) Structure and mutants of the CSS.1 aptamer. (D)ITC traces of cortisol into CSS.1 (left), CSS.1-mt1(middle), CSS.1-mt2 (right). (A) and (B) adapted with permission from Ref [87] Copyright (2022) American Chemical Society. (C) and (D) adapted from Ref [88] with permission from the Royal Society of Chemistry.

Truncations can change the secondary structure of the aptamer as well as how well it binds its target.[89] An aptamer for the pyrimidine ribonucleotide uridine was selected using capture-SELEX (Uri1). Removal of an outer loop resulted in a loss of binding (Figure 1.25A and B)[90]. An example in which binding is not completely lost upon truncation is the sulforhodamine aptamer (SRhB1). Three truncations (SRhB1-a, SRhB1-b, and SRhB1-c) were tested using a fluorescence assay in which the K_d was reduced by 2-fold to 4-fold compared to the wild type SRhB1[91] (Figure 1.24C and D). This showed that this aptamer is very tolerant to truncation and can still bind its target.

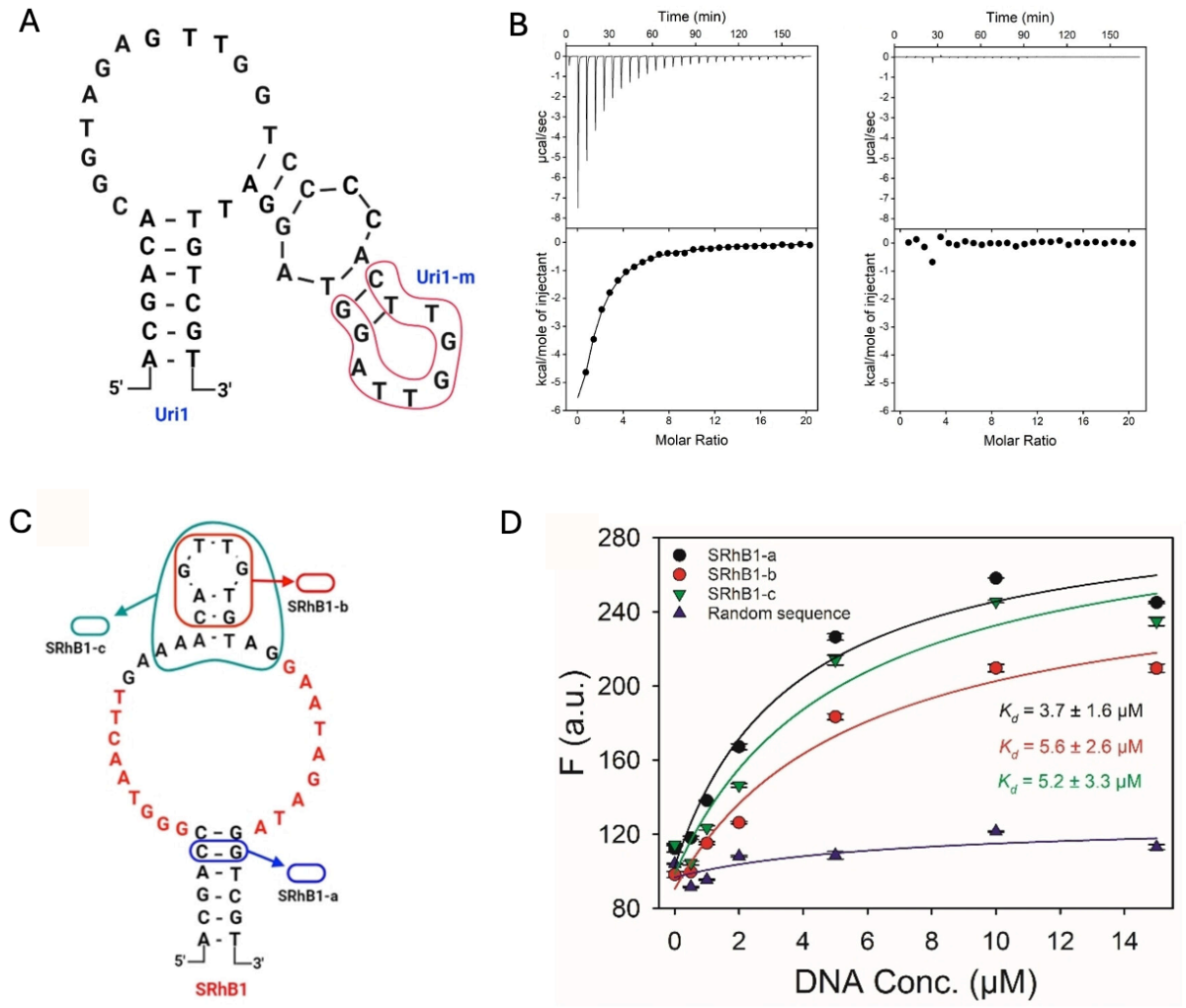


Figure 1.25. (A) Structure and truncation of Uri1 aptamer (B) ITC traces of uridine into the Uri1 aptamer (left) and Uri-m (right). (C) Structure and truncations of SRhB1 aptamer. (D) Fluorescence titration and fitted K_d of the SRhB1 mutants. (A) and (B) adapted from Ref [90]. (C) and (D) adapted from Ref [91].

1.4.6 Sensor Development

Finally, the selected aptamers can be applied in biosensor designs. Some popular aptamer sensors include paper-based sensors (Figure 1.26) [92,93] lateral-flow sensors (Figure 1.27),[94,95] electrochemical sensors,[96] and ELASA[97] (enzyme-linked aptamer sorbent assay, similar to ELISA but using aptamers instead of antibodies). Splitting an aptamer can also lead to different sensor designs.[98,99]

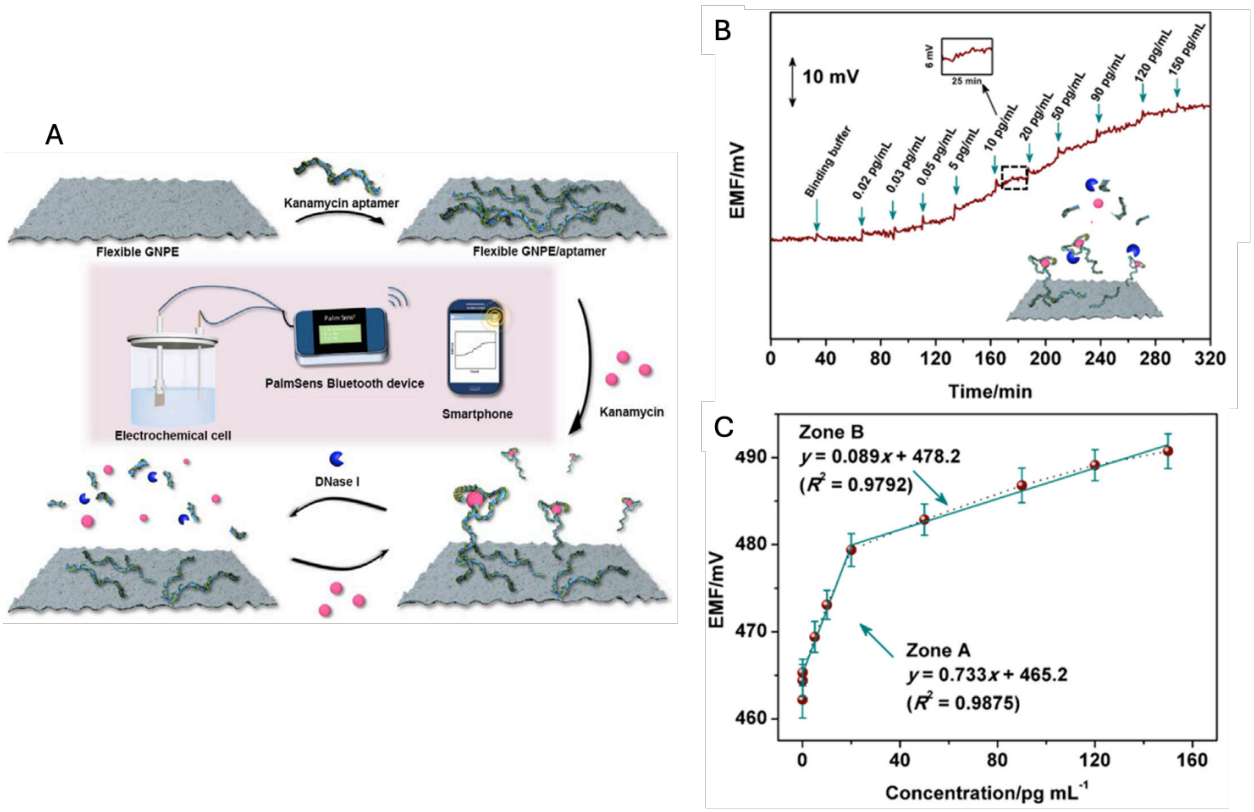


Figure 1.26. (A) Schematic of a paper-based sensor for kanamycin detection. (B) Potentiometric response of sensor with increasing amounts of kanamycin and (C) calibration curve generated. Reprinted from Ref [93] Copyright (2019), with permission from Elsevier.

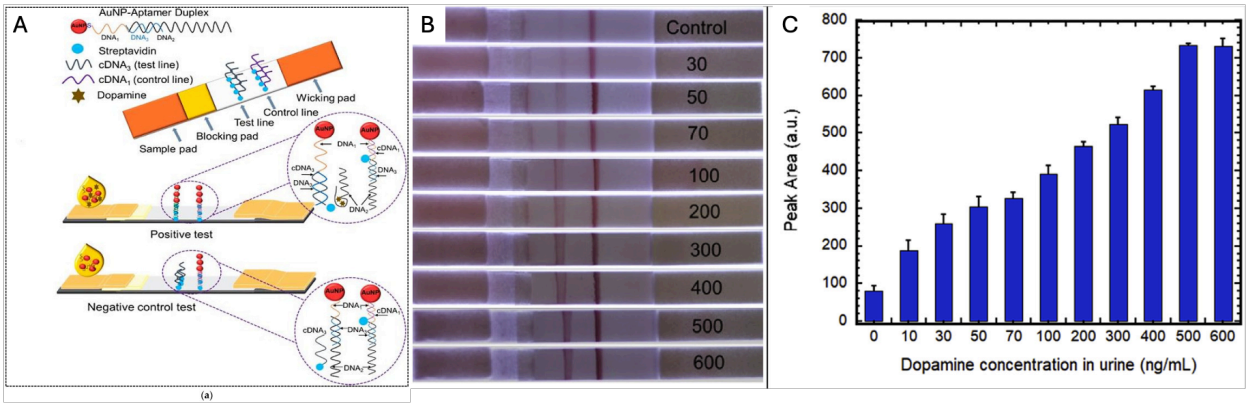


Figure 1.27. (A) Schematic of a lateral flow sensor using an aptamer for dopamine. (B) visual observation of the effect of dopamine concentration on color intensity of the test line; (C) peak area value of intensity to quantify dopamine presence at 15 min. Reprinted from Ref [95] Copyright (2019), with permission from Elsevier.

1.5 Thesis goals

Many of the previously selected aptamers against small molecule antibiotics have been shown not to bind their respective targets when subjected to more vigorous and robust binding assays. This may be due to the SELEX method used where the target was chemically altered through immobilization. Therefore, the goals of this these are to select new aptamers using the library immobilized capture-SELEX method, use reliable binding assays with mutation studies to properly characterize the dissociation constant (K_d), and to use these new aptamers as biosensors.

Chapter 2 An Aptamer for Tetracycline Antibiotics

The results presented in this section have been published as:

Yichen Zhao, Steven Ong, Yijing Chen, P.J Jimmy Huang, and Juewen Liu. Label-free and dye-free fluorescent sensing of tetracyclines using a Capture-Selected DNA aptamer. *Analytical Chemistry,* **2022**, 94 (28), 10175–10182

2.1 Introduction

The tetracyclines refer to a family of linearly fused four-ring antibiotics that inhibit bacterial protein synthesis by impeding aminoacyl-tRNA attachment to ribosomes.[100] In 1949, oxytetracycline (OTC, trade name Terramycine) was among the first discovered antibiotics in the tetracycline family as a natural product isolated from soil. A few years later, tetracycline (TC) was discovered. Since they stain the bones and teeth, TC and OTC are currently used mostly in animals.[101] Due to incomplete metabolism, their traces can be found in animal tissues or excreted and released into the environment.[102,103] Studies in OTC led to the discovery of doxycycline (DOX) with a longer half-life in the body and better absorption, which becomes a highly popular antibiotic to date.

TC is known to interact with various RNA with micromolar affinities including the 30S ribosomal RNA, tRNA and some ribozymes.[104] Aptamers are single-stranded oligonucleotides that can selectively bind target molecules.[105–107] An RNA aptamer for TC was reported by Berens et al in 2001 with a K_d of around 100 nM.[104] A subsequent study optimized the sequence and achieved an even lower K_d based on the same core sequence.[51] By rational randomization of this RNA aptamer, Tickner et al selected an aptamer for DOX.[52] A motivation of selecting RNA aptamers is to design artificial riboswitches.[108]

DNA aptamers are more stable and easier to modify compared to RNA aptamers,[105–107,109,110] and thus are more attractive for biosensor development.[105–107,109] DNA aptamers for tetracyclines have also been reported. In 2008, the first DNA aptamer for OTC was reported by Niazi et al, where the best aptamer (named No. 4) had a K_d of 10 nM and the aptamer had little binding to TC or DOX.[35] The same group then selected another aptamer using different magnetic beads respectively coated with TC, OTC and DOX, and the resulting general aptamer was reported to bind all the three antibiotics.[53] Using a gold nanoparticle based colorimetric assay, this general aptamer was truncated down to just 8 nucleotides.[37] So far, all of these aptamers were obtained by immobilization of target molecules.[35,47,53] Library-immobilized SELEX (also called capture SELEX) allows the use of unmodified free targets. [76,111–115]Many aptamers with tight binding affinities have been selected using this method (e.g. sub-μM K_d for cortisol, dopamine and serotonin).[76,87,111,112,116–122]

TC, OTC and DOX are all fluorescent with a large Stokes shift. [123]Their fluorescence could be enhanced by binding to the RNA aptamers, which was used for the characterization of aptamer binding.[51,52] However, this property has yet to be used for developing biosensors. In this study, new DNA aptamers were selected using OTC as a target through library-immobilized SELEX. The resulting aptamer could bind OTC, TC and DOX with a similar affinity. A label-free and dye-free fluorescent biosensor was demonstrated using the intrinsic fluorescence of the tetracyclines, which outperformed the strand-displacement sensor using a covalently labeled fluorophore and quencher.

2.2 Materials and Methods

2.2.1 Chemicals

All of the DNA oligonucleotides were purchased from Integrated DNA Technologies (Coralville, IA). The DNA library consisted of a randomized region of 30 nucleotides flanked by primer binding sequences. See Table 2.1 for the DNA sequences. TC, OTC, DOX and other chemicals were from Sigma-Aldrich.

Table 2.1 DNA Sequences used in this study.

DNA Name	Sequence and modification (From 5' to 3')
N30 Library	GGA GGC TCT CGG GAC GAC (N30)-GTC GTC CCG CCT TTA GGA TTT ACA G
Forward primer	GGA GGC TCT CGG GAC GAC
Reverse primer	CTG TAA ATC CTA AAG GCG GGA CG
Biotin-reverse primer	/5Biosg/ CTG TAA ATC CTA AAG GCG GGA CG-3
Biotin-column	GTCGTCCCGAGAGCCATA/3BioTEG/
OTC1	ACG ACC ACA GCT TGC TGC ATG ATC TTC TCT TGT AGG TCG T
OTC1-mutant	ACG ACC ACA GGT TCC TGC ATG ACA AAT TCT TGT AGG TCG T
OTC5	ACG ACA TTC CGT TGA TCT CTC CCT TTT GGG TTG GTG TCG T
OTC5-mutant	ACG ACA TTC CTG GTA TCT CTC CCT TTT GGG TTG GTG TCG T
OTC5-truncate	ACG ACA TTC CGT TGA TCT CTC GTT GGT GTC GT
FAM-OTC5	/56-FAM/CT CTC GAC GAC ATT CCG TTG ATC TCT CCC TTT TGG GTT GGT GTC GT
Quencher-DNA	TGT CGT CGA GAG /3IABkFQ/

Note: /5Biosg/ is biotinylation at the 5′-end, and /3BioTEG/ is biotinylation at the 3′-end with extended spacer. 56-FAM is derivative of fluorescein with maximum excitation at 495 nm and maximum emission 520 nm. 3IABkFQ is Iowa Black FQ with absorbance range from 420-620 nm. The two blue regions in the N30 Library sequence are complementary. The mutated bases are indicated in red.

2.2.2 Preparation of OTC solutions

During the aptamer selection, solutions of 2 mM and 0.5 mM OTC were prepared in 1× selection buffer. For rounds 1-14, the selection buffer was 50 mM Tris-HCl, pH 7.8, 300 mM NaCl, 5 mM KCl, 10 mM $MgCl_2$ with 2% dimethyl sulfoxide (DMSO). DMSO was included to increase

the solubility of OTC. For rounds 15-20, the OTC concentration was lowered to 0.5 mM and 0.1 mM and thus the same buffer without DMSO was used. For each selection round, OTC was freshly weighed and dissolved to avoid its degradation.[32] Similarly, TC and DOX solutions were also freshly prepared before use.

2.2.3 SELEX for OTC Aptamers

Selection of DNA aptamers was conducted using the library immobilization method as previously described.[87,111] For each round of selection, the DNA library was first annealed with the biotinylated capture strand. A column loaded with streptavidin-coated agarose microbeads was washed 5 times with 250 μL of 1× selection buffer. The library was then loaded onto the microbeads and washed 10 times with the selection buffer. The last three washes were kept as a background reference. 750 μL of the target solution was then passed through the library and the target bound run off was collected, purified by a 3k molecular weight cut-off spin column and concentrated to around 60 μL. The spin column was centrifuged at 17530 xg for 12 times to wash out target and concentrate the DNA. The concentration of OTC was 2 mM from round 1 to round 14, 0.5 mM from round 15 to round 17, and 0.1 mM from round 18 to round 20. Polymerase chain reaction (PCR) was then used to amplify the eluted pool and one of the primers contained a biotin label. After incubation of the PCR products with the streptavidin beads, they were then denatured using 0.2 M NaOH to recover the single-stranded library for the next round of selection. The final library was analyzed using deep sequencing at McMaster University as described previously.[87]

2.2.4 ITC

Isothermal titration calorimetry (ITC) was performed using a MicroCal VP-ITC.[26] Both the target and the aptamer were in the same buffer. Background heat of titrating antibiotics into the buffer was subtracted. Data analysis was done using the accompanying Origin software.

2.2.5 Fluorescence polarization

To measure fluorescence polarization, change of OTC upon binding to its aptamer, 100 nM OTC was dissolved in 100 µL buffer. The buffers were 25 mM Tris (pH 8.3) containing different concentrations of $MgCl_2$ (1, 2 or 10 mM) and NaCl (0, 100 or 300 mM). To the OTC samples, various concentrations of OTC5 aptamer were titrated (0, 10, 20, 70, 120, 220, 620 and 1020 nM), and each experiment was repeated 3 times. To measure polarization (Tecan Spark microplate reader), the excitation wavelength was set at 370 nm, and the emission wavelength was 520 nm. The change in polarization relative to the sample without the aptamer (ΔP) was plotted. All the binding curves were fitted using $y = y_0 + a[C]/(K_d + [C])$, where [C] is the concentration of the titrated molecule, and a is the maximal signal change upon saturated binding.

2.2.6 Fluorescence Measurements

The experiments were performed on a Varian Eclipse fluorimeter and a Tecan Spark microplate reader with excitation wavelength set for OTC at 370 nm. The emission spectra were collected from 500 nm to 600 nm. Emission was determined to be 530 nm. To determine the K_d, 100 nM OTC, TC or DOX was dissolved in 500 µL buffer (10 mM Tris HCl, pH 7.8, 60 mM NaCl, 2 mM $MgCl_2$, 1 mM KCl). The OTC5 aptamer was titrated such that the final volume increase was less than 10%. The solution was mixed during each titration step and allowed to equilibrate for 1 min before data collection. Similar methods were used for the measurement of OTC-dependent fluorescence without or with 2 µM OTC5 aptamer.

2.2.7 Detection in milk

Milk (2% fat) was from a local supermarket. Six 1.2 mL milk samples were first spiked with different concentrations of OTC. To remove the proteins, 30 µL HCl (1 M) was added to each milk sample and the samples were centrifuged for 15 min at 14000 rpm. The supernatant was then removed and diluted 100× in 1× Dulbecco's PBS buffer (pH 7.2) containing calcium and magnesium. 98 µL of this solution was then added to each well in a 96-well plate. Two blanks of water and buffer were also added to the plate. The base fluorescence was read using the Tecan microplate reader. Then, 2 µL of 100 µM OTC5 aptamer (in water) was added for a final of 2 µM OTC5. The fluorescence was immediately read.

2.2.8 Fluorescence biosensor based on strand displacement

20 nM of FAM-labeled aptamer and 40 nM of the quencher-labeled strand were first hybridized in the selection buffer by heating for 1 min at 95°C and cooled to room temperature. This hybridized solution was diluted to 10 nM in 1× selection buffer and was added to each well of a 96-well microplate. The fluorescence was monitored at 520 nm with 485 nm excitation. The background was run prior to the addition of the target to ensure a low background signal. Then various concentrations of OTC were added at the 5 min mark.

2.2.9 Split Aptamer Studies

Fluorescence experiments were performed on an Eclipse fluorescence spectrometer. A solution of 1 µM doxycycline was prepared in 10 mM MES pH 6 buffer with 2 mM $MgCl_2$. OTC5a and the different stem lengths of OTC5b were pre-annealed in the same buffer for 5 min at 90°C followed by cooling slowly to room temperature. The annealed split aptamers were then titrated into the doxycycline solution up to a final concentration of 2 µM aptamer. The fluorescence was

then read immediately after each addition using an excitation wavelength of 370 nm and emission wavelength of 535 nm.

Isothermal titration calorimetry was performed using a MicroCal ITC200 instrument. Data analysis was done using the accompanying Origin software. ITC was carried out at 20°C. 10 μM aptamer and 150 μM doxycycline were used for these experiments. The split OTC5a with OTC5b4/5 or OTC5b7/5 was pre-annealed for 5 min at 90°C then allowed to cool slowly to 20°C before loading. All solutions were prepared using 20 mM MES pH 6 with 50 mM NaCl and 1 mM $MgCl_2$.

2.3 Results and Discussion

2.3.1 Aptamer selection

OTC has a –OH group at both the 5′ and 6′ positions (Figure 2.1A). Replacing the 5′-OH with a proton results in TC, while replacing the 6′-OH with a proton results in DOX. In this study, we used OTC as the target due to its similarity to these two analogs, and we hoped to obtain an aptamer that can bind all these three tetracyclines. We performed DNA aptamer selection using the library-immobilization method.[77,87,111] The DNA library contained 30 random nucleotides flanked by two constant primer binding regions. The primer binding regions can form a 9-base-pair stem (Table 2.1), thus folding the library to an overall hairpin structure. The library was first hybridized to a short complementary strand with a biotin tag for immobilization on streptavidin-coated agarose beads. The selected sequences can bind to OTC and promote the formation of the hairpin. Thus, they were released from the beads for PCR amplification.

The resulting PCR amplicons from round 20 were deep sequenced. Around 30,000 sequences were obtained and they were processed using the Geneious software. We then took the

most abundant 15 sequences (which together counted for 65.3% of the entire library), and aligned them with the help of Cluster Omega (Figure 2.1B). These 15 sequences can be grouped into four families. Family 1 is represented by sequence OTC1, which can fold into a secondary structure shown in Figure 2.1C. The regions in green covaried to form a base paired stem, while the nucleotides between them are rich in pyrimidines. The rest of the sequences were also well aligned (highlighted in blue). The next family is represented by OTC5 and it has a very small hairpin with a 3 base pair stem and a 4-nt loop (Figure 2.1D). The loop is rich in thymine but can also contain other nucleotides (see Family 2 alignment in Figure 2.1B). The other two families have lower abundance and were not further analyzed.

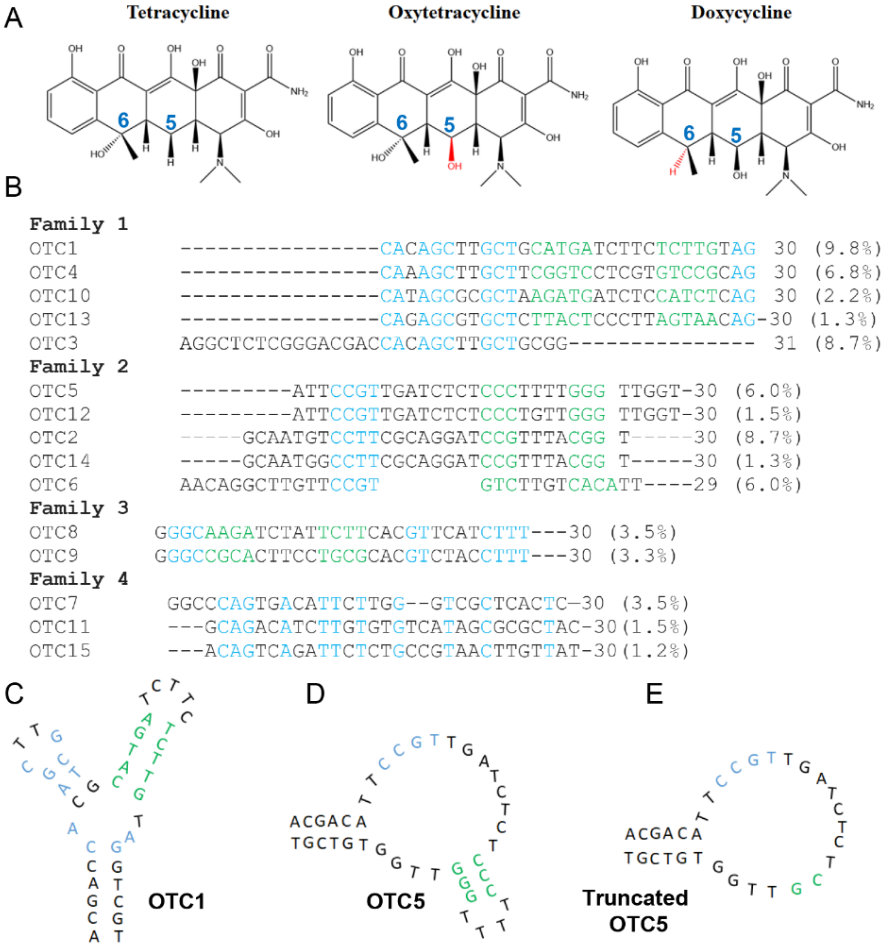


Figure 2.1. (A) The structures of the three tetracycline antibiotics used in this study. (B) Alignment of the most abundant 15 sequences. Within each family, the nucleotides in green can base pair, while those in blue are identical. Mfold predicted secondary structures of (C) the OTC1 aptamer, (D) the OTC5 aptamer and (E) a truncated OTC5 aptamer with the small hairpin removed.

We also compared with the previously reported OTC DNA aptamers obtained from target-immobilized selections.[35,53] We aligned the No. 4 aptamer[35] against our top sequences, but they do not have sequence homology (Figure 2.2). We also searched for the truncated 8-mer aptamer (CGGTGGTG),[37] and no consensus was found with our top 15 sequences either. Therefore, what we obtained were new aptamers. Since we used unmodified OTC, aptamers can access all its surfaces for binding. For the immobilized OTC, part of the molecule became unavailable for aptamer binding and thus the resulting aptamers could bind differently.

```
C10      ----------------CATAGCGCGCTAAGA-TGATCTCCATCTCAG-   30
C4       ----------------CAAAGCTTGCTTCGG-TCCTCGTGTCCGCAG-   30
C3       AGGCTCTCGGGACGACCACAGCTTGCTGCGG-----------------   31
C1       ----------------CACAGCTTGCTGCAT-GATCTTCTCTTGTAG-   30
C8       --------GGGCAA-GATCTATTCTTCACGTTCATC   TTTGTCGT --30
C9        --------GGGCCGCACT TCCTGCGCACG TCTACC TTTGTCGT --30
C2       --------- GCAATGTCCTTCGCAGGATCCGTTTACGGT----       30
C5       ------------------ATTCCGTTGATCTCTCCCTTTTGGGTTGGT   30
C6       ----------------AACAGGCTTGTTCCG-TGTCTTGTCACATT--   29
C7       --------GGCCCAGTGACATTCTTGGGTCGCTCACTC----------   30
C1        ---CACAGCTTGCTGCATGATCTTCTCTTGTAG------- 30
No.4      CGACGCGCGTTGGTGGTGGATGGTGTGTTACACGTGTTGT 40
```

Figure 2.2. Alignment of previously reported No. 4 aptamer with the top 10 sequences from our selection.

2.3.2 Aptamer binding assay using ITC

To characterize binding of the aptamers, isothermal titration calorimetry was used. For the sequences in Family 1, we first titrated OTC into aptamer OTC1 (Figure 2.3A). The downward spikes indicated an exothermic reaction, and based on the integrated heat, a K_d of 0.6 μM was fitted. A mutant of OTC1 was also tested and no binding was detected (Figure 2.4A), indicating the binding of OTC1 was specific. For the Family 2 sequences, we studied OTC5 (Figure 2.3B), and an even lower K_d (0.15 μM) was achieved. To confirm specific binding, an OTC5 mutant was tested by changing a fraction of the loop sequence from GTTG to TGGT, and this modification resulted in a loss of binding (Figure 2.4B). To confirm whether the small hairpin is important or not, we further tested a truncated version (Figure 2.1E), which had little heat release as well (Figure 2.4C). Thus, this small hairpin cannot be removed. The covariation of the stem region (the green bases in Family 2, Figure 2.1A) suggests that it is a real hairpin structure. We also tested the binding of TC and DOX by OTC5 and they both showed a similar binding affinity (Figure 2.4C, D and Table 2.2). Based on the lower K_d of OTC5 than OTC1 and its ability to bind all the three tetracyclines, our subsequent studies focused on OTC5.

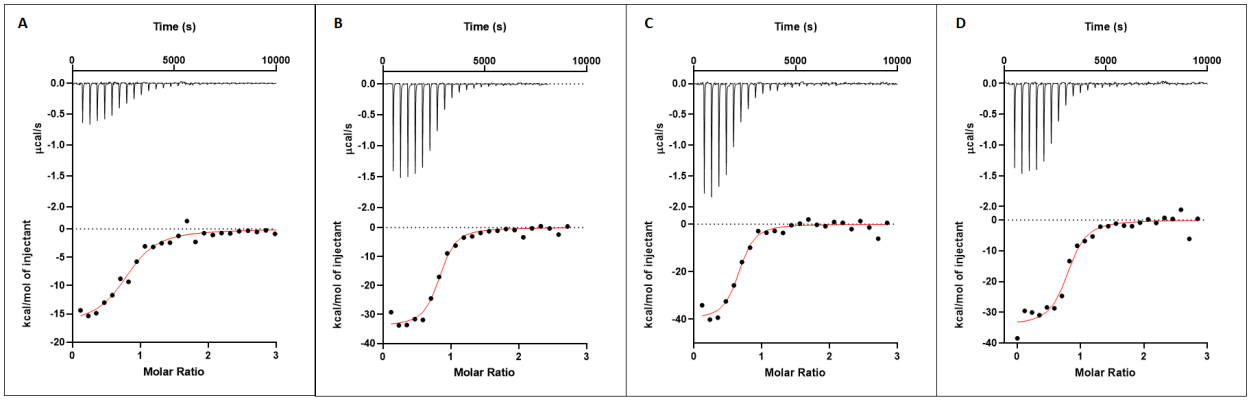


Figure 2.3. ITC traces and integrated heat of (A) titrating OTC into the OTC1 aptamer; and titrating (B) OTC, (C) TC and (D) DOX into the OTC5 aptamer. For each titration, 150 μM of target was titrated into 9 μM of DNA aptamer in the SELEX buffer at 25°C.

Table 2.2 Thermodynamic values of the aptamers based on ITC. Binding ratio (N), dissociation constant (K_d), enthalpy change (ΔH) and entropy change (ΔS) of the binding reactions are supplied.

Aptamer	Target	N	K_d (μM)	ΔH (cal/mol)(× 10^4)	ΔS (cal/mol/k)
OTC1	OTC	0.81 ± 0.03	0.6 ± 0.1	-1.7 ± 0.9	-28.1
OTC5	OTC	0.80 ± 0.03	0.15 ± 0.05	-3.3 ± 1.6	- 79.3
OTC5	TC	0.63 ± 0.02	0.18 ± 0.05	-4.0 ± 1.9	- 104
OTC5	DOX	0.77 ±0.03	0.25 ± 0.6	-3.4 ± 1.6	-84.9

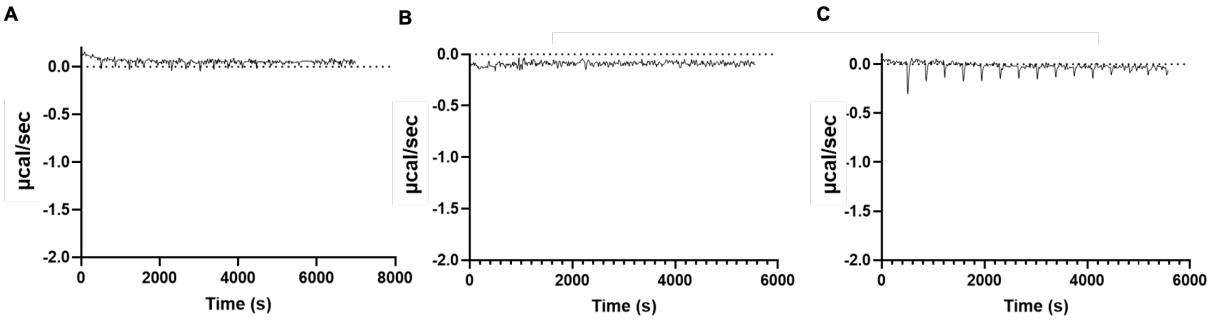


Figure 2.4. ITC of (A) the mutant of OTC1 (B) the mutant of OTC5 and (C) the truncated OTC5 with the hairpin removed.

2.3.3 Intrinsic Fluorescence Enhancement by The OTC5 aptamer

The tetracycline group of antibiotics have an intrinsic fluorescence[124] that can be exploited for sensing purposes. When the OTC5 aptamer was titrated into 100 nM OTC, the fluorescence gradually increased (Figure 2.5A), and we fitted the increase of the peak fluorescence to obtain a

K_d of 98 nM (Figure 2.5B), which was comparable to the values obtained from ITC and FP. If the non-binding mutant was titrated, no fluorescence change was observed (Figure 2.5B). We also did the same experiment with TC (Figure 2.5C) and DOX (Figure 2.5D), and they also showed a similar fluorescence enhancement with a K_d of 264 nM TC and 145 nM DOX. The aptamer provided a more hydrophobic environment for the tetracyclines, which can slow down non-radiative processes leading to enhanced fluorescence.

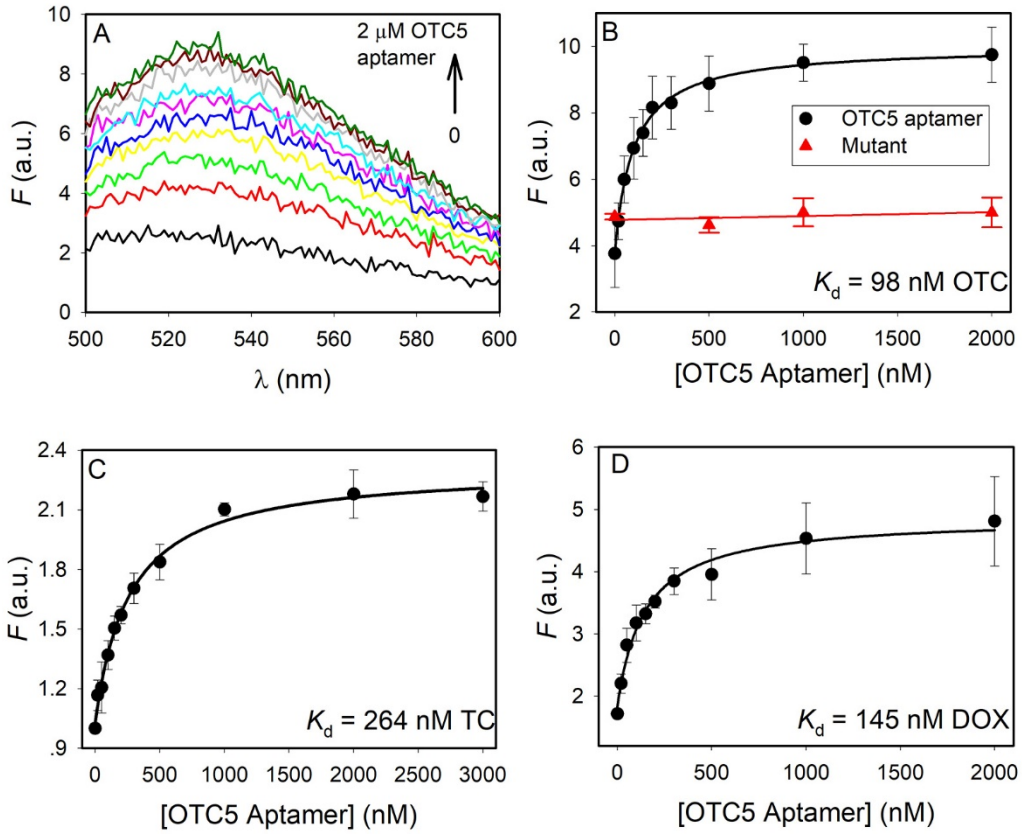


Figure 2.5. (A) Fluorescence spectra of 100 nM OTC in the presence of various concentration of the OTC5 aptamer with 370 nm excitation. The fluorescence increases of 100 nM (B) OTC, (C) TC, and (D) DOX with increasing concentration of the OTC5 aptamer. The data were fitted to a one-site binding curve. In (B), the non-binding mutant was also tested.

Such a unique aptamer-induced fluorescence increase might be useful for detection. We can divide analytes into three types. First, non- fluorescent molecules would have no fluorescence before or after aptamer addition. Second, most fluorophores would not be affected by the aptamer either. Thus, only the tetracyclines can show increased fluorescence. Since no covalent labels or DNA staining dyes were used,[125,126] it is a label-free and dye-free method of sensing . We measured the fluorescence of OTC as a function of its concentration in the absence and presence of 2 μM OTC5 aptamer (Figure 2.6). The increased fluorescence by the added OTC5 aptamer in the absence of OTC was attributed to the intrinsic fluorescence of DNA.[127]

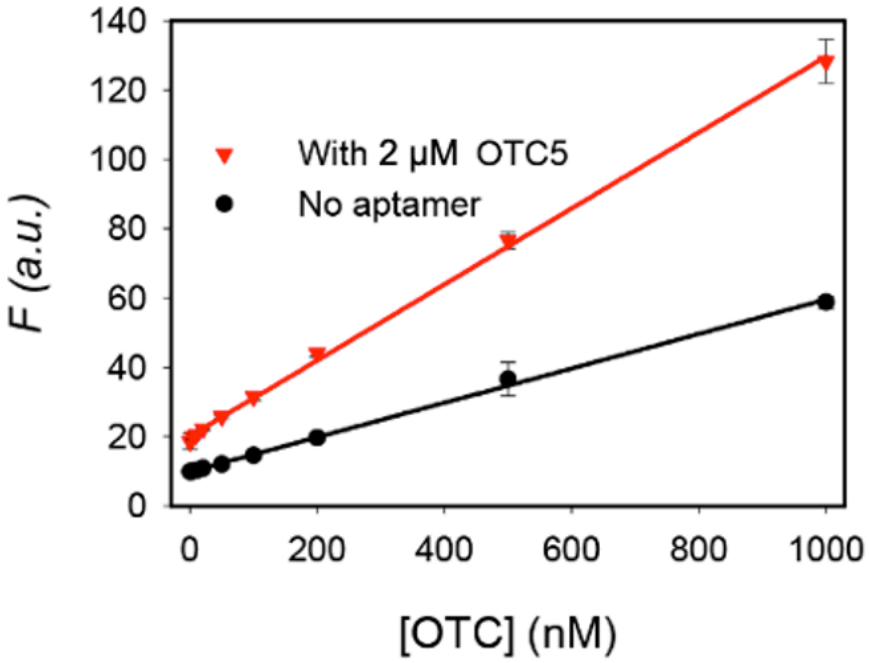


Figure 2.6. Fluorescence of OTC with and without the OTC aptamer.

Johnson and coworkers reported strong quenching of the intrinsic fluorescence of quinine and cocaine upon aptamer binding. While useful for the characterization of aptamer binding, fluorescence quenching is less favorable for biosensors. Manderville and coworkers used the intrinsic fluorescence of ochratoxin A for its detection, where signal-on sensing was achieved only

when exciting the aptamer at 256 nm followed by energy transfer.[128] While many fluorogenic aptamers were reported,[129,130] their ligands are typically not considered as target molecules. To the best of our knowledge, this was the first time that the intrinsic fluorescence of tetracyclines was used for designing aptamer-based signal-on biosensors.

The results presented in the following section have been published as:

Zhao, Y., Gao, B., Sun, P., Liu, J. Metal and pH-Dependent Aptamer Binding of Tetracyclines Enabling Highly Sensitive Fluorescence Sensing. *Biosensors* 2022, 12, 717.

2.3.4 pH and Metal Ion Dependency

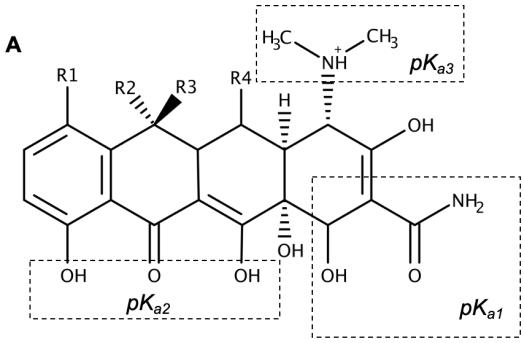
Tetracyclines have a number of pK_a's and changing pH can influence the charge of the molecule. During the selection process, most of the binding assays were done in the selection buffer, which had a pH of 7.8. This pH is close to the pK_{a2} of the antibiotics and thus they were a mixture of protonated and deprotonated forms. To test the effect of pH on aptamer binding and fluorescence enhancement, we herein systematically varied the pH to be either below or above the pK_{a2}. We picked pH 6.0 and 8.3 since they are below or above pK_{a2} of these three tetracyclines. So, at pH 6.0, the tetracyclines are charge neutral, whereas at pH 8.3, they carry one negative charge.

In addition, tetracyclines are known to bind to divalent metal ions[131–133] which may also affect their fluorescence.[134] Metal ions can also affect aptamer binding.[121,135] Thus, the effect of metal ions coupled with the change of pH needs to be studied to characterize aptamer binding and related biosensors. In this work, we systematically studied the effect of pH and metal ions on the sensing of the tetracyclines by the OTC5 aptamer. At slightly acidic conditions and with Mg^{2+}, up to 20-

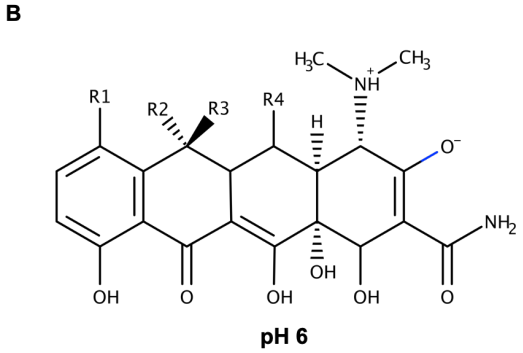
fold fluorescence enhancement was achieved, allowing highly sensitive detection down to sub-nanomolar level.

The structures of OTC, TC and DOX and their pK_a values are shown in Figure 2.7A. At pH 6.0, all the three antibiotics are nearly charge neutral, whereas at pH 8.3, the majority of them are negatively charged (Figure 2.7B). The secondary structure of the OTC5 aptamer is shown in Figure 2.7C, which has a similar affinity for binding these three antibiotics[136]. The majority of the previous studies were performed at pH 7.8, which was used for the selection of the OTC5 aptamer. Here, we studied both pH 6.0 and pH 8.3 to understand the effect of pH.

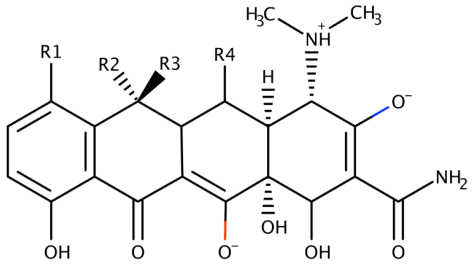
Based on the aptamer-binding induced fluorescence enhancement of the tetracyclines, we developed a label-free and dye-free sensing method as described in Figure 2.7D. When the OTC5 aptamer is added, only the tetracyclines became fluorescent, whereas other molecules, even fluorophores, had no fluorescence change. To achieve better sensitivity, it is desirable to have a low background fluorescence and a large fluorescence enhancement upon aptamer binding.



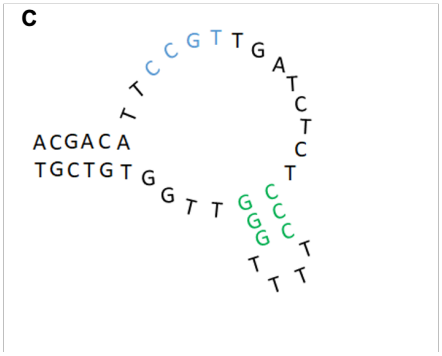
Antibiotic	R1	R2	R3	R4	pK_{a1}, pK_{a2},pK_{a3}
OTC	H	CH_3	OH	OH	3.3 , 7.3, 9.1
TC	H	CH_3	OH	H	3.3, 7.7, 9.7
DOX	H	H	CH_3	OH	3.0, 7.9, 9.1



pH 6



pH 8.3



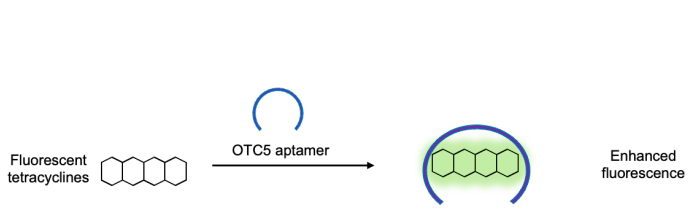


Figure 2.7. (A) The general structure of the tetracyclines with their respective pK_a values.[137] pK_a values adapted from ref.129(B) The structure of tetracyclines at pH 6 and pH 8.3. (C) The secondary structure of the OTC5 aptamer. (D) A cartoon showing the fluorescence enhancement of the tetracyclines upon aptamer binding.

2.3.5 pH and Mg^{2+}- dependent fluorescence of the tetracyclines

We first measured the intrinsic fluorescence of the three tetracyclines as a function of Mg^{2+} concentration at two pH (Figure 2.8). They all had lower fluorescence at pH 6.0 than at pH 8.3. Thus, protonation of them lowered the quantum yield. At both pH, adding Mg^{2+} increased their fluorescence, and the fluorescence enhancement was higher at pH 8.3. If we fit a binding curve to these data, the KD for Mg^{2+} was below 0.5 mM at pH 8.3, whereas the K_d was higher than 5 mM at pH 6.0. At pH 6.0, the pK_{a2} position is protonated. It is likely that this position is involved in binding Mg^{2+} since its protonation decreased Mg^{2+} binding. These antibiotics are known to chelate divalent metal ions and such binding can enhance their fluorescence. Therefore, when testing the effect of the OTC5 aptamer, we need to study the effect of pH and Mg^{2+}.

For the detection of the tetracyclines using the method in Figure 2.7D, having a lower background fluorescence in the absence of the OTC5 aptamer is advantageous. To find out the optimal Mg^{2+} concentration, we then compared the fluorescence of the samples in the absence and presence of 2 μM OTC5 aptamer, and the highest fluorescence increase occurred at above 0.5 mM Mg^{2+} (Figure 2.8D-F). When the Mg^{2+} concentration was higher than 5 mM, the fluorescence enhancement also decreased. Thus, we picked 2 mM Mg^{2+} for our subsequent studies.

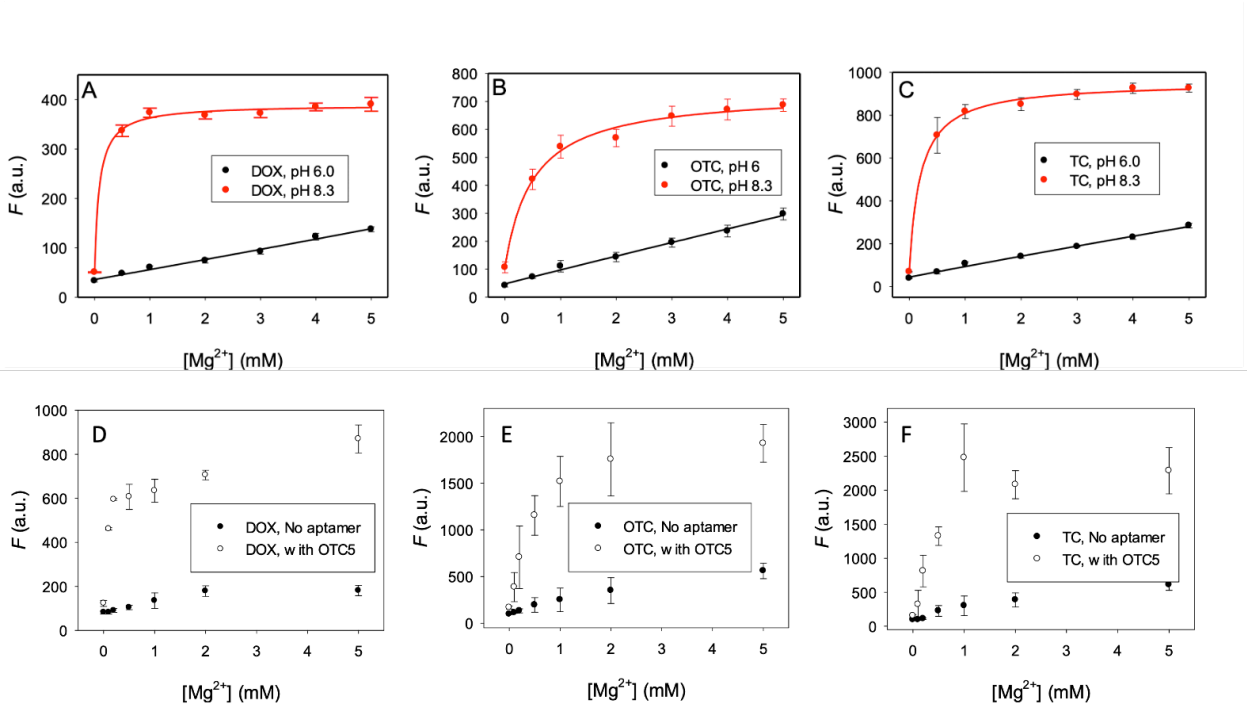


Figure 2.8 The fluorescence of the tetracycline antibiotics at pH 6.0 and 8.3 in the presence of increasing concentration of Mg^{2+}: (A) DOX, (B) OTC and (C) TC. The fluorescence intensity of 100 nM (D) DOX, (E) OTC, and (F) TC alone and with 2 μM of the OTC5 aptamer with increasing concentration of Mg^{2+} in 10 mM MES, pH 6.0 with 50 mM NaCl.

2.3.6 pH and Mg^{2+} dependent aptamer binding

We then tested the fluorescence change of OTC with the addition of the OTC5 aptamer. At pH 6.0, the background fluorescence of 100 nM OTC is quite low, but with the addition of 2 μM OTC5 aptamer, a large enhancement was achieved (Figure 2.9A). We then systematically tested the response over a broad pH range from 4 to 8 (Figure 2.9B). Although pH 5 showed the highest fold of fluorescence enhancement, pH 6 gave higher fluorescence intensities. In addition, TC and OTC are less stable at acidic pH.[138] Therefore, we chose pH 6 as our acidic pH for subsequent studies.

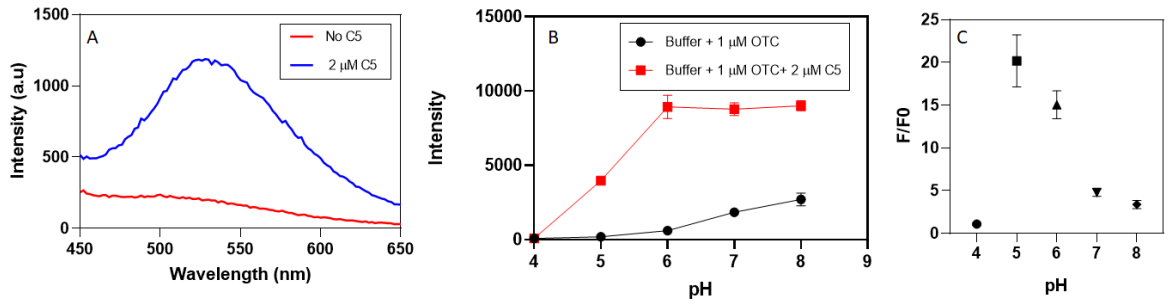


Figure 2.9. (A) Fluorescence spectra of 100 nM OTC in the absence and presence of 2 μM OTC5 aptamer at pH 6.0. (B) pH-dependent fluorescence of 1 μM OTC in the absence and presence of 2 μM OTC5 aptamer. pH 4 and 5: acetate buffer; pH 6, 7: phosphate buffer; pH 8: Tris buffer. All with 10 mM Mg^{2+}. (C) The fold of fluorescence enhancement at different pH due to the addition of OTC5.

We then measured the OTC5 aptamer binding to 100 nM DOX pH 6.0. By gradually titrating aptamer, over 20-fold fluorescence enhancement was achieved with 3.7 μM aptamer added (Figure 2.10A, red line). The K_d was fitted to be 0.39 μM. Without Mg^{2+}, the fluorescence barely changed, indicating a lack of binding. Therefore, this aptamer requires Mg^{2+} for target binding.

We then repeated this experiment at pH 8.3 (Figure 2.10B). In this case, for the 2 mM Mg^{2+} added sample, the background fluorescence was higher, and the final fluorescence was lower. The fluorescence enhancement was only 4-fold, although the K_d was slightly smaller (0.24 μM). Still, when no $Mg^{2+}$was added, the binding was lost, and the fluorescence barely changed upon titration of the OTC5 aptamer. The same experiments were also performed for OTC (Figure 2.10C, D) and TC (Figure 2.10E, F), and the conclusions were the same. For OTC, at pH 6.0, the K_d for the aptamer was 0.14 μM, slightly higher than that at pH 8.3 (0.06 μM), but the fluorescence

enhancement upon aptamer binding was much higher. For TC, at pH 6.0, the K_d for the aptamer was 0.36 µM, about 1-fold higher than that at pH 8.3 (0.16 µM).

Therefore, to use the aptamer-binding induced fluorescence for the detection of these antibiotics, pH 6.0 appeared to be a better condition due to its much higher fluorescence enhancement. In all cases, Mg^{2+} was required for aptamer binding.

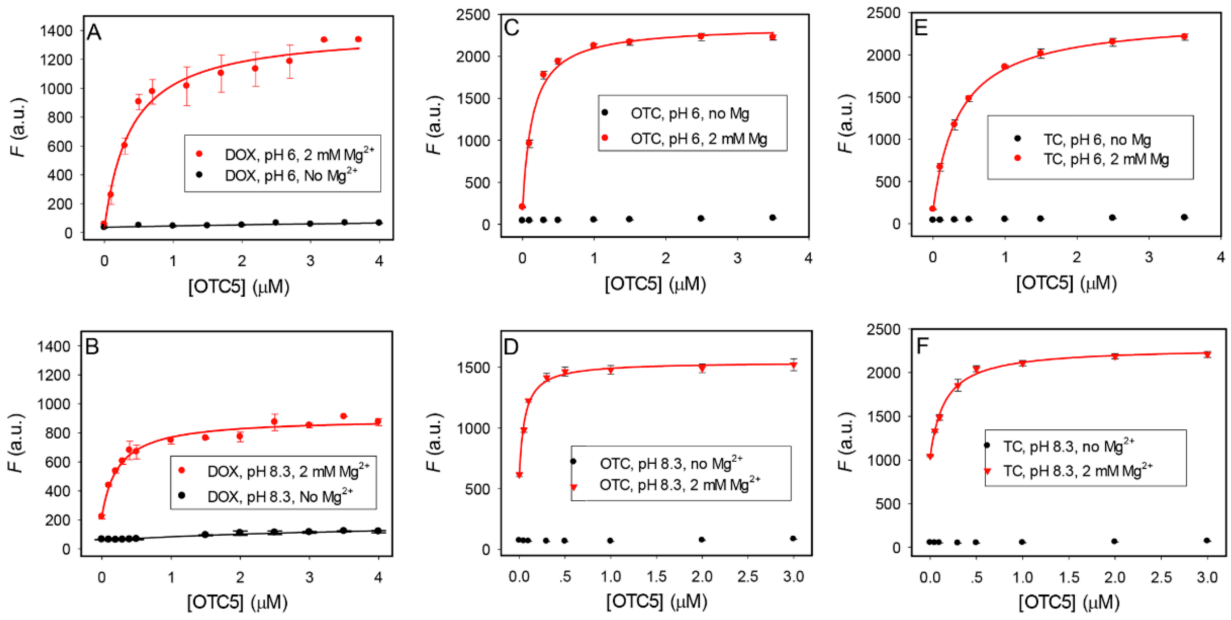


Figure 2.10. Aptamer binding curves for (A, B) DOX, (C, D) OTC, and (E, F) TC in (A, C, E) pH 6.0 buffer and (B, D, F) pH 8.3 buffer in the absence or presence of 2 mM Mg^{2+}.

2.3.7 pH and Mg^{2+} Binding Assay using ITC

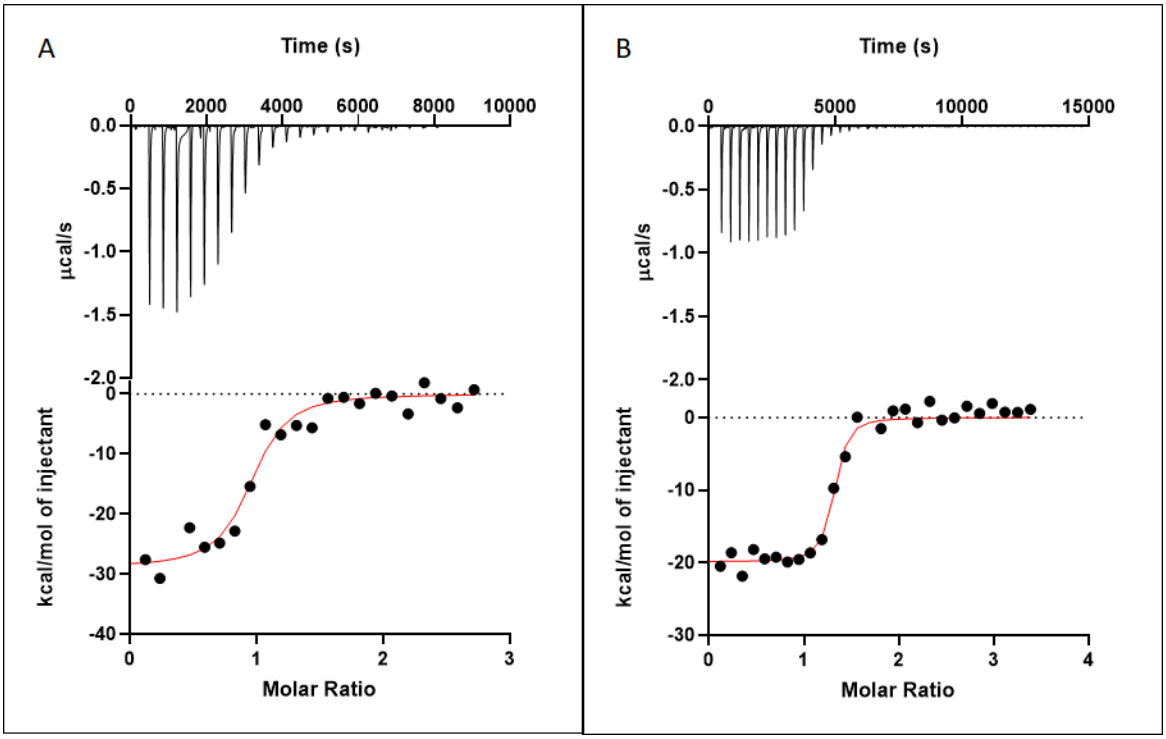


Figure 2.11. ITC traces of 150 µM OTC titrated into 9 µM OTC5 at (**A**) pH 6.0 with 2 mM Mg^{2+} and (**B**) pH 8.3 with 2 mM Mg^{2+}

To further characterize the binding of the aptamers at different pH, ITC was used. OTC was titrated into the OTC5 aptamer at pH 6.0 (Figure 2.11A) and pH 8.3 (Figure 2.11B). The downward spikes indicated an exothermic reaction. By integrating the heat, the K_d at pH 6.0 was fitted to be 0.20 µM. The K_d at pH 8.3 was fitted and found to be almost 10 times lower at 0.03 µM. Comparing the K_d's at pH 6.0 and 8.3 to the previously reported K_d at pH 7.8, the KD of OTC5 at pH 6.0 is very similar to the value of 0.15 µM at pH 7.8.[136] However, the K_d at pH 8.3 is much lower indicating stronger binding which also agrees with the fluorescence measurements.

Table 2.3 Thermodynamic Values of the Aptamers Based on ITC. Binding ratio (N), dissociation constant (K_d), enthalpy change (ΔH), and entropy change (ΔS) of the binding reactions are supplied.

Aptamer	Target	pH	N	K_d (μM)	ΔH (cal/mol) (x 10^4)	ΔS(cal/mol/K)
C5	OTC	6.0	0.92 ± 0.03	0.2 ± 0.4	-2.89 ± 1.5	-66.3
C5	OTC	8.3	1.27 ± 0.02	0.03 ± 0.08	-1.99 ± 0.45	-32.6

2.3.8 Effect of other metal ions

After knowing the importance of Mg^{2+} for aptamer binding and fluorescence-based detection, we then studied the effect of some other divalent metal ions. Since the behavior of these antibiotics were similar, we focused on OTC. We first replaced Mg^{2+} with Ca^{2+} (Figure 2.12A). Ca^{2+} can also enhance the fluorescence of OTC, indicating binding. However, the addition of OTC5 aptamer did not bring much fluorescence enhancement for the Ca^{2+} sample (only ~20%). When we tested Mn^{2+}, the fluorescence of OTC dropped with in-creasing concentration of Mn^{2+} (Figure 2.12B). Although fluorescence was enhanced with the addition of the OTC5 aptamer, the increase was quite modest (less than 1-fold). Therefore, the sensor would work the best in the presence of Mg^{2+}. With Zn^{2+}, the fluorescence enhancement was more and adding OTC5 induced a significant increase (Figure 2.12C).

This could be related to the selection condition, where 10 mM Mg^{2+} was used.[136] Since the tetracyclines can bind to various metal ions, [53,139,140] we reason that Mg^{2+} must be involved in bridging OTC and the aptamer instead of acting as a general salt to screen charge repulsion. Zn^{2+} can replace the role of Mg^{2+} and support aptamer binding. Zn^{2+} and Ca^{2+} can partially replace the role of Mg^{2+} and support aptamer binding. Since the least fluorescence change by adding the OTC5 aptamer was seen with Mn^{2+}, we then tested whether we could rescue the sensor performance by adding extra Mg^{2+}. We performed the aptamer titration with 0.5 mM Mn^{2+} alone and with an additional 2 mM Mg^{2+} Figure (2.12D). With the extra Mg^{2+}, 5-fold fluorescence enhancement was

achieved, and the overall fluorescence was also much higher. Therefore, adding extra Mg^{2+} can be a useful method for samples with unknown metal compositions.

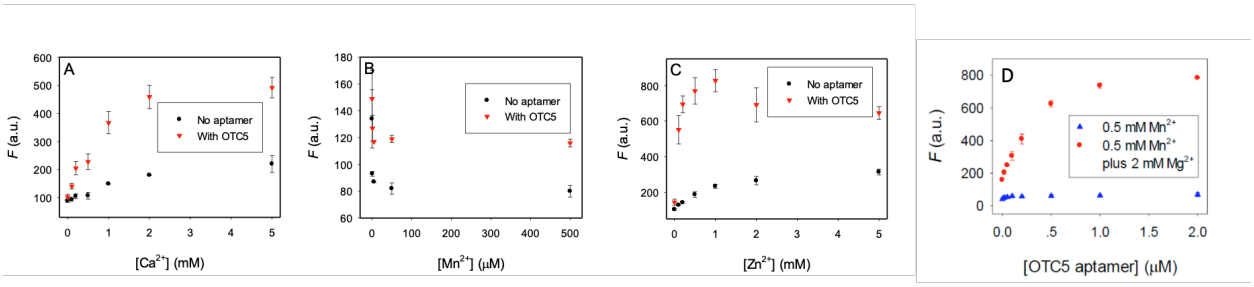


Figure 2.12. The fluorescence of 100 nM OTC alone and with 2 μM OTC5 aptamer as a function of (A) Ca^{2+}, (B) Mn^{2+} and (C) Zn^{2+} concentration. All in pH 6.0 MES buffer. (D) The fluorescence of 100 nM OTC as a function of OTC5 aptamer concentration in 0.5 mM Mn^{2+} alone and with 0.5 mM Mn^{2+} and 2 mM Mg^{2+} mixture. The buffer was 10 mM MES, pH 6.0 with 100 mM NaCl.

2.3.9 Sensing of the Tetracyclines using OTC5.

To achieve quantitative detection, we then resorted to exploiting the binding-induced fluorescence intensity change described above. We tested the selectivity of this sensor against a few other antibiotics (ampicillin, chloramphenicol, kanamycin and streptomycin). Since they are nonfluorescent, the signals were close to zero (Figure 2.13A). We also tested a few fluorescent compounds (fluorescein, dopamine, quinine). With 370 nm excitation, only fluorescein showed a strong 520 nm fluorescence emission (Figure 2.13B), yet its fluorescence was not affected by the OTC5 aptamer. As a result, the fluorescence difference before and after adding the aptamer was also close to zero (Figure 2.13A). Therefore, the background fluorescence in the sample would not affect the performance of the sensor. OTC, TC and DOX showed a similar response, and thus this sensor can detect them as a group.

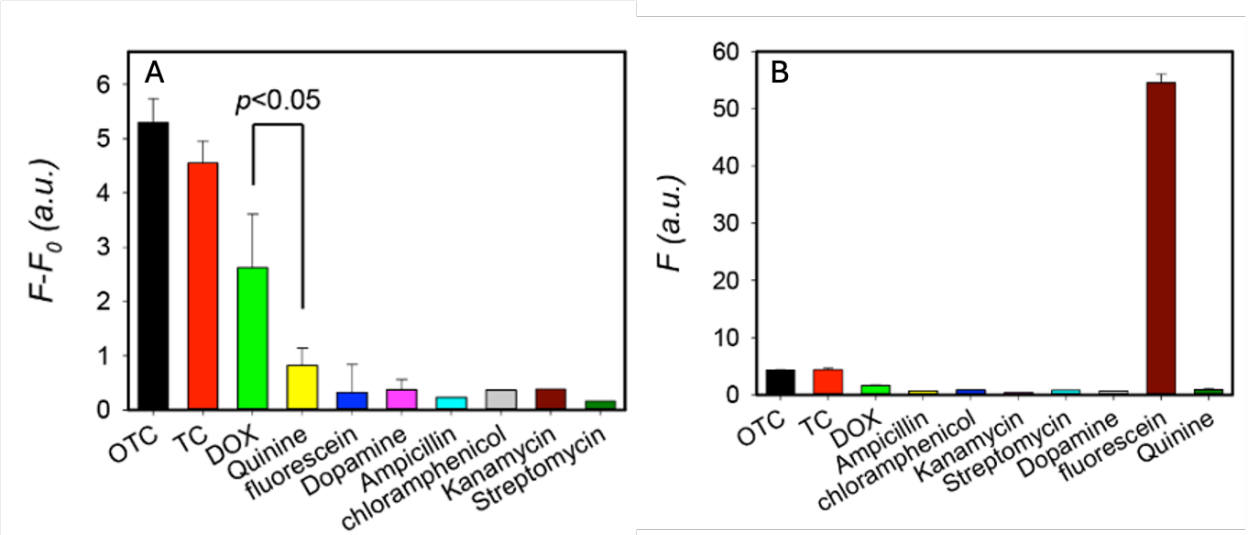


Figure 2.13. (A) Fluorescence difference of various molecules in the absence and presence of 2 μM OTC5 aptamer. (B) Fluorescence intensity at 520 nm of 100 nM of each of the molecules excited at 370 nm. The buffer was 10 mM Tris HCl, pH 7.8, 60 mM NaCl, 2 mM $MgCl_2$, 1 mM KCl.

We then tested the sensitivity of the sensors using the method described in Figure 2.7D. For each analyte concentration, two measurements were performed: before and after adding 2 μM OTC5 aptamer. For all the three antibiotics, we observed linear responses (Figure 2.14A-C) and the slopes of the samples with OTC5 were much higher. We then calculated the fluorescence difference of the two lines and plotted then in Figure 2.14D-F, which were the calibration curves for the tetracyclines. Based on them, we calculated the limit of detection (LOD) to be 0.7 nM, 0.5 nM and 0.1 nM for DOX, OTC and TC, respectively. For comparison, without optimized conditions, the LOD for OTC was 25 nM,[136] and our new condition allowed a 50-fold improvement. This detection method did not involve any covalent fluorophore labels or DNA staining dyes and we solely relied on the intrinsic fluorescence of the tetracyclines.

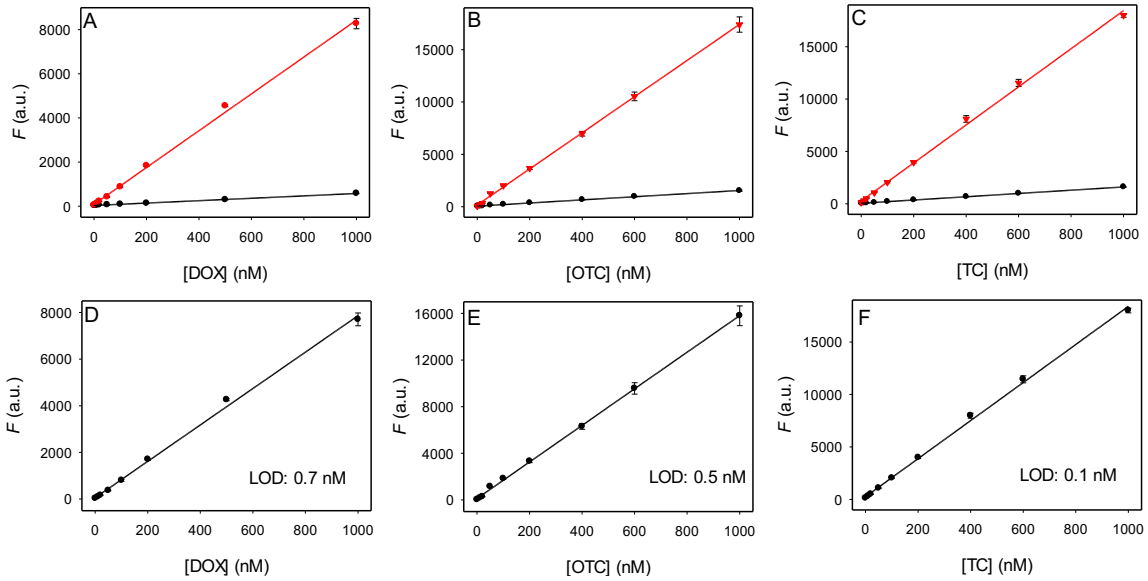


Figure 2.14. Fluorescence intensity of (A) DOX, (B) OTC, and (C) TC in the absence (black dots) and presence (red dots) of 2 μM OTC5 aptamer. Fluorescence difference of (D) DOX, (E) OTC, and (F) TC in the absence and presence of 2 μM OTC5 aptamer. The measurements were performed in pH 6 buffer with 2 mM Mg^{2+}.

We then tested the selectivity of the sensors at different pH against the series of different antibiotics (streptomycin, penicillin, ampicillin, chloramphenicol, and kanamycin). These antibiotics are not fluorescent at both pH 6.0 and 8.3 their signals are close to zero (Figure 2.15A and 2.15B). OTC, DOX, and TC did show significant fluorescence increase. From highest to lowest fluorescence enhancement: TC>OTC>DOX and pH 6.0> pH 8.3 (Figure 2.15C).

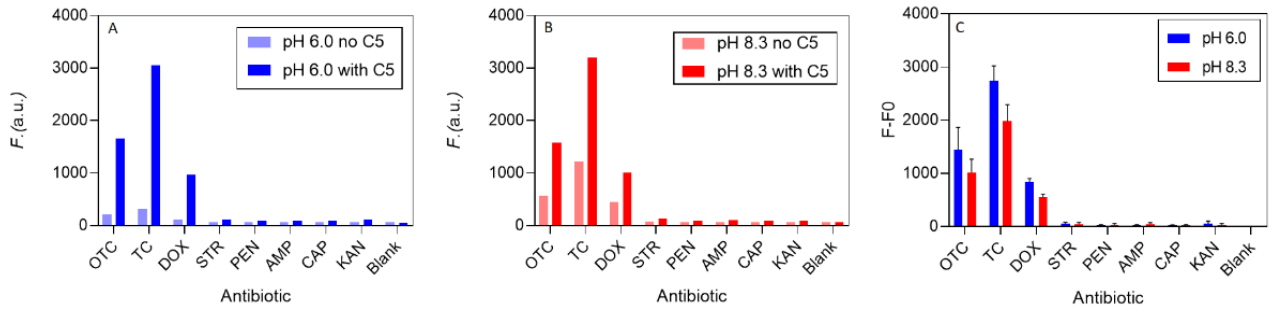


Figure 2.15. Selectivity of the OTC5 aptamer in (A) pH 6.0 MES buffer and (B) pH 8.3 Tris buffer each with 2 mM Mg^{2+}. 2 µM of OTC5 was added to 100 nM of antibiotic. Samples were scanned at an excitation wavelength of 370 nm and emission of 530 nm. (C) The fluorescence difference at pH 6.0 and 8.3 with and without OTC5.

2.3.10 Sensing of OTC in milk

We then tested this sensor using milk samples. Milk (2% fat) was spiked with various amounts of OTC. Since tetracyclines are known to bind to the proteins in milk, samples were first treated with HCl, centrifuged then diluted in buffer before detection. In the treated milk, the sensor showed slightly better performance at pH 6.0 (Figure 2.16A). The detection limit (3σ/slope where σ is the background variation) was also calculated to be 16 nM at pH 6.0 (Figure 2.16B).

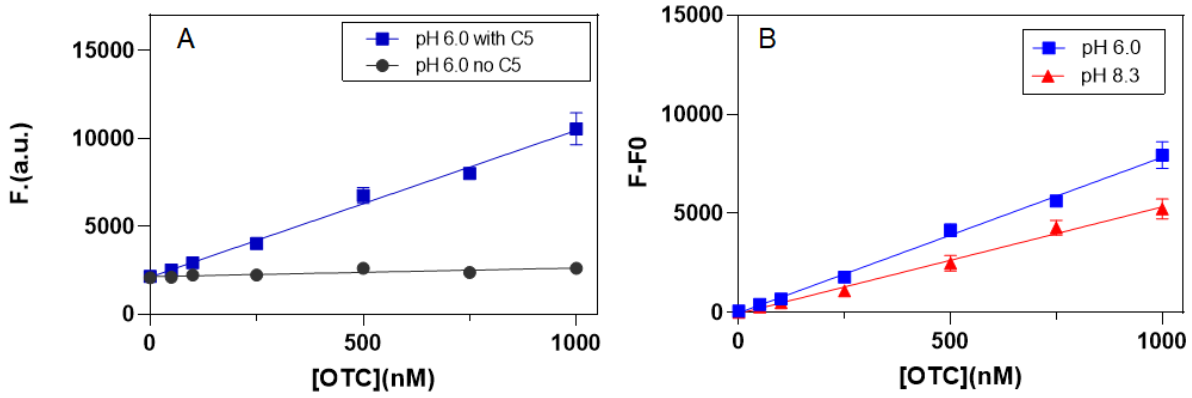


Figure 2.16. Fluorescence intensity as a function of OTC concentration in spiked milk samples after extraction without and with 2 μM OTC5 aptamer at (A) pH 6.0 with 2 mM Mg^{2+}. (B) Fluorescence difference as a function of OTC concentration at pH 6.0.

2.3.11 Labeled fluorescent sensing of OTC

Finally, we also designed a strand-displacement fluorescent sensor with a covalently labeled fluorophore and quencher. The aptamer was extended by six nucleotides on the 5′-end and hybridized with a 12-mer 3′-end quencher-labeled oligo.[141] In the presence of OTC, the aptamer would bind to it and released the quencher-labeled strand resulting in fluorescence enhancement (Figure 2.17A).

The background of the sensor was run prior to the addition of OTC to ensure a stable background signal (Figure 2.17B). Then various concentrations of OTC were added at the 5-min mark. After 5 min of reaction, the fluorescence reached stable values for all samples. With 36 μM of target, over 20-fold increase in the fluorescence signal was observed after 20 min. A calibration curve was obtained showing a typical binding curve (Figure 2.17C). An apparent K_d of 12 μM was obtained. This value was much higher than what was obtained from the ITC experiments due to competition with the complementary strand.[47] Below 4 μM OTC, the response was linear (Figure 2.17C, inset). Using this sensor, the limit of detection was calculated to be 1.2 μM OTC, which was nearly 50-fold worse than the above label-free and dye-free sensing method. The increased apparent K_d can explain the increased detection limit. For the selectivity test of the aptamer, 8 μM of different antibiotics were screened (Figure 2.17D). As expected, the tetracyclines showed a similar response, while the other antibiotics were silent. Overall, this sensor is more expensive yet less sensitive than the label-free and dye-free method.

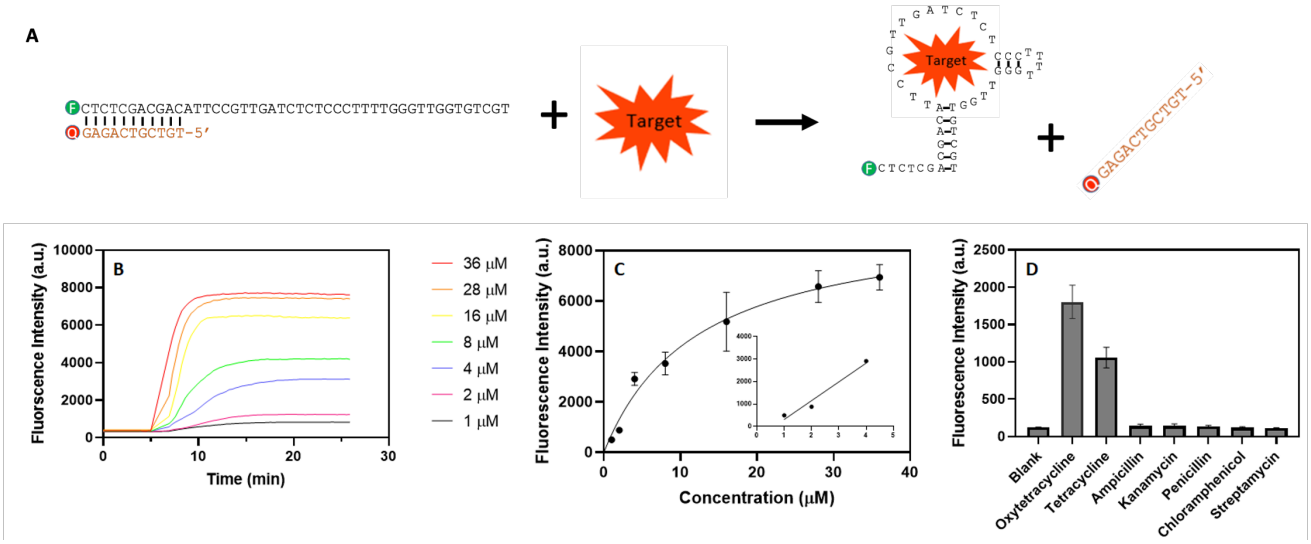


Figure 2.17. (A) Schematic of the strand-displacement biosensing system with a covalently linked fluorophore and quencher. (B) Kinetics traces of the sensor in the presence of various concentrations of OTC in the selection buffer. OTC was added at 5 min. (C) Fluorescence intensity as a function of OTC concentration. Inset: linear response at lower concentrations. (D) Sensor selectivity against various antibiotics at 8 μM.

2.4 A Split aptamer biosensor

The results presented in the following section have been published as:

Zhao, Y., Patel, N., Sun, P., Faulds, K., Graham, D., & Liu, J. (2023). Light-up split aptamers: binding thermodynamics and kinetics for sensing. *The Analyst*, 148(22), 5612–5618.

Splitting an aptamer into two halves is another popular way to achieve a range of signaling methods[98,142] from fluorescence,[143] colorimetric,[144] to Raman-based detection.[99] In a typical design, an aptamer is split from two base paired regions and the two halves would not bind to each other until a target molecule is added. Binding of the two split aptamer halves would bring them from infinitely far away to close proximity, resulting in a larger signal change compared to typical full-length aptamers.

Previous work on split aptamers has focused mainly on sensor design,[98,142,145–148] or other applications but fundamental binding properties of split aptamers versus full-length aptamers have yet to be studied.[149] For example, it is perceived that split aptamers would suffer from a lower binding affinity due to disfavored entropy contributions, but the quantitative effects remain unknown. Understanding of these properties would be valuable for rational design of split aptamer biosensors.

Part of the reason for the lack of systematic binding assays is attributable to difficulties associated with small molecule aptamer binding assays.[150–152] For a systematic study to test many sequences, it is expensive to synthesize fluorescently labeled DNA. Recently, a few aptamers have been reported to show binding-induced fluorescence change.[128,136,153–155] In those examples, target molecules are fluorescent, and the fluorescence intensity is either enhanced or quenched upon aptamer binding. We aimed to take advantage of such fluorescence to perform binding assays to understand split aptamers. In the following section, we measured both the thermodynamic and kinetic properties of the full-length and split aptamers using fluorescence spectroscopy and isothermal titration calorimetry (ITC),

2.4.1 Splitting the OTC5 aptamer

While numerous split aptamers have been reported,[98,142] we focused on the OTC5 aptamer.[136] The OTC5 aptamer has a similar affinity to tetracycline antibiotics such as tetracycline, oxytetracycline (OTC) and doxycycline (K_d ~100 nM).[136] Binding to the OTC5 aptamer can induce a strong fluorescence increase of the tetracycline antibiotics. OTC5 is featured with a large loop and two short stems connecting them, and thus it is quite straightforward to split it through the two stems (Figure 3.1A). In the original aptamer, the two stems have 7 and 3 base pairs (bps), respectively. Since the 3 bp stem is in a hairpin, it also has a high stability.[156,157] After splitting,

however, a 3 bp duplex is unlikely to be stable enough and thus we extended it by two bases to make a total of five base pairs in that stem (Figure 2.18A). Of the two split halves, one was named OTC5a and the other OTC5b. To have a systematic understanding, we fixed the OTC5a sequence but varied OTC5b to form different base pairs. The OTC5b shown in Figure 1A can form 7 and 5 bps in the two stems, respectively, and thus it was named OTC5b7/5. We also used a few other shorter OTC5b sequences such as OTC5b5/6, OTC5b4/6 and OTC5b5/4.

The main tool used in this work is fluorescence spectroscopy. The fluorescence spectrum of the OTC5 full length aptamer was first measured. Doxycycline was chosen as the target molecule for these studies due to its better stability compared to tetracycline and oxytetracycline.[158] 1 μM of doxycycline was dissolved in MES pH 6.0 buffer with 2 mM $MgCl_2$. $MgCl_2$ is necessary to facilitate the binding of the aptamer as well as enhance the fluorescence signal.[155] The fluorescence spectrum was measured at an excitation wavelength of 370 nm and emission from 430 nm to 650 nm, both before and after the addition of 2 μM OTC5 (Figure 2.18B). After the addition of 2 μM OTC5, the fluorescence peak at 535 nm showed an 8-fold increase. This fluorescence enhancement was visible by eye under UV excitation in a dark room (Figure 2.18C).

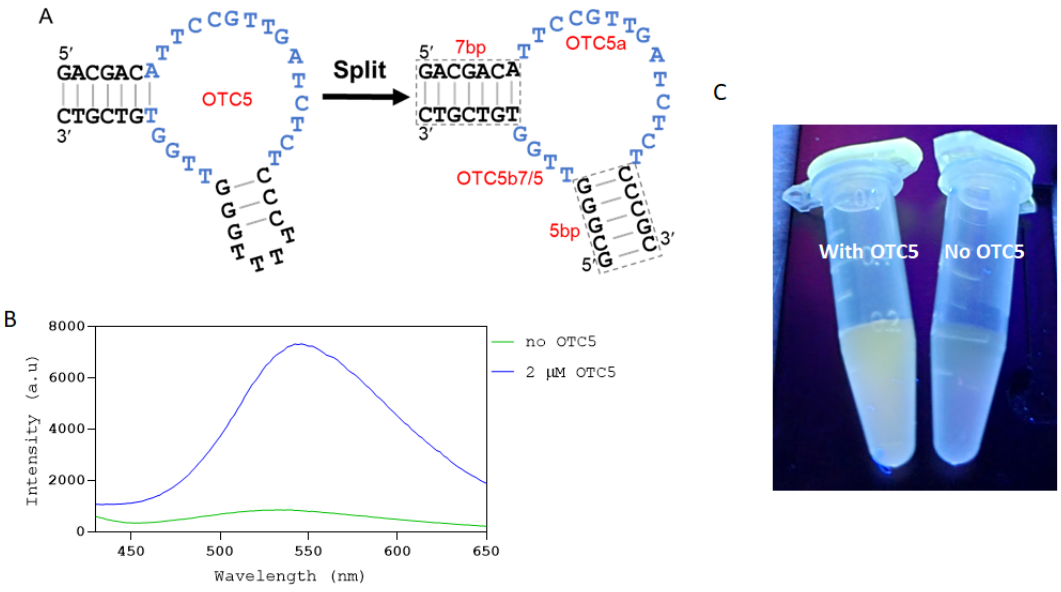


Figure 2.18. (A) The full-length OTC5 aptamer and the strategy of splitting. In this study, the OTC5a strand was fixed and the length of OTC5b strand varied to tune the number of base pairs. In the current figure, the two stems have 7 and 5 base pairs, respectively. (B) Fluorescence spectra of 1 μM doxycycline in the absence and presence of 2 μM of the full length OTC5 aptamer. Buffer for OTC5: 2 mM Mg2+, 10 mM MES, pH 6.0. (C) Photograph showing fluorescence enhancement of 2 μM doxycycline in the presence and absence of 5 μM C5 in the previously mentioned buffer.

2.4.2 Fluorescence change and binding affinity at different stem lengths

To quantitatively measure the effect of split aptamer on the binding affinity, we titrated the aptamers into their targets and monitored the fluorescence change. For the split OTC5 aptamers with various stem lengths, the OTC5b7/5 was the closest in value to the full-length aptamer with a K_d of 0.55 μM (Figure 2.19). For comparison, the full-length has a fitted value of 0.27 μM. By shortening the stems to 5/6, the K_d kept increasing to 1.8 μM. The signal of the 4/6 and 5/4 aptamers failed to saturate, and accurate K_d values cannot be obtained. Overall, this experiment showed that their ability to bind doxycycline was deteriorating by shortening the stems. Thus, the stem length

is very important to tune the binding affinity of split aptamers. Shorter stems can better disrupt the initial aptamer complex, but the binding ability is also more compromised.

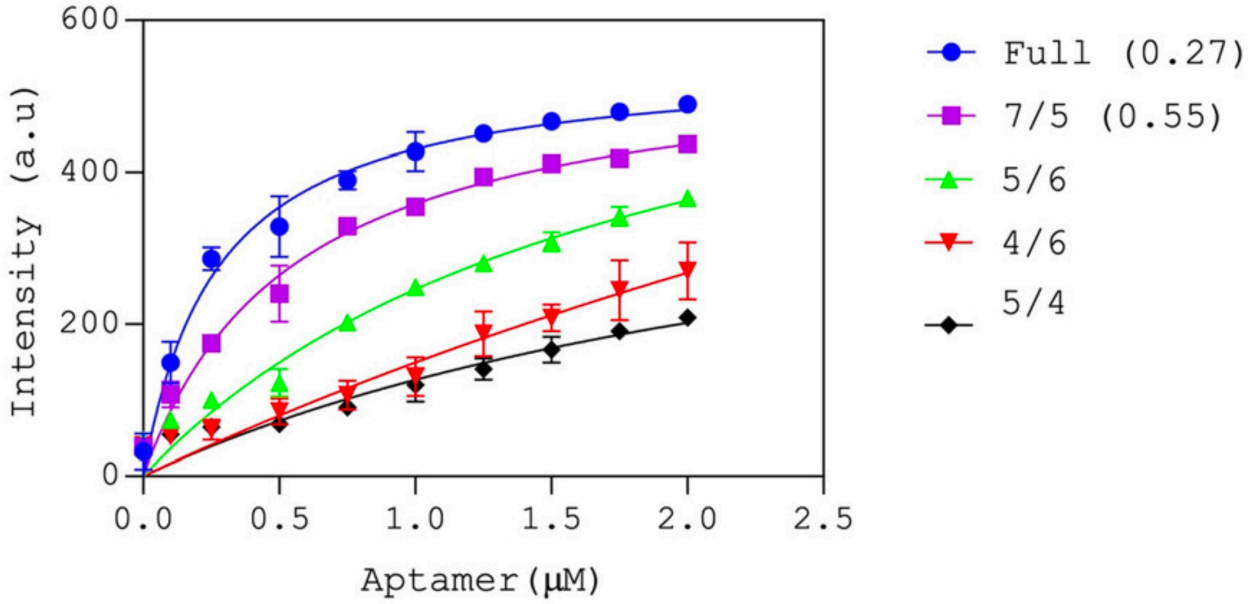


Figure 2.19. Fluorescence titration of each split aptamer into1 μM doxycycline. Fitted K_d values in μM are in brackets. Split aptamers were pre-annealed at 90°C for 5 min and allowed to cool to room temperature before measurements.

2.4.3 Temperature-dependent binding

For a typical binding reaction, it is expected that increasing temperature would weaken binding due to increased entropy contributions. To understand the temperature range for split aptamers, we first mixed aptamers with their targets and then gradually increased temperature. For the full-length OTC5, we observed two stages of fluorescence dropping. The first transition occurred below 20°C, and we attributed it to weak nonspecific association between doxycycline and the aptamer (Figure 2.20, blue trace).[159] Then, relatively stable fluorescence was observed until 30°C, after which, another large fluorescence drop was observed, which was assigned to the dissociation

of the aptamer complex. The melting temperature (T_m) of this step was calculated to be 34°C. At 40°C, the fluorescence dropped to the background level.

For the split OTC5 aptamer (Figure 2.20, red trace), fluorescence drop started from 18°C, and the T_m was fitted to be 23°C. Therefore, in this case, splitting dropped the T_m by 11°C, despite that additional two base pairs were added to one of the stems. Therefore, splitting the aptamer has decreased the thermostability of the binding complex. This can again be rationalized by an even larger entropy loss for the split aptamer upon target binding.

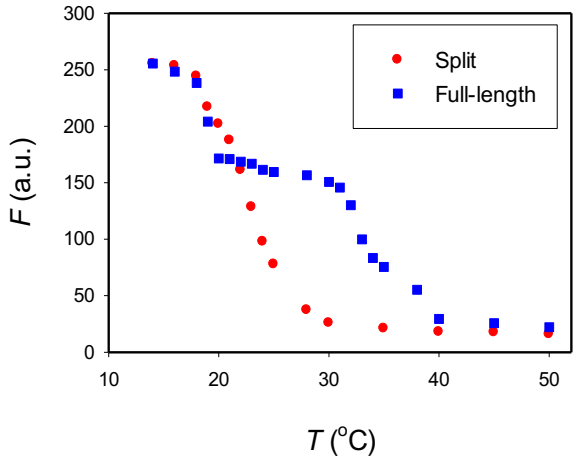


Figure 2.20. Temperature-dependent 1 μM doxycycline fluorescence in the presence of 2 μM of the full-length or the split (5/6 bp) OTC5 aptamer. The measurement was performed in 10 mM MES buffer pH 6.0, 1 mM $MgCl_2$ and 50 mM NaCl.

2.4.4 Thermodynamics of binding using ITC

To further understand the thermodynamics of binding, ITC was performed on the full-length aptamer and two split aptamers with different stem lengths: OTC5b5/4 and OTC5b7/5 (Figure 2.21). ITC can provide full thermodynamic information regarding aptamer binding.[160] All

the aptamers showed exothermic peaks, and the fitted thermodynamic parameters are shown in Table 2.3. The original full length aptamer and OTC5b7/5 stem showed a 3 fold difference in K_d values, but with similar enthalpy change and entropy change, indicating a small drop in affinity.. However, when the stem was shortened further, the K_d was 85-fold higher. Thus, for split aptamers with long stems, likely the initial state was already hybridized and its binding to the target was similar to full-length aptamers.

It was interesting to note that the split aptamers released even more heat or had a more negatively enthalpy change. This can be understood from that the split aptamer had two separate pieces. When they hybridize to form a full aptamer, a lot of hydrogen bonds were formed and they contributed to the heat release. The major factor for the decreased binding affinity was from the entropy term, changing from -61.2 cal/mol·K for the full-length aptamer to -175 cal/mol·K to the split aptamer. Going from a split aptamer to a single binding complex resulted in a much larger entropy loss.

Based on the ITC data and the previous temperature-dependent fluorescence study, at low temperature, when the two halves of a split aptamer are already hybridized even in the absence of a target molecule, the binding performance of split aptamer and full-length aptamers are expected to be similar. However, split aptamers are more susceptible to high temperature due to a very large entropy loss.

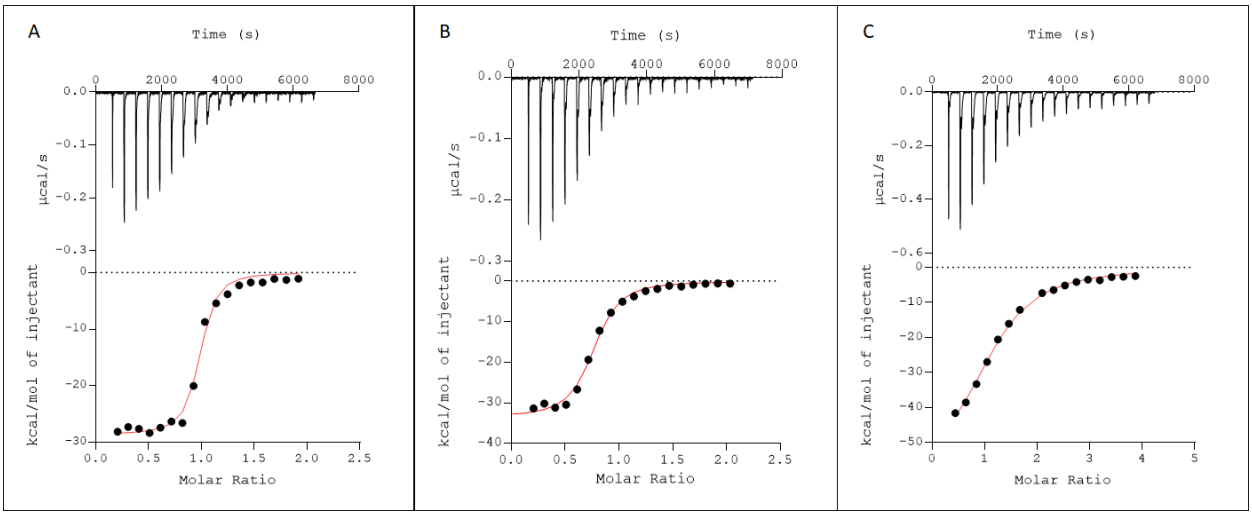


Figure 2.21. ITC traces of (A) the full length OTC5, (B) OTC5a+ OTC5b7/5 aptamer, and (C) OTC5a+OTC5b5/4. All aptamers were pre-annealed for 5 min at 90°C and allowed to cool to room temperature before loading. Experiments were carried out at 20°C.

Table 2.3 Fitted thermodynamic values of ITC experiments.

Aptamer	**Target**	***N***	***K_d* (µM)**	***ΔH* (cal/mol) (x10^4)**	***ΔS*(cal/mol/K)**
Full-length OTC5	Doxycycline	0.95 ± 0.01	0.06 ± 0.02	-2.9±0.6	-64.2
Split OTC5b7/5	Doxycycline	0.74 ± 0.01	0.19 ± 0.13	-3.4 ± 0.2	-83.8
Split OTC5b5/4	Doxycycline	1.1 ± 0.03	2.3 ± 0.13	-5.9 ± 0.2	-175

2.4.5 Binding Kinetics of the Split Aptamers

After understanding the binding thermodynamics, we then studied the effect of reaction kinetics. For split aptamers, there are two ways of mixing. First, we annealed split aptamers and then add target molecules (Figure 2.22, black trace). Alternatively, one half of the aptamer can be

mixed with target analyte first followed by the addition of the other half (Figure 2.22, red and green traces). In this way, we also examined the hybridization kinetics. For biosensor applications, both types of mixing are important. When the split aptamer was annealed prior to addition, the fluorescence increase was instantaneous to a maximum of 4-fold enhancement of doxycycline fluorescence. When the two strands were added separately, the fluorescence only showed a significant increase when the second strand was added, and the kinetics was still very fast. Therefore, in this particular case, using split aptamers did not show a large adverse effect in signaling kinetics.

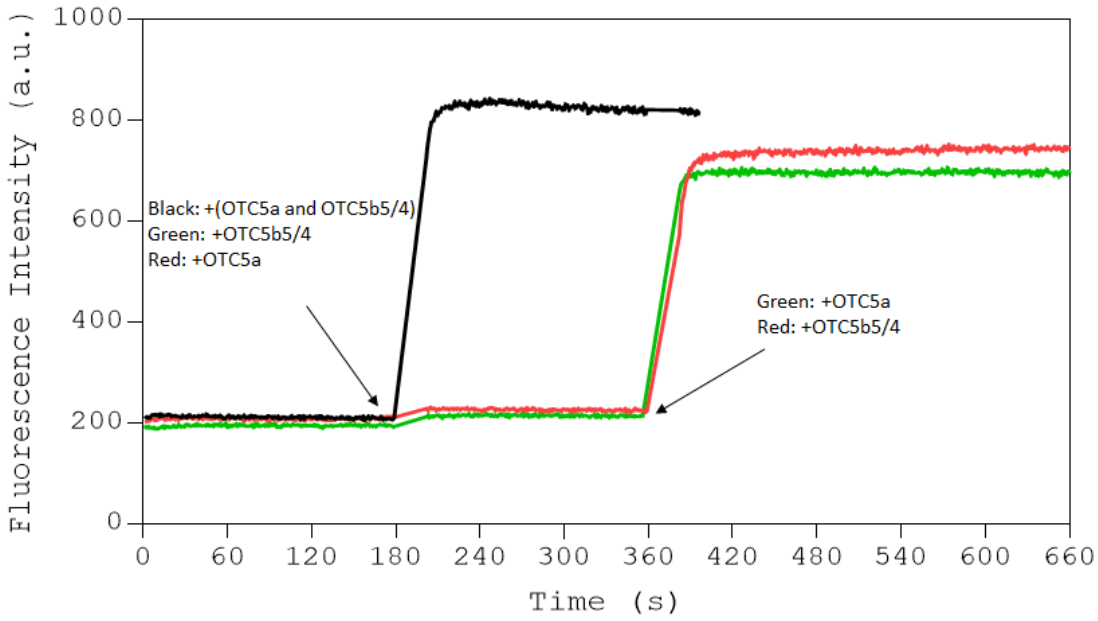


Figure 2.22. Kinetics of the split OTC5a and OTC5b5/4. Black: OTC5a and OTC5b5/4 were pre-annealed at 90°C and 1 μM of the annealed solutions was added at 180 s. Red: 1 μM OTC5a was added at 180 s followed by 1 μM OTC5b5/4 at 360 s. Green: 1 μM OTC5b5/4 was added at 180 s followed by 1 μM OTC5a at 360 s. Excitation was at 370 nm and emission at 535 nm. 200 nM

doxycycline in MES pH 6.0 buffer with 1 mM $MgCl_2$ was read for 180 s to ensure a stable background before the addition of the split aptamer.

2.5 Conclusions

In this work, we used the library-immobilization method (capture SELEX) to select new DNA aptamers for OTC. At least four families of aptamer sequences were obtained, and the OTC5 sequence was studied in detail due to its high binding affinity and generality. Similar binding to OTC, TC and DOX with K_d's around 100 nM to 400 nM was observed using ITC, FP and fluorescence intensity measurements.

These aptamers were different from previously reported ones based on sequence alignment. The intrinsic fluorescence of these tetracyclines allowed for a highly sensitive and selective label-free and dye-free sensing. We then investigated the pH and metal-ion dependency of the OTC5 aptamer and its relevance in the fluorescent detection of tetracycline antibiotics. The sensing performance of the OTC5 aptamer was studied at pH 6.0 and pH 8.3, at which the antibiotics were in charge neutral and negative charged states, respectively. In addition, the effect of a few common divalent metal ions was studied. When compared to other metal ions (Mn^{2+}, Zn^{2+} and Ca^{2+}), Mg^{2+} showed the best fluorescence increase and is required for OTC5 to bind. The optimal concentration of Mg^{2+} was determined to be 2 mM. At pH 6.0, fluorescence enhancement upon binding OTC5 was shown to be greater than at pH 8.3 but had a higher K_d. ITC experiments confirmed this by obtaining fitted K_d values of 0.2 μM and 0.03 μM at pH 6.0 and pH 8.3, respectively. Optimized sensors for TC, OTC, and DOX were developed at pH 6.0 with 2 mM Mg^{2+}. Limits of detection of 0.1, 0.5, and 0.7 nM were achieved using this system TC, OTC, and DOX respectively. This sensor also showed good selectivity when compared with other antibiotics. Milk samples were also tested at pH 6.0. The extracted milk samples showed LODs of 16 nM.. With these optimized

conditions, much more sensitive fluorescence sensors have been developed for the detection of these tetracycline compounds.

Finally, we used this aptamer to study fundamental binding properties of split aptamers. The OTC5 aptamer was then split into stems with different lengths to observe the effects on binding. Kinetics studies of the split aptamers showed that both components of the split aptamer are necessary for detectable fluorescence enhancement, but the order of addition had little effect. The enhancement in each case was also instantaneous. However, splitting the full-length aptamer does decrease binding affinity, except when long binding stems were designed, in which case the initial state of the aptamer is still a full aptamer even without the target. ITC experiments further showed this loss of binding can be attributed to the greater loss in entropy. This understanding allowed us to design a colorimetric signaling method by pre-assemble aptamer complex in the presence of doxycycline. This is the first thorough study of the binding property of split aptamers, and it will be useful for researchers to rationally design biosensors.

Chapter 3 Characterization of an Aptamer Array for the Tetracyclines

The results presented in the following section have been published as:

Zhao, Y., Gao, B., Chen, Y., & Liu, J. (2023). An aptamer array for discriminating tetracycline antibiotics based on binding-enhanced intrinsic fluorescence. *The Analyst*, 148(7), 1507–1513.

Zhao, Y., Gao, B., & Liu, J. (2024). Characterization of the Binding Properties of Ten Aptamers Using the Intrinsic Fluorescence of Oxytetracycline. *ChemistryOpen*.

We recently reported a number of DNA aptamers for tetracycline antibiotics that could all enhance the intrinsic fluorescence of the antibiotics. This fluorescence property allowed us to explore a new method for their detection and for fundamental studies. Only the fluorescence of tetracyclines could be enhanced by adding the aptamers. The fluorescence intensity of other molecules, regardless of whether they fluoresce or not, would not the changed by the addition of the aptamers.

Due to the relatively large structure of tetracyclines, there are many ways for aptamers to bind, and we did indeed observe at least ten families of DNA aptamer sequences that bind.[8] In order to better understand the binding of aptamers to tetracyclines, it is important to perform biochemical binding assays. The intrinsic fluorescence of tetracyclines allows various ways to study binding. More importantly, we want to understand why some aptamers enhance the fluorescence more than others. Since oxytetracycline (OTC) was used as a target to obtain the aptamers, in this study, it was used as the ligand for the binding assays.

3.1 Materials and Methods

3.1.1 Chemicals

All of the DNA samples were purchased from Integrated DNA Technologies (Coralville, IA, USA). OTC and other chemicals were from Sigma-Aldrich. Milli-Q water was used to prepare all the buffers and solutions. Solutions of 100 nM OTC were diluted in a buffer of 10 mM MES pH 6.0, 50 mM NaCl, and 2 mM $MgCl_2$. Each day, OTC solutions were prepared fresh by weighing new powders.

3.1.2 Fluorescence Spectroscopy

The experiments were performed on a Tecan Spark microplate reader with an excitation wavelength set at 370 nm and an emission at 535 nm. For titrations, 100 nM OTC, TC, or DOX was dissolved in buffer (10 mM MES, pH 6.0, 50 mM NaCl, 0 or 2 mM $MgCl_2$). The 10 aptamers were titrated such that the final volume change was kept to be less than 10%. The solution was well mixed after each titration and allowed to equilibrate for 1 min before reading. To study the effect of Mg^{2+}, 100 nM OTC was dissolved in buffer (10 mM MES, pH 6.0, 50 mM NaCl, 0, 0.2, 1, 2 and 5 mM $MgCl_2$). Then each was titrated.

3.1.3 Fluorescence Lifetime

To measure the lifetime of free OTC and the aptamer bound OTC, the experiments were performed on a Horiba Fluorimeter. A solution of 1 μM OTC was dissolved in 500 μL buffer (10 mM MES, pH 6.0, 50 mM NaCl and 2 mM $MgCl_2$). In addition, samples were prepared to contain 2 μM of aptamers. The excitation was a laser with a wavelength of 450 nm, and the emission monochromator was set at 520 nm. The detector voltage ranged from 750 volts to 900 volts, and the measurement range was set to 100 ns and the data were collected for 10000 counts. Each experiment was performed in triplicate.

3.1.4 Isothermal Titration Calorimetry (ITC)

Isothermal titration calorimetry was performed using a MicroCal VP-ITC. 150 μM of OTC was titrated into 9 μM of aptamer. The aptamer and target were both dissolved in pH 6.0 MES buffer with 50 mM NaCl and 2 mM $MgCl_2$. The background heat of target into plain buffer was subtracted and the data was analyzed using the accompanying Origin software.

3.1.5 Selectivity of the sensors

To test the selectivity of the sensors against a series of different molecules (fluorescein, dopamine, quinine, chloramphenicol, kanamycin, ampicillin, and penicillin), 100 nM of each molecule was dissolved in buffer. The fluorescence intensities of these molecules were measured before and after adding 2 μM OTC2, OTC22, or OTC43 aptamers.

3.1.6 Sensor array

To test if our proposed OTC sensor array could discriminate between the different tetracyclines, the fluorescence difference of 50 nM antibiotics in the presence of 0 or 2 μM OTC2, OTC22 or OTC43 aptamers were run in six replicates and the data was analyzed using principal component analysis (PCA, R software). Different OTC concentrations were also tested in a separate study.

3.2 Results and Discussion

3.2.1 The ten oxytetracycline binding aptamers

In this work, we aimed to analyze more sequences to understand the binding of different aptamers, selected using oxytetracycline as the target. To be comprehensive, we analyzed the top 100 most abundant sequences, which collectively represented >65% of the final library (round 20). Using ClustalOmega and manual analysis,[161] we divided these 100 sequences into 10 families along with eight orphan sequences. We chose one sequence from each family and the predicted secondary structures of the ten sequences are shown in Figure 3.1. All of the aptamers have bulged

two-way or three-way junction structures. The internal hairpin regions are colored green/orange, whereas the sequences in the potential binding loops are shown in blue. We previously studied OTC5 (Figure 3.1J) can bind to all the three tetracyclines with K_d values of approximately100 nM.

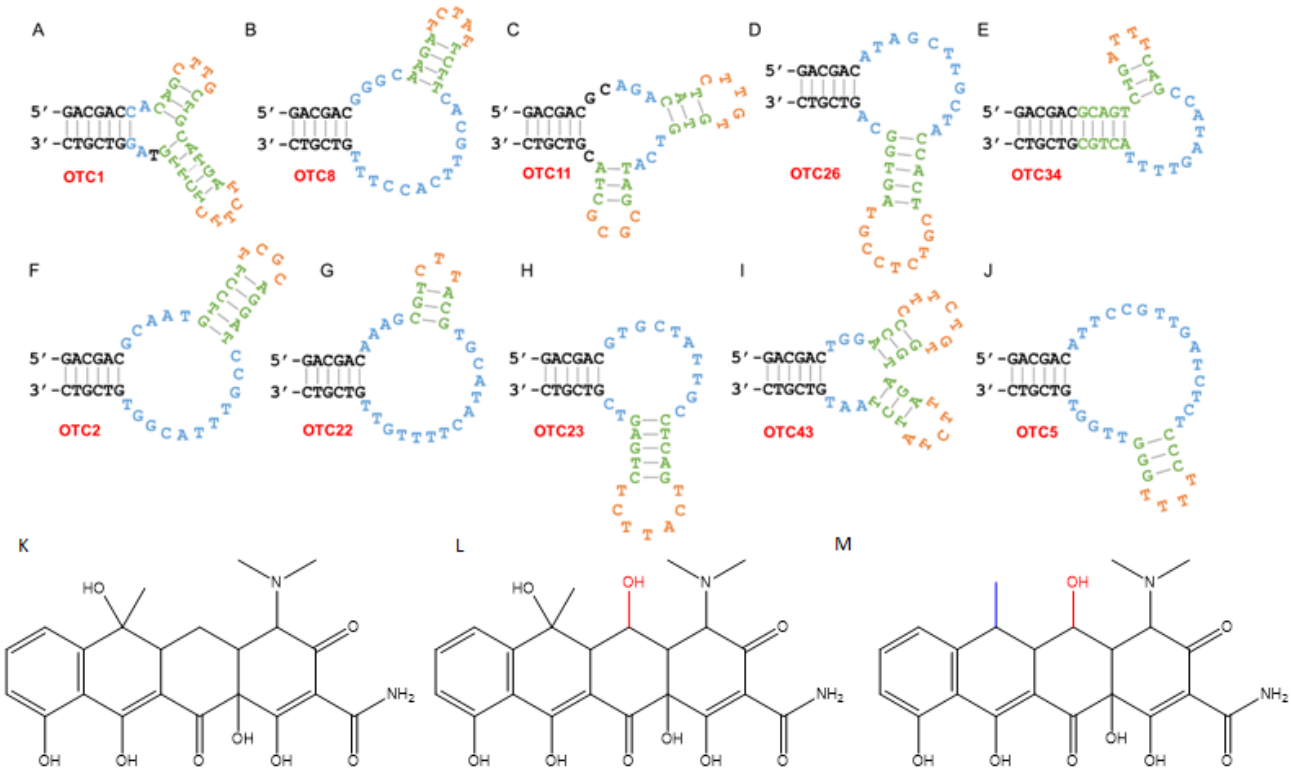


Figure 3.1. The Mfold predicted secondary structures of the ten OTC aptamers studied in this work: (A) OTC1, (B) OTC8, (C) OTC11, (D) OTC26, (E) OTC34, (F) OTC2, (G) OTC22, (H) OTC23, (I) OTC43 and (J) OTC5. The structures of (K) tetracycline, (L) oxytetracycline and (M) doxycycline.

3.2.2 Effect of Mg^{2+}

We first studied the effect of Mg^{2+} on aptamer binding, which was able to affect the intrinsic fluorescence of OTC,[134] and also the binding reaction.[155] We added 2 μM aptamer to 100

nM OTC and compared the fold of fluorescence increase brought upon by the aptamers (F/F_0, Figure 3.2A). Without Mg^{2+}, the fluorescence enhancement of OTC due to aptamer binding was less than 100% for all the ten aptamers (black bars), and all the aptamers behaved similarly. With 2 mM Mg^{2+}, the fluorescence enhancement was quite diverse. Except for OTC26 and OTC34, which showed little fluorescence change even after adding Mg^{2+}, the other eight aptamers were significantly enhanced by Mg^{2+}. This could be related to our selection condition, where 10 mM Mg^{2+} was included. Since OTC2 showed a large fluorescence enhancement, we also measured the aptamer binding in the presence of various concentrations of the aptamer (Figure 3.2B). Without Mg^{2+}, no binding occurred regardless of the OTC2 aptamer concentration. Even concentrations as low as 0.2 mM Mg^{2+} promoted binding. The effect of Mg^{2+} binding saturated around 2 mM Mg^{2+}. Therefore, in the subsequent studies, we included 2 mM Mg^{2+} for all the experiments.

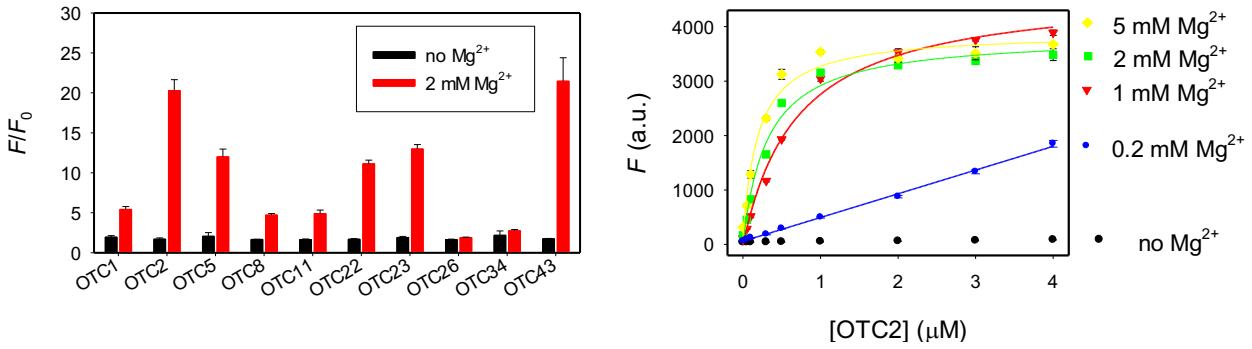


Figure 3.2. (A) The fluorescence intensity ratios of 100 nM OTC in the presence and absence of 2 μM of various aptamers. (B) The fluorescence of 100 nM OTC in the presence various concentrations of OTC2 aptamer at different Mg^{2+} concentrations.

3.2.3 High affinity binding aptamers.

We then measured the binding affinities of these aptamers by gradually titrating each aptamer into 100 nM of OTC solution. For all the aptamers, they induced gradually enhanced fluorescence. Note that each figure has a different *y*-axis scale to best show the binding curves. We previously reported the K_d of OTC5 aptamer to be 0.15 μM (Chapter 2). All the other aptamers, except for OTC8 with a K_d of 2 μM, showed nanomolar binding affinities (Figure 3.3). At this point, it is unclear whether all the aptamers bind OTC in different ways or whether some aptamers belong to the same family. Nevertheless, we have provided a large group of different aptamers for tetracycline antibiotics.

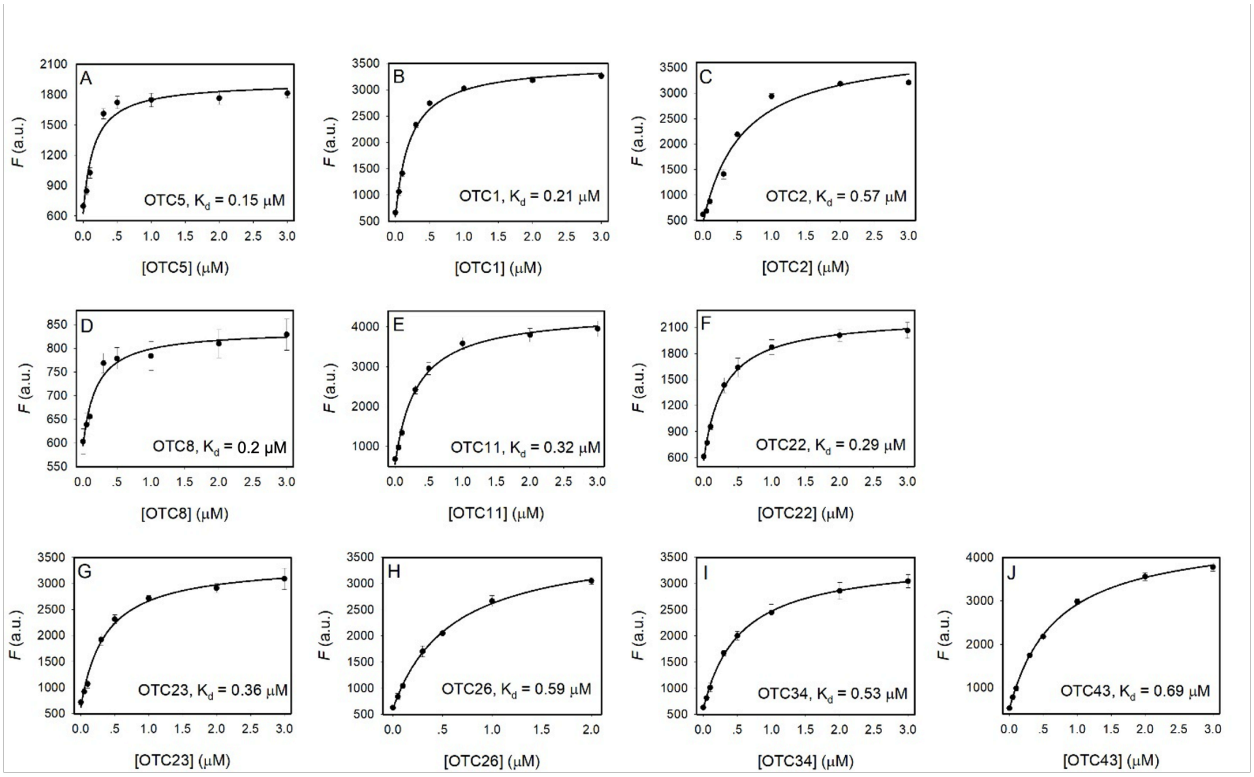


Figure 3.3. Titration curves of various aptamers: (A) OTC1, (B) OTC2, (C) OTC3, (D) OTC5, (E) OTC8, (F) OTC11, (G) OTC22, (H) OTC23, (I) OTC26 and (J) OTC43.

3.2.4 Fluorescence lifetime.

To further understand the mechanism of fluorescence enhancement, fluorescence lifetime measurements were performed. OTC has a quite short sub nanosecond lifetime in aqueous solutions,[123] and our 1 μM OTC showed an average lifetime of 0.65 ns. When 2 μM aptamers were added, the fluorescence lifetime all increased and the largest increase was seen for the OTC43 aptamer, which also had the highest fluorescence intensity enhancement (Figure 3.4A, 3.4B). When we plotted the average lifetime of OTC in the presence of each aptamer, a good correlation between fluorescence intensity increase and lifetime can be observed (Figure 3.4C). Fluorescence quantum yield can be written as $\Phi = \tau/\tau_n$, where τ and τ_n are the measured lifetime and intrinsic lifetime (when quantum yield is 1). Therefore, the increased OTC quantum yield in the presence of the aptamer can be explained by the increased lifetime (Figure 3.4C). We reason that the aptamers provide a more hydrophobic environment for OTC, which decreased collisions with water molecules and thus decreased the rate of non-radiative decay.

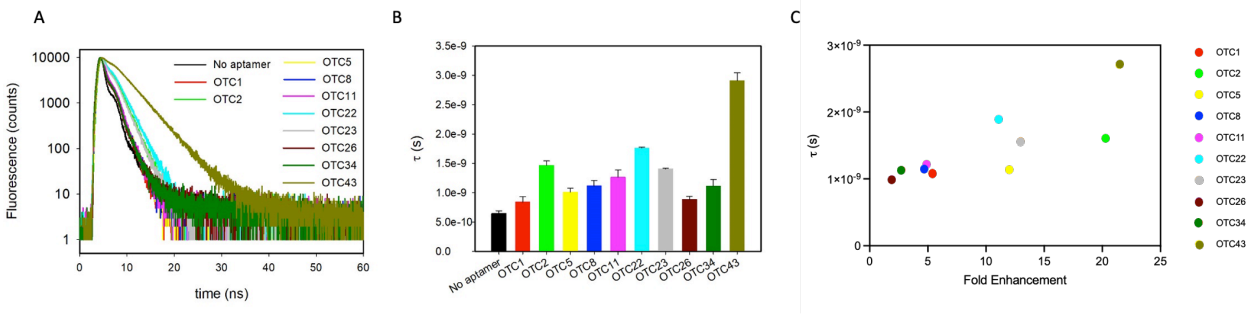


Figure 3.4. (A) Fluorescence lifetime decay traces of 1 μM OTC alone and in the presence of 2 μM aptamers. (B) Average lifetime of the samples. (C) Average fluorescence lifetime vs folds of fluorescence enhancement. The measurements were performed in 10 mM pH 6.0 MES buffer with 50 mM NaCl and 2 mM $MgCl_2$.

3.2.5 Isothermal Titration Calorimetry

To further understand aptamer binding, we picked a few of them for ITC study. We picked OTC2 and OTC22 for their slow kinetics. We also picked OTC43 for its very large fluorescence enhancement. All the binding reactions were exothermic. Both OTC2 and OTC22 showed a similar 1:1 binding of aptamer to target molecule, although OTC2 had a K_d that was ~8 times lower than OTC22. OTC43 had an even higher K_d of >1 μM. OTC43 also generated less heat than OTC2 or OTC22 which were similar to each other. Both the enthalpy and entropy values for OTC2 and OTC22 were similar but OTC43 had a smaller ΔH and less negative ΔS.

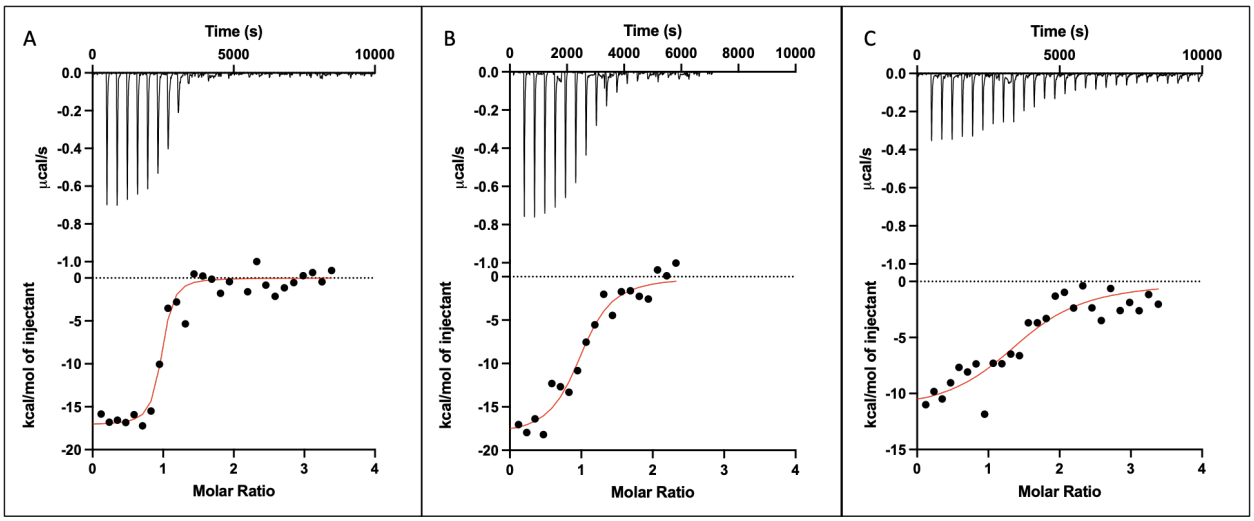


Figure 3.5. ITC traces of (A) OTC2, (B) OTC22, and (C) OTC43. All experiments were done in 10 mM pH 6.0 MES buffer with 50 mM NaCl and 2 mM Mg^{2+}, 9 μM aptamer and 150 μM OTC at 25°C.

Table 3.1. Fitted thermodynamic values of ITC traces.

Aptamer	**Target**	***N***	**K_d (μM)**	**ΔH (cal/mol) (x10^4)**	**ΔS (cal/mol/K)**
OTC2	OTC	0.93 ± 0.02	0.062 ± 0.02	-1.7 ± 0.7	-24.1

OTC22	OTC	0.99 ± 0.05	0.49 ± 0.11	-1.8 ± 0.1	-32.9
OTC43	OTC	1.5 ± 0.1	1.6 ± 0.57	-1.1 ± 0.1	-12.9

Previous work has also reported RNA aptamers that bind tetracyclines and enhance their fluorescence. Some RNA aptamers that were isolated have K_d from 1.7 nM to 600 nM for binding with OTC.[51] Another group reported RNA aptamers with K_d of 7.6 nM that were specific for an analogue of OTC, doxycycline.[52] These K_d values were also determined using fluorescence titration spectroscopy and ITC. The RNA aptamers could enhance the intrinsic fluorescence of the tetracycline antibiotics around 2-3 fold with the doxycycline RNA aptamer able to reach around 6-fold enhancement. ITC studies also showed a similar 1:1 binding stoichiometry for all aptamers and enthalpy values in the same range.

3.2.6 Aptamer binding induced fluorescence changes.

From the studies above, the optimal condition for fluorescence enhancement was determined to be with 2 mM Mg^{2+} at pH 6.0 and we used this condition for all the work here. Figure 3.6A shows the fluorescence spectra of 100 nM OTC after the addition of 2 μM OTC2 aptamer. A large fluorescence enhancement was observed. Such enhancement can also be readily observed by the naked eye (Figure 3.6B). The enhanced fluorescence can be attributed to the aptamer providing a hydrophobic binding pocket to decrease other pathways of relaxation of excited OTC. Binding curves were obtained by gradually titrating the aptamers (Figure 3.7). These curves all have a similar *y*-axis scale (except for Figure 3.7B) to highlight the different extents of fluorescence enhancement in different aptamers. The aptamers can be divided into two groups based on the amount of fluorescence enhancement.

For biosensor applications, the group in the bottom row of Figure 3.7 is more interesting due to a much larger fluorescence enhancement. Outside the 10 families, we also tested an orphan sequence, OTC7, and barely any fluorescence change was observed (Figure 3.8). Therefore, OTC7 served as a negative control to show that not all DNA sequences can enhance the fluorescence of the tetracyclines. The folds of fluorescence enhancement were plotted in Figure 3.6C. Based on these data, five aptamers stood out due to their exceptionally high fluorescence enhancement (OTC2, OTC22, OTC23, OTC43 and the previously studied OTC5).

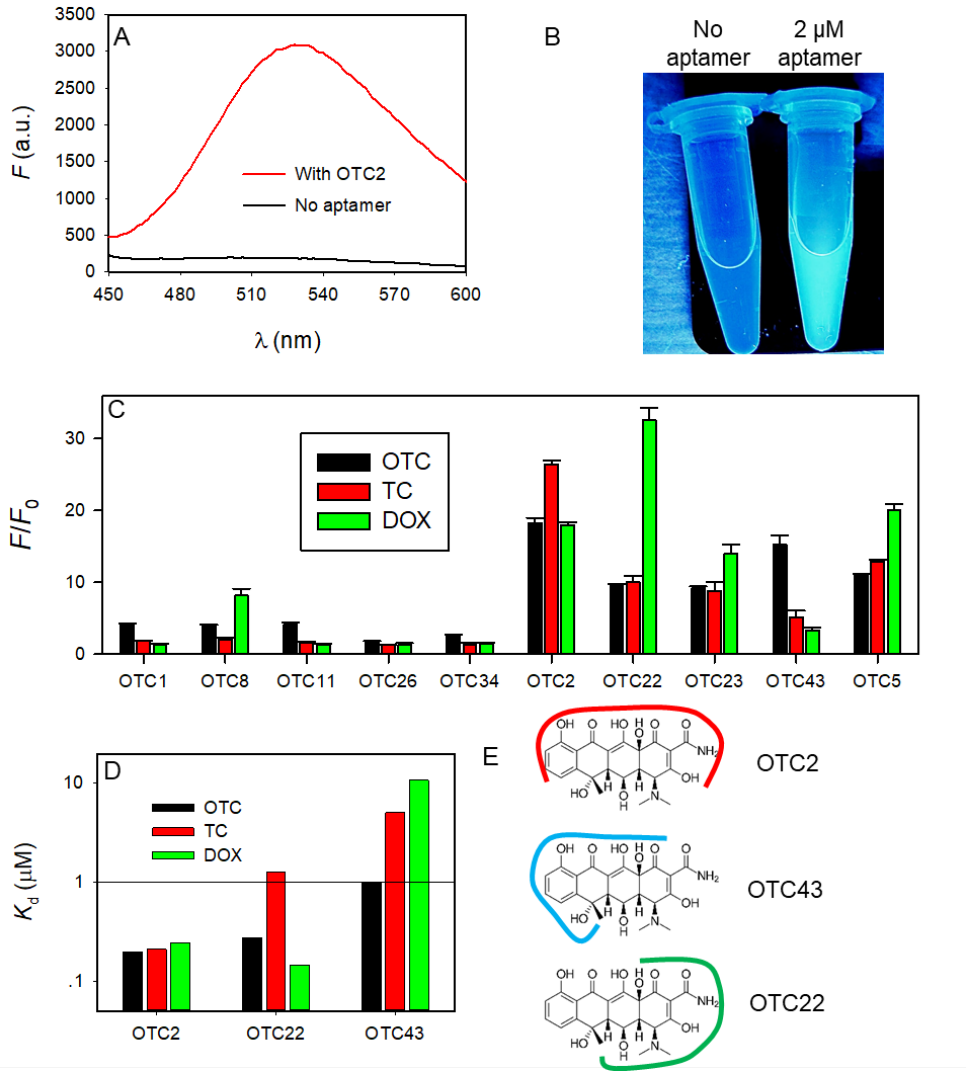


Figure 3.6. (A) Fluorescence spectra of 100 nM OTC before and after adding 2 μM OTC2 aptamer. (B) A fluorescent photograph of 500 nM OTC with (right) and without (left) 2 μM OTC2 aptamer. (C) The fold of fluorescence enhancement of the ten aptamers to the three tetracyclines. (D) The K_d values of the three aptamers. Note the *y*-axis is in log scale. (E) Structures showing aptamers binding to OTC in three different ways, which can explain their selectivity for the three tetracycline antibiotics.

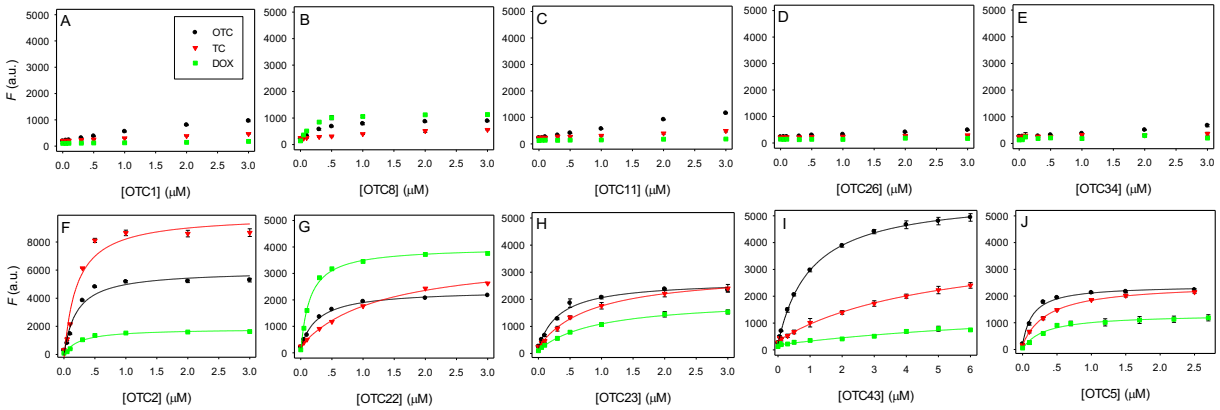


Figure 3.7. The aptamer-dependent fluorescence enhancement of 100 nM of the three tetracyclines in pH 6.0 buffer with 2 mM Mg^{2+} with (A) OTC1, (B) OTC8, (C) OTC11, (D) OTC26, (E) OTC34, (F) OTC2, (G) OTC22, (H) OTC23, (I) OTC43 and (J) OTC5 aptamers.

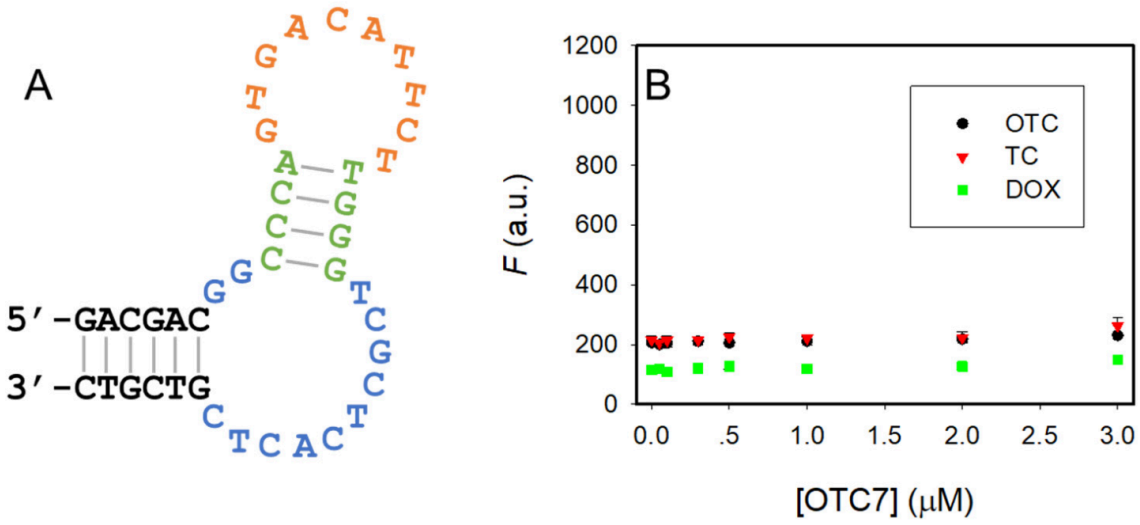


Figure 3.8. (A) The secondary structure of the OTC7, which is an orphan sequence that cannot be assigned to a family. (B) The change of fluorescence of the three antibiotics in the presence of increasing concentration of OTC7. The lack of fluorescence change indicates no binding.

Based on the subtle structural differences of the tetracyclines, we can deduce the binding mechanism. One major type of aptamer has the highest affinity for OTC, followed by TC, and barely binds to DOX (e.g. OTC1, OTC11, OTC26 and OTC43). These aptamers are likely to bind to the common structures of OTC and TC. The other type has the highest affinity for DOX (for example OTC8 and OTC22). OTC2, on the other hand, likely bind in the manner indicated in the top panel of Figure 3.6E, and all three tetracyclines can be bound.

We did not observe absolute selectivity for any of the tetracyclines. The previously reported RNA aptamer had excellent affinity and specificity for DOX.[52] However, that was a much longer sequence and even the truncated aptamer contained 74-nt. Our DNA aptamers were approximately 42-nt, and the binding contact points could be less.

The main goal of this study was to distinguish these three tetracyclines, for which we needed to have probes that have differential responses to them. Therefore, we chose OTC2, OTC22 and OTC43 since they each responded the most to a different tetracycline. We also plotted the K_d values (Figure 3.6D). We focused on these three aptamers for continuing studies.

3.2.7 Highly sensitive detection.

Among the three with the highest fluorescence enhancement, OTC43 had the best selectivity for OTC, OTC22 had the best selectivity for DOX, and OTC2 had the highest response for TC, although the difference was quite small for OTC2. None of the aptamers showed absolute selectivity for any of the tetracyclines. This is understandable since the difference in structure is very small within such large molecules.

We then tested the sensitivity of label-free detection using the respective best aptamers (Figure 3.9). The assays followed the label-free detection method by first measuring the fluorescence of a target tetracycline followed by the addition of an aptamer (Figure 3.9A-C), and the quantification was based on the difference between these two (Figure 3.9D-F). Only the tetracycline antibiotics produced enhanced fluorescence by the aptamers, which is the basis for selective detection. The responses were all linear for target molecules up to 1 μM. The detection limits were calculated to be 0.7 nM OTC, 0.3 nM TC, and 0.4 nM DOX.

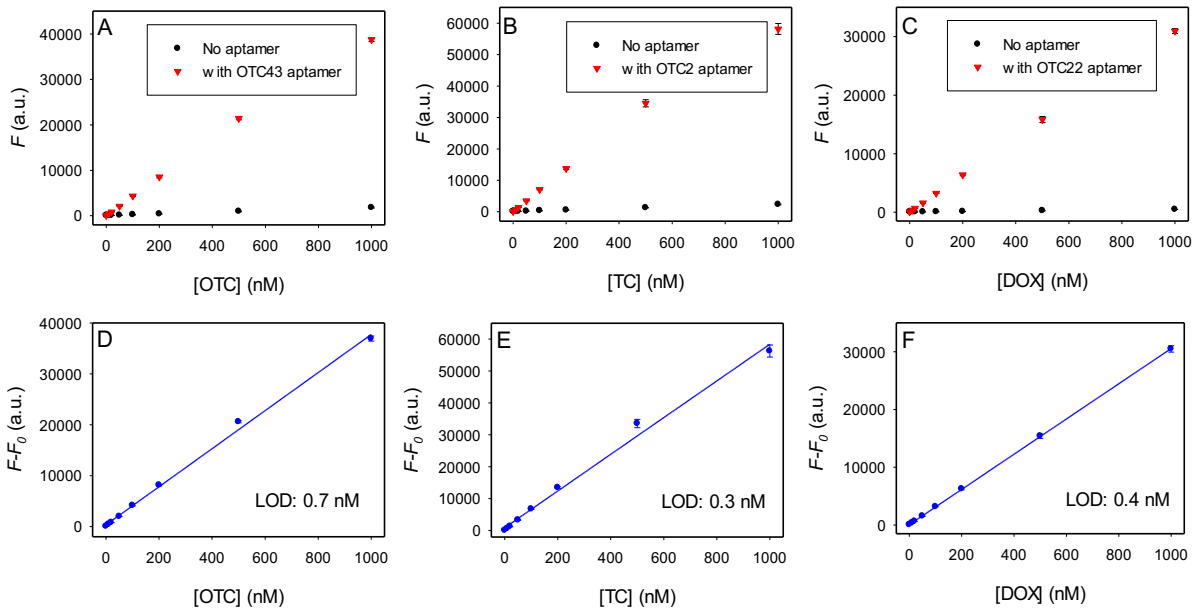


Figure 3.9. The fluorescence of (A) free OTC and after adding 2 μM OTC43 aptamer, (B) free TC and after adding 2 μM OTC2 aptamer, and (C) free DOX and after adding 2 μM OTC22 aptamer. The fluorescence intensity difference before and after adding the aptamers for the detection of (D) OTC, (E) TC, and (F) DOX using their respective aptamers.

3.2.8 A sensor array for discriminating the three antibiotics.

After confirming excellent sensitivity, we measured the selectivity of the three aptamers. As shown in Figure 2.13 in Chapter 2, only the three tetracyclines showed increased fluorescence upon addition of the aptamers. Other molecules such as fluorescein and quinine, although fluorescent, did not show a fluorescence change by the aptamers. The remaining antibiotics were not fluorescent and also did not show any fluorescence changes by the aptamers. Therefore, all these three aptamers are highly selective for the tetracyclines.

Based on the data in Figure 3.10A, we used principal component analysis, which is a powerful data treatment method to maximally differentiate target molecules based on sensor array data.[162–

[164] As shown in Figure 3.10B, with 50 nM antibiotics, TC, DOX, and OTC were well separated, and the rest of the antibiotics were clustered in another region. In addition, we measured the responses to different concentrations of OTC (Figure 3.10). Because the second principal component (PC2) did not exceed 40%, the first principal component (PC1) could be used to quantify the responses (Figure 3.10D). The linear range of detection for OTC was found to be from 10 nM to 200 nM.

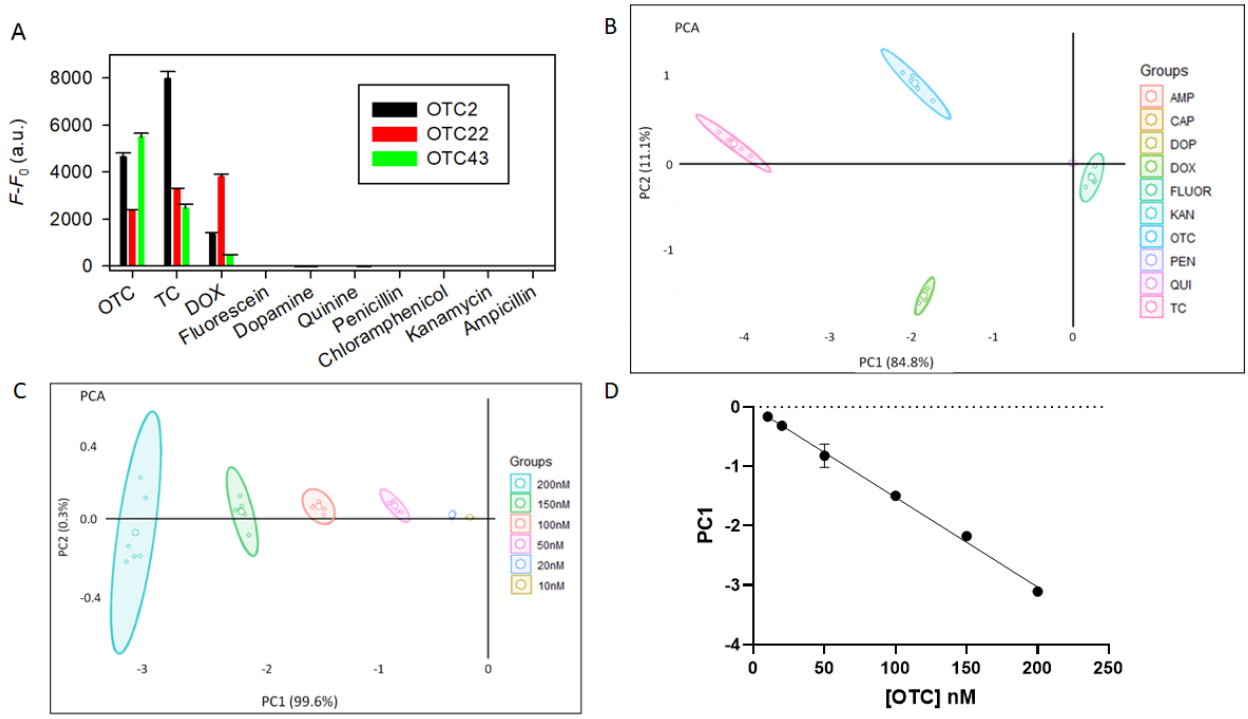


Figure 3.10. Discrimination of different antibiotics using the sensor array. (A) Fluorescence intensity increase among different antibiotics. (B) Canonical score plots of fluorescence responses obtained for different antibiotics at 50 nM antibiotic. (C) Score plots for fluorescence response obtained using varying concentrations of OTC. (D) Plots of PC1 vs concentration of OTC.

3.3 Conclusions

The intrinsic fluorescence of OTC allowed us to conveniently characterize its binding by aptamers. In this work we described 10 aptamers for oxytetracycline that enhance its intrinsic fluorescence to various degrees. Fluorescence enhancement was probed using fluorescence titration spectroscopy and isothermal titration calorimetry. We believe this is the first study in the aptamer field to characterize up to ten aptamers to the same target. Most targets have just one or two representative aptamers. The tetracyclines have a larger structure allow different ways of target binding by aptamers. These ten aptamers all had high binding affinities with nine of them showing nanomolar affinities. They all require Mg^{2+} to promote binding. The increased fluorescence intensities correlated with the increased fluorescence lifetimes and some aptamers showed different reaction kinetics. Using the enhancement of the intrinsic fluorescence of the tetracyclines for binding assays, three aptamers were able to differentiate between three different tetracyclines and their binding led to a more than 10-fold increase in fluorescence. OTC43 was found to be specific to OTC with a limit of detection of 0.7 nM, OTC22 was found to be specific to DOX with a LOD of 0.4 nM, and OTC2 was found to be specific to TC with a LOD of 0.3 nM under optimal buffer conditions. Principal component analysis showed that these new sequences could differentiate between the three tetracyclines as well as other antibiotics and fluorescent molecules. We hypothesize that this selectivity could be due to the way each aptamer binds to a different edge of the tetracycline molecules. This label-free, highly selective aptamer sensor array can be readily paired with other techniques to form improved sensing platforms for different tetracycline antibiotics, especially for portable sensors.

Chapter 4 An Aptamer for Chloramphenicol

The results presented in the following section have been published as:

Zhao, Y., Li, A. Z., & Liu, J. (2023). Capture-SELEX for Chloramphenicol Binding Aptamers for Labeled and Label-Free Fluorescence Sensing. *Environment & Health*, 1(2), 102–109.

4.1 Introduction

Chloramphenicol (CAP) is a broad-spectrum antibiotic used to treat a wide range of bacterial infections by binding to prokaryotic ribosomes and preventing peptide bond formation. Due to its many side effects such as aplastic anemia, leukemia and grey baby syndrome,[165] its use has been banned in most countries.[166] However, its continued illicit use has led to residues being found in the environment, which can increase antibiotic resistance and contaminate the environment.[167]

Aside from instrumentation-based analytical methods, detection of CAP has usually been achieved with immunoassays.[168,169] For small molecule detection, immunoassays have to be performed in a competitive format therefore aptamer-based detection has gained popularity.[170–173] RNA aptamers for CAP with dissociation constants (K_d) <100 μM were previously isolated by Burke et al. in 1997.[55] These RNA aptamers were mainly used to study the RNA-antibiotic interactions and not for developing biosensors. In 2011, DNA aptamers for CAP with reported K_d of 0.8-1 μM were reported by Mehta et al, which were obtained by immobilization of the CAP base (Figure 4.1A).[46] In CAP base, the two chlorine atoms were removed from the CAP structure, which can also compromise the quality of the obtained aptamers. While the full length aptamer is 80-nt, a truncated 40-nt sequence has been used for the development of various biosensors.[45,56,69,174] However, there were varied reports on the binding affinity of this truncated aptamer to CAP.[56,69] In 2016, Duan *et al* used a similar immobilization chemistry and reported

another set of aptamers for CAP, where the claimed K_d reached 0.03 to 0.1 μM.[57] However, no systematic truncation was performed and the full-length aptamers were around 80-nt, which were much less used for the detection of CAP due to its length. [175]

All of the previously mentioned aptamers were isolated by immobilization a CAP analog onto a solid substrate.[46,55,57] This method disallowed access to the entire target due to the covalent linker. In order to access all parts of the unmodified target molecule, capture- SELEX was used. Capture-SELEX involves immobilization of a DNA library onto a substrate and then the target is flowed through to harvest eluted aptamers. Many aptamers with good binding affinities have been selected using this method.[113,116,136] In this study, we selected a few short DNA aptamers for CAP using the capture-SELEX method and compared our new aptamer with a previously reported aptamer. The use of the new aptamer for the detection of CAP in real water samples was also demonstrated.

4.2 Materials and Methods

4.2.1 Chemicals.

All of the DNA oligonucleotides were purchased from Integrated DNA Technologies (Coralville, IA, USA). The DNA sequences and modifications are listed in Table 4.1. CAP and other chemicals were from Sigma-Aldrich. The reagents for aptamer selection were mainly from New England Biolabs.[30] CAP was dissolved in 1× selection buffer (1× SB, 50 mM Tris-HCl, pH 7.8, 300 mM NaCl, 5 mM KCl, 10 mM $MgCl_2$) at final concentrations of 5 mM, 1 mM, and 0.1 mM for the selection. CAP solution was freshly made for each round of the selection to avoid potential degradation.[31] The wastewater was from the City of Kitchener, ON, Canada.

Table 4.1 List of sequences used in this study

DNA Name	Sequence and modification (From 5′ to 3′)
N30 Library	GGAGGCTCTCGGGACGAC(N30)GTCGTCCCGCCTTTAGGATTTACAG
Forward primer	GGAGGCTCTCGGGACGAC
Reverse primer	CTGTAAATCCTAAAGGCGGGACG
Biotin-reverse primer	/5Biosg/ CTGTAAATCCTAAAGGCGGGACG-3
Biotin-column	GTCGTCCCGAGAGCCATA/3BioTEG/
CAP1	CGACATAGAGGATCCATCTTGGGGTGTGTAGTGTGTCG
CAP1short	CGACATAGAGGAT----------GGTGTGTAGTGTGTCG
CAP1mut	CGACATAGGAAGTCCATCTTGGGGTGTGTAGTGTGTCG
CAP3	CGACCTAGTGTCCATCGTTCAGTTCCGATTTCTGGTCG
CAP4	CGACATATGCTAATCTTGTAGATGTACTCTATGTGTCG
FAM-CAP1	/56-FAM/CTCTCGACGACACGACATAGAGGATCCATCTTGGGGTGTGTAGTGTGTCGT
Quencher-DNA	TGT CGT CGA GAG /3IABkFQ/
CAM80	AGCAGCACAGAGGTCAGATGACTTCAGTGAGTTGTCCCACGGTCGGCGAGTCGGTGGTAGCCT ATGCGTGCTACCGTGAA

Note: /5Biosg/ is biotinylation at the 5′-end, and /3BioTEG/ is biotinylation at the 3′-end with extended spacer. 56-FAM is derivative of fluorescein with maximum excitation at 495 nm and maximum emission 520 nm. 3IABkFQ is Iowa Black FQ with absorbance range from 420-620 nm. The two blue regions in the N30 Library sequence are complementary. In CAP1short, the dashed region indicate the deleted hairpin in CAP1. The mutated bases are indicated in red.

4.2.2 Capture-SELEX for CAP.

Our selection was done using the previously described capture-SELEX method.[30] The initial concentration of CAP was 5 mM dissolved in 1× SB. The concentration of CAP was reduced at round 9 to 1 mM and at round 12 to 0.1 mM. A total of 13 rounds of selection was done before the final library was sent for deep sequencing (McMaster University). Since the convergence of the

library was low, four more rounds of selection were carried out using the library from the end of the previous round 11 using 1 mM CAP.

4.2.3 ITC.

Isothermal titration calorimetry (ITC) was performed using a MicroCal VP-ITC. 0.4 mM of CAP was titrated into 20 μM aptamer (CAP1 and CAP3) at 25°C. For CAP4, 2 mM CAP was titrated into 50 μM aptamer. Aptamers were pre-annealed at 90°C for 5 min in 1× SB and allowed to cool to room temperature before loading into the ITC cell. Both the target and the aptamer were dissolved in the same selection buffer. Background heat of titrating antibiotics into the buffer was subtracted. Data were analyzed using the accompanying Origin software.

4.2.4 Biosensor based on the strand displacement reaction

FAM-labeled aptamer (5 μM) and quencher-labeled strand (10 μM) were first hybridized in 1× SB by heating for 3 min at 95°C followed by gradual cooling to room temperature. This hybridized solution was diluted to 100 nM in 1× SB and was added to each well of a 96-well microplate. The fluorescence was monitored at 520 nm with 485 nm excitation. The background was run prior to the addition of the target to ensure a stable background signal. Then various concentrations of CAP were added after the background had stabilized. The same was repeated for real water samples.

4.2.5 Thioflavin-T (ThT) based fluorescence sensing.

CAP1 aptamer (1 μM) and ThT (500 nM) were mixed in Tris-HCl buffer pH 7.8 with 10 mM Mg^{2+}. The fluorescence emission at 495 nm was first read with an excitation wavelength of 425 nm. The background signal was run for approximately 12 min to ensure a stable background before CAP was added and fluorescence changes were recorded. The buffer was then replaced with real water samples for the detection.

4.3 Results and Discussion

4.3.1 Capture selection of CAP binding aptamers.

The structure of CAP is shown in Figure 4.1A (left). Unlike the previous selections using immobilized CAP base (Figure 4.1A, right), our capture-SELEX method used unmodified CAP. The DNA library contained a region of 30 random nucleotides flanked on each side by a primer binding region.[136] The primer binding regions formed a stem, which would fold the library into a hairpin structure.[77] The library was first hybridized with a short complementary strand bearing a biotin tag. Streptavidin-coated agarose beads were used as the substrate for immobilization. Upon incubation with CAP, aptamer sequences were released from the beads by the formation of the hairpin structure, collected, and amplified using PCR.

A total of 13 rounds of selection were performed, during which the concentration of CAP was gradually decreased from 5 mM to 0.1 mM. The round 13 PCR amplicons were deep-sequenced. The sequencing results were processed with the Geneious software and the most abundant family made up less than 1% of the final library. We suspected that the affinity of CAP binding aptamers might not be very high and using too low of CAP concentration may lead to relative more nonspecific dissociation. We then decided to keep 1 mM CAP and re-started from the end of round 11 for three more rounds. The final PCR amplicons from the re-selected round 14 were also deep-sequenced. A total of 80,865 sequences were obtained and the sequence with the highest percentage was the same as that in the previous round 13 (before the re-selection, Figure 4.1B).

4.3.2 Three families of CAP binding aptamers.

We then aligned the top 10 sequences from both sequencing results together (Figure 4.1B), and three families were identified. Family 1 contained only three sequences and we named the most abundant sequence CAP1. The sequences in Family 1 appear to be highly conserved and only one position switched from a guanine to an adenine. Two identical sequences were found in Family 2, and we named this sequence CAP3 (the third most abundant sequence from the first sequencing result). Family 3 contained a lot more sequences, although each at a lower abundance, and we can identify two conserved regions linked by a small hairpin structure. Circular permutation was observed for these two conserved regions, which is often an indication of the same way of aptamer binding to two orientations of the target molecule (flipped by 180 degree).[121,176,177] A representative sequence in this family is named CAP4. Aside from these, there are also a few orphan sequences that cannot be assigned to any of the above families. Due to their low abundance, they were not analyzed further. The Mfold predicted secondary structures of the three representative aptamers are shown in Figure 4.1C-E, respectively. They all appeared to have an internal hairpin structure. The sequence of the hairpin is conserved in CAP1 and CAP3, whereas CAP4 has a variable hairpin.

CAP1 is more G-rich (>35%) than the other sequences. We also compared our newly selected aptamer to a previously reported CAP aptamer (CAM80), but did not find any sequence overlap (Figure 4.2), indicating that we have selected new aptamers. In addition, the RNA aptamer is featured with two A-rich loops, while our aptamer is rich in guanine.

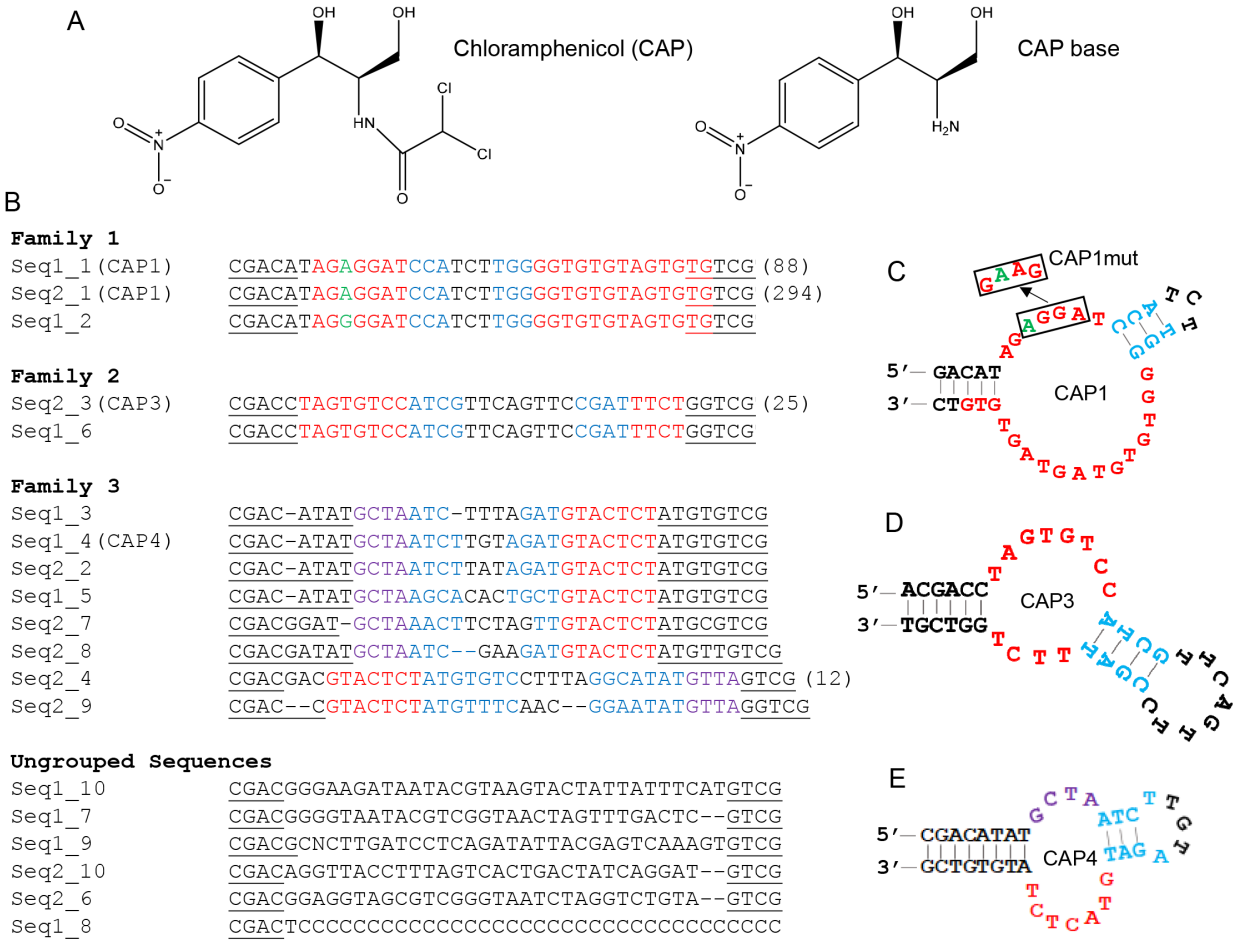


Figure 4.1. (A) Structures of CAP and CAP base. (B) Top 10 most abundant sequences after sequencing from the first (Seq1) and the second (Seq2) sequencing. The bases in red are conserved within each family, whereas the remaining sequences have little to no homology. The number of copies of each sequence is in brackets for the selected sequences. The sequences without a copy number contained less than 10 copies. Secondary structures of the (C) CAP1, (D) CAP3, and (E) CAP4 aptamers predicted using Mfold.



Figure 4.2. Alignment of selection results with CAM80 with the help of ClustalOmega. From the results, CAM80 and other sequences from a selection done by Duan *et al* (No, 1,4,5,6 and 10), do not align with the sequences obtained in this work.

4.3.3 Binding Assay using ITC.

Characterization of aptamer binding was first performed using isothermal titration calorimetry (ITC). In our experiment, 0.4 mM CAP was titrated into 20 μM of CAP1 aptamer at 25°C in the 1× SB (Figure 4.3A). The downward spikes indicate an exothermic binding interaction and a dissociation constant (K_d) of 9.8 μM was fitted. A K_d of 9.8 μM is comparable with the previously reported RNA aptamer, for which the best K_d was 2.1 μM.[15] During this experiment, we noticed that annealing the aptamer was important. The CAP1 aptamer was annealed by heating the aptamer in the buffer followed by gradually cooling to room temperature before ITC experiments. This was done to promote the formation of proper secondary structures. Without annealing, we obtained a smaller heat (only 64% of the annealed sample) and the data cannot be properly fitted (binding stoichiometry much smaller than 1), suggesting a fraction of the aptamers were misfolded before annealing (Figure 4.4D, K_d = 5.6 μM, fitted by forcing N=1 , ΔH = -4703 cal/mol, ΔS = 8.3). Without pre-annealing the heat generated is around 70% lower. However, without forcing N=1,

the fitted value for the binding stoichiometry (N) was very small (N=0.05, ΔH = -9.3x104 cal/mol, ΔS = -289), and the data could not be properly fitted.

To further understand the binding of the aptamer, we then studied a few mutants of CAP1. First, a truncated version of the CAP1 aptamer was tested, where the smaller stem loop was removed (CAP1short), but no binding was observed (Figure 4.4A). Thus, this hairpin structure is important. We further tested a mutant (CAP1mut) by changing the four bases in the main loop from AGGA to GAAG (Figure 4.1C green bases), for which no sign of binding was observed either (Figure 4.4B). This indicates that the loop may be directly involved in the binding of CAP. These mutation studies indicated that the binding of CAP1 aptamer to CAP was specific.

CAP3 also showed some binding but to a lesser degree than CAP1 with a fitted K_d of 78 μM (Figure 4.3A). CAP4 had even weaker binding and a K_d of 98 μM was obtained (Figure 4.3C). For CAP1, the binding stoichiometry was 1:1. It has a large entropy loss upon target binding and thus the binding was mainly driven by enthalpy. Overall, CAP1 was our best aptamer candidate. A K_d of 9.8 μM was quite reasonable for a molecule like CAP containing a single aromatic ring and a few hydrogen bond donors/acceptors. For comparison, the classical adenosine aptamer has a K_d of around 6 μM.[178,179] We reason that reports of K_d values down to 0.03 μM CAP[57] might not be from aptamer binding to CAP but from some other events. [68,151,152,180]

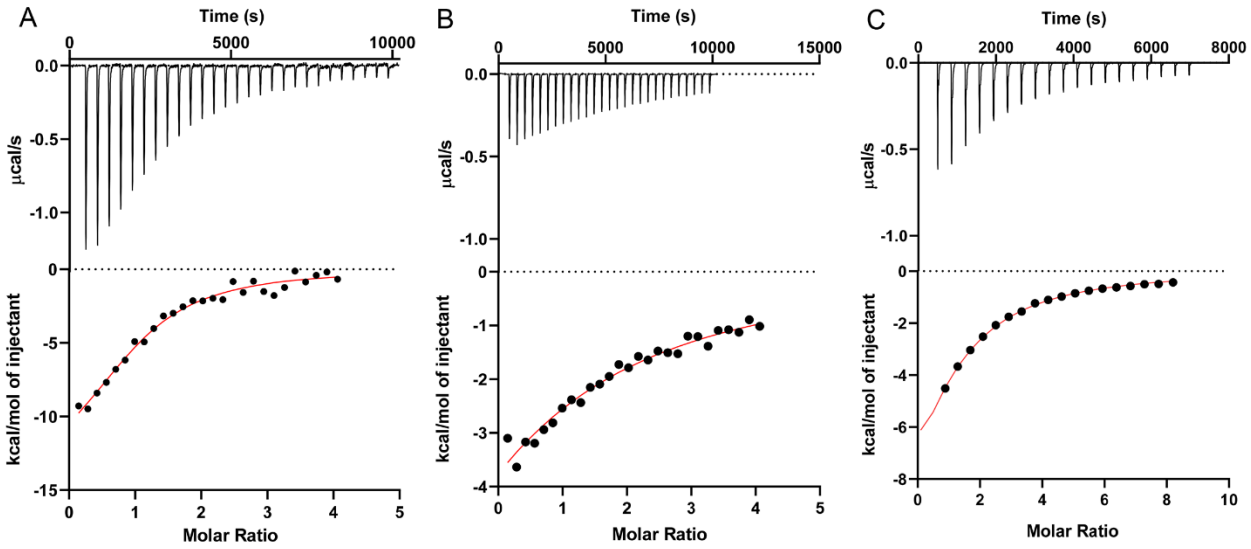


Figure 4.3. ITC traces of (A) 0.4 mM CAP into 20 µM CAP1 aptamer, (B) 0.4 mM CAP into 20 µM of CAP3, and (C) 2 mM CAP into 50 µM CAP4 at 25°C. Aptamers were pre-annealed at 90°C for 5 min in 1× SB.

Table 4.2. Thermodynamic values of titrating CAP into various aptamers based on ITC.

Aptamer	N	K_d (µM)	ΔH (cal/mol) (× 10^4)	ΔS (cal/mol/k)
CAP1	1.0 ± 0.1	9.8 ± 0.5	-1.5 ± 0.2	-27.0
CAP3	1.7 ± 0.5	52 ± 14	-8.9 ± 3.6	-10.5
CAP4	0.7 ± 0.1	112 ± 6	-2.9 ± 0.5	-80.2
CAM80	-	-	-	-

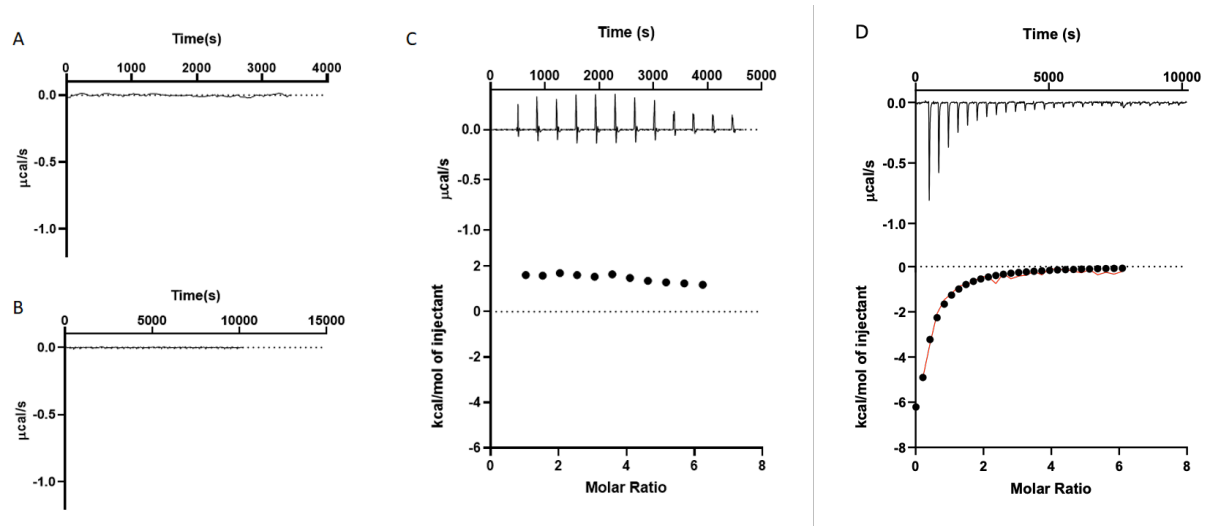


Figure 4.4. ITC traces of (A) a truncated CAP1 (CAP1short) aptamer, and (B) a mutant of CAP1 (CAP1mut) titrated with 0.4 mM CAP and 20 µM aptamer at 25°C in 1× SB. (C) ITC trace of 20 µM CAM80 and 1 mM CAP using the original selection buffer conditions (20 mM Tris-HCl pH 7.6, 100 mM NaCl, 5 mM KCl, 2 mM $MgCl_2$, 1 mM $CaCl_2$). (D) ITC trace of CAP1 without pre-annealing.

4.3.4 Comparison with previously reported aptamers

As mentioned in the section 4.1 and section 1.2.7, two DNA aptamers and an RNA aptamer were previously reported. One of the DNA aptamers were most extensively used, and the secondary structure of the full-length 80-mer aptamer is shown in Figure 4.5A.[46] The 40-mer sequence in the random region was used in most sensor work (shown in yellow), where the two fixed primer binding regions were removed (Figure 4.5B).[69] While all the literature showed a structure in the bottom of Figure 4.5B, this structure was not predicted by Mfold and we saw a structure on the top panel of Figure 4.5B. We previously did ITC on the 40-mer truncated sequence but observed no binding.[69] We used 10 µM aptamer for that experiment, which should be sufficient if it has a literature reported K_d of around 1 µM. Ma *et al* also performed ITC studies on the 40-mer sequence,

and they obtained a K_d value of 237 μM CAP, which was much higher than the previously claimed K_d of around 1 μM.[56] Ma *et al* used an aptamer concentration of 22 μM and 3 mM CAP for this experiment with buffer conditions of 20 mM Tris-HCl pH 7.6, 50 mM $MgCl_2$, 5 mM KCl, 2 mM $CaCl_2$ (experimental conditions obtained from personal communications). We previously made the argument that if the full-length 80-mer can bind, the truncated 40-mer is unlikely to bind due to their very different predicted secondary structures.[69] Since previous ITC was performed using the truncated 40-mer, we herein also tested the full-length 80-mer. Under the same buffer conditions and pre-annealing as CAP1 (50 mM Tris-HCl, pH 7.8, 300 mM NaCl, 5 mM KCl, 10 mM $MgCl_2$), no binding was observed (Figure 4.5D). To further confirm it, we also tried the buffer reported in the original paper (20 mM Tris-HCl, pH 7.6, 100 mM NaCl, 5 mM KCl, 2 mM $MgCl_2$, 1 mM $CaCl_2$) but still no binding was observed (Figure 4.4C). Therefore, our ITC experiments did not support binding of the 80-mer sequence.

The structure of the RNA aptamer for CAP is shown in Figure 4.5C.[55] It has very interesting adenine-rich loops, which is very different from our reported aptamers. CAP1 is a shorter sequence with a well-defined secondary structure. Since DNA has higher stability and lower cost compared to RNA, we believe that CAP1 will be useful for developing analytical biosensors.

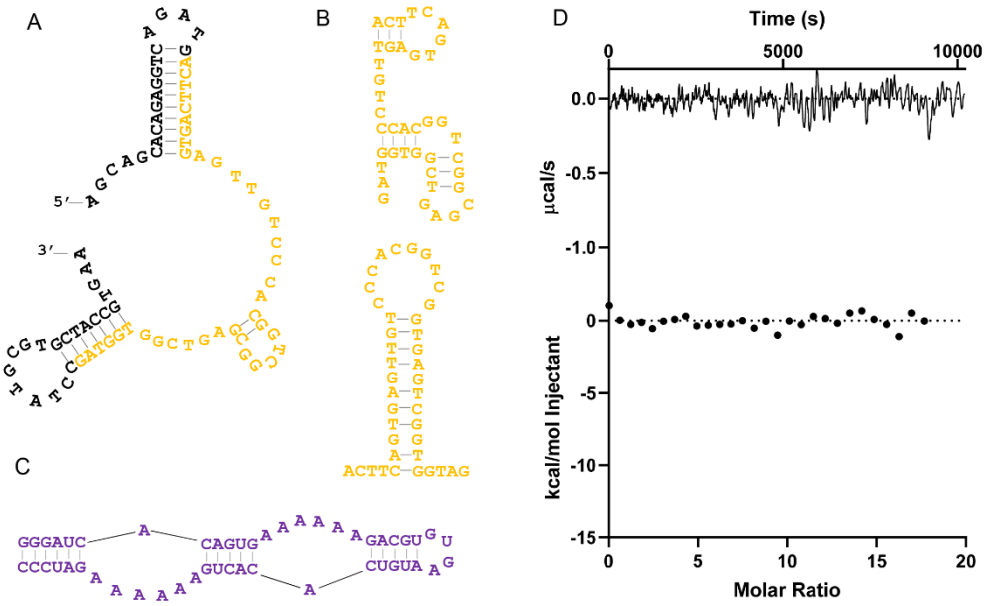


Figure 4.5. Secondary structures of (A) the full length 80-mer CAP aptamer, (C) the truncated 40-mer of the CAP aptamer (from the yellow region in panel (B)) predicted by Mfold (top) and from the literature (bottom). (C) The RNA aptamer for CAP. (D) ITC of 3 mM CAP into 34.5 µM previously reported 80-nt CAM80 aptamer.

4.3.5 Strand displacement reaction for sensing of CAP

After confirming binding, we then designed a strand-displacement fluorescent sensor by using a covalently labelled carboxyfluorescein (FAM) and quencher system (Figure 4.6A). The CAP1 aptamer was extended on the 5′ end that would be complementary to the 12-mer quencher-labeled strand. The background signal was allowed to run prior to the addition of CAP to ensure a stable background. The fluorescence intensity jumped and stabilized almost instantaneously upon addition of CAP (Figure 4.6B). We then varied the concentration of CAP, and the fluorescence was immediately read. A binding curve was obtained with an apparent K_d of 377 µM CAP, much higher than what was measure by ITC. This is due to competition with the complementary strand to increase the apparent K_d value, which was well documented in the literature.[116,141,181]

Using this system, a limit of detection of 14 μM CAP was calculated (3σ/slope, where σ is the background fluorescence variation without CAP). A selectivity test was also done using 0.15 mM of other antibiotics (Figure 4.6D). The sensor showed very good selectivity for CAP as no signal was observed with the other tested antibiotics. This was not surprising since these antibiotics have quite different structures. This limit of detection is not very low, but this assay further confirmed specific aptamer binding. Given the similar K_d of CAP1 and the adenosine/ATP aptamer, similar signal amplification methods can also be applied to the detection of CAP.

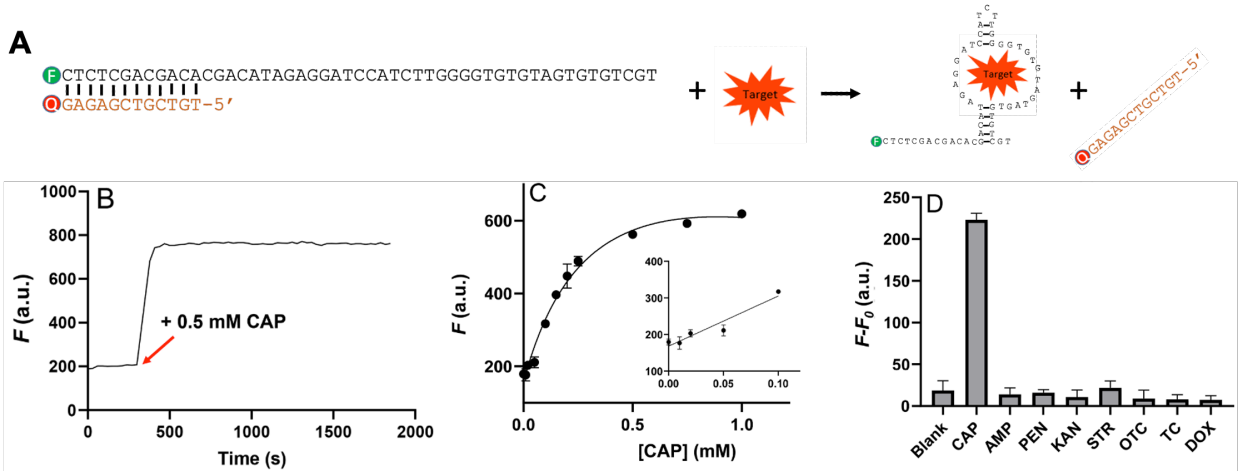


Figure 4.6. (A) Schematic of the strand displacement fluorescent sensor. (B) Kinetics of 100 nM sensor with the addition of 0.5 mM CAP in 1× SB. (C) Fluorescence intensity as a function of CAP concentration. Inset: linear response at low concentrations. (D) Selectivity of sensor against 0.15 mM antibiotic: penicillin (PEN), kanamycin (KAN), streptomycin (STR), oxytetracycline (OTC), tetracycline (TC), and doxycycline (DOX).

4.3.6 Fluorescence Sensing Using ThT

Since the sensitivity of the strand displacement-based assay was low, we further explored a label-free detection method. Thioflavin-T (ThT) is a small molecule that can bind to G-rich DNA, which can enhance its fluorescence intensity.[125] Since the CAP1 aptamer is rich in guanine, we then used

ThT staining. By mixing ThT and the CAP1 aptamer, the fluorescence of ThT would increase. CAP binding might displace ThT, leading to decreased fluorescence (Figure 4.7A). This was previously observed for the adenosine aptamer.[182] The excitation wavelength was set at 425 nm and emission at 495 nm. The CAP1-ThT sensor exhibited around a final drop of around 70% when more than 50 μM CAP was added. Using various concentrations of CAP, a calibration curve was generated with a measured K_d of 4.2 μM (Figure 4.7B). This value was comparable with the value obtained from ITC. In buffer (50 mM Tris-HCl, pH 7.8, 10 mM $MgCl_2$), the limit of detection was calculated to be 1 μM. A high salt concentration is often used in aptamer selection to screen nonspecific electrostatic interactions. Na^+ and Mg^{2+} were studied using ThT and fluorescence. Measurements were done at an excitation wavelength of 425 nm and an emission wavelength of 495 nm with 1 μM CAP1 and 0 or 100 μM CAP in 50 mM Tris-HCl buffer pH 7.8 with varying concentrations of salt. Each salt was done separately. Without Mg^{2+}, adding NaCl did not affect the fluorescence change much, indicating that Mg^{2+} was required for aptamer binding. Without Na^+, Mg^{2+} alone can support aptamer binding, and the best signal change was seen with 10 mM Mg^{2+}, which was used for our ThT experiments. NaCl was determined to be nonessential for CAP1 binding and was thus eliminated from the buffer for the ThT assays (Figure 4.8A). For the ThT assay, a lower salt concentration is preferred to increase binding between ThT and DNA. Using this label-free method, we obtained 14-fold better limit of detection compared to using the strand-displacement assay. The binding between ThT and CAP1 aptamer was also studied by titrating up to 10 μM CAP1 into 2.5 μM of ThT and a K_d of 2.3 μM was fitted (Figure 4.8B). Given the similar K_d values obtained from ITC and ThT, and the low concentration of ThT used (500 nM), ThT did not serve as a strong competitor in this reaction. The selectivity of this system was then tested against various antibiotics and this system was also very selective for CAP (Figure 4.7C).

Given the simplicity of this method, we also used ThT staining to test the binding of the CAP3 and CAP4 aptamers. CAP3 showed a K_d of 46 μM (Figure 4.8C), comparable to the value obtained from ITC. The CAP4 data cannot be fitted but the K_d should be close to 100 μM (Figure 4.8D). This experiment also confirmed that CAP1 was the best aptamer for binding CAP.

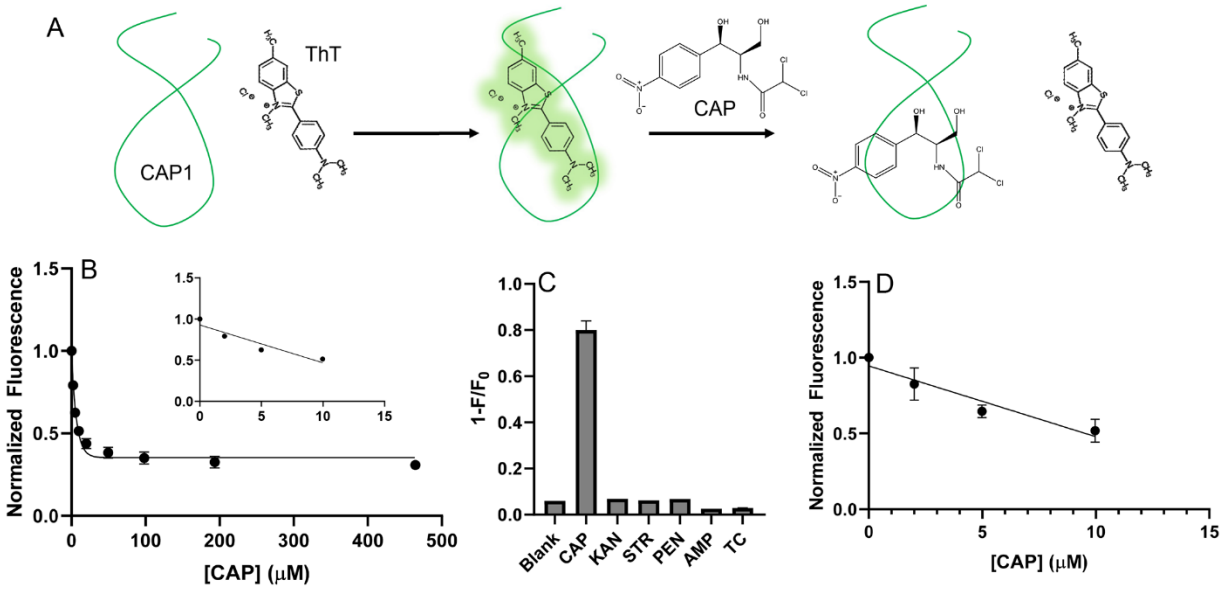


Figure 4.7. (A) Scheme of using ThT and CAP1 to detect CAP. (B) Calibration curve using 1 μM CAP1 and 0.5 μM ThT in 50 mM, pH 7.8 Tris-HCl buffer with 10 mM $MgCl_2$. Inset: the linear region at low CAP concentrations. (C) Selectivity of the ThT sensor with various antibiotics. (D) Fluorescence intensity after the addition of varying amounts of CAP in filtered Lake Ontario water.

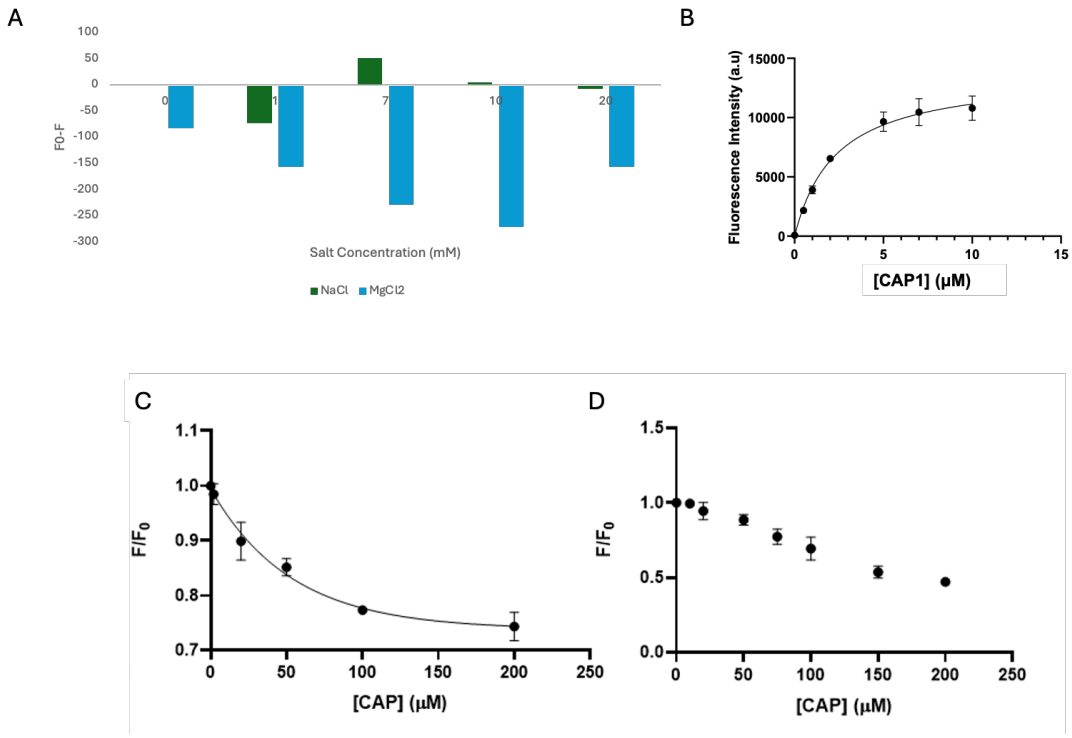


Figure 4.8.(A) The effect of different concentrations of NaCl and $MgCl_2$ on the fluorescence change of the CAP1-ThT system. (B) Titration curve of CAP1 aptamer into 2.5 μM Thioflavin-T in 20 mM Tris-HCl pH 7.8, 10 mM $MgCl_2$. A K_d of 2.3 μM was fitted.(C) CAP3 (K_d = 46 μM), and (C) CAP4 (unable to fit K_d) and 0.5 μM ThT.

4.3.7 Real Water Samples with the ThT-based Sensor.

This ThT-based sensing system was then tested using filtered lake water from Lake Ontario. The filtered water was buffered to contain 20 mM Tris-HCl, pH 7.8 with 10 mM $MgCl_2$. The buffered lake water was then spiked with varying concentrations of CAP before 100 nM CAP1 and 500 nM of ThT was added. From this, a linear drop was also observed in low CAP concentrations and a limit of detection of 1.8 μM was obtained (Figure 4.7D). This value was comparable with that in the clean buffer, confirming that this aptamer can also work in environmental water samples. A

similar experiment was conducted using even more challenging a wastewater sample, in which a limit of detection of 3.6 μM was obtained (Figure 4.9).

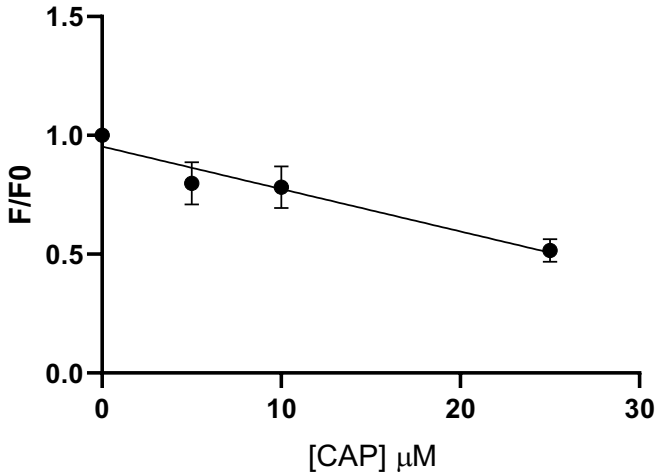


Figure 4.9. Fluorescence intensity of ThT/CAP1 after the addition of varying amounts of CAP in wastewater. The wastewater was buffered the same way as the lake water. A LOD of 3.6 μM was achieved.

4.4 Conclusions

We used the library immobilization method to obtain a few new DNA aptamers that bind the antibiotic CAP. The best aptamer named CAP1 came from the most abundant family after sequencing and showed a K_d of 9.8 μM using ITC. CAP1 shares no sequence homology with CAM80 or other previously claimed aptamers for CAP. ITC was also done with the previously selected CAM80 aptamer, which did not support binding with CAP. An advantage of the CAP1 aptamer is its short length and well-defined secondary structure showing the structure-switching property (switching from the complementary DNA binding state to the target binding state).[42] A fluorescent strand-displacement sensor showed a limit of detection of 14 μM. The CAP1 aptamer

can also enhance the fluorescence of ThT. This fluorescence could then be lowered with the addition of CAP, and a limit of detection of 1 μM was achieved this way. Sensing was also demonstrated in both a lake water sample and a wastewater sample. This newly selected aptamer is both shorter and has shown better binding affinity than previously reported CAP aptamers, and can be integrated into many sensing platforms for the detection of CAP.

Chapter 5 pH-Directed Capture-SELEX Aptamers for Kanamycin Detection

5.1 Introduction

Kanamycin antibiotics are broad-spectrum aminoglycosides useful for treating infections caused by Gram negative bacteria in both humans and animals. Kanamycin has three forms (A, B, and C), and the main therapeutic form is kanamycin A. Kanamycin binds to the bacterial 30s ribosomal subunit inhibiting the synthesis of vital proteins.[183] Similar to other aminoglycoside antibiotics, kanamycin has a narrow therapeutic window for safe use. In addition, it can quickly accumulate in animal by-products if not controlled properly.[184] Current methods of kanamycin detection have been limited to instrumental analysis such as high-performance liquid chromatography (HPLC) and mass spectrometry.[185] In addition, immunoassays have been developed.[186] Although instrumentation analysis is sensitive and can generate reliable results, it requires expensive equipment and skilled technicians. Immunoassays are faster but antibodies are expensive and have shorter shelf lives. For small molecules like kanamycin, immunoassays have to take a competitive assay format. Taking advantage of the rich amino groups in kanamycin, various nanomaterial-based detection methods were also reported, but such sensing mechanisms often lack a high specificity.[187]

Therefore, aptamers present an alternative sensing method. Previously, an RNA aptamer for kanamycin B was selected by Kwon et al. using the target immobilization method, which achieved a dissociation constant (K_d) of 4400 nM kanamycin A and 181 nM kanamycin B.[58] Song et al. selected a DNA aptamer with a reported K_d of 78.8 nM kanamycin A.[59] However, such K_d was obtained using immobilized target, and homogenous assays can avoid artifacts such as nonspecific adsorption to beads.[188] Further binding employed the label-free gold nanoparticle colorimetric assay, which was later demonstrated to be unsuitable for kanamycin A.[70] Stoltenburg

et al. selected DNA aptamers for kanamycin A using capture-SELEX (by immobilization of a DNA library) with different K_d values ranging from 3.9 to 24 μM.[60] However, these values could not be validated in a later study.[61] The Heemstra group used a restriction enzyme SELEX (RE-SELEX) method to isolate aptamers for kanamycin A and their aptamer had a K_d of 340 μM based on microscale thermophoresis (MST).[61] The Plaxco group has been pushing for continuous in vivo monitoring of kanamycin, and the researchers had to use a DNA aptamer converted from an RNA sequence.[189,190] So, a high quality aptamer for kanamycin is still in strong demand by the analytical field.

Kanamycin has a number of primary amine groups with pK_a values ranged from 6.2 to 7.6 (Figure 5.1A). Thus, we reasoned that pH might have a huge influence on aptamer selection and binding. All of the previously reported kanamycin aptamers, regardless of RNA or DNA, were selected in the pH range of 7.5-8.0. In this work, we aim to compare the binding of aptamers for kanamycin selected at a lower pH (pH 6.0) to the more commonly used pH 8.0. Thus, two selections were run in parallel. Indeed, pH 6 enriched high-quality aptamers, which also worked optimally at pH 6. At pH 8, binding can still occur, although it has a strong dependency on salt concentration. Finally, a label-free fluorescent sensing method was demonstrated using thioflavin T (ThT).

5.2 Materials and Methods

5.2.1 Chemicals.

All of the DNA oligonucleotides were purchased from Integrated DNA Technologies (Coralville, IA). See Table 5.1 for sequences. Kanamycin was purchased from Bio Basic Canada Inc. and other reagents were purchased from Sigma-Aldrich. The kanamycin sample used in this study was Kanamycin A (Product number KB0286Alrich catalog number).

Table 5.1. DNA sequences used in this work

DNA	Sequence (5′ – 3′)
N30 Library	GGAGGCTCTCGGGACGAC-(N30)-GTCGTCCCGCCTTTAGGATTTACAG
Forward Primer	GGAGGCTCTCGGGACGAC
Reverse Primer	CTGTAAATCCTAAAGGCGGGACG
Biotinylated Reverse Primer	/5Biosg/ CTGTAAATCCTAAAGGCGGGACG
Biotin Capture Strand	GTCGTCCCGAGAGCCATA/3BioTEG/
KAN6-1	GACGACGAGGGCCTGAAACTTGCTGGAACGGTTTAAGTCGTC
KAN6-5	CGACGCAGTTGGCTTAGCGTAGGTAAAGGTCGTAGTCGTC
Mutant 1	GACGACGGAGGCCTGAAACTTGCTGGAACGGTTTAAGTCGTC
Mutant 2	GACGACGAGGGCCTGAAACTTGCTGGAACGTGTTAAGTCGTC
Ky2	TGGGGGTTGAGGCTAAGCCGA

5.2.2 Buffer and Kanamycin Solution Preparation

Two buffers at pH 6.0 and pH 8.0 were used for aptamer selection. The pH 6.0 buffer contained 50 mM MES pH 6.0 with 300 mM NaCl, 10 mM $MgCl_2$, and 5 mM KCl (SB1). The pH 8.0 buffer contained 50 mM Tris-HCl pH 8.0 with 300 mM NaCl, 10 mM $MgCl_2$ and 5 mM KCl (SB2). Kanamycin solutions were prepared in SB1 and SB2 buffers for the two selections.

5.2.3 Kanamycin Selection.

The capture-SELEX method was used for the selection of kanamycin binding aptamers, which detailed methods are mentioned in previous chapters. In brief, an initial library consisting of a random 30 nucleotide random region flanked by two primer binding regions were used for selection. The first round used 500 pmol library and all the subsequent rounds used 100 pmol. The selections at pH 6.0 (SB1) and pH 8.0 (SB2) were done in parallel. SELEX was done for a total of

11 rounds before sequencing. The initial target kanamycin concentration was 1 mM for both selections and decreased at round 7 to 100 μM and round 9 to 10 μM.

5.2.4 Isothermal Titration Calorimetry.

Isothermal Titration Calorimetry (ITC) was performed using a MicroCal VP-ITC. 20 μM of aptamer was titrated with 200 μM target at 25°C using either SB1 or SB2. Data analysis and fitting was done using accompanying Origin software.

5.2.5 Thioflavin-T Fluorescence Assay.

1 μM of each of the kanamycin aptamers and 1 μM of thioflavin-T (ThT) were mixed together on a 96-well plate. 1 μM of kanamycin (or other antibiotic) was added, and fluorescence was read using a Tecan Spark plate reader after incubating for 5 min. Fluorescence was measured at an excitation wavelength of 425 nm and emission at 495 nm.

5.3 Results and Discussion

5.3.1 Capture-SELEX of Kanamycin Binding Aptamers at Two pH Values

The structure of kanamycin A is shown in Figure 5.1A. A key feature of this molecule is the presence of four amino groups with pK_a values all around 7. Therefore, a small change in pH can significantly change its charge and interactions with strongly negatively charged DNA. Kanamycin A has been a very popular target for aptamer selection, and we summarized some previous selection conditions and binding assays in Table 5.1. All of the previous selections were carried out at slightly basic conditions (pH 7.5 to 8.0), at which kanamycin A is close to charge neutral. Since selections in such a pH range failed to generate high affinity aptamers, we hypothesized that a lower pH might be a better condition since the target molecule became

positively charged. To understand the effect of pH on aptamer selection, in this work, two parallel selections for kanamycin A were performed at pH 6.0 and pH 8.0, respectively.

Table 5.1. SELEX parameters and dissociation constants of previous selections for kanamycin A.

Aptamer	**Type of SELEX**	**pH**	**Salt**	**K_d (μM) and assay used**
RNA	Target-Immobilized	7.5	250 mM Na^+, 1 mM Mg^{2+}	4.4 (Fluorescence anisotropy)[58]
DNA	Target-Immobilized	8.0	50 mM Na^+, 5 mM Mg^{2+}, 5 mM K^+	~0.08 (FAM-labeled aptamer to target-immobilized beads)[59]
DNA	Capture-SELEX (library immobilized)	7.6	100 mM Na^+, 2 mM Mg^{2+}, 5 mM K^+, 1 mM Ca^{2+}	3.9-24 (Strand-displacement);[60] 260 (MST)[61]
DNA	Restriction enzyme-SELEX	7.9	6 mM Mg^{2+}, 28 mM K^+	340 (MST)[61]

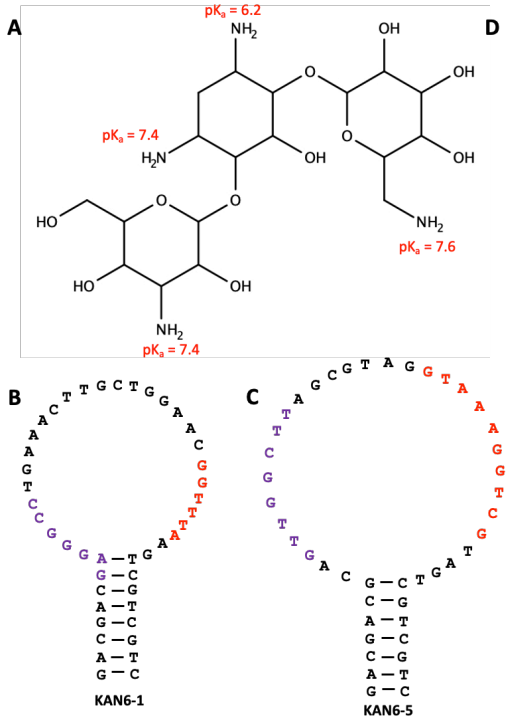
Our DNA library containing a 30-nucleotide (nt) random region was first annealed with a biotinylated capture strand and immobilized on streptavidin-coated agarose beads. The library had two primer binding regions, which could form a 10-base pair (bp) duplex region. Upon binding with the target, the binding sequences would adopt this structure, be released from the bead column, and be amplified by PCR. A total of 11 rounds of selection was done at each pH with kanamycin A concentration gradually decreased from 1 mM to 10 μM. The resulting PCR amplicons from each selection at the end of round 11 were sent for deep sequencing. A total of 46151 sequences were obtained for the selection at pH 6, and 36466 sequences at pH 8. The pH 6 selection showed a good sequence enrichment, although the selection at pH 8 did not converge well and the top

sequence made up less than 0.1% of the final library. This result already suggested that pH 6 might be a better pH for the selection of kanamycin aptamers.

An alignment was performed using the top 20 most abundant sequences from the selection at pH 6, and two main families were identified. The top sequence of the first family (named KAN6-1) comprised around 10% of the final library. This family (Figure 5.1D) has two conserved regions separated by a random region. The random region sequences do not seem to form any stable secondary structures (e.g. no stem-loop structures identified). So, we tend to believe that the entire structure is a big loop as drawn in Figure 5.1B. This top sequence was named KAN6-1 and was used for further analysis.

Family 2 also has two conserved regions separated by a random region (Figure 5.1C, D), although the conserved sequences are different from that in family 1. Therefore, a sequence from family 2 name KAN6-5 was also synthesized for further testing. These sequences were also aligned with the previous reported kanamycin aptamers, and we did not find any sequence homology (Figure 5.1D). So, we obtained new aptamers. Aside from these two families, the rest sequences also contained some common regions. Since they have a much lower abundance, we did not analyze them further. Since kanamycin is a relatively large molecules, it is reasonable that aptamers can have different ways to bind it and thus different aptamers can be generated.

The sequence enrichment for the selection done at pH 8 was less optimal, and the most abundant sequence has only 21 copies (Figure 5.1D). It is possible that at pH 8, kanamycin being a charge neutral molecule lacks charge attraction with DNA, whereas at pH 6, it is positively charged. Interestingly, the next three sequences from the pH 8 selection were also found in family 1 from the pH 6 selection. So, the pH 8 selection might still be successful, and it is just that the sequence enrichment was much slower suggesting weaker binding affinities.



Family 1 (pH 6)

KAN6-1	GAC---GAGGGCCTGAAACTTGCTGGAACGGTTTAAGTCGTC	(3438)
KAN6-2	GACGCCGAGGGCCGAAAACTGA-------GGTTTAAAGACGTCGTC	(2833)
KAN6-3	GACGC-GAGGGCCCATTGTACAGGT----GGTTTAAGTGTCGTC	(2125)
KAN6-8	GAC---GAGGGCCCGGAGTCTGTAGAAGTGGTTTAAGTCGTC	(973)
KAN6-10	GAC---GAGGGCCCGGATAGTGAAAAAGTGGTTTGAGTCGTC	(943)
KAN6-11	GACT--GAGGGCCGATGGATTCAGCGA--GGTTTAAGGTCGTC	(934)
KAN6-13	GACC--GAGGGCCTAGCTTTGGTCCAT--GGTTTAAGGTCGTC	(832)
KAN6-14	GACGT-GAGGGCCGACAACTTTTGA----GGTTTAAGCGTCGTC	(734)
KAN6-15	GAC---GAGGGCCGATGGAAGGAGACAGAGGTTTAAGTCGTC	(549)
KAN6-18	GAC---GAGGGCCTGGAAGTAGTTGACATGGTTTAAGTCGTC	(345)

Family 2 (pH 6)

KAN6-4	GACGCAAGTTGGCTTTCACTTG-G-AA-GGTCGAGTGTCGTC	(1286)
KAN6-5	GACGCA-GTTGGCTTAGCGTAG-GTAAAGGTCGTA-GTCGTC	(1132)
KAN6-16	GACGAA-GTTGGCTTTATCAATTGTAAAGGTCGA--GTCGTC	

Remaining Sequences (pH 6)

KAN6-6	GACAGGAATTACCCGTCTAGGCCCTTCTAGGGTGTCGTC	(1050)
KAN6-9	GACCGGAATTACCCAAATTTTGGCCCGTAGGGGGTCGTC	(949)
KAN6-12	GACGTAGTCGGCTGGTGCATGCTTCAGGTCGTAGTCGTC	(894)
KAN6-17	GACTGGAGTATAGGTCAAAGTCGGCTTATTGCAGTCGTC	(382)
KAN6-7	GACGCGGCTCATTTATTGCCTTGTGTTTGGTCCGTCGTC	(1024)
KAN6-19	GACGGTCTTTAACATGTACCTTCGGTACTGATTGTCGTC	(315)
KAN6-20	GACGTCGGCTGATATATCATTCAGGTCGCAGTCGTCCCG	(314)

pH 8

KAN8-1	GACGCAGTCGGCTTTTGCGGGAAAAAGGTCGGAGTCGTC	(21)
KAN8-2	GACCGAGGGCCCAGCTGGTCGTGT-----GGTTTAATGGTCGTC	(19)
KAN8-3	GAC-GAGGGCCTCGATCGTTCACGTGAGTGGTTTAAGTCGTC	(8)
KAN8-4	GAC-GAGGGCCCTCAGCATAGCGTTAGT-GGTTTAAGTCGTC	(6)

Figure 5.1. (A) The structure of kanamycin A and the pK_a values of its four amino groups.[32] The secondary structures of the (B) KAN6-1 and (C) KAN6-5 aptamers. (D) The top 20 most abundant sequences from SELEX done at pH 6, and the top 4 sequences from SELEX done at pH 8 as well as the previously selected aptamers. The number of copies of each sequence is in brackets. The colored regions are the conserved sequences.

5.3.2 A Strong Effect of pH for Binding in High Salt Buffers

To evaluate aptamer binding, we first used thioflavin-T (ThT) fluorescence spectroscopy. ThT is a fluorescent small molecule that can bind to DNA and enhance its fluorescence.[125] Although ThT is best known as a G-quadruplex binder, it can also bind to other DNA sequences. ThT is particularly useful for evaluating aptamer binding. By adding the KAN6-1 aptamer to ThT, the

ThT fluorescence would increase due to their weak binding. The addition of kanamycin would displace some ThT from the aptamer and lower the fluorescence of the sample (Figure 5.2A). This was previously observed for many other aptamers such as those for adenosine aptamer and chloramphenicol.[191,192] Measurements were performed at an excitation wavelength of 425 nm and an emission wavelength of 495 nm. Since a main goal of this work is to understand the effect of pH, we first measured binding pH 6, 7 and 8. In the selection buffer at pH 6, when we titrated kanamycin A, a gradual decrease in fluorescence was observed, suggesting aptamer binding (Figure 5.2B). With just 2 μM kanamycin, approximately 60% fluorescence drop was achieved (fitted K_d 820 nM). At pH 7, the binding was decreased, whereas at pH 8, the binding was negligible. Therefore, KAN6-1 is indeed a strongly pH-dependent aptamer, and the pH-dependent binding was consistent with our prediction of electrostatic interactions.

To confirm the results, we then performed a few control experiments. First, free ThT (no DNA added) was titrated with kanamycin and no fluorescence change was observed (Figure 5.3A). Second, we mixed an unrelated DNA with ThT and then titrated kanamycin, and no fluorescence change was observed either (Figure 5.3B). Therefore, ThT is a reliable assay for evaluating the binding of kanamycin aptamers.

To more accurately measure binding, we then performed isothermal titration calorimetry (ITC), which also provides thermodynamic information of aptamer binding. The aptamer was first annealed at 95°C and slowly cooled to room temperature. 100 μM of kanamycin was titrated into 10 μM of aptamer. The downward spikes indicate an exothermic binding interaction (Figure 5.4A), and the strong heat release was consistent with enthalpy-driven binding (e.g. electrostatic interactions and hydrogen bonding). The negative entropy change also confirmed this hypothesis (Table 5.2). The K_d was fitted to be 320 nM, which was slightly lower than the 820 nM K_d from

the ThT assay performed above. ITC is a more reliable method of quantitative measurement of binding, since ThT acts as a competitor that can lower the observed binding affinity. At pH 8, ITC also showed very little binding (Figure 5.4B), consistent with the ThT results. We also tested the binding of the KAN6-5 aptamer from family 2 (Figure 5.4C), and a K_d value of 800 nM was obtained. Since KAN6-1 has stronger binding, this study is focused on this aptamer.

It has been demonstrated many times that DNA selections often yield sequences that work optimally under the condition of selection. For example, the Li group selected a series of RNA-cleaving DNAzymes from pH 3 to 7. Except for pH 7, the rest selections all resulted DNAzymes that worked the best under the selection pH.[193] The fact that the pH 8 selection in our work did not enrich new sequences indicated that kanamycin A probably needs to be selected at a lower pH to have most of the amine groups protonated. Previously, a streptavidin aptamer was selected that can bind at pH 7.4 but not at pH 5.2.[194] There are also studies to understand the effect of pH for aptamer binding.[195–197] Our work is different in that we have taken into account the property of the target molecule and used pH to our advantage to evolve better aptamers.

5.3.3 pH-insensitive Binding in Low Salt Buffers

It is known that in a high ionic strength buffer, charges are screened and electrostatic interactions are weakened. The above experiments were carried out in the high salt selection buffers containing 300 mM NaCl and 10 mM $MgCl_2$, and thus charge attractions are relatively weak. To further understand charge or electrostatic interactions, we studied the effect of ionic strength. We omitted MgCl2 and NaCl from the buffer. In addition, to fully eliminate possible divalent metal ions, we also added 2 mM EDTA. Under this no salt condition, the KAN 6-1 aptamer retained its target binding from the ThT fluorescence (Figure 5.2C). The fluorescence drop even reached 90% with a fitted K_d of around 460 nM. We further performed the same experiment in pH 7 and 8 in the no-

salt buffer, and similar binding as that in pH 6 was also observed. This is a very interesting result, since this aptamer became pH-dependent in the absence of salt. This result can be rationalized by that pKa values would decrease when ionic strength decreases.[198] Thus, kanamycin might still have a favorable electrostatic attraction with the aptamer at higher pH in the absence of salt.

Overall, at pH 6, the KAN6-1 aptamer is very robust and insensitive to salt, whereas at pH 8, it only binds to kanamycin strongly in the absence of salt. This result can explain the poor aptamer enrichment in our pH 8 selection since the selection buffer contained a high salt concentration. Since our capture-SELEX method relied on DNA hybridization for capturing the DNA library, a high ionic strength was required. Under this confinement, pH 6 is a better condition than pH 8 for the selection of kanamycin aptamers.

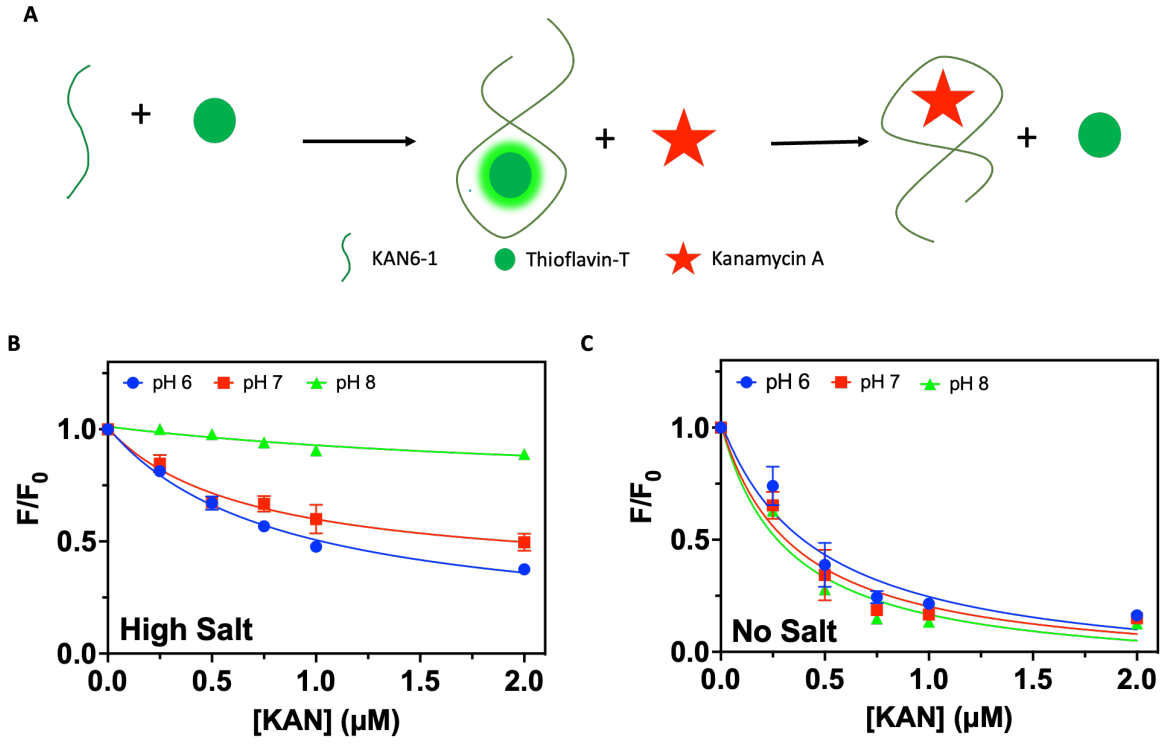


Figure 5.2. (A) A scheme showing the ThT-based fluorescence assay of kanamycin A (KAN) binding and it can also be used as a label-free detection method. Fluorescence titration curve of adding kanamycin A into 1 µM KAN6-1 aptamer in the presence of 1 µM ThT in either (B) high salt buffers (50 mM MES, pH 6 or HEPES, pH 7 and 8 with 300 mM NaCl, 10 mM MgCl2, and 5 mM KCl), or (C) no salt buffers 50 mM MES (pH 6) or HEPES (pH 7 and 8) buffer but with 2 mM EDTA.

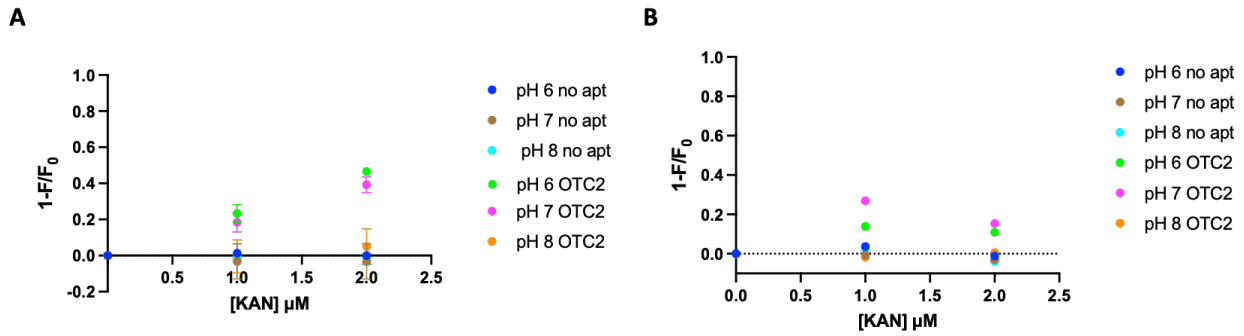


Figure 5.3. The fluorescence of Thioflavin-T with and without a non-binding aptamer sequence for control. (A) No salt in 50 mM pH 6 MES buffer, pH 7 HEPES, and pH 8 HEPES all with 2mM EDTA.(B) Same buffers but all with 300 mM NaCl, 10 mM $MgCl_2$, and 5 mM KCl.

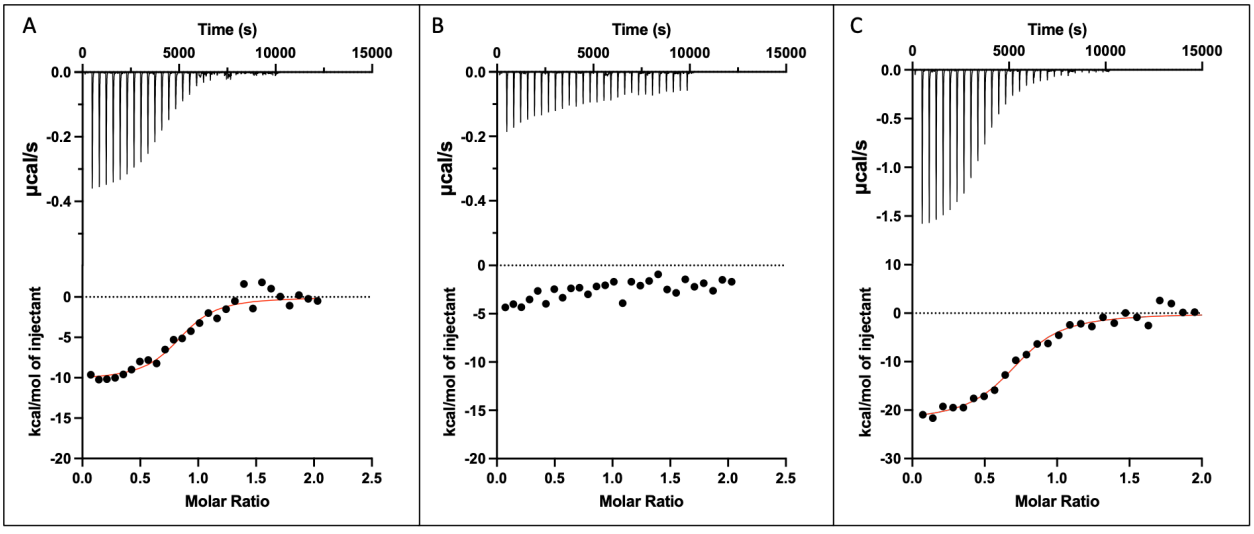


Figure 5.4. ITC trace of titrating 100 μM kanamycin A into 10 μM KAN6-1 aptamer in (A) 50 mM pH 6.0 MES with 300 mM NaCl, 10 mM MgCl2, 5 mM KCl; (B) 50 mM pH 8.0 HEPES with 300 mM NaCl, 10 mM MgCl2, 5 mM KCl. (C) ITC trace of titrating 200 μM kanamycin A into 20 μM KAN6-5 aptamer in pH 6.0 SB1 buffer.

Table 5.2. Fitted thermodynamic values from ITC traces.

Aptamer	**pH**	**Salt**	***N***	K_d **(μM)**	**Δ*H* (kcal/mol)**	**Δ*S* (cal/mol/K)**
KAN6-1	6.0	SB1	0.84± 0.03	0.32 ± 0.1	-10.3 ± 0.5	-4.8
KAN6-1	8.0	SB2	N/A	N/A	N/A	N/A
KAN6-5	6.0	SB1	0.72 ± 0.02	0.8 ± 0.2	-22.3 ± 0.9	-46.9
Ky2	8.0	Ky2 SB*	N/A	N/A	N/A	N/A

*Ky2 SB: 50 mM pH 8.0 Tris-HCl, 100 mM NaCl, 5 mM $MgCl_2$, 5 mM KCl,

5.3.4 Mutation Studies

At pH 6.0, kanamycin A is a positively charged and DNA is highly negatively charged. Therefore, there is a chance that the observed binding was simply due to nonspecific electrostatic interactions. To confirm the binding of the aptamer, mutants were tested (Figure 5.5A). One mutation (mutant 1) was made on the first conserved region by swapping the positions of a guanine and an adenine. The ThT assay showed that mutant 1 failed to respond to kanamycin (Figure 5.5B). We then tested mutant 2, where on the second conserved region a GT was swapped to TG, and this mutant also failed to bind kanamycin. Since neither mutant changed the base composition or the secondary structure of the aptamer, their lack of binding indicated that the binding of KAN6-1 was specific.

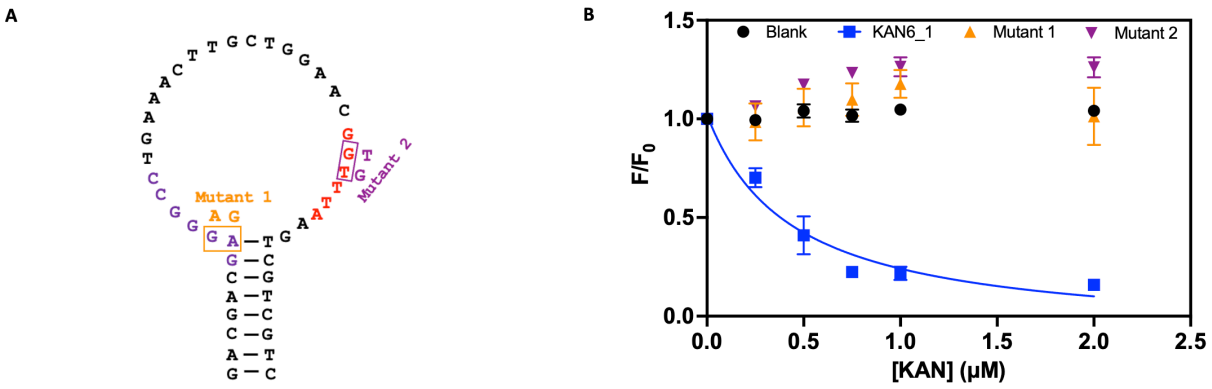


Figure 5.5. (A) Two aptamer mutants based on KAN6-1. (B) Fluorescence binding assays of mutant 1 and 2 using ThT.

5.3.5 Comparison with previously published aptamers

Kanamycin A has been previously used as a target for aptamer selections. From sequence alignment, we showed that our aptamers are different (Figure 5.6). Of these aptamers, the one from the RE-SELEX was reported to have a K_d of approximately 400 μM[61]. In the same paper, the authors also measured the K_d of another aptamer,[60] with a K_d of 260 μM. So, the only other possible high affinity DNA aptamer was Ky2,[59] which had a K_d of 78 nM from FAM-labeled aptamer binding to immobilized kanamycin. The secondary structure of Ky2 is shown in Figure 5A, and this is also a very short sequence. Since this K_d was measured using immobilized target, we herein performed two homogenous assays to verify binding. In the selection buffer reported by the authors, no ThT fluorescence change was observed when we titrated up to 2 μM kanamycin (Figure 5.7B). At the same time, no heat change was observed when 10 μM Ky2 was titrated with 100 μM kanamycin A using ITC (Figure 5.7C). Therefore, we do not believe that this Ky2 sequence is an aptamer for kanamycin.

```
KAN6-5          ------------------------------------------------------------GACGCAGTTGGCTTAGCGTAGGTAAAGGTCGTAGTCGTC--
KAN8-1          ------------------------------------------------------------GACGCAGTCGGCTTTTGCGGGAAAAAGGTCGGAGTCGTC--
KAN6-1          ------------------------------------------------------------GACGAGGGCCTGAAACTTGCTGGAACGGTTTAAGTCGTC--
KAN6-2          ---------------------------------------------------------GACGCCGAGGGCCGAAAACTGAGGTTTAAAGACGTCGTC------
KAN6-3          ------------------------------------------------------------GACGCGAGGGCCCATTGTACAGGTGGTTTAAGTGTCGTC--
KAN6-4          ------------------------------------------------------------GACGCAAGTTGGCTTTCACTTGGAAGGTCGAGTGTCGTC--
KAN6-6          ------------------------------------------------------------GACAGGAATTACCCGTCTAGGCCCTTCTAGGGTGTCGTC--
KAN6-7          ------------------------------------------------------------GACGCGGCTCATTTATTGCCTTGTGTTTGGTCCGTCGTC--
Ky2             ----------------------------------------------------------------------GGGGGTTGAGGCTAAGCCGA---------
K16-1           -------------CGCATACCAGCTTAGTTCAGAATTCATTGGAGCGTGGCGTGGATGCCCGATGGACGCCCCAGGGTGCAGATAGTAAGTGCAATCTCGGC
3_17            ATACCAGCTTATTCAATTAGCATGGTGCTGAGGCTTGATCTGGAGGTCGTGAACGAAAATTGGTCGTTTAGTTGGCTCGTAGATAGTAAGTGCAATC------
```

Figure 5.6. Alignment of the top 7 sequences from our pH 6 kanamycin selection and previously reported aptamers (Ky2, K16-1, 3_17) using Clustal Omega. There is little sequence homology between our newly selected aptamers and the previously reported ones.

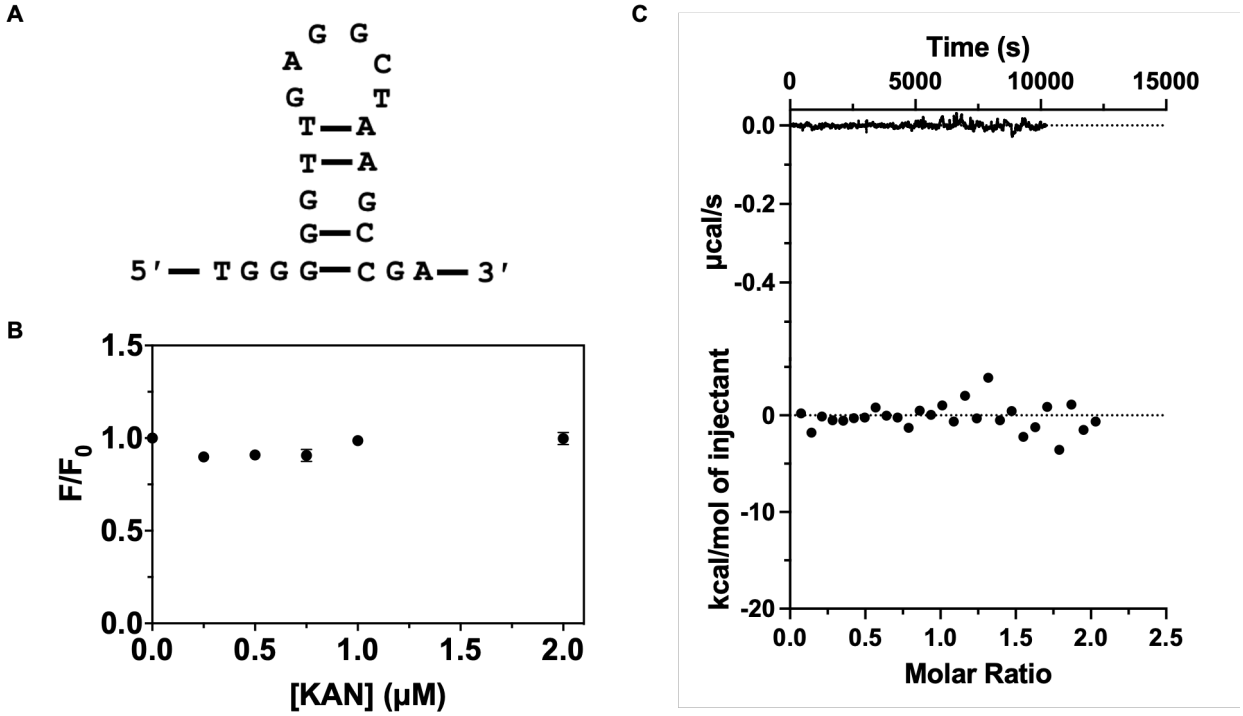


Figure 5.7 (A) The secondary structure of Ky2 predicted my Mfold. (B) Thioflavin-T assay of the Ky2 aptamer in its selection buffer (20 mM Tris-HCl pH 8.0 100 mM NaCl, 5 mM MgCl2, 5 mM KCl). (C) ITC trace of 100 μM kanamycin A into 10 μM Ky2 aptamer in its selection buffer.

5.3.6 Selectivity of the KAN6-1 aptamer

The above assays have confirmed binding of the KAN6-1 aptamer. Using the ThT assay, a few other aminoglycoside antibiotics, including tobramycin and lincomycin, were screened for cross-reactivity and selectivity (Figure 5.8A). When 1 μM antibiotics was added, tobramycin also lowered the fluorescence by around 60%, similar to the response of kanamycin (Figure 5.8B). The other tested antibiotics did not show much fluorescence change. We then performed a ThT fluorescence titration using tobramycin and a K_d of 1 μM was obtained (Figure 5.8C), which was similar to that of binding to kanamycin (850 nM) in SB1 buffer. The structures of tobramycin and kanamycin are the most similar out of the aminoglycosides tested, the only differences being a hydroxyl group at the 3′ position and the absence of an amine group at the 2′ position (Figure 5.8A). Based on these differences in structure we hypothesized that the aptamer may bind to the structure that both kanamycin and tobramycin have in common (Figure 5.8A, red lines). Other aminoglycosides with this structural motif might also bind to this aptamer, which may make this a broad-spectrum aptamer for the detection of these aminoglycosides as a group.

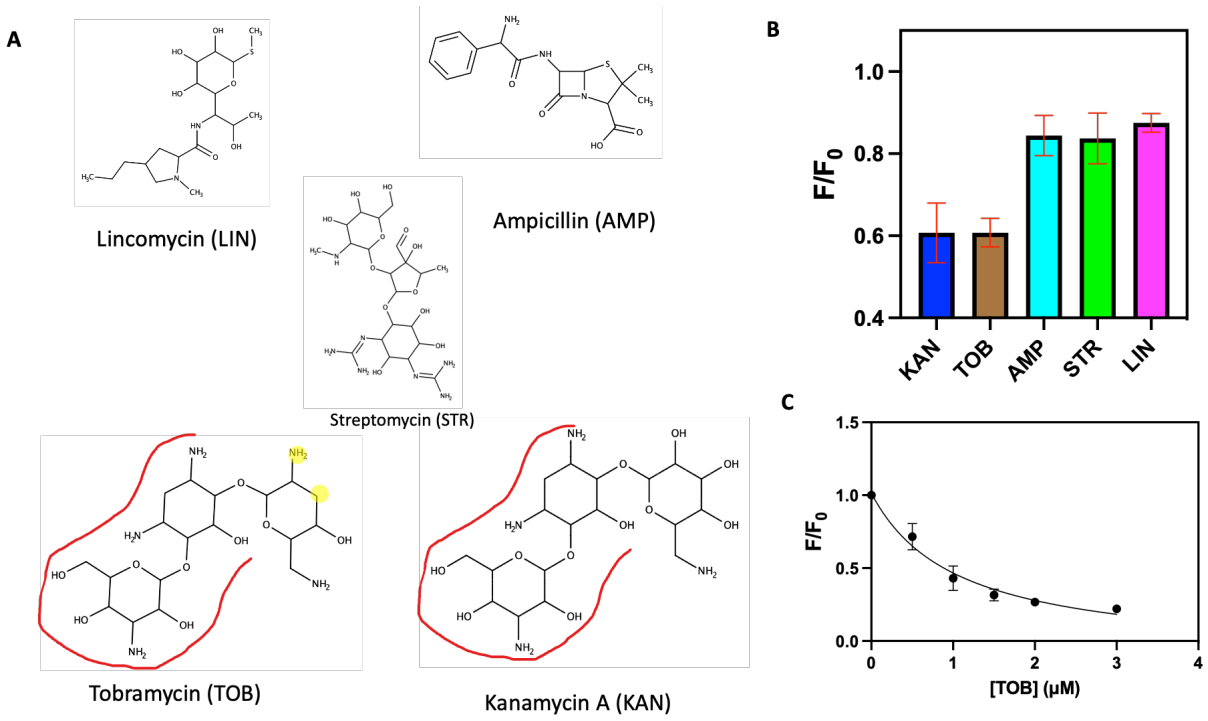


Figure 5.8 (A) Structures of the antibiotics used in the selectivity study. The highlighted regions in TOB are the differences between tobramycin and kanamycin A. The red line represents a possible binding region for the aptamers. (B) Selectivity of the KAN6-1 aptamer with 1 μM different antibiotics in SB1 buffer. (C) A ThT fluorescence titration curve of tobramycin.

5.3.7 Detection of kanamycin A in Lake Water

The ThT fluorescence assay can also be used as a label-free method for the detection of kanamycin. We fitted the initial linear response part of the response in the salt-free buffer, and a limit of detection of 0.3 μM kanamycin was obtained based on the equation of 3σ/slope, where σ is the standard deviation of the fluorescence variation in the absence of kanamycin (Figure 5.9A). Finally, the KAN6-1 aptamer was tested using filtered Lake Ontario water. The filtered water was buffered using 50 mM MES pH 6.0 with 2 mM EDTA. The water was then spiked with varying concentrations of kanamycin before 1 μM KAN6-1 and 1 μM ThT was added, and a fluorescence

drop was observed. Using the lake water, a K_d of 1 µM was fitted with a limit of detection of 0.1 µM (Figure 5.9B). This LOD is comparable to that in the buffer (Figure 5.9A). Therefore, the lake water did not interfere with the binding of the aptamer or the detection.

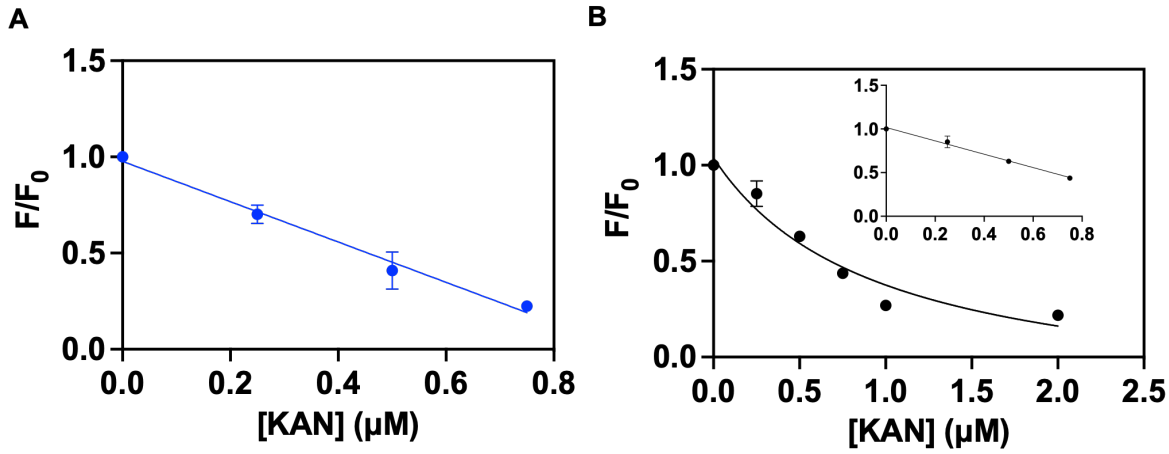


Figure 5.9. ThT-based assay using (A) pH 6 MES buffer with 2 mM EDTA. (B) Filtered Lake Ontario water. Inset: Linear region at low concentrations of kanamycin.

5.4 Conclusions

In this work, we have performed a parallel capture-SELEX at pH 6.0 and pH 8.0 for isolating aptamers for kanamycin A. The final library of the pH 6.0 selection converged well, while the selection at pH 8.0 did not. The best aptamer from the pH 6.0 selection was named KAN6-1 and it had a K_d of around 300 nM at pH 6.0 based on ITC. However, as the pH increased, the binding of KAN6-1 decreased. In particular, in high salt buffers, pH 8 failed to show good binding. Therefore, an important contribute we made here is to show the huge influence of pH for the selection of aptamers for kanamycin. This observation can likely be extended to target molecules with pK_a near 7. The isolation of sub-optimal aptamers in previous studies can probably be

attributed to the use of both a high pH and a high salt concentration. A ThT fluorescence assay was used to analyze the selectivity of the aptamer and was found that it had similar affinity to tobramycin, another aminoglycoside with a very similar structure. For practical applications of kanamycin detection in vivo, this aptamer probably needs to be applied in tissues with a slightly acid pH for best sensitivity. Alternatively, extracted bodily fluids (e.g. by microneedles) can be buffered for measurement.[199,200] For environmental monitoring, it is quite easy to tune the pH of the sample to 6.0 using a buffer, and the insensitivity to salt of this aptamer can make it a robust probe.

Chapter 6 Conclusions and Future Work

6.1 Conclusions

DNA aptamers present a novel and inexpensive way to sense antibiotics. In this thesis, I selected multiple aptamers for different antibiotics and apply them for biosensing. Some goals of these studies were to re-select aptamers to bind their targets, a more fundamental study on how aptamers bind their targets, as well as how selection conditions can influence aptamer binding.

In Chapter 2, I selected aptamers for the tetracycline group of antibiotics using oxytetracycline as the target. This family of antibiotics all share a four ringed structure with different side groups. At least four families of aptamer sequences were obtained, and the OTC5 sequence was studied in detail due to its high binding affinity and generality. Similar binding to OTC, TC and DOX with K_d's around 100 nM to 400 nM was observed. The intrinsic fluorescence of these tetracyclines allowed for a highly label-free and dye-free sensing with a LOD of 25 nM OTC. I then took a closer look at the results of the previous oxytetracycline selection and took a more fundamental approach to analyze the binding of the aptamers to oxytetracycline, tetracycline, and doxycycline. I investigated the pH and metal-ion dependency of the OTC5 aptamer and its relevance in the fluorescent detection of tetracycline antibiotics. At pH 6.0, fluorescence enhancement upon binding OTC5 was shown to be greater than at pH 8.3 but had a higher K_d. ITC experiments confirmed this by obtaining fitted K_d values of 0.2 μM and 0.03 μM at pH 6.0 and pH 8.3, respectively. When compared to other metal ions (Mn^{2+}, Zn^{2+} and Ca^{2+}), Mg^{2+} showed the best fluorescence increase and is required for OTC5 to bind. The optimal concentration of Mg^{2+} was determined to be 2 mM. The OTC5 aptamer was then split into stems with different lengths to observe the effects on binding. Kinetics studies of the split aptamers showed that both components of the split aptamer are necessary for detectable fluorescence enhancement, but the

order of addition had little effect. Splitting the full-length aptamer does decrease binding affinity, except when long binding stems were designed. ITC experiments showed this loss of binding can be attributed to the greater loss in entropy.

In Chapter 3, The intrinsic fluorescence of OTC allowed us to conveniently characterize its binding by aptamers. 10 aptamers were found for oxytetracycline that enhance its intrinsic fluorescence to various degrees. Fluorescence enhancement was probed using fluorescence titration spectroscopy and isothermal titration calorimetry. These ten aptamers all had high binding affinities with nine of them showing nanomolar affinities and all require Mg^{2+} to promote binding. Three aptamers were able to differentiate between three different tetracyclines and their binding led to a more than 10-fold increase in fluorescence. OTC43 was found to be specific to OTC with a limit of detection of 0.7 nM, OTC22 was found to be specific to DOX with a LOD of 0.4 nM, and OTC2 was found to be specific to TC with a LOD of 0.3 nM under optimal buffer conditions.

In Chapter 4, I selected a new aptamer for chloramphenicol and proved its binding to the target using ITC. The aptamer named CAP1 came from the most abundant family after sequencing and showed a K_d of 9.8 μM using ITC. CAP1 shares no sequence homology with CAM80 or other previously claimed aptamers for CAP. ITC was also done with the previously selected CAM80 aptamer, which did not support binding with CAP. A fluorescent strand-displacement sensor showed a limit of detection of 14 μM. The CAP1 aptamer can also enhance the fluorescence of ThT. This fluorescence could then be lowered with the addition of CAP, and a limit of detection of 1 μM was achieved this way.

In Chapter 5, I studied the effect of selection pH on aptamer binding by performing a parallel capture-SELEX at pH 6.0 and pH 8.0 for isolating aptamers for kanamycin A. The final library of the pH 6.0 selection converged well, while the selection at pH 8.0 did not. The best

aptamer from the pH 6.0 selection was named KAN6-1 and it had a K_d of around 300 nM at pH 6.0 based on ITC. However, as the pH increased, the binding of KAN6-1 decreased. In high salt buffers, pH 8 failed to show good binding. Therefore, pH has a huge influence on the selection of aptamers for kanamycin. This observation can likely be extended to target molecules with pK_a near 7. A ThT fluorescence assay was used to analyze the selectivity of the aptamer and was found that it had similar affinity to tobramycin, another aminoglycoside with a very similar structure.

6.2 Original Contributions

Based on the above work, I have made the following original contributions:

1. A new aptamer for tetracyclines called OTC5 was selected using capture-SELEX and oxytetracycline as the target. This aptamer had different affinities for TC, DOX and OTC and could enhance the intrinsic fluorescence of the tetracyclines. This could also be used as a label and dye free sensor. Splitting aptamers can also affect their binding capabilities, proven using ITC.

2. From the remaining pool of aptamers from the previous selection, ten aptamers were identified to have different affinities for each tetracycline and could distinguish them from each other using fluorescence.

3. A new aptamer for chloramphenicol was selected using capture-SELEX called CAP1. This aptamer was compared to previously selected aptamers and was shown to actually bind the target. A thioflavin-T assay was then designed for the label free detection of chloramphenicol.

4. A parallel selection for kanamycin A was performed at pH 6.0 and pH 8.0 to observe the effects of selection pH on the resulting aptamers. The selection pH had a big influence on the binding of the resulting aptamers.

6.3 Future Work

The results presented in this thesis provide new insights into aptamer selection as well as improving the quality of aptamers available for biosensor development. It has also provided some information on the fundamental of antibiotic binding aptamers.

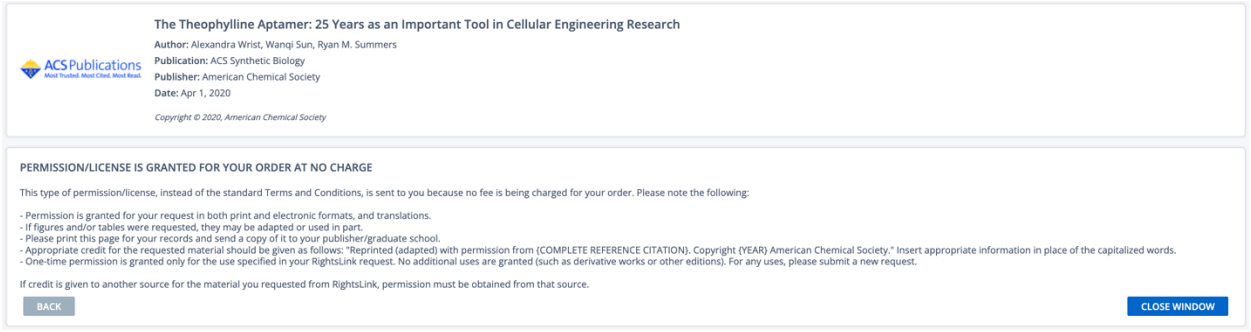
The OTC5 and the other tetracycline family binding aptamers described above could be easily adapted to different sensing methods such as paper-based, lateral flow, and electrochemical sensors. The fundamental study on splitting an aptamer can pave the way for more advanced biosensor designs.

Some older and previously selected aptamers may not bind to their respective targets. Therefore, re-selections of other previously selected targets could be done in order to yield better aptamers for previous targets (such as the chloramphenicol aptamer).

Finally, other selection conditions other than pH (such as salt concentration, temperature, library design, etc.) could be studied more in depth. We have already seen the huge influence that pH can have on the final aptamers, altering other parameters may also affect the final aptamers.

Letters of Copyright Permission

Figure 1.3



ACS Publications
Most Trusted. Most Cited. Most Read.

The Theophylline Aptamer: 25 Years as an Important Tool in Cellular Engineering Research

Author: Alexandra Wrist, Wanqi Sun, Ryan M. Summers
Publication: ACS Synthetic Biology
Publisher: American Chemical Society
Date: Apr 1, 2020

Copyright © 2020, American Chemical Society

PERMISSION/LICENSE IS GRANTED FOR YOUR ORDER AT NO CHARGE

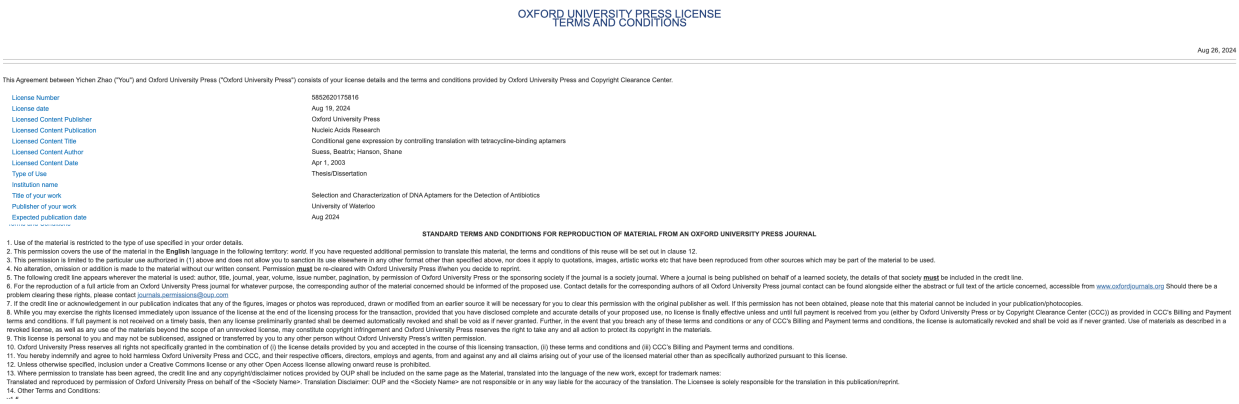
This type of permission/license, instead of the standard Terms and Conditions, is sent to you because no fee is being charged for your order. Please note the following:

- Permission is granted for your request in both print and electronic formats, and translations.
- If figures and/or tables were requested, they may be adapted or used in part.
- Please print this page for your records and send a copy of it to your publisher/graduate school.
- Appropriate credit for the requested material should be given as follows: "Reprinted (adapted) with permission from {COMPLETE REFERENCE CITATION}. Copyright {YEAR} American Chemical Society." Insert appropriate information in place of the capitalized words.
- One-time permission is granted only for the use specified in your RightsLink request. No additional uses are granted (such as derivative works or other editions). For any uses, please submit a new request.

If credit is given to another source for the material you requested from RightsLink, permission must be obtained from that source.

BACK CLOSE WINDOW

Figure 1.5:



OXFORD UNIVERSITY PRESS LICENSE
TERMS AND CONDITIONS

Aug 26, 2024

This Agreement between Yichen Zhao ("You") and Oxford University Press ("Oxford University Press") consists of your license details and the terms and conditions provided by Oxford University Press and Copyright Clearance Center.

License Number	5852620175816
License date	Aug 19, 2024
Licensed Content Publisher	Oxford University Press
Licensed Content Publication	Nucleic Acids Research
Licensed Content Title	Conditional gene expression by controlling translation with tetracycline-binding aptamers
Licensed Content Author	Suess, Beatrix; Hanson, Shane
Licensed Content Date	Apr 1, 2003
Type of Use	Thesis/Dissertation
Institution name	
Title of your work	Selection and Characterization of DNA Aptamers for the Detection of Antibiotics
Publisher of your work	University of Waterloo
Expected publication date	Aug 2024

STANDARD TERMS AND CONDITIONS FOR REPRODUCTION OF MATERIAL FROM AN OXFORD UNIVERSITY PRESS JOURNAL

1. Use of the material is restricted to the type of use specified in your order details.
2. This permission covers the use of the material in the **English** language in the following territory: world. If you have requested additional permission to translate this material, the terms and conditions of this reuse will be set out in clause 12.
3. This permission is limited to the particular use authorized in (1) above and does not allow you to sanction its use elsewhere in any other format other than specified above, nor does it apply to quotations, images, artistic works etc that have been reproduced from other sources which may be part of the material to be used.
4. No alteration, omission or addition is made to the material without our written consent. Permission must be re-cleared with Oxford University Press if/when you decide to reprint.
5. The following credit line appears wherever the material is used: author, title, journal, year, volume, issue number, pagination, by permission of Oxford University Press or the sponsoring society if the journal is a society journal. Where a journal is being published on behalf of a learned society, the details of that society must be included in the credit line.
6. For the reproduction of a full article from an Oxford University Press journal for whatever purpose, the corresponding author of the material concerned should be informed of the proposed use. Contact details for the corresponding authors of all Oxford University Press journal contact can be found alongside either the abstract or full text of the article concerned, accessible from www.oxfordjournals.org Should there be a problem clearing these rights, please contact journals.permissions@oup.com
7. If the credit line or acknowledgement in our publication indicates that any of the figures, images or photos was reproduced, drawn or modified from an earlier source it will be necessary for you to clear this permission with the original publisher as well. If this permission has not been obtained, please note that this material cannot be included in your publication/photocopies.
8. While you may exercise the rights licensed immediately upon issuance of the license at the end of the licensing process for the transaction, provided that you have disclosed complete and accurate details of your proposed use, no license is finally effective unless and until full payment is received from you (either by Oxford University Press or by Copyright Clearance Center (CCC)) as provided in CCC's Billing and Payment terms and conditions. If full payment is not received on a timely basis, then any license preliminarily granted shall be deemed automatically revoked and shall be void as if never granted. Further, in the event that you breach any of these terms and conditions or any of CCC's Billing and Payment terms and conditions, the license is automatically revoked and shall be void as if never granted. Use of materials as described in a revoked license, as well as any use of the materials beyond the scope of an unrevoked license, may constitute copyright infringement and Oxford University Press reserves the right to take any and all action to protect its copyright in the materials.
9. This license is personal to you and may not be sublicensed, assigned or transferred by you to any other person without Oxford University Press's written permission.
10. Oxford University Press reserves all rights not specifically granted in the combination of (i) the license details provided by you and accepted in the course of this licensing transaction, (ii) these terms and conditions and (iii) CCC's Billing and Payment terms and conditions.
11. You hereby indemnify and agree to hold harmless Oxford University Press and CCC, and their respective officers, directors, employs and agents, from and against any and all claims arising out of your use of the licensed material other than as specifically authorized pursuant to this license.
12. Unless otherwise specified, inclusion under a Creative Commons license or any other Open Access license allowing onward reuse is prohibited.
13. Where permission to translate has been agreed, the credit line and any copyright/disclaimer notices provided by OUP shall be included on the same page as the Material, translated into the language of the new work, except for trademark names:
Translated and reproduced by permission of Oxford University Press on behalf of the <Society Name>. Translation Disclaimer: OUP and the <Society Name> are not responsible or in any way liable for the accuracy of the translation. The Licensee is solely responsible for the translation in this publication/reprint.
14. Other Terms and Conditions:

Figure 1.6

License Details

This Agreement between Yichen Zhao ("You") and Elsevier ("Elsevier") consists of your license details and the terms and conditions provided by Elsevier and Copyright Clearance Center.

Print Copy

License Number	5852621091458
License date	Aug 19, 2024
Licensed Content Publisher	Elsevier
Licensed Content Publication	Bioorganic & Medicinal Chemistry
Licensed Content Title	A tetracycline-binding RNA aptamer
Licensed Content Author	Christian Berens,Alison Thain,Renée Schroeder
Licensed Content Date	Oct 1, 2001
Licensed Content Volume	9
Licensed Content Issue	10
Licensed Content Pages	8
Type of Use	reuse in a thesis/dissertation
Portion	figures/tables/illustrations
Number of figures/tables/illustrations	1
Format	electronic
Are you the author of this Elsevier article?	No
Will you be translating?	No
Title of new work	Selection and Characterization of DNA Aptamers for the Detection of Antibiotics
Institution name	University of Waterloo
Expected presentation date	Aug 2024
Portions	Figure 2
The Requesting Person / Organization to Appear on the License	Yichen Zhao

License Details

This Agreement between Yichen Zhao ("You") and Oxford University Press ("Oxford University Press") consists of your license details and the terms and conditions provided by Oxford University Press and Copyright Clearance Center.

Print Copy

License Number	5852620516964
License date	Aug 19, 2024
Licensed Content Publisher	Oxford University Press
Licensed Content Publication	Nucleic Acids Research
Licensed Content Title	Thermodynamic characterization of an engineered tetracycline-binding riboswitch
Licensed Content Author	Müller, Michael; Weigand, Julia E.
Licensed Content Date	Jan 1, 2006
Licensed Content Volume	34
Licensed Content Issue	9
Type of Use	Thesis/Dissertation
Requestor type	Educational Institution/Non-commercial/ Not for-profit
Format	Electronic
Portion	Figure/table
Number of figures/tables	1
Will you be translating?	No
Title of new work	Selection and Characterization of DNA Aptamers for the Detection of Antibiotics
Institution name	University of Waterloo
Expected presentation date	Aug 2024
Portions	Figure 4
The Requesting Person / Organization to Appear on the	Yichen Zhao

Figure 1.7

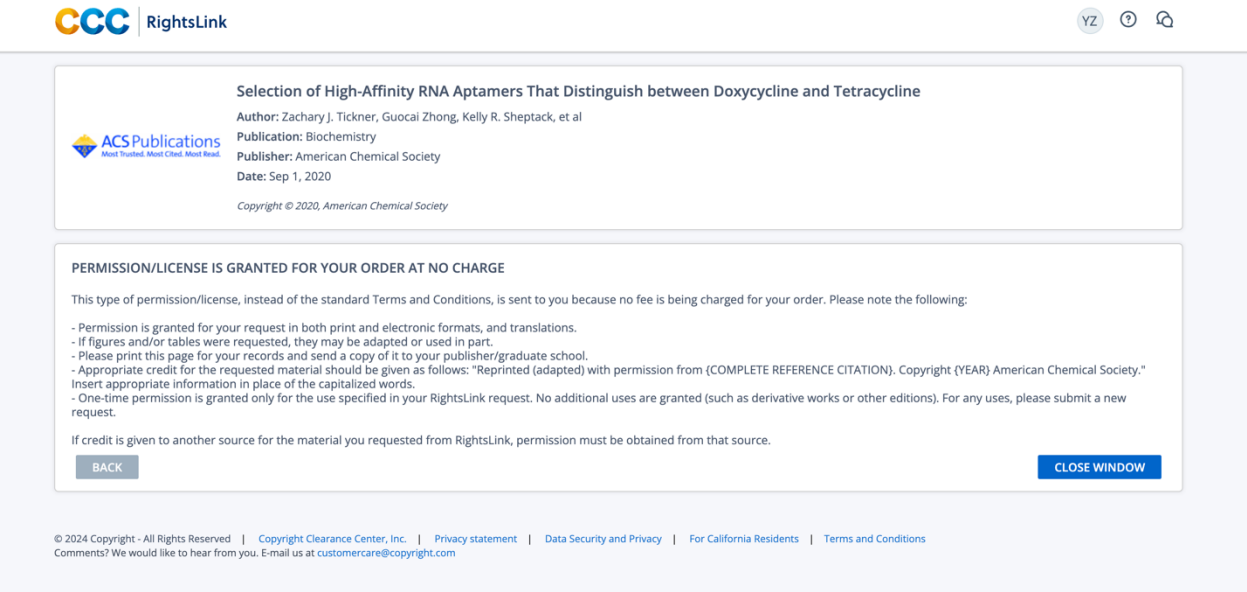


Figure 1.8

License Details

This Agreement between Yichen Zhao ("You") and Elsevier ("Elsevier") consists of your license details and the terms and conditions provided by Elsevier and Copyright Clearance Center.

Print Copy

License Number	5852630319272
License date	Aug 19, 2024
Licensed Content Publisher	Elsevier
Licensed Content Publication	Bioorganic & Medicinal Chemistry
Licensed Content Title	ssDNA aptamers that selectively bind oxytetracycline
Licensed Content Author	Javed H. Niazi,Su Jin Lee,Yeon Seok Kim,Man Bock Gu
Licensed Content Date	Feb 1, 2008
Licensed Content Volume	16
Licensed Content Issue	3
Licensed Content Pages	8
Type of Use	reuse in a thesis/dissertation
Portion	figures/tables/illustrations
Number of figures/tables/illustrations	2
Format	electronic
Are you the author of this Elsevier article?	No
Will you be translating?	No
Title of new work	Selection and Characterization of DNA Aptamers for the Detection of Antibiotics
Institution name	University of Waterloo
Expected presentation date	Aug 2024
Portions	Figure 4, Figure 5
The Requesting Person / Organization to Appear on the License	Yichen Zhao

Figure 1.9

License Details

This Agreement between Yichen Zhao ("You") and Elsevier ("Elsevier") consists of your license details and the terms and conditions provided by Elsevier and Copyright Clearance Center.

Print Copy

License Number	5852630536405
License date	Aug 19, 2024
Licensed Content Publisher	Elsevier
Licensed Content Publication	Bioorganic & Medicinal Chemistry
Licensed Content Title	Single-stranded DNA aptamers specific for antibiotics tetracyclines
Licensed Content Author	Javed H. Niazi,Su Jin Lee,Man Bock Gu
Licensed Content Date	Aug 1, 2008
Licensed Content Volume	16
Licensed Content Issue	15
Licensed Content Pages	9
Type of Use	reuse in a thesis/dissertation
Portion	figures/tables/illustrations
Number of figures/tables/illustrations	2
Format	electronic
Are you the author of this Elsevier article?	No
Will you be translating?	No
Title of new work	Selection and Characterization of DNA Aptamers for the Detection of Antibiotics
Institution name	University of Waterloo
Expected presentation date	Aug 2024
Portions	Figure 4, Table 1
The Requesting Person / Organization to Appear on the License	Yichen Zhao

Figure 1.10

License Details

This Agreement between Yichen Zhao ("You") and Elsevier ("Elsevier") consists of your license details and the terms and conditions provided by Elsevier and Copyright Clearance Center.

Print Copy

License Number	5852630752229
License date	Aug 19, 2024
Licensed Content Publisher	Elsevier
Licensed Content Publication	Chemistry & Biology
Licensed Content Title	RNA aptamers to the peptidyl transferase inhibitor chloramphenicol
Licensed Content Author	Donald H. Burke,David C. Hoffman,Analisa Brown,Mark Hansen,Arthur Pardi,Larry Gold
Licensed Content Date	Nov 1, 1997
Licensed Content Volume	4
Licensed Content Issue	11
Licensed Content Pages	11
Type of Use	reuse in a thesis/dissertation
Portion	figures/tables/illustrations
Number of figures/tables/illustrations	2
Format	electronic
Are you the author of this Elsevier article?	No
Will you be translating?	No
Title of new work	Selection and Characterization of DNA Aptamers for the Detection of Antibiotics
Institution name	University of Waterloo
Expected presentation date	Aug 2024
Portions	Figure 3, Table 1
The Requesting Person / Organization to Appear on the License	Yichen Zhao

Figures 1.11, 1.13

License Details

This Agreement between Yichen Zhao ("You") and Springer Nature ("Springer Nature") consists of your license details and the terms and conditions provided by Springer Nature and Copyright Clearance Center.

Print Copy

License Number	5852631459952
License date	Aug 19, 2024
Licensed Content Publisher	Springer Nature
Licensed Content Publication	Microchimica Acta
Licensed Content Title	Detection of chloramphenicol with an aptamer-based colorimetric assay: critical evaluation of specific and unspecific binding of analyte molecules
Licensed Content Author	Xiaoqi Tao et al
Licensed Content Date	Nov 19, 2020
Type of Use	Thesis/Dissertation
Requestor type	academic/university or research institute
Format	electronic
Portion	figures/tables/illustrations
Number of figures/tables/illustrations	1
Will you be translating?	no
Circulation/distribution	50000 or greater
Author of this Springer Nature content	no
Title of new work	Selection and Characterization of DNA Aptamers for the Detection of Antibiotics
Institution name	University of Waterloo
Expected presentation date	Aug 2024
Portions	Figure 1
The Requesting Person / Organization to Appear on the License	Yichen Zhao

License Details

This Agreement between Yichen Zhao ("You") and Elsevier ("Elsevier") consists of your license details and the terms and conditions provided by Elsevier and Copyright Clearance Center.

Print Copy

License Number	5852631102703
License date	Aug 19, 2024
Licensed Content Publisher	Elsevier
Licensed Content Publication	Journal of Biotechnology
Licensed Content Title	In vitro selection and characterization of DNA aptamers recognizing chloramphenicol
Licensed Content Author	Jaytry Mehta,Bieke Van Dorst,Elsa Rouah-Martin,Wouter Herrebout,Marie-Louise Scippo,Ronny Blust,Johan Robbens
Licensed Content Date	Oct 10, 2011
Licensed Content Volume	155
Licensed Content Issue	4
Licensed Content Pages	9
Type of Use	reuse in a thesis/dissertation
Portion	figures/tables/illustrations
Number of figures/tables/illustrations	4
Format	electronic
Are you the author of this Elsevier article?	No
Will you be translating?	No
Title of new work	Selection and Characterization of DNA Aptamers for the Detection of Antibiotics
Institution name	University of Waterloo
Expected presentation date	Aug 2024
Portions	Figures 3,6,7,10
The Requesting Person / Organization to Appear on the License	Yichen Zhao

Figures 1.12, 1.13

License Details

This Agreement between Yichen Zhao ("You") and Springer Nature ("Springer Nature") consists of your license details and the terms and conditions provided by Springer Nature and Copyright Clearance Center.

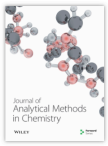
Print Copy

License Number	5852640303628
License date	Aug 19, 2024
Licensed Content Publisher	Springer Nature
Licensed Content Publication	Applied Biochemistry and Biotechnology
Licensed Content Title	Selection and Identification of Chloramphenicol-Specific DNA Aptamers by Mag-SELEX
Licensed Content Author	Ye Duan et al
Licensed Content Date	Sep 9, 2016
Type of Use	Thesis/Dissertation
Requestor type	academic/university or research institute
Format	electronic
Portion	figures/tables/illustrations
Number of figures/tables/illustrations	5
Will you be translating?	no
Circulation/distribution	50000 or greater
Author of this Springer Nature content	no
Title of new work	Selection and Characterization of DNA Aptamers for the Detection of Antibiotics
Institution name	University of Waterloo
Expected presentation date	Aug 2024
Portions	Figures 1, 4,5,6, Table 1
The Requesting Person / Organization to Appear on the License	Yichen Zhao

Figure 1.14, 1.15

Journal of Analytical Methods in Chemistry

Forward Series



All articles

Research Article | Open Access

Capture-SELEX: Selection of DNA Aptamers for Aminoglycoside Antibiotics

Regina Stoltenburg, Nadia Nikolaus, Beate Strehlitz

First published: 30 December 2012 | https://doi.org/10.1155/2012/415697 | Citations: 3

Academic Editor: Songbai Zhang

Details

Copyright © 2012 Regina Stoltenburg et al.

This is an open access article distributed under the Creative Commons Attribution License, which permits unrestricted use, distribution, and reproduction in any medium, provided the original work is properly cited.

Check for updates

Publication History

Issue Online:
30 December 2012

Version of Record online:
30 December 2012

Manuscript accepted:
26 September 2012

Manuscript received:
19 July 2012

RE-SELEX: restriction enzyme-based evolution of structure-switching aptamer biosensors

A. A. Sanford, A. E. Rangel, T. A. Feagin, R. G. Lowery, H. S. Argueta-Gonzalez and J. M. Heemstra, *Chem. Sci.*, 2021, **12**, 11692 **DOI:** 10.1039/D1SC02715H

This article is licensed under a Creative Commons Attribution-NonCommercial 3.0 Unported Licence. **You can use material from this article in other publications, without requesting further permission** from the RSC, provided that the correct acknowledgement is given and it is not used for commercial purposes.

License URLs: https://creativecommons.org/licenses/by/3.0/, https://creativecommons.org/licenses/by-nc/3.0/

Figure 1.16:

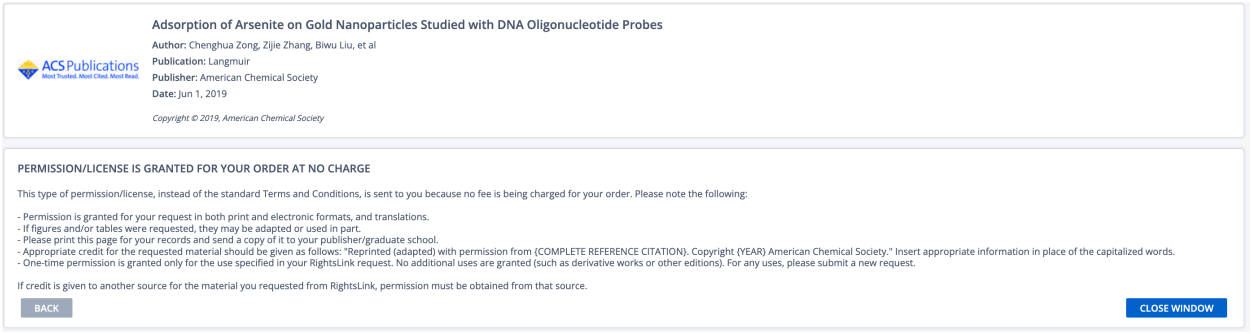
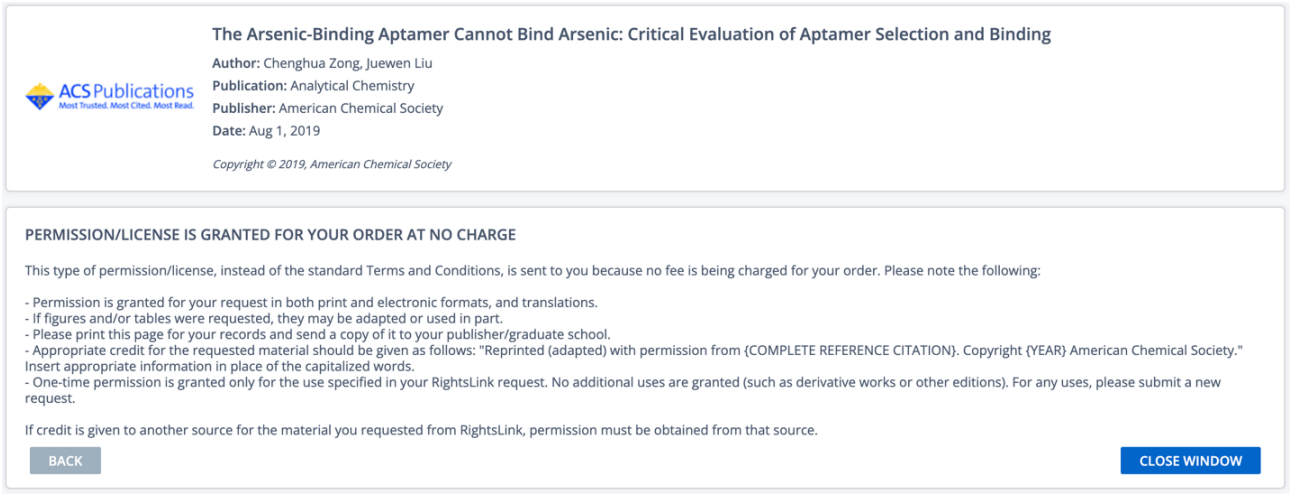


Figure 1.17



The Arsenic-Binding Aptamer Cannot Bind Arsenic: Critical Evaluation of Aptamer Selection and Binding

Author: Chenghua Zong, Juewen Liu
Publication: Analytical Chemistry
Publisher: American Chemical Society
Date: Aug 1, 2019

Copyright © 2019, American Chemical Society

PERMISSION/LICENSE IS GRANTED FOR YOUR ORDER AT NO CHARGE

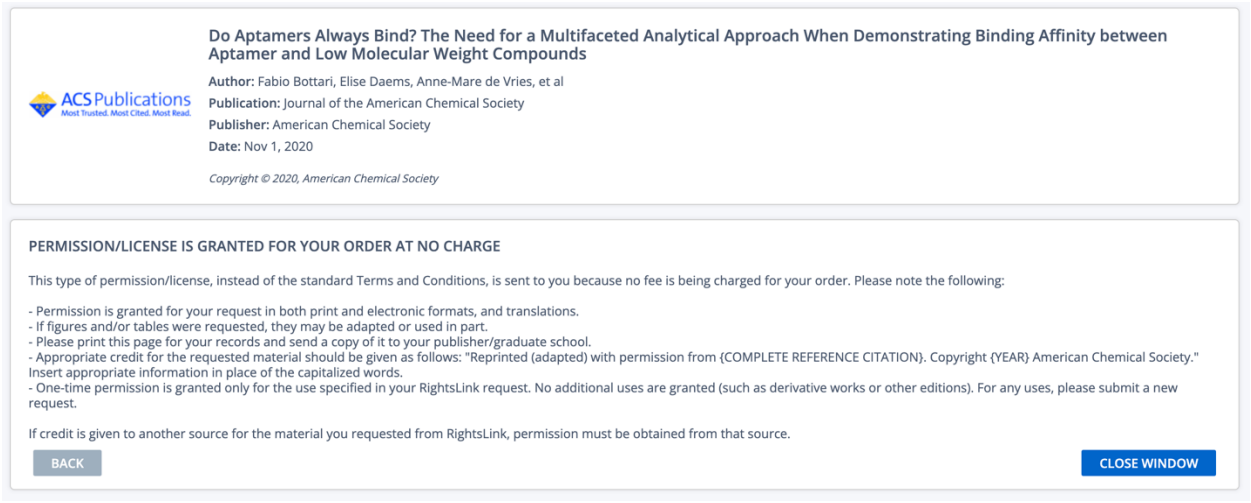
This type of permission/license, instead of the standard Terms and Conditions, is sent to you because no fee is being charged for your order. Please note the following:

- Permission is granted for your request in both print and electronic formats, and translations.
- If figures and/or tables were requested, they may be adapted or used in part.
- Please print this page for your records and send a copy of it to your publisher/graduate school.
- Appropriate credit for the requested material should be given as follows: "Reprinted (adapted) with permission from {COMPLETE REFERENCE CITATION}. Copyright {YEAR} American Chemical Society." Insert appropriate information in place of the capitalized words.
- One-time permission is granted only for the use specified in your RightsLink request. No additional uses are granted (such as derivative works or other editions). For any uses, please submit a new request.

If credit is given to another source for the material you requested from RightsLink, permission must be obtained from that source.

BACK CLOSE WINDOW

Figure 1.18



Do Aptamers Always Bind? The Need for a Multifaceted Analytical Approach When Demonstrating Binding Affinity between Aptamer and Low Molecular Weight Compounds

Author: Fabio Bottari, Elise Daems, Anne-Mare de Vries, et al
Publication: Journal of the American Chemical Society
Publisher: American Chemical Society
Date: Nov 1, 2020

Copyright © 2020, American Chemical Society

PERMISSION/LICENSE IS GRANTED FOR YOUR ORDER AT NO CHARGE

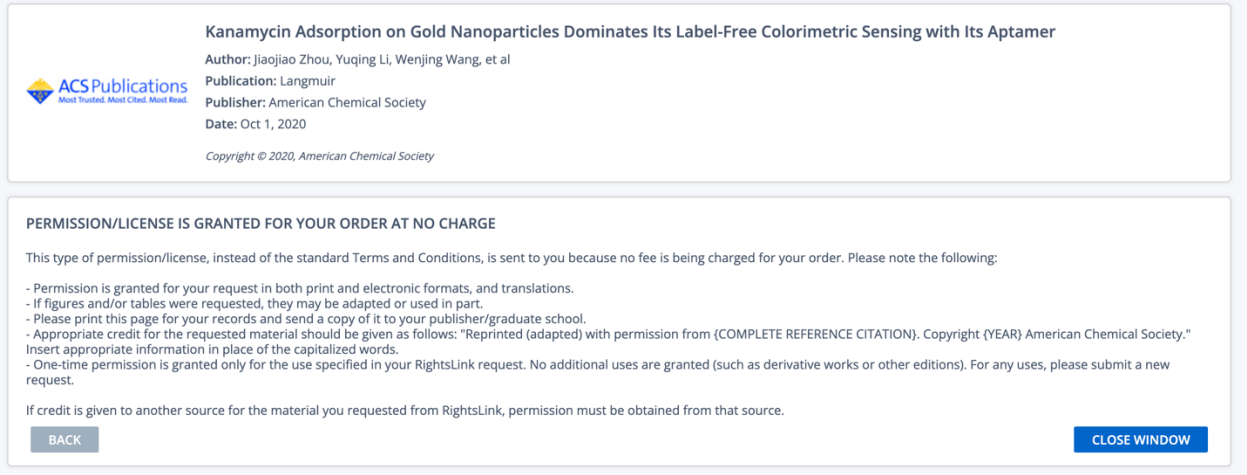
This type of permission/license, instead of the standard Terms and Conditions, is sent to you because no fee is being charged for your order. Please note the following:

- Permission is granted for your request in both print and electronic formats, and translations.
- If figures and/or tables were requested, they may be adapted or used in part.
- Please print this page for your records and send a copy of it to your publisher/graduate school.
- Appropriate credit for the requested material should be given as follows: "Reprinted (adapted) with permission from {COMPLETE REFERENCE CITATION}. Copyright {YEAR} American Chemical Society." Insert appropriate information in place of the capitalized words.
- One-time permission is granted only for the use specified in your RightsLink request. No additional uses are granted (such as derivative works or other editions). For any uses, please submit a new request.

If credit is given to another source for the material you requested from RightsLink, permission must be obtained from that source.

BACK CLOSE WINDOW

Figure 1.19



Kanamycin Adsorption on Gold Nanoparticles Dominates Its Label-Free Colorimetric Sensing with Its Aptamer

Author: Jiaojiao Zhou, Yuqing Li, Wenjing Wang, et al
Publication: Langmuir
Publisher: American Chemical Society
Date: Oct 1, 2020

Copyright © 2020, American Chemical Society

ACS Publications
Most Trusted. Most Cited. Most Read.

PERMISSION/LICENSE IS GRANTED FOR YOUR ORDER AT NO CHARGE

This type of permission/license, instead of the standard Terms and Conditions, is sent to you because no fee is being charged for your order. Please note the following:

- Permission is granted for your request in both print and electronic formats, and translations.
- If figures and/or tables were requested, they may be adapted or used in part.
- Please print this page for your records and send a copy of it to your publisher/graduate school.
- Appropriate credit for the requested material should be given as follows: "Reprinted (adapted) with permission from {COMPLETE REFERENCE CITATION}. Copyright {YEAR} American Chemical Society." Insert appropriate information in place of the capitalized words.
- One-time permission is granted only for the use specified in your RightsLink request. No additional uses are granted (such as derivative works or other editions). For any uses, please submit a new request.

If credit is given to another source for the material you requested from RightsLink, permission must be obtained from that source.

BACK

CLOSE WINDOW

Figure 1.20



Angewandte International Edition Chemie
GDCh A Journal of the German Chemical Society

Communication | Open Access

Selective Hemin Binding by a Non-G-quadruplex Aptamer with Higher Affinity and Better Peroxidase-like Activity

Lide Gu, Yuzhe Ding, Yang Zhou, Prof. Dr. Yao Zhang, Prof. Dr. Deli Wang, Prof. Dr. Juewen Liu

First published: 27 December 2023 | https://doi.org/10.1002/anie.202314450 | Citations: 4

Volume 63, Issue 6
February 5, 2024
e202314450

Metrics

Citations: 4
Full text views: 3,420

Details

© 2023 The Authors. Angewandte Chemie International Edition published by Wiley-VCH GmbH

This is an open access article under the terms of the Creative Commons Attribution-NonCommercial License, which permits use, distribution and reproduction in any medium, provided the original work is properly cited and is not used for commercial purposes.

Figure 1.24

Comparing two cortisol aptamers for label-free fluorescent and colorimetric biosensors

C. Niu, Y. Ding, C. Zhang and J. Liu, *Sens. Diagn.*, 2022, **1**, 541 **DOI:** 10.1039/D2SD00042C

This article is licensed under a Creative Commons Attribution 3.0 Unported Licence. **You can use material from this article in other publications without requesting further permissions** from the RSC, provided that the correct acknowledgement is given.

Read more about how to correctly acknowledge RSC content.

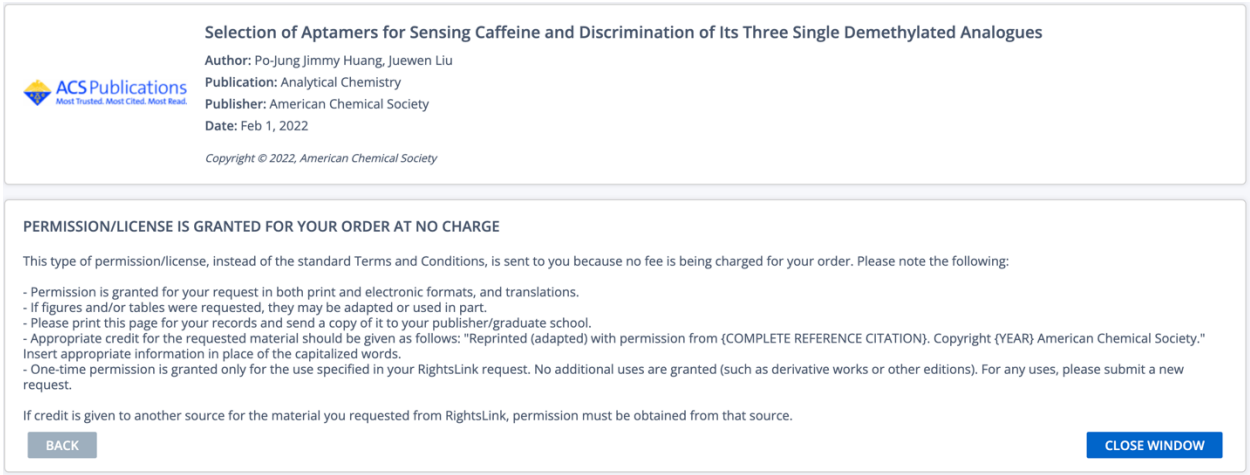


Figure 1.25



Figure 1.26

License Details

This Agreement between Yichen Zhao ("You") and Elsevier ("Elsevier") consists of your license details and the terms and conditions provided by Elsevier and Copyright Clearance Center.

Print Copy

License Number	5853141305184
License date	Aug 20, 2024
Licensed Content Publisher	Elsevier
Licensed Content Publication	Biosensors and Bioelectronics
Licensed Content Title	Flexible freestanding graphene paper-based potentiometric enzymatic aptasensor for ultrasensitive wireless detection of kanamycin
Licensed Content Author	Yao Yao,Chengmei Jiang,Jianfeng Ping
Licensed Content Date	Jan 1, 2019
Licensed Content Volume	123
Licensed Content Issue	n/a
Licensed Content Pages	7
Type of Use	reuse in a thesis/dissertation
Portion	figures/tables/illustrations
Number of figures/tables/illustrations	2
Format	electronic
Are you the author of this Elsevier article?	No
Will you be translating?	No
Title of new work	Selection and Characterization of DNA Aptamers for the Detection of Antibiotics
Institution name	University of Waterloo
Expected presentation date	Aug 2024
Portions	Scheme 1, Figure 3
The Requesting Person / Organization to Appear on the License	Yichen Zhao

Figure 1.27

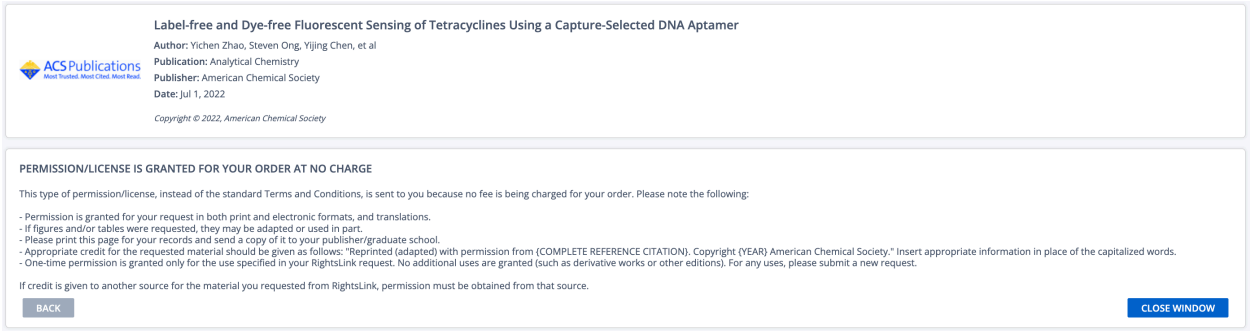
License Details

This Agreement between Yichen Zhao ("You") and Elsevier ("Elsevier") consists of your license details and the terms and conditions provided by Elsevier and Copyright Clearance Center.

Print Copy

License Number	5853150554060
License date	Aug 20, 2024
Licensed Content Publisher	Elsevier
Licensed Content Publication	Analytical Biochemistry
Licensed Content Title	Lateral flow assay using aptamer-based sensing for on-site detection of dopamine in urine
Licensed Content Author	Shima Dalirirad,Andrew J. Steckl
Licensed Content Date	1 May 2020
Licensed Content Volume	596
Licensed Content Issue	n/a
Licensed Content Pages	1
Type of Use	reuse in a thesis/dissertation
Portion	figures/tables/illustrations
Number of figures/tables/illustrations	2
Format	electronic
Are you the author of this Elsevier article?	No
Will you be translating?	No
Title of new work	Selection and Characterization of DNA Aptamers for the Detection of Antibiotics
Institution name	University of Waterloo
Expected presentation date	Aug 2024
Portions	Figures 2,3
The Requesting Person / Organization to Appear on the License	Yichen Zhao

Articles in Chapter 2



Label-free and Dye-free Fluorescent Sensing of Tetracyclines Using a Capture-Selected DNA Aptamer

Author: Yichen Zhao, Steven Ong, Yijing Chen, et al
Publication: Analytical Chemistry
Publisher: American Chemical Society
Date: Jul 1, 2022

Copyright © 2022, American Chemical Society

PERMISSION/LICENSE IS GRANTED FOR YOUR ORDER AT NO CHARGE

This type of permission/license, instead of the standard Terms and Conditions, is sent to you because no fee is being charged for your order. Please note the following:

- Permission is granted for your request in both print and electronic formats, and translations.
- If figures and/or tables were requested, they may be adapted or used in part.
- Please print this page for your records and send a copy of it to your publisher/graduate school.
- Appropriate credit for the requested material should be given as follows: "Reprinted (adapted) with permission from {COMPLETE REFERENCE CITATION}. Copyright {YEAR} American Chemical Society." Insert appropriate information in place of the capitalized words.
- One-time permission is granted only for the use specified in your RightsLink request. No additional uses are granted (such as derivative works or other editions). For any uses, please submit a new request.

If credit is given to another source for the material you requested from RightsLink, permission must be obtained from that source.

BACK CLOSE WINDOW

Zhao, Y., Gao, B., Sun, P., Liu, J. Metal and pH-Dependent Aptamer Binding of Tetracyclines Enabling Highly Sensitive Fluorescence Sensing. Biosensors 2022, 12, 717. Is under an Open Access License.

1. The Analyst

Billing Status: Open

Article: Light-up split aptamers: binding thermodynamics and kinetics for sensing.

Print License

Order License ID	1512498-1	**Type of Use**	Republish in a thesis/dissert...
Order detail status	Completed	**Publisher**	ROYAL SOCIETY OF CHEMIST...
ISSN	0003-2654	**Portion**	Chapter/article

0.00 CAD

Hide Details

Republication Permission

LICENSED CONTENT

Publication Title	The Analyst	**Rightsholder**	Royal Society of Chemistry
Article Title	Light-up split aptamers: bin...	**Publication Type**	Journal
Author / Editor	ROYAL SOCIETY OF CHEMIST...	**Start Page**	5612
Date	01/01/1876	**End Page**	5618
Language	English	**Issue**	22
Country	United Kingdom of Great Bri...	**Volume**	148

REQUEST DETAILS

Portion Type	Chapter/article	**Rights Requested**	Main product
Page Range(s)	5612-5618	**Distribution**	Worldwide
Total Number of Pages	7	**Translation**	Original language of publica...
Format (select all that apply)	Electronic	**Copies for the Disabled?**	No
Who Will Republish the Content?	Academic institution	**Minor Editing Privileges?**	No
		Incidental Promotional Use?	No
Duration of Use	Life of current edition	**Currency**	CAD
Lifetime Unit Quantity	Up to 499		

NEW WORK DETAILS

Title	Selection and Characterizati...	**Institution Name**	University of Waterloo
Instructor Name	Yichen Zhao	**Expected Presentation Date**	2024-08-15

ADDITIONAL DETAILS

The Requesting Person / Organization to Appear on the License	Yichen Zhao

REQUESTED CONTENT DETAILS

Title, Description or Numeric Reference of the Portion(s)	Light-up split aptamers: bin...	**Title of the Article / Chapter the Portion Is From**	Light-up split aptamers: bin...
Editor of Portion(s)	Zhao, Yichen; Patel, Nikesh; ...	**Author of Portion(s)**	Zhao, Yichen; Patel, Nikesh; ...
Volume / Edition	148	**Issue, if Republishing an Article From a Serial**	22
Page or Page Range of Portion	5612-5618	**Publication Date of Portion**	2023-11-06

Articles in Chapter 3

2. The analyst online

Billing Status: Open

Article: An aptamer array for discriminating tetracycline antibiotics based on binding-enhanced intrinsic fluores...

Print License

Order License ID	1512498-2	**Type of Use**	Republish in a thesis/dissert...
Order detail status	Completed	**Publisher**	Royal Society of Chemistry
ISSN	1364-5528	**Portion**	Chapter/article

0.00 CAD

Hide Details

Republication Permission

LICENSED CONTENT

Publication Title	The analyst online	**Publication Type**	e-Journal
Article Title	An aptamer array for discri...	**Start Page**	1507
Author / Editor	Royal Society of Chemistry (...	**End Page**	1513
Date	01/01/1876	**Issue**	7
Language	English	**Volume**	148
Country	United Kingdom of Great Bri...	**URL**	http://www.rsc.org/is/journa...
Rightsholder	Royal Society of Chemistry		

REQUEST DETAILS

Portion Type	Chapter/article	**Rights Requested**	Main product
Page Range(s)	1507-1513	**Distribution**	Worldwide
Total Number of Pages	7	**Translation**	Original language of publica...
Format (select all that apply)	Electronic	**Copies for the Disabled?**	No
Who Will Republish the Content?	Academic institution	**Minor Editing Privileges?**	Yes
		Incidental Promotional Use?	No
Duration of Use	Life of current edition	**Currency**	CAD
Lifetime Unit Quantity	Up to 499		

NEW WORK DETAILS

Title	Selection and Characterizati...	**Institution Name**	University of Waterloo
Instructor Name	Yichen Zhao	**Expected Presentation Date**	2024-08-15

ADDITIONAL DETAILS

The Requesting Person / Organization to Appear on the License	Yichen Zhao

REQUESTED CONTENT DETAILS

Title, Description or Numeric Reference of the Portion(s)	An aptamer array for discri...	**Title of the Article / Chapter the Portion Is From**	An aptamer array for discri...
Editor of Portion(s)	Zhao, Yichen; Gao, Biwen; C...	**Author of Portion(s)**	Zhao, Yichen; Gao, Biwen; C...
Volume / Edition	148	**Issue, if Republishing an Article From a Serial**	7
Page or Page Range of Portion	1507-1513	**Publication Date of Portion**	2023-03-27

ChemistryOpen

Chemistry Europe
European Chemical Societies Publishing

Research Article | Open Access

Characterization of the Binding Properties of Ten Aptamers Using the Intrinsic Fluorescence of Oxytetracycline

Yichen Zhao, Biwen Gao, Juewen Liu

First published: 05 February 2024 | https://doi.org/10.1002/open.202300250 | Citations: 2

Details

© 2024 The Authors. ChemistryOpen published by Wiley-VCH GmbH

This is an open access article under the terms of the Creative Commons Attribution License, which permits use, distribution and reproduction in any medium, provided the original work is properly cited.

Check for updates

Chapter 4:

Environment & Health > Vol 1/Issue 2 > Article

Open Access

ARTICLE | May 30, 2023

Capture-SELEX for Chloramphenicol Binding Aptamers for Labeled and Label-Free Fluorescence Sensing

Yichen Zhao, Albert Zehan Li, and Juewen Liu*



Environment & Health
Cite this: *Environ. Health* 2023, 1, 2, 102−109

https://doi.org/10.1021/envhealth.3c00017
Published May 30, 2023

Copyright © 2023 The Authors. Co-published by Research Center for Eco-Environmental Sciences, Chinese Academy of Sciences, and American Chemical Society. This publication is licensed under CC-BY-NC-ND 4.0.

References

1. Kratschmer, C. & Levy, M. Effect of Chemical Modifications on Aptamer Stability in Serum. *Nucleic Acid Ther* **27**, 335–344 (2017).

2. Morrissey, D. V. *et al.* Activity of stabilized short interfering RNA in a mouse model of hepatitis B virus replication. *Hepatology* **41**, 1349–1356 (2005).

3. Dass, C. R., Saravolac, E. G., Li, Y. & Sun, L.-Q. Cellular Uptake, Distribution, and Stability of 10-23 Deoxyribozymes. *Antisense Nucleic Acid Drug Development* **12**, 289–299 (2002).

4. Kurreck, J., Wyszko, E., Gillen, C. & Erdmann, V. A. *Design of Antisense Oligonucleotides Stabilized by Locked Nucleic Acids*. *Nucleic Acids Research* vol. 30 (2002).

5. Zhou, J. & Rossi, J. Aptamers as targeted therapeutics: Current potential and challenges. *Nat Rev Drug Discov* **16**, 181–202 (2017).

6. Tuerk, C. & Gold, L. Systematic Evolution of Ligands by Exponential Enrichment: RNA Ligands to Bacteriophage T4 DNA Polymerase. *Science (1979)* **249**, 505–510 (1990).

7. Ellington, A. D. & Szostak, J. W. In vitro selection of RNA molecules that bind specific ligands. *Nature* **346**, 818–822 (1990).

8. Ellington, A. D. & Szotak, J. W. Selection in vitro of single. stranded DNA molecules that fold into specific ligand binding structures. *Nature* **355**, 1809–1816 (1992).

9. Homann, M. & Göringer, H. U. *Combinatorial Selection of High Affinity RNA Ligands to Live African Trypanosomes*. *Nucleic Acids Research* vol. 27 https://academic.oup.com/nar/article/27/9/2006/2847998 (2006).

10. Ng, E. W. M. *et al.* Pegaptanib, a targeted anti-VEGF aptamer for ocular vascular disease. *Nat Rev Drug Discov* **5**, 123–132 (2006).

11. Shakeel, L., Khan, A. & Akilimali, A. "Izervay (avacincaptad pegol): paving the way for vision preservation in geographic atrophy". *Annals of Medicine & Surgery* **86**, 2413–2416 (2024).

12. Wang, M. *et al.* Selection and identification of diethylstilbestrol-specific aptamers based on magnetic-bead SELEX. *Microchemical Journal* **159**, (2020).

13. Lam, S. Y., Lau, H. L. & Kwok, C. K. Capture-SELEX: Selection Strategy, Aptamer Identification, and Biosensing Application. *Biosensors (Basel)* **12**, (2022).

14. Guan, J., He, K. & Gunasekaran, S. Selection of ssDNA aptamer using GO-SELEX and development of DNA nanostructure-based electrochemical aptasensor for penicillin. *Biosens Bioelectron X* **12**, (2022).

15. Narayan, C., Veeramani, S. & Thiel, W. H. Optimization of RNA Aptamer SELEX Methods: Improved Aptamer Transcript 3′-End Homogeneity, PAGE Purification Yield, and Target-Bound Aptamer RNA Recovery. *Nucleic Acid Ther* **32**, 74–80 (2022).

16. Sakamoto, S. *et al.* Enzyme-linked immunosorbent assay for the quantitative/qualitative analysis of plant secondary metabolites. *J Nat Med* **72**, 32–42 (2018).

17. Jayasena, S. D. Aptamers: An Emerging Class of Molecules That Rival Antibodies in Diagnostics. *Clin Chem* **45**, 1628–1650 (1999).

18. Nakhjavani, M. *et al.* A Flow Cytometry-Based Cell Surface Protein Binding Assay for Assessing Selectivity and Specificity of an Anticancer Aptamer. *Journal of Visualized Experiments* (2022) doi:10.3791/64304.

19. Spizzo, G. *et al.* High Ep-CAM Expression is Associated with Poor Prognosis in Node-positive Breast Cancer. *Breast Cancer Res Treat* **86**, 207–213 (2004).

20. Went, P. T. H. *et al.* Frequent EpCam protein expression in human carcinomas. *Hum Pathol* **35**, 122–128 (2004).

21. Yoshida, W. *et al.* Selection of DNA aptamers against insulin and construction of an aptameric enzyme subunit for insulin sensing. *Biosens Bioelectron* **24**, 1116–1120 (2009).

22. Ferrannini *et al.* Insulin: new roles for an ancient hormone. *Eur J Clin Invest* **29**, 842–852 (1999).

23. Zhang, Z. *et al.* High-Affinity Dimeric Aptamers Enable the Rapid Electrochemical Detection of Wild-Type and B.1.1.7 SARS-CoV-2 in Unprocessed Saliva. *Angewandte Chemie* **133**, 24468–24476 (2021).

24. Martínez-Roque, M. A. *et al.* DNA aptamer selection for SARS-CoV-2 spike glycoprotein detection. *Anal Biochem* **645**, 114633 (2022).

25. Russo Krauss, I. *et al.* High-resolution structures of two complexes between thrombin and thrombin-binding aptamer shed light on the role of cations in the aptamer inhibitory activity. *Nucleic Acids Res* **40**, 8119–28 (2012).

26. Gu, C., Lan, T., Shi, H. & Lu, Y. Portable Detection of Melamine in Milk Using a Personal Glucose Meter Based on an in Vitro Selected Structure-Switching Aptamer. *Anal Chem* **87**, 7676–7682 (2015).

27. Xu, S. *et al.* Selection of DNA aptamers against polychlorinated biphenyls as potential biorecognition elements for environmental analysis. *Anal Biochem* **423**, 195–201 (2012).

28. Jo, M. *et al.* Development of Single-Stranded DNA Aptamers for Specific Bisphenol A Detection. *Oligonucleotides* **21**, 85–91 (2011).

29. Dolgosheina, E. V. *et al.* RNA Mango Aptamer-Fluorophore: A Bright, High-Affinity Complex for RNA Labeling and Tracking. *ACS Chem Biol* **9**, 2412–2420 (2014).

30. Reinemann, C., Freiin von Fritsch, U., Rudolph, S. & Strehlitz, B. Generation and characterization of quinolone-specific DNA aptamers suitable for water monitoring. *Biosens Bioelectron* **77**, 1039–1047 (2016).

31. Zhou, N. *et al.* Selection and identification of streptomycin-specific single-stranded DNA aptamers and the application in the detection of streptomycin in honey. *Talanta* **108**, 109–116 (2013).

32. Wrist, A., Sun, W. & Summers, R. M. The Theophylline Aptamer: 25 Years as an Important Tool in Cellular Engineering Research. *ACS Synth Biol* **9**, 682–697 (2020).

33. Larsson, D. G. J. & Flach, C.-F. Antibiotic resistance in the environment. *Nat Rev Microbiol* **20**, 257–269 (2022).

34. Danner, M.-C., Robertson, A., Behrends, V. & Reiss, J. Antibiotic pollution in surface fresh waters: Occurrence and effects. *Science of The Total Environment* **664**, 793–804 (2019).

35. Niazi, J. H., Lee, S. J., Kim, Y. S. & Gu, M. B. ssDNA aptamers that selectively bind oxytetracycline. *Bioorg Med Chem* **16**, 1254–1261 (2008).

36. Kim, K. *et al.* High-sensitivity detection of oxytetracycline using light scattering agglutination assay with aptasensor. *Electrophoresis* **31**, 3115–3120 (2010).

37. Kwon, Y. S., Ahmad Raston, N. H. & Gu, M. B. An ultra-sensitive colorimetric detection of tetracyclines using the shortest aptamer with highly enhanced affinity. *Chem. Commun.* **50**, 40–42 (2014).

38. Zhou, N., Luo, J., Zhang, J., You, Y. & Tian, Y. A label-free electrochemical aptasensor for the detection of kanamycin in milk. *Analytical Methods* **7**, 1991–1996 (2015).

39. Khabbaz, L. S. *et al.* Detection of kanamycin by using an aptamer-based biosensor using silica nanoparticles. *Analytical Methods* **7**, 8611–8616 (2015).

40. Wang, Y. & Rando, R. R. Specific Binding of Aminoglycoside Antibiotics to RNA. *Chem Biol* **2**, 281–290 (1995).

41. Song, K. M. *et al.* Gold nanoparticle-based colorimetric detection of kanamycin using a DNA aptamer. *Anal Biochem* **415**, 175–181 (2011).

42. Wang, J., Ma, K., Yin, H., Zhou, Y. & Ai, S. Aptamer based voltammetric determination of ampicillin using a single-stranded DNA binding protein and DNA functionalized gold nanoparticles. *Microchimica Acta* **185**, 68 (2018).

43. Lee, A.-Y. *et al.* Development of a ssDNA aptamer for detection of residual benzylpenicillin. *Anal Biochem* **531**, 1–7 (2017).

44. Song, K.-M., Jeong, E., Jeon, W., Cho, M. & Ban, C. Aptasensor for ampicillin using gold nanoparticle based dual fluorescence–colorimetric methods. *Anal Bioanal Chem* **402**, 2153–2161 (2012).

45. Wu, S. *et al.* Aptamer-based fluorescence biosensor for chloramphenicol determination using upconversion nanoparticles. *Food Control* **50**, 597–604 (2015).

46. Mehta, J. *et al.* In vitro selection and characterization of DNA aptamers recognizing chloramphenicol. *J Biotechnol* **155**, 361–369 (2011).

47. Berens, C., Thain, A. & Schroeder, R. A tetracycline-binding RNA aptamer. *Bioorg Med Chem* **9**, 2549–2556 (2001).

48. Wallace, S. T. & Schroeder, R. In vitro selection and characterization of streptomycin-binding RNAs: recognition discrimination between antibiotics. *RNA* **4**, 112–23 (1998).

49. Ciesiołka, J., Michałowski, D., Wrzesinski, J., Krajewski, J. & Krzyżosiak, W. J. Patterns of cleavages induced by lead ions in defined RNA secondary structure motifs. *J Mol Biol* **275**, 211–220 (1998).

50. Suess, B. Conditional gene expression by controlling translation with tetracycline-binding aptamers. *Nucleic Acids Res* **31**, 1853–1858 (2003).

51. Muller, M., Weigand, J. E., Weichenrieder, O. & Suess, B. Thermodynamic characterization of an engineered tetracycline-binding riboswitch. *Nucleic Acids Res* **34**, 2607–2617 (2006).

52. Tickner, Z. J., Zhong, G., Sheptack, K. R. & Farzan, M. Selection of High-Affinity RNA Aptamers That Distinguish between Doxycycline and Tetracycline. *Biochemistry* **59**, 3473–3486 (2020).

53. Niazi, J. H., Lee, S. J. & Gu, M. B. Single-stranded DNA aptamers specific for antibiotics tetracyclines. *Bioorg Med Chem* **16**, 7245–7253 (2008).

54. Jenison, R. D., Gill, S. C., Pardi, A. & Polisky, B. High-Resolution Molecular Discrimination by RNA. *Science (1979)* **263**, 1425–1429 (1994).

55. Burke, D. H. *et al.* RNA aptamers to the peptidyl transferase inhibitor chloramphenicol. *Chem Biol* **4**, 833–843 (1997).

56. Ma, P. *et al.* Structure-switching fluorescence aptasensor for sensitive detection of chloramphenicol. *Microchimica Acta* **187**, 505 (2020).

57. Duan, Y. *et al.* Selection and Identification of Chloramphenicol-Specific DNA Aptamers by Mag-SELEX. *Appl Biochem Biotechnol* **180**, 1644–1656 (2016).

58. Kwon, M., Chun, S.-M., Jeong, S. & Yu, J. In Vitro Selection of RNA against Kanamycin B. *Mol Cells* **11**, 303–311 (2001).

59. Song, K.-M. *et al.* Gold nanoparticle-based colorimetric detection of kanamycin using a DNA aptamer. *Anal Biochem* **415**, 175–181 (2011).

60. Stoltenburg, R., Nikolaus, N. & Strehlitz, B. Capture-SELEX: Selection of DNA Aptamers for Aminoglycoside Antibiotics. *J Anal Methods Chem* **2012**, 1–14 (2012).

61. Sanford, A. A. *et al.* RE-SELEX: restriction enzyme-based evolution of structure-switching aptamer biosensors. *Chem Sci* **12**, 11692–11702 (2021).

62. Bissen, M. & Frimmel, F. H. Arsenic — a Review. Part I: Occurrence, Toxicity, Speciation, Mobility. *Acta hydrochimica et hydrobiologica* **31**, 9–18 (2003).

63. Kim, M. *et al.* Arsenic Removal from Vietnamese Groundwater Using the Arsenic-Binding DNA Aptamer. *Environ Sci Technol* **43**, 9335–9340 (2009).

64. Matsunaga, K. *et al.* Development of a simple analytical method to determine arsenite using a DNA aptamer and gold nanoparticles. *Chemosphere* **224**, 538–543 (2019).

65. Wu, Y., Liu, L., Zhan, S., Wang, F. & Zhou, P. Ultrasensitive aptamer biosensor for arsenic(iii) detection in aqueous solution based on surfactant-induced aggregation of gold nanoparticles. *Analyst* **137**, 4171 (2012).

66. Zong, C., Zhang, Z., Liu, B. & Liu, J. Adsorption of Arsenite on Gold Nanoparticles Studied with DNA Oligonucleotide Probes. *Langmuir* **35**, 7304–7311 (2019).

67. Zong, C. & Liu, J. The Arsenic-Binding Aptamer Cannot Bind Arsenic: Critical Evaluation of Aptamer Selection and Binding. *Anal Chem* **91**, 10887–10893 (2019).

68. Bottari, F. *et al.* Do Aptamers Always Bind? The Need for a Multifaceted Analytical Approach When Demonstrating Binding Affinity between Aptamer and Low Molecular Weight Compounds. *J Am Chem Soc* **142**, 19622–19630 (2020).

69. Tao, X. *et al.* Detection of chloramphenicol with an aptamer-based colorimetric assay: critical evaluation of specific and unspecific binding of analyte molecules. *Microchimica Acta* **187**, 668 (2020).

70. Zhou, J. *et al.* Kanamycin Adsorption on Gold Nanoparticles Dominates Its Label-Free Colorimetric Sensing with Its Aptamer. *Langmuir* **36**, 11490–11498 (2020).

71. Mendonsa, S. D. & Bowser, M. T. In Vitro Evolution of Functional DNA Using Capillary Electrophoresis. *J Am Chem Soc* **126**, 20–21 (2004).

72. Bruno, J. G. & Kiel, J. L. Use of Magnetic Beads in Selection and Detection of Biotoxin Aptamers by Electrochemiluminescence and Enzymatic Methods. *Biotechniques* **32**, 178–183 (2002).

73. Gu, L. *et al.* Selective Hemin Binding by a Non-G-quadruplex Aptamer with Higher Affinity and Better Peroxidase-like Activity. *Angewandte Chemie International Edition* **63**, (2024).

74. Chodosh, L. A. & Buratowski, S. Purification of DNA-Binding Proteins Using Biotin/Streptavidin Affinity Systems. *Curr Protoc Protein Sci* **12**, (1998).

75. Sullivan, R., Adams, M. C., Naik, R. R. & Milam, V. T. Analyzing Secondary Structure Patterns in DNA Aptamers Identified via CompELS. *Molecules* **24**, 1572 (2019).

76. Nutiu, R. & Li, Y. In vitro selection of structure-switching signaling aptamers. *Angewandte Chemie - International Edition* **44**, 1061–1065 (2005).

77. Yang, K.-A., Pei, R. & Stojanovic, M. N. In vitro selection and amplification protocols for isolation of aptameric sensors for small molecules. *Methods* **106**, 58–65 (2016).

78. Yang, K.-A., Pei, R., Stefanovic, D. & Stojanovic, M. N. Optimizing Cross-reactivity with Evolutionary Search for Sensors. *J Am Chem Soc* **134**, 1642–1647 (2012).

79. Gu, L. *et al.* Capture-SELEX for a short aptamer for label-free detection of salicylic acid. *Smart Molecules* **1**, (2023).

80. Paniel, N. *et al.* Selection of DNA aptamers against penicillin G using Capture-SELEX for the development of an impedimetric sensor. *Talanta* **162**, 232–240 (2017).

81. Mencin, N. *et al.* Optimization of SELEX: Comparison of different methods for monitoring the progress of in vitro selection of aptamers. *J Pharm Biomed Anal* **91**, 151–159 (2014).

82. Reuter, J. A., Spacek, D. V. & Snyder, M. P. High-Throughput Sequencing Technologies. *Mol Cell* **58**, 586–597 (2015).

83. Liu, L. *et al.* Comparison of Next-Generation Sequencing Systems. *J Biomed Biotechnol* **2012**, 1–11 (2012).

84. Velázquez-Campoy, A., Ohtaka, H., Nezami, A., Muzammil, S. & Freire, E. Isothermal Titration Calorimetry. *Curr Protoc Cell Biol* **23**, (2004).

85. Ruscito, A. & DeRosa, M. C. Small-Molecule Binding Aptamers: Selection Strategies, Characterization, and Applications. *Front Chem* **4**, (2016).

86. Katilius, E., Flores, C. & Woodbury, N. W. Exploring the sequence space of a DNA aptamer using microarrays. *Nucleic Acids Res* **35**, 7626–7635 (2007).

87. Huang, P.-J. J. & Liu, J. Selection of Aptamers for Sensing Caffeine and Discrimination of Its Three Single Demethylated Analogues. *Anal Chem* **94**, 3142–3149 (2022).

88. Niu, C., Ding, Y., Zhang, C. & Liu, J. Comparing two cortisol aptamers for label-free fluorescent and colorimetric biosensors. *Sensors & Diagnostics* **1**, 541–549 (2022).

89. Wen, X. *et al.* Selection and truncation of aptamers as fluorescence sensing platforms for selective and sensitive detection of nitrofurazone. *Anal Chim Acta* **1252**, 341044 (2023).

90. Gu, L., Zheng, J., Zhang, Y., Wang, D. & Liu, J. Selection and Characterization of DNA Aptamers for Cytidine and Uridine. *ChemBioChem* **25**, (2024).

91. Gu, L., Zheng, J., Zhang, Y., Wang, D. & Liu, J. Capture-SELEX of DNA Aptamers for Sulforhodamine B and Fluorescein. *Chemistry – A European Journal* **29**, (2023).

92. Economou, A., Kokkinos, C., Bousiakou, L. & Hianik, T. Paper-Based Aptasensors: Working Principles, Detection Modes, and Applications. *Sensors* **23**, 7786 (2023).

93. Yao, Y., Jiang, C. & Ping, J. Flexible freestanding graphene paper-based potentiometric enzymatic aptasensor for ultrasensitive wireless detection of kanamycin. *Biosens Bioelectron* **123**, 178–184 (2019).

94. Majdinasab, M., Badea, M. & Marty, J. L. Aptamer-Based Lateral Flow Assays: Current Trends in Clinical Diagnostic Rapid Tests. *Pharmaceuticals* **15**, 90 (2022).

95. Dalirirad, S. & Steckl, A. J. Lateral flow assay using aptamer-based sensing for on-site detection of dopamine in urine. *Anal Biochem* **596**, 113637 (2020).

96. Jarczewska, M., Górski, Ł. & Malinowska, E. Electrochemical aptamer-based biosensors as potential tools for clinical diagnostics. *Analytical Methods* **8**, 3861–3877 (2016).

97. Moore, M. D., Escudero-Abarca, B. I. & Jaykus, L.-A. An Enzyme-Linked Aptamer Sorbent Assay to Evaluate Aptamer Binding. in 291–302 (2017). doi:10.1007/978-1-4939-6857-2_18.

98. Debiais, M., Lelievre, A., Smietana, M. & Müller, S. Splitting aptamers and nucleic acid enzymes for the development of advanced biosensors. *Nucleic Acids Res* **48**, 3400–3422 (2020).

99. Zhou, C. *et al.* Split aptamer-based detection of adenosine triphosphate using surface enhanced Raman spectroscopy and two kinds of gold nanoparticles. *Microchimica Acta* **186**, 251 (2019).

100. Chopra, I. & Roberts, M. Tetracycline Antibiotics: Mode of Action, Applications, Molecular Biology, and Epidemiology of Bacterial Resistance. *Microbiology and Molecular Biology Reviews* **65**, 232–260 (2001).

101. Granados-Chinchilla, F. & Rodríguez, C. Tetracyclines in Food and Feedingstuffs: From Regulation to Analytical Methods, Bacterial Resistance, and Environmental and Health Implications. *J Anal Methods Chem* **2017**, 1–24 (2017).

102. Daghrir, R. & Drogui, P. Tetracycline antibiotics in the environment: a review. *Environ Chem Lett* **11**, 209–227 (2013).

103. Mehlhorn, A., Rahimi, P. & Joseph, Y. Aptamer-Based Biosensors for Antibiotic Detection: A Review. *Biosensors (Basel)* **8**, 54 (2018).

104. Berens, C., Thain, A. & Schroeder, R. A tetracycline-binding RNA aptamer. *Bioorg Med Chem* **9**, 2549–2556 (2001).

105. Wu, L. *et al.* Aptamer-Based Detection of Circulating Targets for Precision Medicine. *Chem Rev* **121**, 12035–12105 (2021).

106. McConnell, E. M., Nguyen, J. & Li, Y. Aptamer-Based Biosensors for Environmental Monitoring. *Front Chem* **8**, (2020).

107. Yu, H., Alkhamis, O., Canoura, J., Liu, Y. & Xiao, Y. Advances and Challenges in Small-Molecule DNA Aptamer Isolation, Characterization, and Sensor Development. *Angewandte Chemie International Edition* **60**, 16800–16823 (2021).

108. Wurmthaler, L. A., Sack, M., Gense, K., Hartig, J. S. & Gamerdinger, M. A tetracycline-dependent ribozyme switch allows conditional induction of gene expression in Caenorhabditis elegans. *Nat Commun* **10**, 491 (2019).

109. Wu, Y., Belmonte, I., Sykes, K. S., Xiao, Y. & White, R. J. Perspective on the Future Role of Aptamers in Analytical Chemistry. *Anal Chem* **91**, 15335–15344 (2019).

110. Debiais, M., Lelievre, A., Smietana, M. & Müller, S. Splitting aptamers and nucleic acid enzymes for the development of advanced biosensors. *Nucleic Acids Res* **48**, 3400–3422 (2020).

111. Nakatsuka, N. *et al.* Aptamer–field-effect transistors overcome Debye length limitations for small-molecule sensing. *Science (1979)* **362**, 319–324 (2018).

112. Yang, K.-A. *et al.* Recognition and sensing of low-epitope targets via ternary complexes with oligonucleotides and synthetic receptors. *Nat Chem* **6**, 1003–1008 (2014).

113. Yu, H. *et al.* Isolation of Natural DNA Aptamers for Challenging Small-Molecule Targets, Cannabinoids. *Anal Chem* **93**, 3172–3180 (2021).

114. Yu, H. *et al.* In vitro isolation of small-molecule-binding aptamers with intrinsic dye-displacement functionality. *Nucleic Acids Res* **46**, e43–e43 (2018).

115. Lyu, C., Khan, I. M. & Wang, Z. Capture-SELEX for aptamer selection: A short review. *Talanta* **229**, 122274 (2021).

116. Yang, K.-A. *et al.* High-Affinity Nucleic-Acid-Based Receptors for Steroids. *ACS Chem Biol* **12**, 3103–3112 (2017).

117. Yang, W. *et al.* In vitro isolation of class-specific oligonucleotide-based small-molecule receptors. *Nucleic Acids Res* **47**, e71–e71 (2019).

118. Gao, H. *et al.* Universal Design of Structure-Switching Aptamers with Signal Reporting Functionality. *Anal Chem* **91**, 14514–14521 (2019).

119. Luo, Y., Wang, J., Yang, L., Gao, T. & Pei, R. In vitro selection of DNA aptamers for the development of fluorescent aptasensor for sarcosine detection. *Sens Actuators B Chem* **276**, 128–135 (2018).

120. Tian, H., Duan, N., Wu, S. & Wang, Z. Selection and application of ssDNA aptamers against spermine based on Capture-SELEX. *Anal Chim Acta* **1081**, 168–175 (2019).

121. Liu, Y. & Liu, J. Selection of DNA Aptamers for Sensing Uric Acid in Simulated Tears. *Analysis & Sensing* **2**, (2022).

122. Luo, Y., Jin, Z., Wang, J., Ding, P. & Pei, R. The isolation of a DNA aptamer to develop a fluorescent aptasensor for the thiamethoxam pesticide. *Analyst* **146**, 1986–1995 (2021).

123. Carlotti, B., Fuoco, D. & Elisei, F. Fast and ultrafast spectroscopic investigation of tetracycline derivatives in organic and aqueous media. *Physical Chemistry Chemical Physics* **12**, 15580 (2010).

124. Pautke, C. *et al.* Characterization of eight different tetracyclines: advances in fluorescence bone labeling. *J Anat* **217**, 76–82 (2010).

125. Yeasmin Khusbu, F., Zhou, X., Chen, H., Ma, C. & Wang, K. Thioflavin T as a fluorescence probe for biosensing applications. *TrAC Trends in Analytical Chemistry* **109**, 1–18 (2018).

126. Sun, C. *et al.* Label-free fluorescent sensor based on aptamer and thiazole orange for the detection of tetracycline. *Dyes and Pigments* **149**, 867–875 (2018).

127. Gustavsson, T. & Markovitsi, D. Fundamentals of the Intrinsic DNA Fluorescence. *Acc Chem Res* **54**, 1226–1235 (2021).

128. Armstrong-Price, D. E., Deore, P. S. & Manderville, R. A. Intrinsic "Turn-On" Aptasensor Detection of Ochratoxin A Using Energy-Transfer Fluorescence. *J Agric Food Chem* **68**, 2249–2255 (2020).

129. Autour, A. *et al.* Fluorogenic RNA Mango aptamers for imaging small non-coding RNAs in mammalian cells. *Nat Commun* **9**, 656 (2018).

130. Truong, L. & Ferré-D'Amaré, A. R. From fluorescent proteins to fluorogenic RNAs: Tools for imaging cellular macromolecules. *Protein Science* **28**, 1374–1386 (2019).

131. Jezowska-Bojczuk, M., Lambs, L., Kozlowski, H. & Berthon, G. Metal ion-tetracycline interactions in biological fluids. 10. Structural investigations on copper(II) complexes of tetracycline, oxytetracycline, chlortetracycline, 4-(dedimethylamino)tetracycline, and 6-desoxy-6-demethyltetracycline and discussion of their binding modes. *Inorg Chem* **32**, 428–437 (1993).

132. Lambs, L., Decock-Le Reverend, B., Kozlowski, H. & Berthon, G. Metal ion-tetracycline interactions in biological fluids. 9. Circular dichroism spectra of calcium and magnesium

complexes with tetracycline, oxytetracycline, doxycycline, and chlortetracycline and discussion of their binding modes. *Inorg Chem* **27**, 3001–3012 (1988).

133. Lambs, L., Brion, M. & Berthon, G. Metal ion-tetracycline interactions in biological fluids. Part 3. Formation of mixed-metal ternary complexes of tetracycline, oxytetracycline, doxycycline and minocycline with calcium and magnesium, and their involvement in the bioavailability of these antibiotics in blood plasma. *Agents Actions* **14**, 743–750 (1984).

134. Schneider, S. *et al.* Fluorescence kinetics of aqueous solutions of tetracycline and its complexes with Mg2+ and Ca2+. *Photochemical & Photobiological Sciences* **2**, 1107–1117 (2003).

135. Lorsch, J. R. & Szostak, J. W. In vitro selection of RNA aptamers specific for cyanocobalamin. *Biochemistry* **33**, 973–982 (1994).

136. Zhao, Y., Ong, S., Chen, Y., Jimmy Huang, P.-J. & Liu, J. Label-free and Dye-free Fluorescent Sensing of Tetracyclines Using a Capture-Selected DNA Aptamer. *Anal Chem* **94**, 10175–10182 (2022).

137. Li, Y., Wang, H., Liu, X., Zhao, G. & Sun, Y. Dissipation kinetics of oxytetracycline, tetracycline, and chlortetracycline residues in soil. *Environmental Science and Pollution Research* **23**, 13822–13831 (2016).

138. Xuan, R., Arisi, L., Wang, Q., Yates, S. R. & Biswas, K. C. Hydrolysis and photolysis of oxytetracycline in aqueous solution. *Journal of Environmental Science and Health, Part B* **45**, 73–81 (2009).

139. Scaria, J., Anupama, K. V. & Nidheesh, P. V. Tetracyclines in the environment: An overview on the occurrence, fate, toxicity, detection, removal methods, and sludge management. *Science of The Total Environment* **771**, 145291 (2021).

140. Guerra, W., Silva-Caldeira, P. P., Terenzi, H. & Pereira-Maia, E. C. Impact of metal coordination on the antibiotic and non-antibiotic activities of tetracycline-based drugs. *Coord Chem Rev* **327–328**, 188–199 (2016).

141. Nutiu, R. & Li, Y. Structure-Switching Signaling Aptamers. *J Am Chem Soc* **125**, 4771–4778 (2003).

142. Qi, X., Yan, X., Zhao, Y., Li, L. & Wang, S. Highly sensitive and specific detection of small molecules using advanced aptasensors based on split aptamers: A review. *TrAC Trends in Analytical Chemistry* **133**, 116069 (2020).

143. Stojanovic, M. N., de Prada, P. & Landry, D. W. Fluorescent Sensors Based on Aptamer Self-Assembly. *J Am Chem Soc* **122**, 11547–11548 (2000).

144. Li, F. *et al.* Adenosine detection by using gold nanoparticles and designed aptamer sequences. *Analyst* **134**, 1355 (2009).

145. Yu, H., Canoura, J., Guntupalli, B., Lou, X. & Xiao, Y. A cooperative-binding split aptamer assay for rapid, specific and ultra-sensitive fluorescence detection of cocaine in saliva. *Chem Sci* **8**, 131–141 (2017).

146. Chen, A., Yan, M. & Yang, S. Split aptamers and their applications in sandwich aptasensors. *TrAC Trends in Analytical Chemistry* **80**, 581–593 (2016).

147. Ye, H. *et al.* Split aptamer acquisition mechanisms and current application in antibiotics detection: a short review. *Crit Rev Food Sci Nutr* **63**, 9098–9110 (2023).

148. Liu, X. *et al.* Recent Advances of Biosensors Based on Split Aptamers in Biological Analysis: A Review. *IEEE Sens J* **22**, 12460–12472 (2022).

149. Wang, R. *et al.* Unconventional Split Aptamers Cleaved at Functionally Essential Sites Preserve Biorecognition Capability. *Anal Chem* **91**, 15811–15817 (2019).

150. McKeague, M. *et al.* Comprehensive Analytical Comparison of Strategies Used for Small Molecule Aptamer Evaluation. *Anal Chem* **87**, 8608–8612 (2015).

151. Daems, E., Moro, G., Campos, R. & De Wael, K. Mapping the gaps in chemical analysis for the characterisation of aptamer-target interactions. *TrAC Trends in Analytical Chemistry* **142**, 116311 (2021).

152. Zhao, Y., Yavari, K. & Liu, J. Critical evaluation of aptamer binding for biosensor designs. *TrAC Trends in Analytical Chemistry* **146**, 116480 (2022).

153. Shoara, A. A., Slavkovic, S., Donaldson, L. W. & Johnson, P. E. Analysis of the interaction between the cocaine-binding aptamer and its ligands using fluorescence spectroscopy. *Can J Chem* **95**, 1253–1260 (2017).

154. Shoara, A. A. & Johnson, P. E. Fluorometry studies of aptamers that bind intrinsically fluorescent ligands: techniques, obstacles and optimizations. *Aptamers* **6**, 19–27 (2022).

155. Zhao, Y., Gao, B., Sun, P., Liu, J. & Liu, J. Metal and pH-Dependent Aptamer Binding of Tetracyclines Enabling Highly Sensitive Fluorescence Sensing. *Biosensors (Basel)* **12**, 717 (2022).

156. Zhang, H., Li, F., Dever, B., Li, X.-F. & Le, X. C. DNA-Mediated Homogeneous Binding Assays for Nucleic Acids and Proteins. *Chem Rev* **113**, 2812–2841 (2013).

157. Bezerra, A. B., Kurian, A. S. N. & Easley, C. J. Nucleic-Acid Driven Cooperative Bioassays Using Probe Proximity or Split-Probe Techniques. *Anal Chem* **93**, 198–214 (2021).

158. Hassani, M., Lázaro, R., Pérez, C., Condón, S. & Pagán, R. Thermostability of Oxytetracycline, Tetracycline, and Doxycycline at Ultrahigh Temperatures. *J Agric Food Chem* **56**, 2676–2680 (2008).

159. Oehler, R., Polacek, N., Steiner, G. & Barta, A. Interaction of tetracycline with RNA: photoincorporation into ribosomal RNA of Escherichia coli. *Nucleic Acids Res* **25**, 1219–1224 (1997).

160. Slavkovic, S. & Johnson, P. E. Isothermal titration calorimetry studies of aptamer-small molecule interactions: practicalities and pitfalls. *Aptamers* **2**, 45–51 (2018).

161. Sievers, F. *et al.* Fast, scalable generation of high-quality protein multiple sequence alignments using Clustal Omega. *Mol Syst Biol* **7**, (2011).

162. De, M. *et al.* Sensing of proteins in human serum using conjugates of nanoparticles and green fluorescent protein. *Nat Chem* **1**, 461–465 (2009).

163. Yan, Q. *et al.* pH-Regulated Optical Performances in Organic/Inorganic Hybrid: A Dual-Mode Sensor Array for Pattern-Recognition-Based Biosensing. *Anal Chem* **90**, 10536–10542 (2018).

164. Hizir, M. S. *et al.* Universal sensor array for highly selective system identification using two-dimensional nanoparticles. *Chem Sci* **8**, 5735–5745 (2017).

165. Shen, A. Y., Haddad, E. J., Hunter-Smith, D. J. & Rozen, W. M. Efficacy and adverse effects of topical chloramphenicol ointment use for surgical wounds: a systematic review. *ANZ J Surg* **88**, 1243–1246 (2018).

166. Hanekamp, J. C. & Calabrese, E. J. Chloramphenicol, European Legislation and Hormesis - Commentary. *Dose-Response* **5**, dose-response.0 (2007).

167. Lees, P., Pelligand, L., Giraud, E. & Toutain, P. A history of antimicrobial drugs in animals: Evolution and revolution. *J Vet Pharmacol Ther* **44**, 137–171 (2021).

168. Dasgupta, A. Advances in antibiotic measurement. in 75–104 (2012). doi:10.1016/B978-0-12-394317-0.00013-3.

169. Liu, N. *et al.* A rabbit monoclonal antibody-based sensitive competitive indirect enzyme-linked immunoassay for rapid detection of chloramphenicol residue. *Food Agric Immunol* **25**, 523–534 (2014).

170. Yu, H., Alkhamis, O., Canoura, J., Liu, Y. & Xiao, Y. Advances and Challenges in Small-Molecule DNA Aptamer Isolation, Characterization, and Sensor Development. *Angewandte Chemie International Edition* **60**, 16800–16823 (2021).

171. Wu, L. *et al.* Aptamer-Based Detection of Circulating Targets for Precision Medicine. *Chem Rev* **121**, 12035–12105 (2021).

172. McConnell, E. M., Nguyen, J. & Li, Y. Aptamer-Based Biosensors for Environmental Monitoring. *Front Chem* **8**, (2020).

173. Wu, Y., Belmonte, I., Sykes, K. S., Xiao, Y. & White, R. J. Perspective on the Future Role of Aptamers in Analytical Chemistry. *Anal Chem* **91**, 15335–15344 (2019).

174. Hamidi-Asl, E., Dardenne, F., Blust, R. & De Wael, K. An Improved Electrochemical Aptasensor for Chloramphenicol Detection Based on Aptamer Incorporated Gelatine. *Sensors* **15**, 7605–7618 (2015).

175. Xie, Y., Huang, Y., Tang, D., Cui, H. & Cao, H. A competitive colorimetric chloramphenicol assay based on the non-cross-linking deaggregation of gold nanoparticles coated with a polyadenine-modified aptamer. *Microchimica Acta* **185**, 534 (2018).

176. Huang, P. J. & Liu, J. Simultaneous Detection of L-Lactate and D-Glucose Using DNA Aptamers in Human Blood Serum**. *Angewandte Chemie International Edition* **62**, (2023).

177. Jenison, R. D., Gill, S. C., Pardi, A. & Polisky, B. High-Resolution Molecular Discrimination by RNA. *Science (1979)* **263**, 1425–1429 (1994).

178. Huizenga, D. E. & Szostak, J. W. A DNA Aptamer That Binds Adenosine and ATP. *Biochemistry* **34**, 656–665 (1995).

179. Ding, Y. & Liu, J. Pushing Adenosine and ATP SELEX for DNA Aptamers with Nanomolar Affinity. *J Am Chem Soc* **145**, 7540–7547 (2023).

180. McKeague, M. & DeRosa, M. C. Challenges and Opportunities for Small Molecule Aptamer Development. *J Nucleic Acids* **2012**, 1–20 (2012).

181. Hu, J. & Easley, C. J. A simple and rapid approach for measurement of dissociation constants of DNA aptamers against proteins and small molecules via automated microchip electrophoresis. *Analyst* **136**, 3461 (2011).

182. Zhang, F., Huang, P.-J. J. & Liu, J. Sensing Adenosine and ATP by Aptamers and Gold Nanoparticles: Opposite Trends of Color Change from Domination of Target Adsorption Instead of Aptamer Binding. *ACS Sens* **5**, 2885–2893 (2020).

183. Krause, K. M., Serio, A. W., Kane, T. R. & Connolly, L. E. Aminoglycosides: An Overview. *Cold Spring Harb Perspect Med* **6**, a027029 (2016).

184. Jiang, M., Karasawa, T. & Steyger, P. S. Aminoglycoside-Induced Cochleotoxicity: A Review. *Front Cell Neurosci* **11**, (2017).

185. Zhang, X. *et al.* Determination of Kanamycin by High Performance Liquid Chromatography. *Molecules* **24**, 1902 (2019).

186. Dijkstra, J. A., Voerman, A. J., Greijdanus, B., Touw, D. J. & Alffenaar, J. W. C. Immunoassay Analysis of Kanamycin in Serum Using the Tobramycin Kit. *Antimicrob Agents Chemother* **60**, 4646–4651 (2016).

187. Wang, X. *et al.* Determination of human urinary kanamycin in one step using urea-enhanced surface plasmon resonance light-scattering of gold nanoparticles. *Anal Bioanal Chem* **395**, 2397–2403 (2009).

188. Ding, Y., Liu, X., Huang, P.-J. J. & Liu, J. Homogeneous assays for aptamer-based ethanolamine sensing: no indication of target binding. *Analyst* **147**, 1348–1356 (2022).

189. Rowe, A. A., Miller, E. A. & Plaxco, K. W. Reagentless Measurement of Aminoglycoside Antibiotics in Blood Serum via an Electrochemical, Ribonucleic Acid Aptamer-Based Biosensor. *Anal Chem* **82**, 7090–7095 (2010).

190. Li, H. *et al.* High frequency, calibration-free molecular measurements in situ in the living body. *Chem Sci* **10**, 10843–10848 (2019).

191. Ding, Y., Xie, Y., Li, A. Z., Huang, P.-J. J. & Liu, J. Cross-Binding of Four Adenosine/ATP Aptamers to Caffeine, Theophylline, and Other Methylxanthines. *Biochemistry* **62**, 2280–2288 (2023).

192. Yang, K. *et al.* A functional group–guided approach to aptamers for small molecules. *Science (1979)* **380**, 942–948 (2023).

193. Liu, Z., Mei, S. H. J., Brennan, J. D. & Li, Y. Assemblage of signaling DNA enzymes with intriguing metal-ion specificities and pH dependences. *J Am Chem Soc* **125**, 7539–45 (2003).

194. Gordon, C. K. L., Eisenstein, M. & Soh, H. T. Direct Selection Strategy for Isolating Aptamers with pH-Sensitive Binding Activity. *ACS Sens* **3**, 2574–2580 (2018).

195. Yuan, H. *et al.* Mechanism of pH influence on aptamer binding with Cd2+ revealed by molecular dynamics simulation. *New Journal of Chemistry* **47**, 9239–9249 (2023).

196. Belleperche, M. & DeRosa, M. pH-Control in Aptamer-Based Diagnostics, Therapeutics, and Analytical Applications. *Pharmaceuticals* **11**, 80 (2018).

197. Hianik, T., Ostatná, V., Sonlajtnerova, M. & Grman, I. Influence of ionic strength, pH and aptamer configuration for binding affinity to thrombin. *Bioelectrochemistry* **70**, 127–133 (2007).

198. Ma'mun, S., Chafidz, A., Indrayanto, E. & Setiawan, P. K. The Effect of Ionic Strength on Protonation Constant of Monoethanolamine in Water at 303K. *J Phys Conf Ser* **1295**, 012017 (2019).

199. Min, J., Sempionatto, J. R., Teymourian, H., Wang, J. & Gao, W. Wearable electrochemical biosensors in North America. *Biosens Bioelectron* **172**, 112750 (2021).

200. Kim, J., Campbell, A. S., de Ávila, B. E.-F. & Wang, J. Wearable biosensors for healthcare monitoring. *Nat Biotechnol* **37**, 389–406 (2019).